Sorption enhancement and chemical looping as process intensification measures for the steam reforming of acetic acid

A base-case for the enhanced steam reforming of pyrolysis oils

Oluwafemi Akinbola Omoniyi

Submitted in accordance with the requirements for the degree of

Doctor of Philosophy

School of Chemical and Process Engineering

University of Leeds, UK

June 2017

Acknowledgements

My sincere gratitude goes to God Almighty for the grace and strength to carry out this study. Secondly, I appreciate my parents, Rev Bola Omoniyi and Pastor Mrs Mojisola Omoniyi for the undying support shown to me during the completion of this work.

Special thanks also go to my supervisor Dr Valerie Dupont for her professional and academic guidance throughout the duration of this study. I also appreciate all technical staff particularly at the school of chemical and process engineering in the University of Leeds for their support during my study.

I would like to appreciate The Niger Delta Development Commission (NDDC) Nigeria for providing funding for these work. I also appreciate all colleagues especially Sergio Ramirez, Dr Zainab Ibrahim S G Adiya, Hafizah Yun, Lifita Tande, Dr Feng Chen, Dr Syed Zaheer Abbas, and Dr Guarav Nahar for their support and friendship.

I appreciate my siblings and their families for their prayers and moral support throughout the course of my study; The Ogunjinrin's- Kemi, Ayo, and Lauren Ogunjinrin; the Owolabi's- Tolulope, Bunmi, Temi and Ebun Owolabi; The Ajibade's-Adewale, Funmilola and Demilade Ajibade. I also appreciate Prof Tunde Idowu for words of wisdom and encouragement during the course of my study.

Finally, I appreciate every member at RCCG Powerconnections Leeds particularly the choir team and the pastorate/leaders for their friendship and encouragement during my study.

Thank you all.

Abstract

Chemical looping steam reforming (CLSR) and sorption enhanced chemical looping steam reforming (SE-CLSR) were utilised as process intensification measures to optimise the steam reforming process of acetic acid as a base-case for the enhanced steam reforming of pyrolysis oils. Both processes were carried out in a packed bed reactor, using two conventional nickel-based catalysts ('A' with alumina support and 'B' with calcium aluminate support) with the view of ascertaining optimal conditions for sustained steam reforming, and observing changes in morphology and characteristics in the materials utilised.

An experimental review, carried out on the steam reforming of acetic acid indicates, an acetic acid and water pre-heat temperature < 70°C and > 120°C respectively is ideal for sustained hydrogen production, at weight hourly space velocity (WHSV) set between 2.3 hr^{-1} to 2.5 hr^{-1}, steam reforming temperature (T_{SR}) set to 600°C or 650°C and steam to carbon ratio (S/C) set to 3 for the reactor set up and configuration utilised. Sustained steam reforming was observed at all T_{SR} investigated (550°C – 700°C), at all catalyst sizes compared, and all WHSV utilised (2.1 hr^{-1} to 2.8 hr^{-1}), with acetic acid conversion efficiency >83% realised and a hydrogen yield efficiency >85% realised for all experimental runs when compared to equilibrium values.

Characterisation of the utilised catalyst through SEM images indicates the formation of filamentous carbon on the catalyst surface. Two peaks of CO_2 obtained from the CO_2 chemigram in TGA-FTIR analysis indicates two types of carbon are formed, with amorphous carbon and a polycrystalline pseudo-graphitic carbon observed through TEM images and diffraction patterns.

CLSR has been promoted as a viable measure of improving the efficiency of the steam reforming process. It is a cyclic process that incorporates an oxidation step for material regeneration alongside steam reforming. In this study, it was inferred that the

proficiency of the subsequent steam reforming fuel-steam feed run is dependent on the operating conditions and type of materials utilised in the oxidation step.

Efficient auto-reduction and sustained CLSR close to equilibrium values were observed for both catalysts (S/C of 3, WHSV: 2.36 hr^{-1} and 2.5 hr^{-1}, T_{OX}: 600°C - 800°C, T_{SR}: 600 °C and 650°C) except when oxidation was carried out at 600°C for catalyst A. This exemplifies the advantages of an alkali-based support for reforming catalysts such as the one in catalyst B in reducing thermal decomposition of the fuel and sintering. Study on T_{OX} utilised indicates, an increase in T_{OX} would lead to more efficient carbon and nickel oxidation. Care must be taken however because it also leads to a potential increase of sintering of the catalyst.

SEM-EDX analysis and CHN analysis in this study indicates, there is a close similarity between the oxidised catalyst and fresh as received catalyst B particularly when oxidation is carried out at 800°C. This indicates complete burning of carbon and catalyst oxidation during the oxidation phase utilised for the CLSR experiments. The complete oxidation observed ensured sustained steam reforming over 10 cycles of CLSR investigated in this study (T_{SR} at 650°C, T_{OX}: 800°C, WHSV set to 2.5 $hr^{-1}$and S/C of 3) for catalyst B.

The sustained reforming, across all 10 cycles of CLSR, showed high consistency with >95% of acetic acid converted leading to a hydrogen yield efficiency >88% observed across all 10 cycles, when compared with equilibrium values. A carbon balance of the overall chemical looping reforming process infers most of the carbon share (ca 90%) in the process is utilised for effective steam reforming and hydrogen production.

SE-CLSR entails the addition of a sorbent into the chemical looping reforming material bed. This has been promoted to lead to an increase in hydrogen concentration and yield, due to the shift in equilibrium towards hydrogen production caused by the in-situ carbon-capture during the reforming process. Two stages occur, as in the case of CLSR. Calcining of the sorbent occurs in the oxidation stage alongside other processes that

occur in the oxidation step in CLSR. In-situ carbon capture or carbonation of the calcined sorbent occurs alongside other reactions in the reforming stage.

Three phases were identified for the SE-CLSR reforming stage;

- The pre-breakthrough phase, where complete sorption activity occurs and >99% of all carbon products produced is captured
- The breakthrough phase where a break of CO_2 is observed indicating partial sorption activity
- The post-breakthrough phase where no sorption activity is occurring.

It was inferred that the mass of the sorbent added to the material bed has an influence on the carbonation duration (pre-breakthrough + breakthrough Phase). An increase in the sorbent/ catalyst ratio increases the duration of carbonation and number of moles of carbon captured.

20 cycles of SE-CLSR with T_{SR} at 650°C and T_{OX} set to 850°C using catalyst B with S/C set to 3 and WHSV set to 1.18 was conducted. Sustained and consistent reforming (>80 % of acetic acid converted) was observed across all 20 SE-CLSR cycles; this led to > 78% hydrogen yield efficiency across all 20 SE-CLSR cycles when compared to equilibrium values.

A close observation of the carbonation duration indicates a reduction in the pre-break duration for the first 10 cycles. This led to a decrease in sorbent conversion and efficiency. This was attributed to a change in kinetics and CO_2 capture capacity in the pre-breakthrough phase, caused by sintering in the materials and reduction of open porosity.

At the end of the 20^{th} cycle, the conversion efficiency had dropped to about 50% of the conversion efficiency at the end of the first cycle. This prompts the need for reactivation techniques to reduce the decay of the CaO sorbent across redox cycling.

Steam hydration of the material has been promoted to improve the reactivity of CaO based sorbents and was carried out at 250°C with the view to observe any changes in the conversion of the sorbent. It was observed that on comparison to the SE-CLSR experiments with no hydration at 250°C, there was a higher hydrogen yield and concentration. This was attributed to a higher rate of sorption enhancement as observed in the increased carbonation rate in the pre-breakthrough phase for the experiments with hydration set at 250°C. There is also increased sorption enhanced auto-reduction observed and an improved sorbent conversion outlook over the cycles investigated.

Table of Contents

List of Figures

List of tables

Chapter 1 Introduction

1.1 General overview

Hydrogen is a gas of industrial importance utilised in many processes globally, particularly in the production of ammonia and the upgrading of fuels while refining. Its application in fuel-cells and space vehicles is touted as one of the most sustainable means for transportation applications and for the production of heat and power. It has been promoted as the long-term, optimal solution for the replacement of petroleum fuels, particularly in the energy and electricity sector. Its combustion does not lead to the production of carbonaceous products when compared to other options. Hence, it reduces greenhouse gas emissions (CO_2, CH_4, N_2O), and air pollutants such as carbon monoxide, soot, particulate matter, NOx and ozone formation [1].

The emission profile of hydrogen taking into consideration life cycle assessment and well to wheels' analysis [1] shows that positive environmental attributes that could be potentially realised from the utilisation of hydrogen as an alternative fuel is dependent on the process employed in its production and the raw material utilised.

In terms of production, the exciting prospects and drive for research on the production and utilisation of hydrogen is, there are so many hydrogen-containing compounds and mixtures that could easily or potentially be used for hydrogen production. They range from water, nuclear energy, fossil-fuels such as coal, natural gas, and naphtha also, renewable resources such as biomass resources, wind and solar. Nevertheless, hydrogen is produced majorly from fossil-fuels- particularly naphtha, coal, heavy oils and natural gas, globally as shown in Figure 1.1[2].

[1] Life cycle assessment (LCA) and well to wheel analysis details the environmental impacts of the production, utilisation, and storage or disposal of studied processes and materials with the view to understand processes, proffer an optimal process and determine sustainability.

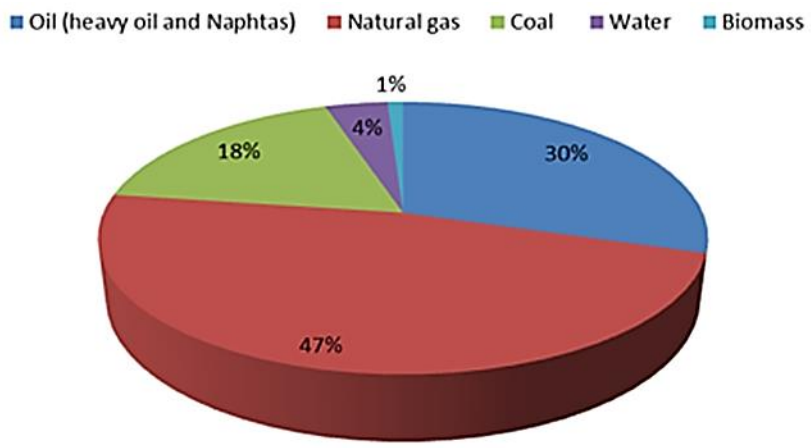

Figure 1.1 Global hydrogen production [3-5]

On large-scale and industrial settings, conventional hydrogen-production processes that majorly lead to a considerable amount of greenhouse-gas emissions could be done semi-centrally or centrally by integrating the production of hydrogen to the eventual process for which it would be utilised for. This is especially seen in the Haber's process for the production of ammonia. Hydrogen could be produced in a distributed setting as well resulting in an increased economies of scale and diversification of its end use; this is used particularly in stationary powers-sites.

This general flexibility in the production of hydrogen is hampered due to costs, safety issues and the lack of available infrastructure for the distribution and storage of hydrogen. Therefore, more research is required with the view to provide a more efficient means for hydrogen storage, particularly in a large-scale setting [6].

Nevertheless, the global need for the production of hydrogen remains essential, due to the numerous applications it is used for, or could be potentially utilised (Figure 1.2). At present, more than 50 million tons of hydrogen are produced globally, with a global market-value of over 40 billion dollars. Estimations indicate the market value could rise to about 180 billion dollars due to the advent of fuel-cell technologies [7].

This high market value is ultimately due to its utilisation in many industrial processes, particularly in food-processing, metallurgical processes, refining and petrochemical industries.

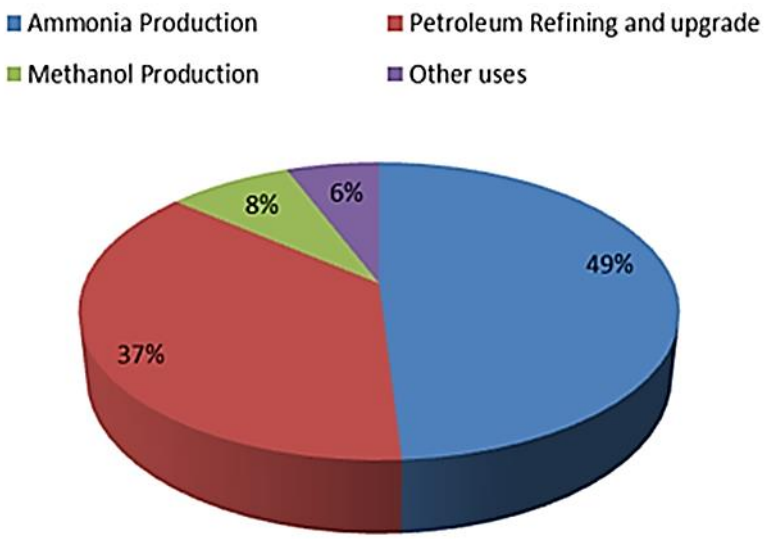

Figure 1.2 Global hydrogen consumption [8, 9]

Hydrogen is utilised in a liquefied form in space shuttles and rockets, with intense research on its utilisation in ultra-sonic and supersonic space vehicles. The major reason for the rise in the research by different organisations on the utilisation of hydrogen is prompted, due to the diverse potential ways by which energy could be produced or harnessed from it in fuel-cells, turbines or even combustion engines or chambers.

This is due to the unique properties of hydrogen as the lightest element and an energy carrier. Hydrogen has energy content higher than all fuels, gasoline included. Its low density indicates, its heating or caloric value would be low on a volumetric basis[10]. Properties such as its viscosity, and thermal conductivity indicate good heat-transfer attributes. There are indications of good combustion characteristics from the utilisation of hydrogen in spark ignition engines [11].

The prospects of the utilisation of hydrogen in fuel-cell applications and as an energy carrier or alternative fuel in transportation, has prompted various governments and private industrial bodies to invest in research and policies with the view to creating, building and maintaining a hydrogen economy.

It is important to reiterate, the potential utilisation of hydrogen in fuel-cells and other new pilot advancements and technologies would compete with present processes that

require hydrogen; hence, the resources utilised in the production of hydrogen might not be able to sustain the growing hydrogen requirements in the long run. It is important to also note, a few concerns have been raised against the utilisation of hydrogen as a fuel substitute, particularly when it is produced from fossil-fuels in terms of sustainability[12]. It is imperative and prudent to ascertain, for a sustainable and efficient hydrogen economy, more sources of hydrogen (notably from renewable options) must be employed.

Many renewable options have been identified for the sustainable production of hydrogen, ranging from wind-power, marine energy, solar radiation and biomass resources[13]. The basic downside of renewable hydrogen is the cost of production and commercialisation of the processes involved, when compared to conventional processes from fossil-fuels. This un-competiveness has raised questions of the overall efficiency of producing renewable hydrogen in place of optimising present processes.

Another challenge, hindering the mass commercialisation and acceptance of renewable hydrogen, is the fact that most of the processes involved produce greenhouse-gases, prominently, carbon-dioxide. This begs the question of the overall advantages of using renewable sources when carbon capture is not applied downstream of the production. Furthermore, many challenges have been raised and encountered on a pilot-scale when studying the efficiency of using renewable resources. Nevertheless, it is important to note, most of these challenges, such as carbon deposition and mechanical problems, are encountered in conventional production of hydrogen from fossil-fuels.

The utilisation of renewable sources for the production of hydrogen is thus essential, particularly on a large-scale basis as it would generally contribute to a greater energy security and would be essential for meeting the growing demand for hydrogen on mid-term and long-term considerations.

1.2 Production of hydrogen

Hydrogen gas can be produced from different sources, using different methods or a series of processes, this is due to its abundance as a chemically bound element in

different renewable and non-renewable sources. Irrespective of its source, its extraction must involve chemical processing and a thermal or energy input[9]; using the nature of the inputs and processes, hydrogen production methods can be classified into three distinct categories (the thermochemical process, biological processes and the electrolytic process) briefly described:

1.2.1 Water splitting/electrolysis

The electrolysis of water for the production of hydrogen is the oldest process for hydrogen production[14]; it has been promoted and researched, due to the ease of operation, maturity and simplicity of the process. It involves passing an electric current or electricity through water with the view to splitting water molecules into hydrogen and oxygen.

This is the cleanest technology for the production of hydrogen. In most cases, it has less efficiency in terms of costs and poor performance, when compared to other means of hydrogen production. It could be very expensive for large-scale production. Nevertheless, there are different technologies applied and developed for this process for small scale production or large-scale production.

An example of technologies developed is advanced alkaline electrolysis (this is shown to have efficiency of up to 90%), the solid polymer electrolysis process and the high temperature steam electrolysis process. Non-renewable sources, such as coal and natural gas, are utilised naturally for this process. The efficiency and environmental performance of the electrolysis of water for hydrogen production could be improved by the use of renewable resources, especially with photovoltaic in the process. These have been researched in many studies [15-18].

Renewable resources such as wind, geothermal and solar hydroelectric power can be used in the hydrogen production process, by utilising them for the generation of electricity or electric current used for the water split. Another means that has been investigated is the use of nuclear energy, or a nuclear reactor, to drive the electrolysis

of water, this certainly improves the efficiency of the general process. It reduces the electric current or electricity utilised.

1.2.2 Biological processes

The production of hydrogen through this route is less energy-intensive, especially when compared to thermochemical processes. The process occurs at ambient temperature and pressure. It entails the utilisation of a microorganism. This is done potentially, using biomass resources, although solar energy is required for some of the processes. In the presence of light, bio-photolysis could occur, leading to the production of hydrogen directly or indirectly.

In direct photolysis, solar energy is used to cleave water into hydrogen and oxygen molecules directly by a green algae or cyano-bacteria. This is a simple process, but said to be inefficient and non-sustainable for continuous hydrogen production, due to the nature of the micro-organism involved [19-21]. Indirect photolysis starts with photosynthesis to form simple sugars; these simple sugars then react with water in a light-induced process to form hydrogen. This is not efficient for continuous hydrogen production. The utilisation of non-waste feedstocks is also a downside for this process.

Another, similar, light-dependent process is photo-fermentation; this occurs in an oxygen and ammonia deficient environment. Like the indirect bio-photolysis process, it involves the formation of hydrogen from simple sugars, in this case, using photosynthetic bacteria. It is said to be more efficient than bio-photolysis, but requires a nitrogenase enzyme to operate. It requires photo bioreactors, but in general, is not a very efficient process[22].

Dark fermentation by anaerobic bacteria, on a carbohydrate rich substrate, can be used to produce hydrogen. This doesn't require solar energy compared to other biological processes, it poses the highest potential in terms of commercialisation. It might lead to the formation of other reduced by-products such as methane, sulphides, butanol and ethanol. This could hinder or reduce hydrogen production; nevertheless, it is promoted to have a commercial value in the future.

Another novel practice is to combine dark fermentation and photo fermentation in a hybrid system, with the view to increasing efficiency and yield.

A comparison of biological processes for the production of hydrogen is given in Table 1.1:

Table 1.1:Biological production of hydrogen [23]

Process	Microorganism used	Advantages
Direct bio-photolysis	Microalgae	▪ Solar conversion energy increased 10-fold as compared to trees, crops
Indirect photolysis	Microalgae, Cyanobacteria	▪ It has the ability to fix N_2 from the atmosphere
Photo-fermentation	Microalgae, Purple bacteria	▪ Uses different waste materials such as distillery effluents, wastes etc.
Dark-Fermentation	Fermentative bacteria	▪ Uses a variety of carbon sources as substrate ▪ Can produce hydrogen without light ▪ Produces valuable metabolites as by-products, e.g. butyric acids, lactic and acetic acids ▪ There is no oxygen-limitation problem
Hybrid system	Fermentative bacteria + anoxygenic phototropic bacteria	▪ Can improve the overall yield of hydrogen

1.2.3 The thermochemical process

This is the most utilised and researched method for hydrogen production. It is generally more energy intensive when compared to other methods of hydrogen production. But it is still the most efficient of all methods. It could be oxidative or non-oxidative, with the non-oxidative process involving splitting of the carbon – hydrogen bond in the feedstocks, using plasma radiation or heat (Reaction 1.1).

Reaction 1.1 The non-oxidative thermochemical Process

$$C_nH_m \xrightarrow{A} qH_2 + pC + C_xH_y$$

'A' could be heat or plasma radiation. The produced hydrocarbon could be any stable hydrocarbon formed after cracking.

The oxidative processes are more common. They are matured industrial processes done at high temperatures, mostly in the presence of an oxidant or a combination of oxidants (in the case of autothermal steam reforming). There are different types of oxidative processes that, potentially could be used for the production of hydrogen. But the most essential industrial methods are: conventional steam reforming, autothermal reforming and partial oxidation.

1.2.3.1 Conventional steam reforming

This is the most efficient, and most developed process for hydrogen production. It has a thermal efficiency of 70-80% compared to other oxidative thermal processes, such as autothermal reforming and the partial oxidation process (thermal efficiency of 60-75%)[24]. The in-corporation and utilisation of steam reforming is beneficial because, with ease, it can be integrated into multi-stage single stream plants.

In petroleum refining, conventional steam reforming could be utilised to supplement the hydrogen required for hydro treating processes. Catalytic reforming of naphtha is regarded as a very important process in the refining industry and produces hydrogen as a by-product. It is required for the production of high- octane gasoline components. It leads to the production of valuable co-products such as BTX[2] (very important in the petrochemical industry). It is regarded as a very efficient process as the hydrogen produced can be reused in the refining process for hydro-treatment and hydro-cracking and other hydrogen required steps. Nevertheless, conventional steam reforming is still utilised as a source of hydrogen in the petroleum refining because of strict

[2] BTX-Benzene, Toluene and Xylenes

environmental legislations and extensive processing of residues which has prompted the increased demand of hydrogen (90% of the total crude run) in the refining process.

At present, the basic utilisation of conventional steam reforming is confined to the reforming of fossil-fuels particularly natural gas. Problems were encountered by the utilisation of natural gas in the steam reforming process particularly due to the formation of carbon deposits. The carbon deposits led to reduction of catalyst activity, restricted heat transfer then eventually led to tube failure.

This discovery led to a series of researches to optimise the steam-reforming process in a bid to promote reformer performance, increase catalytic activity and life, and increase versatility of feedstocks that could be utilised. Present research is centred on the potential reforming of renewable energy sources and optimisation of the present reforming technologies.

It is important to note, the product of the reforming reaction (Reaction 1.2A) is majorly syngas, and not only hydrogen. In most industrial processes, a water-gas shift reaction (Reaction 1.2B) is carried out for the further conversion of carbon monoxide, to produce more hydrogen:

Reaction 1.2 Steam reforming reaction (A) and water gas shift (B)

$$CH_4 + H_2O \rightarrow 3H_2 + CO \ldots\ldots\ldots\ldots\ldots\ldots\ldots\ldots\ldots\ldots A$$

$$CO + H_2O \rightarrow H_2 + CO_2 \ldots\ldots\ldots\ldots\ldots\ldots\ldots\ldots\ldots\ldots B$$

The syngas formed can be used for other industrial applications that requires the products asides its more prominent utilisation in ammonia production, fuel-cells applications or other applications for which hydrogen alone is utilised. For example, methanation of syngas is a precursor of many petrochemical and chemical applications; it could be used in the production of methanol. This is a precursor of many industrial processes. Furthermore, it could be used for electricity generation through combustion.

The major application of syngas is the Fischer-Tropsch process (FT), where syngas is converted to other hydrocarbons or fuels. Research into FT processes, particularly in

gas-to-liquid applications (using unutilised natural gas) is rapidly increasing, due to the diversified products and chemicals that could be produced, when compared to other routes of natural-gas processing, such as liquefaction and compression. Its application is thriving, due to the abundance of most feedstocks utilised and the potential to produce co-products.

Reforming might be carried out using carbon-dioxide instead of steam (Reaction 1.3). However, this leads to a reduction in the H_2/CO ratio in the product. This might be a favourable option if the product required is CO and if the cost of carbon-dioxide is relatively low.

Reaction 1.3: Dry reforming or reforming with carbon-dioxide

$$CH_4 + CO_2 \leftrightarrow 2CO + 2H_2$$

Stand-alone steam reforming is not the preferred nor optimal means of producing syn-gas for massive Gas to Liquid (GTL) applications. This is due to its required high heat duty and poor economy of scale, compared to other means of production [25]. Nevertheless, it is important that it is complemented with other means of production like partial oxidation to achieve optimal performance. Another school of thought is to utilise heat recovery and exchange mechanics in the steam reforming process, with the view to reducing costs, emissions and improving process efficiency[26].

1.2.3.2 Partial oxidation and autothermal reforming

Partial oxidation (Reaction 1.4) is a widely-used method of hydrogen production. It involves a series of flame-homogeneous reactions that occur from burning hydrocarbons in a limited supply of oxygen- to be exact about 40% of the required stoichiometric amount of air or oxygen.

It is an expensive means of hydrogen production that utilises pure oxygen to oxidise fuels partially with the view of producing hydrogen. It comes with a few advantages when compared to other means of hydrogen production such as a very good response time and less fuel sensitivity/diversity. It occurs at high temperatures between 1150°C

and 1315°C, using a wide range of feedstocks or fuels. It has been studied intensely and commercially utilised in the shell process and Texaco process[25]. The high temperature and heat duty utilised leads to the formation of soot in the overall process.

Reaction 1.4: Partial oxidation

$$CH_4 + \frac{1}{2}O_2 \leftrightarrow CO + 2H_2$$

Partial oxidation could be an adiabatic process. This entails the utilisation of internal combustion instead of an external source of heat, which in turn leads to higher conversion rates because they can operate at higher temperatures than the tubular reformer, leading to a better economy of scale. Partial oxidation can occur heterogeneously over catalysts in a process called, '*catalytic partial oxidation*' (CPO). This helps in the prevention of the production of soot and other unwanted oxidation products occurring during homogenous partial oxidation.

Another type commonly researched and utilised is the autothermal reforming (ATR). This starts homogeneously but is completed heterogeneously over catalysts. An autothermal reformer can combine both steam reforming and partial oxidation processes with the view of producing higher efficiency. It is called a *secondary reformer* if it is preceded by another tubular reformer.

The use of CPO and ATR is being researched in Qatar, Nigeria and other sites with large gas to liquid plants. The high flammability associated with premixing hydrocarbons and oxygen might hinder the overall commercialisation of the process, particularly methane[27].

It is imperative to note, both processes (ATR and CPO) have the capability to handle both heavy and light feedstocks. The preheat temperature is limited due to the risk of auto ignition. Both processes differ, in the sense that ATR requires a burner in its combustion zone. The CPO process does not require a burner.

ATR also has a higher thermal efficiency, when compared to CPO or conventional tubular steam reforming. An auto-thermal reformer might contain a pre-combustion chamber before the catalytic bed; this helps in increasing catalytic life as there is less thermal or mechanical stress on the reforming catalyst. This comes with the trade-off of the need of more oxygen to be utilised in the combustion chamber.

The utilisation of a secondary reformer, in the reforming process, brings about flexibility of the operating conditions of the primary reformer; for example, the primary reformer could be set with reduced heat duty or increased pressure. A comparison of the main oxidative thermochemical process is given in Table 1.2;

Table 1.2: Main oxidative thermochemical processes for the production of hydrogen [26, 28]

	Advantages	**Disadvantages**
Conventional steam reforming	Matured and requires a lower heat duty when compared to autothermal reforming and partial oxidation, best H_2/CO ratio for hydrogen production applications.	Highest air emissions particularly carbon-dioxide, complex system.
Autothermal Reforming	Low methane slip, syngas methane content can be tailored by adjusting reformer outlet temperature. No catalyst is required and less pre-treatment is needed when compared to steam reforming.	Limited experience and commercialisation, requires oxygen.
Partial Oxidation	Feedstock pre-treatment in terms of desulphurisation is not required. It is also a very simple process with less cost when compared to steam methane reforming.	Very high temperature is utilised, soot formation, and requires pure oxygen.

As discussed, the oxidative processes for the production of hydrogen are carried out conventionally using natural gas, coal or naphtha; these fossil-fuels, particularly

naphtha, are mostly mixtures. They majorly contain higher hydrocarbons that are first oxidised, reformed or converted in an autothermal reformer. Due to the low operating temperatures utilised, methanation is first carried out to convert higher hydrocarbons to methane, which can then be steam reformed.

This process of converting higher hydrocarbons to methane is generally called pre-reforming (Reaction 1.5) and is essential in the pre-treatment of conventional feedstocks of steam reforming with the view to preventing coking and carbon deposition at reforming temperatures. Pre -reforming is carried out to aid fuel flexibility whilst helping to prevent catalyst deactivation in the primary reformer.

Reaction 1.5: Pre-Reforming

$$C_xH_y + xH_2O \overset{\Delta H \gg 0}{\longleftrightarrow} xCO + (x + \frac{y}{2})H_2$$

$$CO + 3H_2 \leftrightarrow CH_4 + H_2O$$

1.3 Hydrogen production and carbon-dioxide emissions

One of the main drives for hydrogen, particularly in fuel-cells, power and energy applications, is the fact that its combustion releases no greenhouse gas. Most of the production methods, as discussed, still produce a considerable amount of carbon-dioxide and carbon monoxide, deterring the overall benefits of the utilisation of hydrogen.

Carbon-dioxide emission is a major concern globally, as countries try to comply with dictates and agreements by the Kyoto protocol. CO_2 emissions trends, particularly from the combustion of petroleum fuels and fossil-fuels, have been on the rise since 1970. They lead to research on novel ways to improve the environmental impacts of processes, by designing and integrating environmental-friendly and efficient power generation systems[29].

These modifications, while reducing the environmental impacts of applied processes, come with an increased capital and operational cost. This is not ideal for smaller to medium scale plants.

Another school of thought is carbon capture, transportation and sequestration. In the last decade, carbon capture has been the focus of many studies. It can be done through the post-combustion system, where the carbonaceous products released are trapped, then separated from the exhaust streams or flue gases, after combustion as established in many coal-fired gas plants [30-32].

This could be done using a chemical scrub or membrane and sorbent separation technique. An example of these is the use of alkanolamines to absorb CO_2 chemically, or the use of sulfolane and methanol through physical absorption. The drawback of these processes is the corrosion of equipment that might occur, and the dilution of CO_2 with nitrogen, before separation.

Another process utilises pure oxygen in place of air, to burn or combust the fuel, with the view to have products containing CO_2 and water only. They can be separated easily. The oxygen utilised is gotten from air through an energy-intensive cryogenic nitrogen separation. This indicates increased costs.

Another method for carbon capture is the pre-combustion capture system. The carbon is captured mostly through decarbonation before combustion in air. This has been used particularly in processes where oxygen or air naturally are not required, such as in the production of hydrogen from the reforming of natural gas[33]. A main disadvantage of this process is, it cannot be applied in many already established plants, with its application majorly for newer plants.

The carbon-dioxide captured, using any of the carbon-capture systems, can be compressed at 100 bars then easily transported, using pipelines and stored underground, (as practised in many countries) or used in carbonation reactions in industries. Large-scale storage in natural-gas fields or specified reservoirs around the

globe (especially oil and gas reservoirs) have been identified as an appropriate means of storing the captured carbonaceous products.

This is because research indicates, pumping CO_2 into natural-gas fields or oil fields, particularly depleted ones, might enhance the natural-gas extraction and oil production respectively [14]. Mineral carbonation, industrial processes re-use and many other sites, such as saline aquifers and coal-beds for methane recovery have been investigated, due to the surplus CO_2 that could be captured from different processes.

Several questions have been asked concerning the long-time safety, environmental sustainability and reliability of carbon sequestration and storage. Another downside of the mentioned methods of carbon capture is, it involves an external modification to process plants. This would lead to increase costs and economics thereby reducing the general efficiency and profitability of industrial processes [34]. Combustion efficiency of these processes has been debated, as they are essentially very energy extensive.

Another school of thought is the need and support for renewable technologies and processes, with the view to reduce GHG emissions and reduce dependencies on fossil-fuels. Biomass in particular has been promoted as a suitable fuel source to replace fossil-fuels in different processes, particularly thermo-chemical processes, including the production of hydrogen and the reforming process [35]. It is considered to be carbon-neutral according to well to wheels analysis because the amount of carbon released during its utilisation is equivalent to the amount it absorbs. A comparison of the global warming impact of hydrogen produced from different sources is given in Figure 1.3;

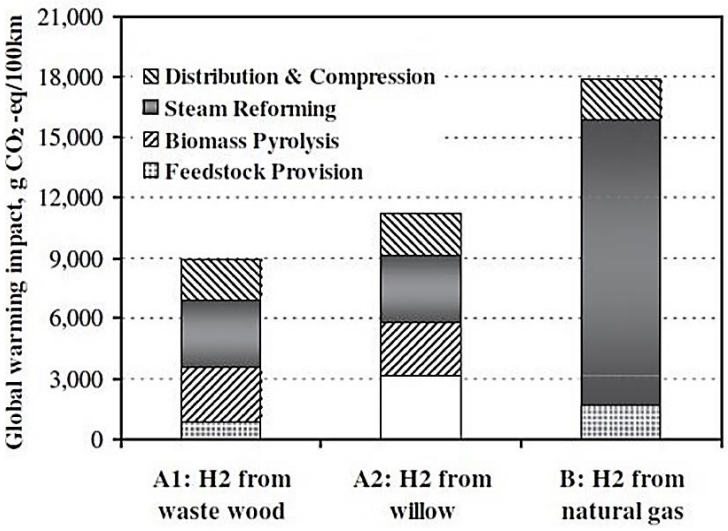

Figure 1.3:Global warming impact of hydrogen production [36]

1.4 Hydrogen production and economics

Most of the hydrogen production methods can utilise renewable sources as feedstocks. Large-scale and industrial production of hydrogen is widely done using fossil-fuels. On the long run, this is unsustainable. One of the main inhibitors for the utilisation of renewable sources and the mass commercialisation of renewable hydrogen is the economics of the process.

Many doubters have claimed, the production of hydrogen from renewable sources cannot be sustainable. It cannot compete economically with the costs incurred from the production of hydrogen from conventional fossil-fuels.

It is important to reiterate, the margin between the production costs of hydrogen from fossil-fuels and that from its subsequent production from renewable sources is reducing, due to the increasing variable cost incurred from fossil-fuel utilisation and the advent of process-intensification measures being studied for the production of hydrogen from renewable sources.

The retail selling price (RSP) [3] for hydrogen, produced from different feedstocks (renewable and non-renewable sources), was compared in a study on the economic prospects of the utilisation of renewable sources, when compared to conventional sources as illustrated in Table 1.3;

Table 1.3:Comparison of the Retail Selling Price (RSP) of hydrogen from different sources [37]

	Energy source	Process	H_2 RSP (S/Kg)
Non-renewable sources	Natural gas	Conventional steam reforming	2.33-3.17
		Conventional steam reforming with carbon sequestration	2.55
	Coal	Gasification without sequestration	1.05 – 1.50
		Gasification with sequestration	0.36 – 1.83
Renewable sources	Nuclear/ Nuclear MHR	Electrolysis	4.36 – 7.36
		Sulphur- iodine thermochemical	1.84 -2.63
	Solar	Photovoltaic, stirling-dish and power tower electrolysis	5.78 – 23.27
		Sulphuric acid /hybrid thermochemical	2.80
		Solar and natural gas (Sulphur-iodine thermochemical)	7.53
	Wind	Electrolysis	3.5 -6.77
	Biomass	Gasification	1.44 – 2.83
		Pyrolysis + SMR	1.47 -2.57

As indicated in Table 1.3, the economics of the processes are dependent on the production method utilised. It is obvious that biomass resources, particularly through the utilisation of pyrolysis oil for the production of hydrogen can compete with fossil-fuels in terms of economics, for the production of hydrogen. It is important to note, the cost mentioned does not take into account recent developing process-intensification measures that could further reduce the cost of production from biomass.

[3] Retail selling price is the price at which hydrogen can be sold at a profit 37. Bartels, J.R., M.B. Pate, and N.K. Olson, *An economic survey of hydrogen production from conventional and alternative energy sources.* International journal of hydrogen energy, 2010. **35**(16): p. 8371-8384.

Nuclear energy could compete with fossil-fuel in terms of cost, depending on the method of production. Full commercialisation of this process might not materialise soon, due to complexities in the intensely researched process. Solar-energy and wind-energy are expensive sources for hydrogen production. Further optimisation of the process could further increase the economies of scale and ensure sustainability in the future.

1.5 Biomass prospects, conversion and utilisation

Biomass resources [4] have been promoted as the most sustainable, efficient and renewable source of hydrogen, because of its abundance globally: also, because it can be harnessed easily and more cost effectively, when compared to other renewable sources being investigated, particularly on a small-scale production process and on a short term or mid-term basis[38-41].

Biomass[5] utilisation and conversion is receiving great interest and research globally, because it could contribute immensely to energy demand. At present, biomass contributes to about 10% of the global energy demand. Estimations indicate, biomass potentially could supply 6 billion tons of oil. This is equivalent to 26% of global energy consumption[23].

Biomass conversion and utilisation, particularly for the production of hydrogen and other energy carriers, could be a cheaper and a more sustainable means for better energy security, particularly in developing countries, with the view that they could be readily harnessed, due to their abundant availability. Using Nigeria as a case study,

[4] Biomass resources in this context refer to biomass residues which entail all *"biomass by-products, residues and waste streams from agriculture, forestry and related industries as well as the non-fossilized and biodegradable organic fractions of industrial and municipal wastes". 24. UNFCCC, Clarifications of definition of biomass and consideration of changes in carbon pools due to a CDM project activity. 2005. p. Appendix 8..*

[5] Biomass as defined by the United Nations Framework Convention on Climate Change is said to be "*a non-fossilized and biodegradable organic material originating from plants, animals and micro-organisms. This shall also include products, by-products, residues and waste from agriculture, forestry and related industries as well as the non-fossilized and biodegradable organic fractions of industrial and municipal wastes*" 24. Ibid.

biomass utilisation could help solve some of the stringent energy challenges encountered.

Biomass utilisation, particularly for the production of hydrogen could proffer cheaper and affordable industrial and social benefits. This would lead to an improved energy security.

1.5.1 Nigerian biomass as a case study

The utilisation and energy potential of biomass resource for bio-energy production in Nigeria has been widely researched; this is due to the general belief, the country has a vast un-utilised biomass resource. If harnessed, it could help solve some of its economic problems particularly electricity generation. Biomass produced and available in Nigeria generally can be categorised into three as illustrated in Table 1.4:

Table 1.4: Biomass resource types in Nigeria [42]

Biomass Type	Typical example
Agricultural sources	Agricultural residues e.g. Maize straw, rice straw, energy crops Jatropha for biodiesel, perennial grasses Food processing residues
Forest residues	Forest residues Loggings, slash, trimmings etc.) Mill residues (saw dust, woodchips, shavings etc.)
Municipal wastes	Organic fractions of municipal solid wastes, urban wood wastes, waste oils, greases

All three types of biomass-resource are abundant in Nigeria, but the quantity available varies across the six geo-political regions of the country. Iye, E.L. and P.E. Bilsborrow [43], in an article, discussed the potential and availability of biomass energy-resources in all six geo-political zones in Nigeria. They concluded, the potential for biomass conversion is greatest in the northern region of Nigeria. This comprises of the north-central, north-east and north-west geographical zones.

Iye, E.L. and P.E. Bilsborrow identified and concluded- of the types of biomass in Nigeria, biomass from agricultural sources is the easiest and most sustainable for use for bio-energy production (medium and large-scale). They arrived at this conclusion due to

serious challenges to be considered in conversion of forest residues and municipal waste to energy, particularly re-afforestation and waste collection respectively. In Nigeria, it is estimated that 21,000 Giga grams and 17000 Giga grams of biomass resources are available, on average, from feed residues and process residues respectively[43].

The exact amount of biomass is uncertain with varying reported estimates. It is believed, potentially Nigeria has an excess of 1.2 mega tonnes/day of biomass in reserve from fuel wood, animal waste, energy crops and agricultural residues, as depicted in Table 1.5.

Table 1.5:Biomass reserve and production in Nigeria [44, 45]

Biomass class	Reserves	Production
Fuel wood	11 -13 million hectares of forest and woodlands	0.10million tonnes/day
Animal waste	211 assorted animals (other estimates indicate that 61 million tonnes/yr. of animal waste is reserved)	0.781 million tonnes of waste per day
Energy crops and Agricultural residues	72 -83 million hectares of agric. land (30% of these represent arable land)	0.256 million tonnes of assorted crops per day

The master-plan on renewable energy in Nigeria estimates, Nigeria produced averagely 144 million tonnes of biomass resource in 2004; More recent studies on biomass conversion for energy and power generation in Nigeria indicate, biomass production is increasing in Nigeria, with an estimated available biomass resource materials of about 157-159 million tons per year in 2011[42].

The conventional utilisation of biomass for energy conversion has not received much attention. More interest and research were centred on solar and hydropower. Basically, this is due to the general belief, they are believed to primitive and unsustainable.

It is imperative to note, major research on biomass cultivation, and its utilisation for energy use in Nigeria, is centred on the production of biogas and recycling of waste or

waste management, with potential production of 6.8 million m^3 of biogas daily, estimated from animal waste alone [46].

1.5.1.1 Agricultural sources

These basically refer to crop residues and animal wastes; Cooper, C. and C. Laing investigated and analysed the energy-generation potential of crop residues and animal waste in Africa. They iterated, Nigeria has abundant biomass resources that could be utilised, using the four crops evaluated as having the greatest residue potential in Africa (coconut, rice, maize and sugarcane) as a base-case. They evaluated, and gave a summary of the residue to production ratio (RDR) of the selected crops. They calculated their energy potential. They reiterated the difficulty in utilising animal wastes for bio-energy conversion, due to the free-range farming system popularly practiced in Nigeria[47].

In terms of agricultural crops, it is essential to note, 80% of the land area in Nigeria supports the growth of cereal crops; the production of cereal crops is necessitated due to their high utilisation and dependability as staple feedstocks. In a bid to re-cultivate, residues from cereal crop are generally burnt or destroyed. Some are used as domestic fuels in stoves.

Unconventional biomass feedstocks and crop residues, such as Jatropha curcas, castor oil and sunflower, are produced in Nigeria. They could potentially be used for biofuel and bio-energy production. These residues are classified as process residues or field residues (Table 1.6); Process residues are those gotten from the processing of the crops. They offer great promise for use as energy sources, compared to field residues- those remaining on the field after crop harvest. Field residues are used as fertiliser or fodder for livestock[6] .It is estimated that only 35% of available field residue can be used sustainably for bio-energy conversion. It is imperative to note, due to the vast resource available, these could amount to a lot in terms of bio-energy generation.

[6] Most field residues are utilised as feed for livestock with the exception of Rice straw whose utilisation as a feedstock for livestock is limited due to its high silica content.

Other agricultural crop residues that could be utilised, due to their high availability, include rice-chaff and bran**.** These are process residues with a huge potential for bio-energy conversion. The potential of rice-chaff as a feedstock for biogas production has been investigated with 161.5 ml and 140.5 ml of biogas produced for a retention time of 60 days and 70 days respectively. Rice bran is also being researched for use in biodiesel production.

Table 1.6: Energy potential of the major crop residues in Nigeria [48]

Crop	**Residues**	**Residue type**	**Tonnage potential (metric tons)**	**Energy potential (TJ)**
Coconut	Crop		158000	
	Husk	Process residue	63200	2844
	Shells		18960	1138
Maize	Crop		5476000	
	Cobs	Process residue	2059759	28837
	Stalks	Field residue	11451685	160324
Rice	Crop		3277000	
	Husks	Process Residue	896260	12548
	Straw	Field residue	6808623	95321
Sugarcane	Crop		682000	
	Bagasse	Process Residue	179025	1253

N.B caloric value of coconut is 18MJ/Kg, maize and rice is 14 MJ/Kg, and sugarcane Bagasse is 7MJ/Kg

Residues from oil palm are of utmost importance, due to the high availability of palm globally. Oil-palm is the highest source of vegetable oil of all the oil-bearing plants in the world. It is found particularly in tropical regions or nations. Globally, Nigeria is the 5th

largest supplier and producer of palm-oil and has vast resources of oil palm in 27 of the 36 states in Nigeria, with annual production estimated at about 855000 tonnes. Palm-oil processing produces waste, including empty fruit bunches (EFBs), palm-oil mill effluent (POME) and mesocarp fibre (MF). They could be channelled for bio energy conversion.

The major challenge with the utilisation of oil palm waste in Nigeria for bio-energy conversion is the fact that it is used for various purposes; the EFB, kernel shell and fibre are used as fuel and manure. The palm leaves and bark are used to make thatch-roofs, beach or village houses, baskets, mats and brooms. Palm sap is used to produce palm wine and sometimes gin.

The wastes from oil palm cultivation and processing have high caloric values. This has led to continuous research on their collection and utilisation in bio-energy generation particularly bio-ethanol production and, in this case, bio-hydrogen;

Using Nigeria as a case study, it is evident, agricultural residues have a huge energy potential. Hence, they could be utilised in bio-energy conversion and for the production of hydrogen. It is important to state, other major crop residues like sorghum, wheat and millet can also be produced in Nigeria and could also help in bio-energy production in countries where they are readily available.

In terms of animal residues[7], the prospect for bio energy conversion is being investigated. Using Nigeria as a case study, they can be found particularly in the northern part of Nigeria, where major livestock rearing occurs. Animal manure is another residue. This is touted and promoted for potential biogas production. The free roaming system, practised in Nigeria and other counties, might make it difficult for waste collection. All the animals are moved to one area at night where waste can be collected easily.

[7] Animal residues in this case refers to animal dung and other livestock residue

1.5.1.2 Forest biomass

Forest residues have been considered for use in bio-energy conversion. Using Nigeria as a case study, the major challenge on the utilisation of forest biomass is its present fragility in the country; forest residues are majorly used as fuel wood, charcoal, ply wood and timber production with little re-afforestation done.

Nigeria still has abundant resources with 12 % of its total land-mass covered with forest and wood that varying depending on region. The north of Nigeria has an open forest structure consisting of shrubs and wood. The southern part of Nigeria encompasses the thick rain-forest. The continuous urbanisation in Nigeria, coupled with the increasing usage of forest materials for fuel wood and charcoal production would compete with the potential utilisation of forest resources [45].

1.5.1.3 Municipal Solid Waste (MSW)

These are materials realised from human activities including open dump and sanitary landfills. Waste management is generally restricted to the urban parts of Nigeria. It varies depending on economic development, and activities in the region. Major research on the utilisation of MSW is on the production of biogas from the anaerobic digestion of the biodegradable portion of MSW and electricity generation from gasification or thermo-conversion.

As detailed in this chapter, the abundant biomass resource in Nigeria is a true representation of many countries globally, where the surplus renewable resources are utilised, for local consumption. Taking into consideration the increasing need for renewable energy and the overall economic and environmental benefits that might be generated from bio-energy conversion. It is important to review biomass conversion technologies with the view to understanding the process of converting the readily available residues, particularly for the production of hydrogen.

1.5.2 Biomass conversion technologies and utilisation

Biomass conversion technologies, for the production of hydrogen and other energy carriers, is either biochemical or thermochemical (Figure 1.4); the biochemical process

is basically the same as the biological process of producing hydrogen, as discussed in earlier parts of these chapter. They include fermentation, anaerobic digestion and bio photolysis.

As discussed earlier in this chapter, the biochemical or biological process is not as efficient, cheap nor sustainable as the thermochemical process, especially for the production of hydrogen. They are used for the production of first generation biofuels that could in turn be used as an energy provider or for the production of hydrogen.

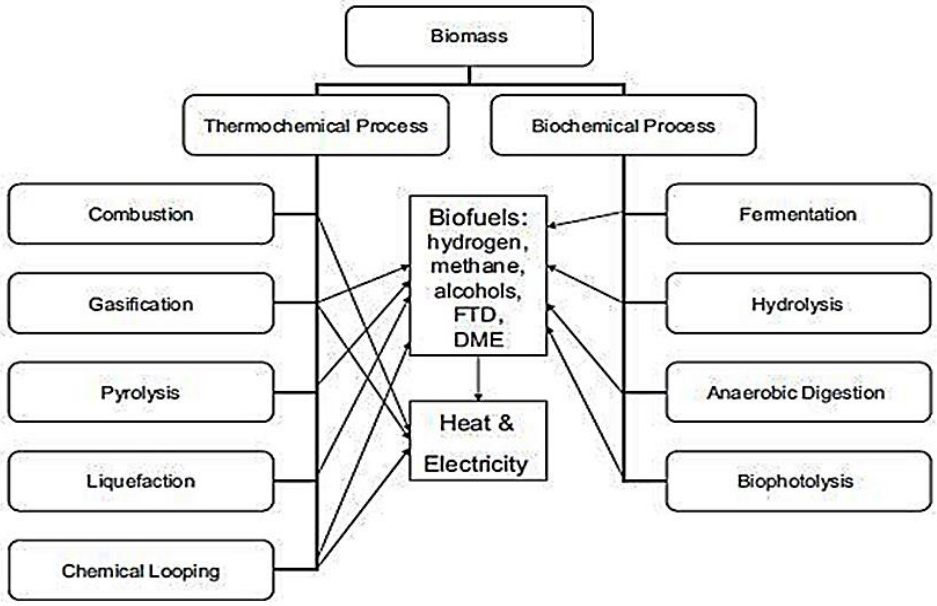

Figure 1.4:Biomass conversion processes [34]

The production of hydrogen, from several liquids of biomass origin, is being investigated immensely. First generation biofuels, prominently ethanol, produced from fermentation have been researched as a potential fuel substitute and hydrogen-source due to the maturity of the process and ease of production in most cases[49].

There are drawbacks in their utilisation. Their continuous production could lead to deforestation. They are majorly produced from energy crops, which inherently means they compete directly or indirectly with food production. The production of first generation biofuels requires a huge consumption of water which, in general sense, is not sustainable.

Nevertheless, the utilisation of first generation biofuels particularly butanol for bio energy and hydrogen production is still being investigated in terms of its overall viability; The catalytic reforming of several organic compounds particularly alcohols has been widely studied on a pilot scale with a theoretical maximum yield of 6, 7 and 12 moles of hydrogen that could be potentially produced from one mole of the widely available ethanol, glycerol and butanol respectively. Research also indicates that at optimal steam to fuel ratio, the reforming of all three alcohols mentioned results in the production of high purity hydrogen of about 70 – 75 % volume [50].

The reforming of butanol has been promoted in literature as a potential process of converting biomass to hydrogen; the general process is the biological conversion of biomass to n-butanol, 2- butanol or the preferred iso-butanol which could be reformed to hydrogen. Each molecule of butanol has the potential to produce as much as 12 molecules of hydrogen and the process using suitable catalysts could be very efficient with little problems or issues associated with conventional reforming [51]. The basic drawback however lies in the conversion of biomass to butanol, as the production process even though severely researched is still complicated in terms of yield and efficiency. Another undesirable issue could be raised with the part of the biomass used in producing butanol as most butanol plants still utilise first generation biomass which invariably means less environmental sustainability. These might change nevertheless with companies and organisations like GEVO, Butamax, and BP and DuPont researching the process of producing butanol from biomass wastes and second generation sources.

Biomass derived vegetable oils, waste cooking oil, sunflower oil, and Jatropha have also shown to be a potential fuel for hydrogen production due to their ease of transportation, and low oxygen content, however this oils are mostly expensive and in the case of some of them not readily available or also utilised as food. Biodiesel which is produced from different bio-oils and vegetable oils has also been widely studied for bio energy production and conversion due to the high efficiency that can be potentially derived from its favourable chemical properties (low sulphur content, and low viscosity). Research on the reforming and ATR of biodiesel show that less or no coking is formed

during the process when compared to other fuel feedstocks however sintering occurred leading to catalyst deactivation[52, 53].

The conversion of the sustainable second generation biomass residues to liquids of biomass origin through biological processes is however still in the pilot scale in most cases with full commercialisation projected just for futuristic long-term goals. Hence the thermal conversion of biomass takes precedent and more priority basically due to its higher efficiency.

The thermal conversion of biomass is however dependent on the chemical structure of the biomass resource to be resourced; the chemical structure of biomass residues varies depending on the type of biomass but can be generally classified into four main organic components. Cellulose and hemicellulose are the most essential components in biomass residues; both components are found more in hardwoods with approximate composition as high 79% when compared to soft wood which has lesser. Another relevant chemical component in biomass are extractives, they exist in little quantities in most cases and generally do not contribute much to the mass of the biomass residues, nevertheless, they play an important role in its utilisation. Lignin is the last organic components that are found in biomass; they range from 10% to 40% by weight in different dry biomass residues. In Hardwood for example lignin composition tend to range from about 10% to 21.7% while in softwood it is not strange to have a lignin content closer to 30% [41].

The chemical structure has a very important part to play in thermochemical processes particularly the pyrolysis of biomass residues; highly cellulosic biomass residues for example would produce pyrolysis oils containing complex compounds particularly organic acids, phenols, esters, aldehydes, and other carbonyl compounds or heterocyclic compounds [54]. The presence of lignin after pyrolysis is also essential as it deters the complete characterisation of pyrolysis oils using high performance liquid chromatography and gas chromatography.

Irrespective of the chemical content or composition of biomass, hydrogen is basically produced thermally through gasification or reforming of biomass derived products. It could also be produced through flash pyrolysis in a direct process (Reaction 1.6);

Reaction 1.6: Flash pyrolysis of Biomass

$$Biomass \xrightarrow{Heat} H_2 + CH_4 + CO$$

The production of hydrogen through this process and from the combustion, and liquefaction of biomass is believed to be unsustainable; this is due to the low efficiency and productivity from the processes and the difficulty of achieving suitable operating conditions in the case of liquefaction of biomass.

Biomass gasification (Figure 1.5) was promoted over combustion due to the lower temperature and better efficiency of the process, it also has an advantage over combustion because several industrially useful products can be formed directly hence increasing flexibility of the process [55-57].

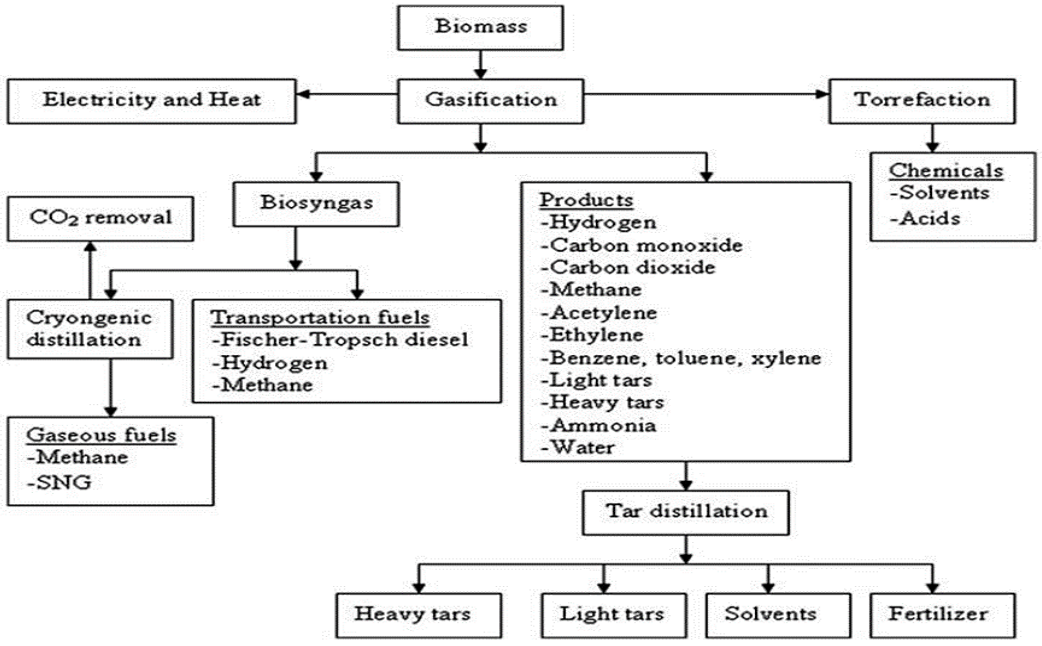

Figure 1.5: Various products from biomass gasification [58]

The presence of air in the gasification process results in increased production of gasses and hence the yield of potential hydrogen also increases, however the efficiency of the process is thwarted due to various challenges that could be encountered like the production of tar, and ash which might reduce the hydrogen production efficiency due to agglomeration, sintering. Another challenge is the increased steam to fuel ratio required and the high heat of duty utilised. Proper process and equipment design of gasifier, and the use of additives, has been promoted to minimise the formation of tar in the gasification process.

Another important initiative is to operate at optimal operating conditions and control in terms of temperature, pressure and residence time. Fractionation or leaching of biomass might also help in reducing the amount of ash however, this might lead to reduced quality [59, 60]. The utilisation of catalyst in the gasification process might also lead to an increased efficiency of the gasification process by the reduced production of CO and increased production of hydrogen; it however does not affect the production of charcoal in the process.

These challenges have also prompted the research on the use of a supercritical water process in gasification; the main difference is the change of the gasifying agent from air or steam to water over its critical point[8]. Supercritical water when compared to subcritical water allows reactions or processes to occur in a single phase with ease. It is also promoted due to higher potential efficiencies, easy carbon separation, low charcoal production, little need for pre-treatment or the removal of sulphur, Nitrogen and halogens, and the production of very rich hydrogen without the need for water gas shift reactions [23].

Another advantage of critical water gasification is the fact that wet biomass can be utilised with high efficiency. This process is however still being studied in the laboratory on a pilot scale due to a few challenges that could be encountered from its utilisation particularly corrosion due to hydrogen peroxide and its cost implications. Another

[8] Water is supercritical above its critical temperature at 274.29°C and critical pressure at 22.089Mpa

modification to the gasification process is the integration of a water hydrocarbon reaction and carbon capture. This process is done under sub-critical and supercritical water conditions (particularly for feedstock with high water or moisture content) the major benefits of this process are that Tar is not formed and the fact that it proves to be economically competitive with other production methods [61].

A better process is to reform the products of fast pyrolysis notably pyrolysis oils (Table 1.7), this has been promoted due to the higher yield of hydrogen that could be produced in this method;

Table 1.7: Hydrogen yield of thermal biomass conversion processes [62]

Process Routes	Yield of Hydrogen (% wt biomass)	Energy Content (HHV) of H_2 / Energy Content of Biomass
Pyrolysis + Catalytic Reforming	12.6	91%
Gasification + Shift Conversion	11.5	83%
Biomass + Steam + External Heat (Theoretical Maximum)	17.1	124%

Bio-oil or pyrolysis oils is produced from the fast pyrolysis of biomass residues; it is produced in high quantities and a high yield of about 80% in optimal conditions with the other products formed majorly charcoal and bio-gasses utilised to supplement the energy need and heat profile of the process.

Fast Pyrolysis of biomass (Figure 1.6) takes place through the following steps;

- *Pre-treatment*- This includes the drying of the biomass with the view to reduce the water content of the pyrolysis oils to be produced and the grinding of the biomass residue. This stage is essential in maximising the quality and yield of pyrolysis oils to be produced.
- *Reaction step:* The grinded residue is heated at 450 -550°C in an oxygen deficient environment over an inert gas for the endothermic pyrolysis reactions to take place.
- *Product Recovery:* The solid products are separated first from the gasses by passing the product stream through cyclones; the gasses are then condensed by cooling to form bio-oil. Other gasses formed can be recycled back into the

process as inert gasses; this integration makes the entire process a self-sustaining model when compared to other biomass conversion processes.

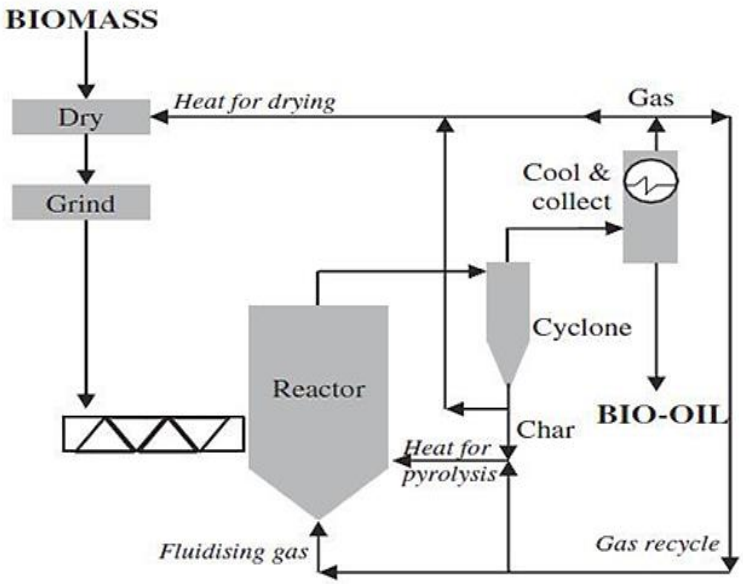

Figure 1.6: Biomass pyrolysis[36, 63]

The utilisation of pyrolysis oils has been promoted to be more sustainable in terms of economics and proficiency due to the ease of transportation and storage of bio-liquids when compared to other biological sources or feedstock of hydrogen production[64]. Pyrolysis oils also have a higher energy density when compared to fuels from gasification of biomass and can be used for small scale or large-scale operations[65].

Another school of thought is that the utilisation of bio-liquids in place of the bulky biomass residue gives more freedom and economies of scales as both processes involved in the conversion from biomass to hydrogen could be done centrally in the same plant or diversified and distributed between different plants or firms with the view of an optimal supply chain. Pyrolysis oils can also be utilised on their own as valuable fuel additives, used to upgrade in the refining process or converted to other high value chemicals increasing the flexibility, and economic potential of this method of production. It is therefore essential to study pyrolysis oils in terms of properties and chemical composition with the view to understand how they could be utilised in bio-energy conversion particularly the production of Hydrogen.

1.6 Properties and utilisation of pyrolysis oil

Pyrolysis oils are smelly, versatile and very complex mixtures which are difficult to elucidate as they could comprise of various compounds. This varying composition is dependent on the biomass from which the oils are produced and, the process and conditions of production or pyrolysis. Storage conditions and ageing also affects the general stability and composition of pyrolysis oils but in general, all pyrolysis oils consist and can be represented by their carbon, hydrogen and oxygen content, with minor elements like Nitrogen and sulphur also taken into account. Pyrolysis oils are also known to have a low energy value and volatility, and are known to be acidic and viscous. It is however important to reiterate that the properties of pyrolysis oils vary with different pyrolysis oils; hence it is essential to review these characteristics with the view to understand how they affect the utilisation of pyrolysis oils.

1.6.1 Characteristics of pyrolysis oils

1.6.1.1 Heating value and viscosity

The heating value of bio-oils is generally dependent on the type of biomass that was pyrolysed; it has been observed from different studies that oil plants like oil palm, sunflower and rape seed tend to produce bio-oils with high heating value when compared to bio-oils produced from wood waste or agricultural residues [66, 67]. Other factors like the production process and the operating conditions for pyrolysis might also have an effect on the eventual heating value of bio-oils[68].

The viscosity of bio-oils is a great test of its fluidisation and eventual application; it varies significantly amongst different bio-oils as some are very viscous and others with low viscosity especially after storage. The problems that arise from the viscosity of bio-oils has prompted the addition of alcohols in different studies on a pilot scale, these not only reduce the viscosity but also increase the overall stability of the bio-oil [69]. Pyrolysis oils could be highly viscous with a low energy value making them not the most suitable candidate for direct use as fuels or energy carriers. However, their utilisation in the

production of other fuels particularly hydrogen has been promoted due to their basic characteristics particularly after upgrading and post-treatment [68, 70].

1.6.1.2 Water and oxygen content

The high water content of bio-oils when compared to heavy oils enhances its fluidisation; it invariable means that bio-oils would have a low viscosity which is one of the important reasons for research into its utilisation as fuels as its high water content means it would be good for internal combustion and atomisation in engines when compared to petroleum fuels, research also indicates that these properties would be enhanced by additional thermal cracking[71]. The high water content however also means that it would have a low flame temperature, ignition properties and caloric value, which deters its eventual application directly.

Bio-oils also have high oxygen content due to the presence of oxygen containing compounds in their complex molecules; the oxygen content like its water content invariably means better combustion as complete combustion can take place however, it also means a lower energy density, immiscibility of the oils, thermal instability, storage instability and consequently a lower efficiency. The high oxygen content of bio-oils also means an increased polarity and immiscibility with non-polar fuels which may be detrimental in its direct utilisation.

1.6.1.3 Acidity and ash content

Bio-oils comprises of different organic acids which invariably reduces its PH, the strong acidity reduces the stability of bio-oils and increases the corrosivity of the oils. The strong acidity of bio-oils means that extra upgrade might be essential before they are utilised in processes or as fuels. The ash content of bio-oils also affects its utilisation particularly as potential fuels, as it could lead to corrosion and other problems; the ash content varies with different biomass residues and could be as high as 15% in agricultural residues compared to very little amount in softwoods [72].

A summary of the main characteristics of pyrolysis oils is given in Table 1.8;

Table 1.8: Characteristics of pyrolysis oils[73]

Properties	Oil Characteristics	Reasons
Appearance	Dark red-brown to dark green	Micro-carbon and chemical composition in oil
Odor	Distinctive odor—an acrid smoky smell	Lower molecular weight aldehydes and acids
Density	Very high compared to fossil fuel Pyrolysis bio-oil: 1.2 kg/liter Fossil oil: 0.85 kg/liter	High moisture and heavy molecule contamination
Viscosity	Can vary from as low as 25 centistokes (cSt) to as high as 1000 cSt	Wide range of feedstock, water content and the amount of light ends collected
Heating value	Significantly lower than fossil oil	High oxygen content
Aging	Viscosity increase, volatility decrease, phase separation and deposition of gum occur with time	Complex structure and high pH value
Miscibility	Miscible with polar solvent but totally immiscible with petroleum fuel	Polar in nature

1.6.1.4 Other properties

The homogeneity of bio-oils has been a debated as most bio-oils appear to be homogeneous while others argue that the presence of extractives inherently shows heterogeneity. The extractives in most bio-oils lead to phase separation in the bio-oil structure particularly after storage; these extractives however vary with different biomass residues. The rheological properties of bio-oils have also been studied extensively; it has been observed that bio-oils that contain a lot of extractives do not behave like non-Newtonian fluids however most bio-oils do exhibit this behaviour.

The flash point, and pour point have also been studied for bio-oils to ascertain its stability and fluidity in low temperatures; the flash point depends on the volatile constituent and could be as high as 100°C in some oils [74] while the pour points which is dependent on how viscous the oils are could be as low as -36°C [74]Though most bio-oils exhibit a pour point between -12°C and -33°C.

1.6.2 Bio-oil upgrading

The properties of bio-oils as detailed indicate that an upgrade might be essential for its eventual utilisation for different applications; this is because they do not possess the

required properties to be utilised as transportation fuels directly in place of petroleum derived fuels, its composition also shows that they are very diverse and can be used in different applications. Bio-oils could be upgraded through different means and processes depending on its eventual application; a review of the methods by which bio-oil could be upgraded highlighted nine ways by which they could be improved for better quality in terms of application [75].

They could be hydro treated in the presence of suitable catalysts under high pressure with the view to deoxygenise the bio-oil mixture; the reduction of oxygen leads to an increased energy density hence increasing the potential of the utilisation of bio-oils. They could also be hydrogenated with the view to decrease unstable acids and aldehydes in the bio-oil mixture; this however leads to more corrosion and complications with application. Organic acids in bio-oil can also be esterified to stable esters through catalytic esterification which boosts the eventual qualities of the bio-oil[76]. These processes however come with a high cost particularly material costs as complex machinery or equipment's might be required. Problems due to clogging and carbon deposition and catalyst life/deactivation have also been experienced. A new and novel process hydrogenates and esterifies the bio-oil to convert unstable compounds to stable components with the use of bi functional catalysts to obtain better efficiency[77].

Catalytic cracking or combined catalytic pyrolysis with catalytic cracking to form lighter compounds has also been identified as a means to upgrade bio-oils; as bio-oils are composed of different compounds, there are a lot of compounds that could be formed from catalytic decomposition. Poor quality of produced compounds and coking issues has been noticed in this process and deterred its application. Nevertheless, substrates like phenols, organic acids which are useful in the resin industry and in the production of valuable products have been extracted from bio-oils. Other additives and flavouring agents particularly in the fertilizer industries, pharmaceutical industries and food industries can also be derived from bio-oils [68].

Another school of thought is the utilisation of a super critical medium or fluids; this could be used to produce bio-oils and also upgrade them; these is slated as not being economically sustainable on a large-scale due to the high costs of the fluids needed[78]. An easier approach to upgrade bio-oils includes purification and separation by molecular distillation; this process nevertheless competes with the other highly regarded molecular distillation applications and would also incur high energy consumption.

Another process for bio-oil conversion and upgrade is particularly important for its application in diesel engines; this is the direct mixing of bio-oils with diesel fuel through emulsification by the use of a surfactant. This process nevertheless comes with high energy consumption, and is not so economical. It also reduces the cetane number of the fuel and might lead to corrosion.

The final process of bio-oil conversion details the base-case for its conversion to hydrogen through steam reforming; these has been the basis of many research due to the importance of hydrogen not just as a potential energy resource but also as an important industrial chemical/precursor. The steam reforming of pyrolysis oils has been investigated by various researchers with a view to ascertain the challenges posed, feasibility, optimality and sustainability of the process [65, 79-81]. This studies indicate that the reforming of bio-oils can occur in different temperatures and wide operating conditions efficiently [82]; It is also evident that the reforming of bio-oil brings good promise for the production of hydrogen with a reported yield of 70 -80% of the theoretical stoichiometric potential produced.

The industrial application of bio-oils for hydrogen production particularly in large-scale centralised or distributed processes is still however in its development stage; this is because of the problems or issues associated with the steam reforming process in general in terms of catalyst life and efficiency, the complexity of bio-oils and the un-competiveness of the process in terms of economics when compared to other processes. It is hence important to review the conventional reforming process with the view to identify challenges and problems encountered and to make a case for

optimisation and process intensification. The complexity of pyrolysis oils has also promoted the study of the reforming of model compounds and oxygenates which are prominent in their composition with the view to easily elucidate and proffer process intensification techniques that would optimise the efficiency of the steam reforming process. The study of model compounds prominently acetic acid as utilised in the study would give a footprint on the efficiency of process intensification measures utilised and how the conventional steam reforming process can be optimised.

Chapter 2 Literature review: Advances in steam reforming processes

2.1 General overview

Steam reforming came into prominence when standard oil from New Jersey applied it for the production of hydrogen from off gases at a refinery. The process was very basic and simple; it occurred in tubes erected vertically and supported in parallel rows in a furnace, heat was supplied by burning fuel in a furnace and the basic feedstock for steam reforming was natural gas and coal. The main drive for reforming was to produce syn-gas for Fischer-Tropsch processes for the eventual production of ammonia, industrial hydrogen and methanol. It is a matured and well developed process because of the variety of fuels or feedstocks that could be utilised; to be precise almost all hydrocarbons and fuels can be steam reformed to form syngas through Reaction 2.1;

Reaction 2.1: Conventional steam reforming

$$C_nH_mO_p + (n-p)H_2O \overset{\Delta H \gg 0}{\longleftrightarrow} nCO + (n-p+0.5m)H_2$$

$$C_xH_y + xH_2O \overset{\Delta H \gg 0}{\longleftrightarrow} xCO + (x+\frac{y}{2})H_2$$

This is an endothermic reaction that is irreversible in higher hydrocarbons and heavy fuel; according to le Chatelier's principle it is generally favoured by high temperature, low pressure and high catalytic activity; however, in large-scale operations, reformers are always operated at higher pressures[9] when compared to those utilised on a pilot scale, this leads to a reduction in cost due to better throughput but might also mean an increased heat duty required for the reaction. The high duty required also means that the process is susceptible to catalyst deactivation due to the formation of whisker carbon and coking on the active site of the catalyst. This has led to intense research on catalyst development and optimisation of the reforming process. Catalyst development is essential due to the operating conditions by which a reformer operates, for example

[9] Steam reformers are generally operated between 20 -26 bars particularly when hydrogen is the main product required.

the heat duty required; it is essential to utilise a catalyst that will not only accelerate the reforming reactions and performance but would be active over a long period of time particularly for large-scale operations.

The need to optimise the reforming process due to the problems experienced in its application has led to different approaches and types of reformers developed; the first major addition was the utilisation of a second reformer after the main or primary reforming process. The secondary reformer was designed and basically used in ammonia production. The reformate gas is partially oxidised and re-reformed in the adiabatic secondary reformer; it is an exothermic process that occurs at a very high temperature which drives the reforming process to completion with little methane formed.

The presence of fouling agents in some feedstocks has also led to the introduction of pre-treatment and pre-reforming; the pre-treatment process involves the removal of fouling agents and contaminants particularly Sulphur. The removal of sulphur is done by the hydrogenation and subsequent adsorption in a zinc oxide bed [83]. The pre-treatment process continues with an adiabatic pre-reforming which converts all higher hydrocarbons heavy hydrocarbons to methane. This leads to optimal performance and production due to fewer loads on the primary reformer especially if a heater is installed after the pre-reformer to preheat the product gas before reforming. It also helps in increasing the life span of the catalyst and reduces the formation of hot bands and hot spots; this is because there is no sulphur poisoning. Furthermore, it eliminates the sensitivity or effects of variant feedstock compositions and steam to carbon ratio to the steam reformer.

The water shift reaction (Reaction 2.2) occurs after secondary reforming in two stages differentiated by the temperature at which they occur; the first water shift occurs at a high temperature before another water shift at the thermodynamically favoured low temperature.

Reaction 2.2 Water gas shift reactions

$$n \times (CO + H_2O \overset{\Delta H<0}{\longleftrightarrow} CO_2 + H_2)$$

The basis for the water gas shift reaction is to remove CO and convert it to CO_2 hence preventing the unwanted utilisation of useful Hydrogen which could also react with CO.

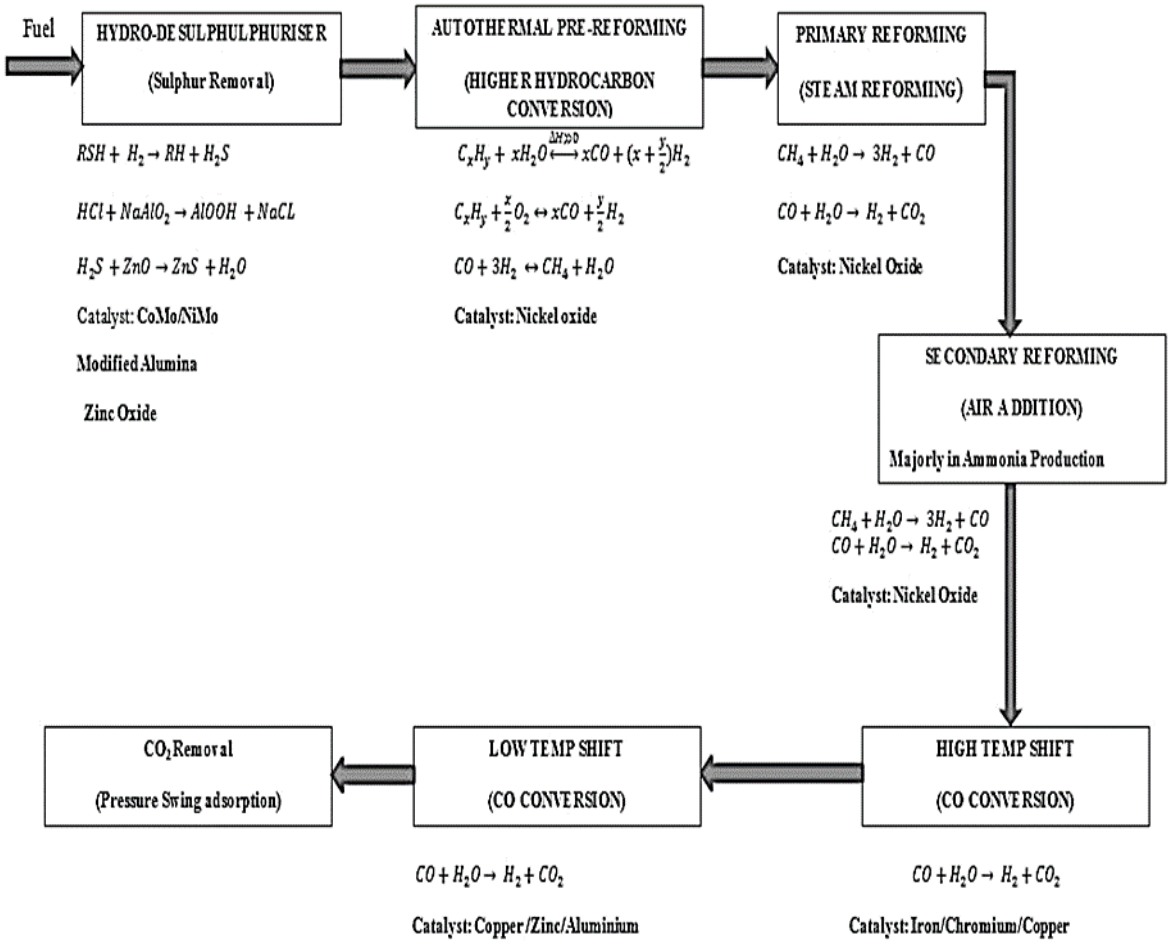

Figure 2.1:The reforming process[83]

The reforming process (Figure 2.1) could be regarded as an energy converter with the heat released from the primary reforming process utilised in the secondary reformer and the optimal performance of the reforming process is basically achieved by having a trade- off on the intensity of action of the different stage of the reforming process. The process could be processed as described previously, or could be processed with a reduction in the heat duty of the primary reformer accompanied with the addition of surplus air in the second reformer.

Another generally accepted process is heat exchange reforming where reuse of waste heat energy is done through process integration (Figure 2.2) [84].

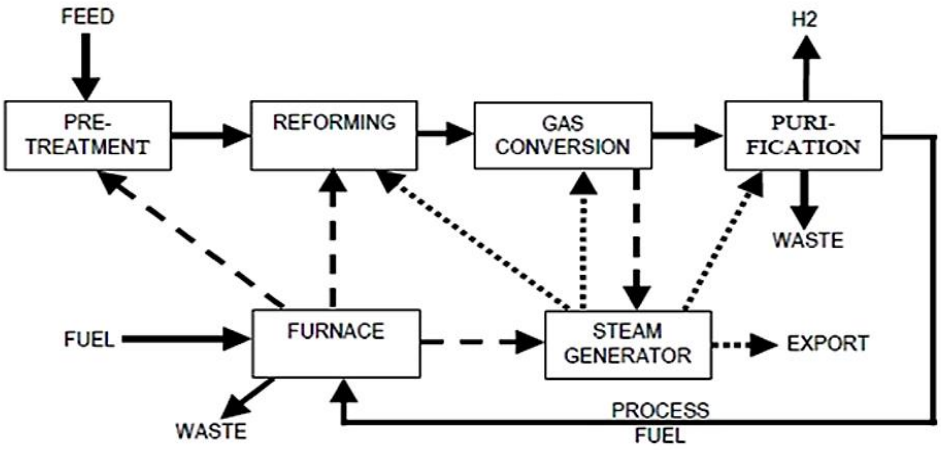

Figure 2.2: Schematic of the reforming process showing heat and materials integration [83]

2.2 Steam reformers

A basic steam reformer consists of several tubes called reformer tubes filled with catalysts; these tubes are held in a furnace box where they are heated and used for the thermo-chemical reforming process. The output generated from the operation of steam reformers are basically dependent and challenged by the mechanical design of the reformer, catalyst function/ activity, and the feedstock/ operating conditions by which it is operated.

2.2.1 Mechanical design of a reformer

The mechanical design describes the dynamics of the tubes used in the reformer, inlet and outlet systems, burner arrangement and the burner characteristics.

2.2.1.1 Reformer tubes

The efficiency of the reformer design is basically affected by the number of reformer tubes, tube design, and dimension; previous studies indicate that it is advisable to increase the dimension of a particular tube than increase the number of tubes in a reformer hence the basic designing mechanical parameters for designing a reforming tube are the tube diameter, length and pitch [85].

- *Tube length and diameter*: Increasing the length of the reforming tube increases the area of reaction and catalysis and generally should increase product formation. It is however limited by restrictions due to the associated pressure drop, design complexity (due to thermal expansion), and the compressive load of the tube at higher temperature. An increase in the diameters of reformer tubes also increases the area available for catalysis and the reforming process. Nevertheless, its effects on hoop stress in the tube, reduction of the heat transfer surface area and the gas side heat transfer coefficient must be considered.
- *Tube pitch:* The distance between the tubes in a reforming reactor is also essential in the reformer design. Generally, the closer the tubes are together, the hotter the tubes get for a particular operation, and this has an important role in the evaluation of the thickness of the tubes which is optimally dependent on the metal temperature of the tube.
- *Tube design*: The materials or metal used to make the reformer tubes are also important for the efficiency of the reformer, reformers are operated at high temperatures hence the tube must be made of alloys with better creep rupture properties. This could be a complex and difficult decision process as various factors like the maximum tube temperature, full understanding of the reaction kinetics must be considered [86]. There have been steady developments on the metallurgy of reformer tubes in a bid to optimise performance and reduce the stress to rupture value or potential of tube materials. Micro alloys containing 25% chromium, 35% nickel, niobium and other transition metals is being used at present because they offer benefits in relation to thermal strength and stability.

2.2.1.2 Reactor size and cost

The primary reformer is constrained by heat flux and its size is determined based on the surface area required for heat transfer. The secondary reformer is however not constrained and is selected based on industry input. This plays an importance in process economics as the primary reformer tends to be more expensive than the secondary

reformer. The increased cost of the primary reformers has led most process designers to optimise the process in a bid to minimise the size of the primary reformer with less detail given to the amount of catalyst in the reformers due to the little order cost incurred. The secondary reformer size should be that the combustion process does not take place close to the catalyst.

2.2.1.3 Burner arrangement

This is essential in the design of the primary/tubular reformer because of the highly endothermic process that occurs within; tubular reformers are generally classified into four distinct categories based on the burner and tube arrangement, also taking into consideration the flow of effluent gasses and means by which the tubes are heated as depicted in Figure 2.3;

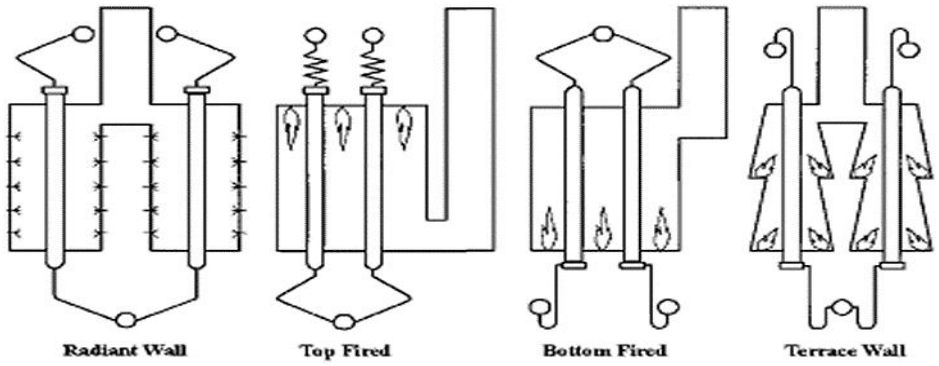

Figure 2.3: Types of burning arrangement in reformers[87]

- *Side fired/radiant wall reformers*: The side fired reformer is designed in a way that the tubes are only heated by radiating heat from the walls of the furnace and flue gas. The burners are arranged with the flames directed towards the wall with the tubes arranged in a single role along the centreline of the furnace. It could also be arranged with two furnaces side by side having or sharing the same inlet and outlet systems. In this type of reformer the flow of the process gas and the effluent flue gas are counter current.

- *Top fire*d: The burners are arranged in-between the tubes, tube rows and furnace wall. It is the commonly used and accepted design for reformers and with the flame directed downward from the ceilings of the furnace, the tubes are heated majorly through radiation of the flue gas to the catalyst tubes, with the reacting gas and the flue gas flowing co-currently.

- *Bottom fired*: This is an out-dated design for reformers and involves the heating of the tubes with the flame directed upward from the bottom of the furnace. It has an advantage of easy access to heat control and the burners however it is limited by the need to control the outlet temperature.

- *Terrace wall*: this is an upgrade of the bottom fired reformers having a slightly lower tube temperature. It involves having burners also at a different level of the furnace. Problem might however arise when the tubes are heated by radiation and flue gas convection at the same time.

2.2.1.4 Inlet and outlet system

The major parameters for the inlet and outlet design (Figure 2.4) are its flexibility to thermal expansion and its ability to withstand heat and stress during operation particularly start up and shutting down operations.

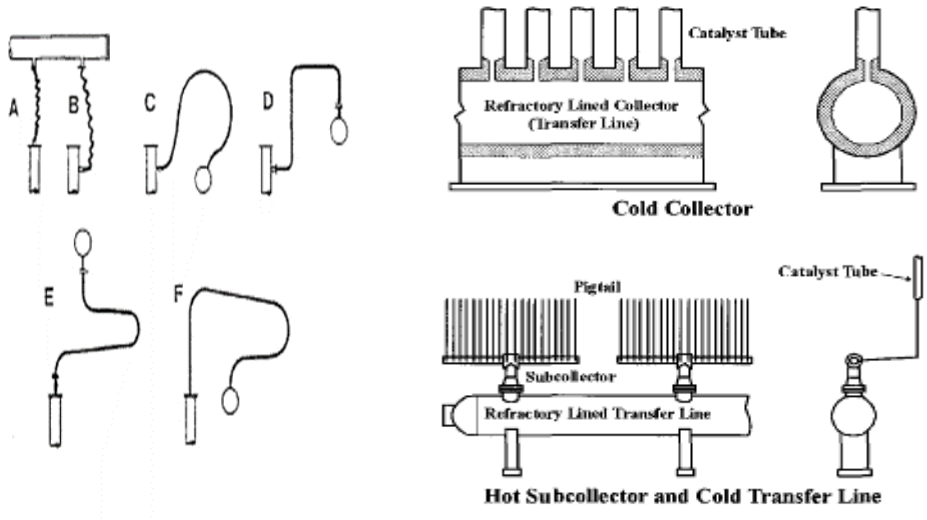

Figure 2.4: Common inlet (left) and outlet (right) designs [86, 87]

The feed stream is connected to the top of the inlet header though an inlet hairpin, the hair-pins might also be connected to the side of the reformer tube if pre-heat of the gas is necessary. The hairpin is flexible and can absorb thermal expansion of the tubes and must also be designed to give access to the tube in case of catalyst replacement. The major attribute required for the outlet system is its capability to handle the associated manifold stress linked to the bottom of the reformer. The method of collection is basically the difference in the different types of outlet systems, in the cold collector system; the reformed gas is transferred directly to the transfer line with the aid of special instruments which connect the hot and cold part of the collector. In the sub collector system; the reformed gas is collected by a sub-collector through pigtails which help to reduce thermal stress before passing them on to the main collector.

2.2.1.5 Burners

The burners used in the furnace are generally designed in a bid to control the combustion intensity, flame shape and heat transfer; more modelling must also be done to curtail environmental issues that might arise like the production of nitrates[86]. These environmental issues have led to the development of burners with air or fuel staging. This entails the control and maintenance of the air and fuel mixture with a view to reduce NOx formation [84].

2.2.2 Operating conditions

The optimal operation of a reformer using specified and controlled conditions is essential in the long-time efficiency of a reformer and helps in determining the effectiveness of the reforming process. The major attributes that needs to be considered are the relative sensitivities of the process in relation to its steam/carbon ratio, operating pressure, temperature, and addition of enriched [88].

2.2.2.1 Steam/Carbon ratio

Steam and Carbon sensitivity is an important factor to consider in tubular/ primary steam reforming; this is because the steam and carbon ratio could help in determining the efficiency and overall effectiveness of the primary reformer especially in preventing

economic and mechanical problems. Basically, it is expedient and more effective to have a higher steam/carbon ratio due to the following reasons;

- A high steam/carbon ratio inhibits carbon formation and deposition from the thermal cracking of the hydrocarbon feedstocks;
- A high steam/carbon ratio also favours product/ syngas formation and eventually hydrogen;
- A high steam/carbon ratio also reduces the amount of unreacted hydrocarbon feedstocks;
- A high steam/carbon ratio also provides steam for the water shift reaction and helps in the conversion and removal of carbon monoxide.

A high steam/carbon ratio however comes at a cost as the required heat duty and fuel consumption of the process increase (fuel for making steam and replacing waste fuel); hence more heat and increased cost would be required [83].

2.2.2.2 Combustion air/oxygen

The addition of oxygen to the reforming process is essentially needed for secondary reforming; oxygen can be added through the addition of excess oxygen purchased from a third party supplier or through the introduction of air, both means of supply however comes with an increased cost due to oxygen purchase or cost of nitrogen removal from air respectively, this extra cost of oxygen addition could be reduced by the use of pure air (21% oxygen, 78% nitrogen, 1% inerts). Oxygen addition however helps in energy saving as the heat realised from the exothermic reaction in the secondary reformer could be integrated and used to heat the primary reformer (heat exchange reforming). Its addition also helps in reducing methane slips. It is however important to note that an increase in oxygen concentration supplied generally leads to a reduction of hydrogen production [88]

2.2.2.3 Pressure

The operating pressure of the primary and secondary reformer is very important depending on the industrial application for which the reforming is performed. Basically a low pressure favours the reforming reaction according to le chatellier's principle; it however leads to increased compression costs incurred in the front end process of the industrial application of the reformed gas. A higher operation pressure is therefore utilised in industrial production of hydrogen which allows for a more compact reactor design, which hence leads to reduction of material cost and increases the throughput of the reactor. The trade-off from the operating pressure is however restricted by the maximum permissible pressure of 40 bar of the material used in the construction of the reforming tube.

2.2.2.4 Temperature

The operating temperature and the resulting heat duty of the reformer (particularly the primary reformer) determine the amount of product formed and then plays an important role in cost and efficiency of the overall process. It is generally accepted that a primary reformer should not run above 800°C because the catalyst melts at 1100°C and the catalyst tubes creep close to 850°C. Nevertheless, it is better to operate the primary reformer at temperatures close to the maximum set to maximise hydrogen production and reduce the amount of unreacted hydrocarbons. This comes with an increased energy cost due to increased heat duty. The secondary reformer is adiabatic and is not constrained by temperature and can be operated at higher temperatures closer to 1000°C, as discussed before the released heat from the secondary reformer could reduce the associated energy cost of primary reforming.

2.2.2.5 Catalysts

The behaviour and activity of reforming catalysts (Figure 2.5) is essential in ascertaining the reaction kinetics and efficiency of the reforming process. The type of catalyst employed is determined by the part of the reforming process where it is utilised and the type or class of feedstocks being reformed; in adiabatic pre-reforming for example, it is desirable to have high catalytic activity using a catalyst with a high surface area while in

tubular reforming and secondary reforming, the major need for the catalyst is to minimise pressure drop and maximise heat transfer as dictated by the mechanical design of the reactor.

Nevertheless, irrespective of the type of catalyst utilised, it is essential for all reforming catalyst to exhibit the following characteristics;

- *Reliability and catalyst activity*: All catalysts used in the reforming process must be reliable for the operation or step by step process for which it is assigned. Processes where catalysis is needed in the reforming operation include pre-reforming which may entail desulphurisation of feedstocks using zinc oxide, removal of produced carbon deposits to methane using an alkali-based metal or a metallic compound as catalyst, and the thermal or oxo-thermal conversion of hydrocarbons to syn-gas. Catalysts with high catalytic activity are also preferable as they could help in the reduction of the heat duty required for the reforming process.
- *Stability*: The catalyst utilised must be stable under all operating conditions particularly during start-up and shut down operations. The catalyst must also be able to withstand the high thermal activity and temperature in the refining process.
- *Versatility, ease/need for reduction and flexibility*: Natural gas and methane is currently the prominent feedstock for steam reforming however it is essential and advisable that catalysts used in the reforming process be flexible and applicable on a wide variety of other feedstocks. Some primary steam reforming catalyst utilised presently contain 10-20 % Ni in its oxidised form hence reduction of the nickel compound is essential before catalytic action can occur. The ease at which this reduction process takes place or the need for reduction is also important in the choice of reforming catalysts. The ease and need for catalyst reduction might affect its speed and activity particularly in start-up operations.
- *Catalyst life:* The catalyst life is also very important in the choice of a catalyst. Most designers prefer to use a catalyst with proven long life. Catalyst life could

also be reduced due to the formation of coke in the reforming process, or the presence of fouling agents. These lead to catalyst deactivation or failure and eventually lead to the formation of hot bands in the reforming tube [89].

- *Catalyst size and shape*: the catalytic reactions in the reforming process occur on the surface of the catalyst hence the geometric surface area of the catalyst is important in designing and achieving optimal catalyst activity. The shape and size of the catalyst also helps in decreasing pressure drop and increasing the heat transfer coefficient. The first common shape of reforming catalyst was the ring shaped reforming catalysts but these has been modified with more complex shapes with multiple holes or the use of flutes. The optimal catalyst choice is one with a high void fraction which helps in-terms of pressure drop, and a high geometric surface area [86].

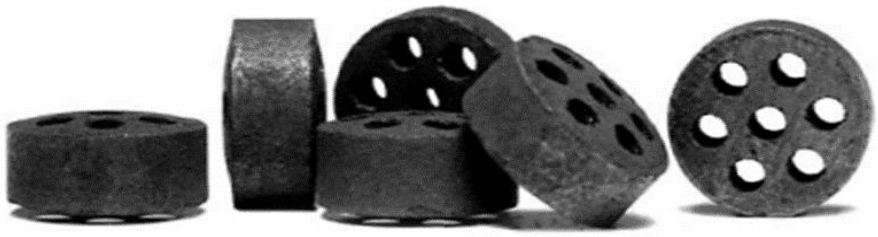

Steam reforming catalyst. Topsøe R-67 R-7H.

Figure 2.5: Steam Reforming catalyst[86]

- *Types of catalysts:* The type of catalyst utilised is basically dependent on the type of feedstock utilised; for light hydrocarbon feeds, it is economical to use non-alkalised catalysts while alkalised (low and high alkalised catalyst) catalyst are utilised for heavy hydrocarbons. Catalysts are basically alkalised by metal predominantly Potassium (due to its high mobility) for the removal and prevention of carbon deposits which might be formed from the thermal cracking of hydrocarbons. Potassium catalyses the hydrogenation or carbonation of the carbon deposition to the products of reforming (syn-gas, carbon mono oxide, or methane); it however inhibits the reforming reaction in the process. Nickel and

Nobel metals are slated to be the most suitable catalysts for steam reforming [90]. Nickel has been researched because it is better than other transition metals that are also researched in terms of conversion and availability, it is also more stable and can be kept or stored in its reduced form during large-scale or industrial use. Nickel catalysis is also essential because the primary feedstock for conventional reforming processes is very stable even at very high temperatures; hence the nickel catalyst is essential for reduction of the operating temperature which helps in reduction of hoop stress and stress to the tubes [91].

Catalytic action in the reforming process may however still be reduced even with the listed characteristic basically due to loss or reduced activity, sintering, poisoning and carbon formation or deposits [92].

2.3 Limitations of conventional steam reforming processes

The major challenge or limitation with the reforming process that reduces its overall efficiency and performance aside from the production of greenhouse gas emission and the high duty required is the life span of most catalyst; most catalysts are naturally designed to have a high life span however loss of activity and catalyst deactivation can easily occur either through poisoning by fouling agents or carbon deposition. This affects the process performance greatly as it leads to the reduction of the desired products in the product stream and could also lead to an increase in required heat duty.

Poisoning by fouling agents notably sulphur, alkali metals and silica occurs greatly in conventional processes due to the presence of this elements in the complex feedstocks utilised; however as discussed earlier the advent of pre-reforming and pre-treatment might reduce the effect of catalyst poisoning.

Catalyst deactivation is also caused by carbon formation; this could be caused basically by decomposition of the fuel or feedstocks by thermal cracking at elevated temperatures (Reaction 2.3);

Reaction 2.3 Thermal cracking of fuel feedstocks

$$CH_4 \leftrightarrows C + 2H_2$$

$$C_nH_m \rightarrow nC + 0.5mH_2$$

It could also be formed from Boudouard reaction (Reaction 2.4) from the dissociation of carbon monoxide; this attributes to a high proportion of carbon deposited in conventional processes and has been researched intensely;

Reaction 2.4 Boudouard reaction

$$2CO \rightleftharpoons C + CO_2$$

Carbon deposition could also occur by the reduction of CO by Hydrogen as slated in Reaction 2.5;

Reaction 2.5: Carbon monoxide reduction

$$CO + H_2 \leftrightarrows C + H_2O$$

This exemplifies the need for the water gas shift reaction with the view to remove CO and convert it to CO_2 hence preventing the unwanted utilisation of useful Hydrogen.

The carbon deposited through the reactions described above are all whisker or graphitic carbons and are majorly formed on the surface or active sites of the catalyst; the amount produced are dependent on the operating conditions particularly S/C ratio and temperature but are more affected by the type of catalyst utilised [93].

Whisker carbon deposition occurs at high temp and still allows catalysis to occur but reduces the stability of the catalyst through disintegration of the catalyst support material [94]. Its effect could be reduced by the addition of an alkali or alkali earth metal which can block the active sites of the catalyst and prevent carbon deposition. This however reduces the efficiency of the catalyst as there is reduced catalytic activity on the active sites of the catalyst. It could also lead to potential sintering[10] [93].

[10] Sintering is basically caused by the movement of the Nickel active surface of the catalyst; it is stimulated at high steam partial pressure and high operating temperatures.

Coke and Pyrolytic carbon also occurs at high temperatures and could be formed from olefins which could be formed from the fuel after thermal dissociation particularly from higher hydrocarbons (Reaction 2.6); this is highly dependent on the fuel feed and the reacting or operating temperature. Pyrolytic carbon is formed due to low catalyst activity in the reactor; these might be attributed to poisoning of the catalyst surface or sintering.

Reaction 2.6: Coke formation

Higher Carbon Fuel → Lower carbon fuel + Coke + gasses

$$C_nH_mO_k \rightarrow xC + kCO + C_{(n-k-x)}H_{(m-2x)} + xH_2$$

Gum and Encapsulating carbon which are formed at lower temperature are not really studied for the reforming reaction because the process conventionally operates at a high temperature; they however occur particularly from heavy feedstocks that might be pre-reformed at low operating temperatures. They can be formed from Reaction 2.7 and is also dependent on the catalyst used.

Reaction 2.7 Gum formation

$$C_nH_m \rightarrow (CH_2) \rightarrow gum$$

It is also important to reiterate that the feedstock utilised might also determine the type of carbon deposited; the type of carbon produced from the reforming of the model compounds of pyrolysis oils for example is majorly graphitic[95] while poly aromatically structured coke are majorly deposited from the reforming of pyrolysis oils after phase separation[96]. An overview of the routes to carbon formation in a steam reformer is given in Table 2.1;

Table 2.1 :Overview of the routes to carbon formation in a reformer[86]

	Critical Parameters	Characteristics	Effects
Whisker carbon	Low H_2O/C Low H_2O/C_nH_m High T	Dissociation of hydrocarbons at the nickel surface and formation of a carbon whisker at the backside of the nickel crystal.	No immediate deactivation but mechanical disintegration of the catalyst and increased ΔP
Pyrolytic carbon	High T Low activity (sulphur poisoning) High partial pressure of C_nH_m	Non-catalytic cracking of higher hydrocarbons to form carbon on catalyst and tube	Carbon formation in tube and on catalyst. Formation of "hot bands" and increased ΔP
Encapsulating carbon	Low T Heavy feed Low H_2O/C Low H_2O/C_nH_m	Encapsulating of the nickel particles by a CH_x film	Deactivation of the catalyst.

2.4 Process intensification measures for hydrogen production

Process intensification and integration measures for the optimisation of conventional reforming processes has been extensively researched[97]; this as discussed in earlier part of this thesis is basically to alleviate problems with conventional reformers, it is also a means to ensure that emerging technologies and processes are fully optimised to prevent present challenges and limitations of conventional processes.

In the base-case, for the production of hydrogen through the reforming of liquids of biomass origin; mechanical problems have been identified on a pilot scale majorly due to catalyst deactivation and carbon deposition. Another school of thought is that the process is still unsustainable due to economic and environmental concerns. However, it is important to reiterate that the basis of process intensification as those to be studied and researched in this study is to alleviate the problems associated with the reforming process particularly carbon deposition, and to establish an affordable model that could be utilised not only on the large-scale but also for small and medium plants.

Another school of thought from emerging studies indicates that carbon deposited particularly on the surface of the reforming catalyst could in the right operational conditions help in reduction of the reforming catalyst in the presence of an inert gas [98]. Hence, it might be beneficial to study the type of carbon deposited if any especially

after process intensification in a packed bed reactor as this might help to determine the efficiency of the process. On this basis, process intensification can be defined as a process of developing a more compact, cleaner, efficient and effective system with the view to obtain optimality in terms of operational stability and sustainability[99].

Process intensification can be done through the following ways; it could be done by utilising process intensifying equipment's like novel reactors and intensive mixing, or by utilising process intensifying methods like heat exchange, process integration and process control mechanics [97]. The process intensification measures that was reviewed and studied in this work are sorption enhanced reforming and cyclic or looping processes; these has been identified to be beneficial to the reforming of liquids of biomass origin particularly pyrolysis oils [100-103].

2.4.1 Chemical looping system and applications

A chemical looping system can be regarded or described as a chemical process normally carried out in two or more reactors in which a regenerating solid material or metal[11] drives the reaction in the reactors involved by circulating between them. It is being applied and investigated for different chemical applications with the basic idea of developing a self-sustaining medium intended to;

- Minimise exergy and energy loss from the reaction scheme;
- Obtain high process efficiency particularly in relation to energy loss and conversion;
- Reduce and maintain the environmental downsides of processes like emissions and pollution especially when integrated with a fossil-fuel conversion system;
- Achieve ease of reaction with economic benefits;
- Drive the equilibrium of reaction towards production of valuable products.

The general chemical lopping approach is similar with the utilisation of intermediates which are reacted and regenerated in the reaction scheme; it has been employed and

[11] Liquid and gaseous material could also be used in chemical looping systems however realistically their utilisation is challenging and commercially impractical.

applied in many chemical reactions (Reaction 2.8) involving carbonaceous and non-carbonaceous reactions like water splitting, fuel combustion, gasification and CO_2 separation. It is a basic Redox process but differs from other oxidation and reduction processes because it utilises a metallic oxide instead of the conventional air or pure oxygen;

Reaction 2.8 Examples of looping reactions and thermochemical cycles

- ***Water splitting Through the Bunsen reaction (*** $H_2O \rightarrow H_2 + 1/2O_2$***)***

$$\mathrm{SO_2} + I_2 + H_2O \rightarrow 2\mathrm{HI} + H_2SO_4$$

$$2HI \rightarrow H_2 + I_2$$

$$H_2SO_4 \rightarrow H_2O + \mathrm{SO_2} + 1/2O_2$$

- ***CO_2 separation and purification;***

$$CO_2\ (impure) \rightarrow \mathrm{CaCO_3} \rightarrow CO_2\ (pure)$$

- ***Carbon gasification (*** $C + 2H_2O \rightarrow CO_2 + H_2$ ***);***

$$2MO + C \rightarrow 2M + CO_2$$

$$2M + 2H_2O \rightarrow 2MO + H_2$$

- ***Water - gas shift reaction*** $(CO + H_2O \rightarrow H_2 + CO_2)$ ***;***

$$CO + H_2O + CAO \rightarrow H_2 + CACO_3$$

$$CaCO_3 \rightarrow CaO + CO_2$$

2.4.1.1 Types of chemical looping systems

Looping reaction systems are categorised based on the type of looping particles or solids used and the type of reactions carried out in the process;

2.4.1.1.1 Type I looping systems (metal-metal oxide)

The basic reactions in the type 1 looping systems are multiple cyclic redox reactions where the solid particles notable metallic oxides are reduced in a reducing reactor and oxidised using air, H_2O or CO_2 in an oxidising reactor or combustor. The metallic particle utilised is expected to be capable of reacting with various carbonaceous fuels and hydrocarbons and must have a high oxygen carrying capacity [104]. The metallic carrier must also have high resistance to attrition, and agglomeration. It is also desirable that

the material utilised must be one that could be produced easily and cost effectively. Here are some of the common metals used as oxygen carriers;

- **Nickel:** It is probably the most utilised and studied catalyst and oxygen carrier [105]. This might be due to high conversion rates and reactivity, good performance even at higher temperatures, low attrition rates and no agglomeration behaviour at operating temperatures. It however is a toxic metal and could be very expensive when compared to other oxygen carriers. It may also react with its supporting material particularly aluminate to form nickel aluminate. It also has the tendency to react with sulphur which leads to catalyst deactivation.
- **Copper:** The utilisation of copper as an oxygen carrier is a cheaper alternative which also exhibit very high reactivity and low sulphur poisoning at typical temperatures [104]; however, it has a low melting point and hence would lead to problems relating to agglomeration.
- **Iron**: Iron has an advantage of being environmental friendly and cheap, it however comes at a cost of low reactivity and poor conversion rates; it however has the advantage of preventing carbon formation and preventing sulphide poisoning. Another researched option is to add nickel particles to increase the conversion rate however this might have a detrimental effect on the mechanical strength of the oxygen carrier.
- **Manganese:** Manganese is another cheap option with an added advantage of it being non-toxic; it has a higher oxygen capacity when compared to iron but also results in low reactivity depending on the supporting material utilised. It is however noted for its resistance to sulphur poisoning. Poor mechanical stability and fluidization properties have also been identified for the utilisation of natural manganese ores as an OC [106]
- **Cobalt:** Cobalt just like nickel materials are also expensive and toxic; it might also not be thermodynamically stable and favourable at higher temperature depending on the oxidation state of the cobalt oxide

2.4.1.1.2 Type II looping system (metal oxide – metal carbonate)

The basic reactions in the type II looping reactions are carbonation and calcinations; the particle utilised is used notable for CO_2 capture but could also be utilised for the removal of other impurities like halides, sulphides. This can be used for the capture of CO_2 and impurities from flue gas and fuel gas when integrated with combustion and gasification of biomass, coal and other feedstocks.

2.4.1.2 Chemical looping applications and hydrogen production

The earlier application of chemical looping in processes was prompted by the need to develop separating and conversion methods and techniques for product generation. Example of earlier processes that utilises looping processes include the Lewis and Gilliland process for CO_2 generation in the beverage industry [107, 108] and, hydrogen production in the steam-iron process [109, 110]. However, with the development of various separation methods, its present utilisation is designed to develop an optimised reaction scheme in terms of efficiency and the effectiveness of chemical processes particularly CO_2 emissions control. Examples of Present chemical looping applications and research are given in Figure 2.6;

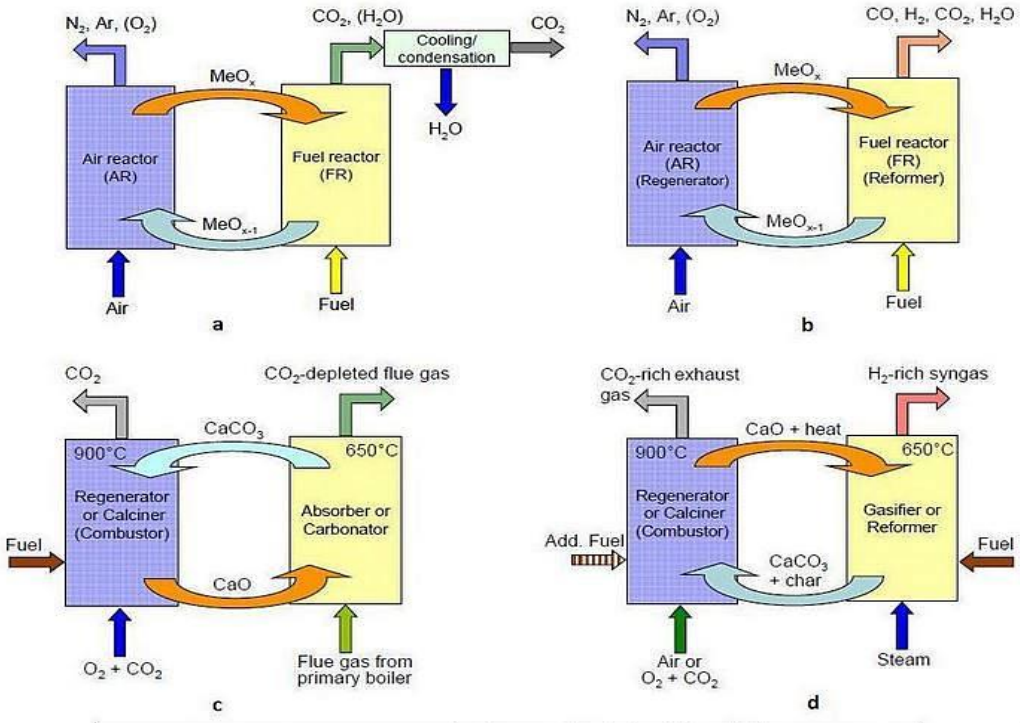

	Technology	Transported reactive species	Circulating solid material	Obtained product
a	Chemical looping combustion (CLC)	O_2	metal oxides	heat, power, CO_2
b	Chemical looping reforming (CLR)	O_2	metal oxides	H_2, CO
c	Carbonate Looping	CO_2	CaO/ $CaCO_3$	clean flue gas, CO_2
d	Sorption enhanced reforming (SER)	CO_2	CaO/ $CaCO_3$	hydrogen rich syngas

Figure 2.6: Chemical looping applications [111]

Chemical looping combustion (a) and carbonate looping (c) are the most important of all the looping applications described in Figure 2.6, this is because they are the basis by which chemical looping steam reforming and sorption enhanced reforming are based; sorption enhanced reforming for example is utilising and integrating a carbonate looping process into steam reforming processes while chemical looping steam reforming or enhanced steam reforming is integrating chemical looping combustion into the reforming process.

Hydrogen production from steam reforming is proving to be the better production mechanism when hydrogen is produced from renewable sources because it is a matured process and it incurs lower costs when compared to gasification and other production methods. Looping processes helps in saving more cost from the reforming process as

cost of extra CO_2 capture is avoided when steam reforming is integrated with chemical looping combustion and more cost relating to an extra air separation unit is avoided in the autothermal chemical looping steam reforming process. Looping process can be incorporated through sorption enhanced reforming or chemical looping steam reforming.

2.4.2 Sorption enhanced reforming

Sorption enhanced reforming has been investigated with the view to improve the efficiency of the conventional reforming process in an intensified single step as supposed to the conventional multi step process [112, 113]; it has been promoted to as a sustainable and economical process for the conversion of natural gas to high purity hydrogen production [114].

This is a single stage four step process that involves the simultaneous and selective removal of CO_2 during the reforming process; in this process, the reforming process, water gas shift reactions and CO_2 removal all happen simultaneously in the presence of a catalyst and an ideal adsorbent or chemisorbent.

The utilisation of Sorption enhanced reforming for the production of hydrogen has been investigated for a long time with the view of carbon sequestration and the first patent for its utilisation was granted in the 1930's [115]; the first experiments was also reported around 1984 on a pilot scale [116]. However, the process is still not mass commercialised as different studies are still being carried out on the various sorbent or minerals required for the process. The use of sorbent to capture CO_2 in-situ in industrial applications in terms of reducing greenhouse gasses and producing environmental friendly industrial final products has been widely and thoroughly researched as it opens an opportunity for more sustainable industrial production and cost saving as the extra cost for CO_2 sequestration is avoided[117-119].

The general basis for the selection of sorbent in sorption enhanced reforming is the stability, kinetics and the adsorption capacity of the material to be utilised [120](Table 2.2); Lithium or sodium based sorbents and hydrotalcites have been reported to be good

sorbents due to their sorption capacity and stability respectively[121]; however, Calcium based sorbents are the most researched and studied due to their good sorption kinetics and good adsorption capacity at operating conditions compatible with simultaneous steam reforming [122], reports nevertheless indicates loss of capacity and activity due to sintering of CaO sorbent after several sorption cycles when they are utilised [123, 124]. Using CaO as a sorbent, the exothermic carbonation reaction (Reaction 2.9) is also added to the reforming and water gas shift reaction.

Reaction 2.9 Carbonation reaction using CaO based sorbents

$$CaO + CO_2 \leftrightarrow CaCO_3$$

Different synthetic sorbents and reactivation techniques have also been suggested and other minerals like synthetic silicates, huntite and metallic zirconates are also a point of interest[125, 126].

Single materials with combined catalytic and sorption activity are being investigated and researched; this is with the view to help reduce the material or solid hold up in the reactor and in order to avoid intra and inter particle diffusion resistance [114, 127, 128]. However, high efficiency in regards to high sorption capabilities and efficient hydrogen production has been ascertained when solo-materials (sorbent and catalysts) are mixed as in the case of this study[129, 130].

Table 2.2:Properties of different sorbent materials [131, 132]

Group	Representative member	Adsorption capability	Stability	Kinetics
Metal oxides	CaO	Good	Poor	Good
Hydrotalcites	$Mg_6Al_2(OH)_{16}(CO_3)\,x4H_2O/K_2CO_3$	Poor	Good	Poor
Double Salts	$(K_2CO_3)(2KHCO_3)(MgCO_3)(MgO)\,xH_2O$	Fair	Unknown	Fair
Li Metal oxides	Li_4SiO_4	Fair	Fair	Good
Supported Sorbent	CaO on Cabot superior micropowder	Fair	Good	Good

The first step of the sorption enhanced reforming process as described by Rashmi Chaubey et al is a pre-saturation step where steam and H_2 are used to saturate the

reactor [9]; the reforming reaction, water gas shift and CO_2 absorption all takes place in the second step of the sequence producing pure H_2 gas. The third step proceeds when the H_2 purity reduces to signal the end of sorption enhancement due to the production of Carbon containing gasses; this involves desorption of absorbed CO_2 through heat and sometimes a mixture of hydrogen and steam, and the final step involves pressurisation of the reactor for preparation for a new cycle.

Exergy analysis for sorption enhancement in comparison to steam reforming analysis indicates that the process can compete and improve the conventional steam reforming process and relative downstream purification processes[133]. Sorption enhanced steam reforming also promotes feedstock conversion according to le Chatelier's principle, and helps in saving costs when compared to conventional processes as an extra separation and purification unit for CO_2 and H_2 is not required and a little extra heat is required. A quick comparison of the conventional steam reforming process and sorption enhanced reforming can be seen in Table 2.3;

Table 2.3: Comparison of conventional steam methane reforming and sorption enhanced reforming [134]

SI. No		Conventional SMR	SER goals
1	Operating Temperature	800 -1000° C	400-500°C
2	CH_4 to H_2 conversion	80-85%	90+ %
3	Reaction Product Composition (dry basis)	73.7%H_2 + 9.4% CO_2 + 12.0CO + 4.8 CH_4	98+ % H_2
4	Product Pressure	14-28 bar	14-28 bar

The basic advantages of using this process over conventional steam reforming is the lower operating temperature and low pressures required and the reduction of side and by-reactions [134]. It is also more efficient in the fact that the reforming reaction and water gas shift can occur simultaneously in one step hence reducing the process steps required as compared to conventional processes. This advantages generally imply that sorption enhanced reforming would reduce cost in terms of energy cost, capital cost and production costs when compared to conventional steam reforming processes. It also

entails that this process could be operated at a small or medium scale and could be adapted and appropriate to the varying distributed biomass sources.

2.4.3 Chemical looping steam reforming

Chemical looping steam reforming (CLSR) is the integration of a chemical looping system with the reforming process. It can be divided into two similar processes; chemical looping combustion integrated with steam reforming (CLC-SR) and autothermal chemical looping steam reforming (a-CLSR), this has been researched in many studies both done with the view to optimise the reforming process, save energy and provide a more viable approach in achieving more conversion of reactants [135-138].

The basic idea of CLC-SR is to supply the heat required for endothermic steam reforming reactions from unmixed combustion which was proposed by Lyon and Cole [139], [140]; it utilises two reactors normally where one acts as a combustor and the other acts as a reformer/ reducing reactor; the combustor is supplied with air which is used to oxidise the circulating metal oxides from its reduced state. This is a very exothermic reaction and the heat realised is used to provide heat for the very endothermic reforming and metal oxide reduction reactions. The utilisation of steam in the place of air in the oxidation stage of the chemical looping process for the production of hydrogen has also been investigated in the steam-iron process and cyclic water gas shift process [141, 142]. This has been promoted to lead to the efficient production of pure hydrogen without complex separation units [143]. The reforming process takes place in reforming catalytic tubes placed in the other reactor followed by water gas shift reactions and pressure swing adsorption to produce more hydrogen and capture carbon-dioxide. The off gasses of the pressure swing adsorption are then used to reduce the metal oxide which then returns to the combustors for another looping cycle. It is important to reiterate that the reduction of the metal oxides do not take place in the catalytic tubes which is utilised for the reforming process alone.

A-CLSR or unmixed steam reforming is promoted and has been identified as an exciting prospect and pathway for sustainable hydrogen production [144]; it could also be operated with a reduced cost in an autothermal process. There is also high potential for

power production when compared to other thermochemical process with an improved heat transfer. Another basic reason for the promotion of unmixed steam reforming is the prospect that issues relating to coking and sulphur poisoning could be avoided or minimised [139]. In this process, the metal oxide carrier is also utilised as the catalyst for the reforming process, hence the choice of the metal oxide for the looping process is vital; the basic properties that influence the choice of catalyst/oxygen carrier in this process are its resistance to attrition, agglomeration and, carbon formation, other factors include the conversion rate and reactivity, and cost of preparation[145]. Nickel is promoted as a very good oxygen carrier for this process because it has a higher conversion rate, lesser tendency to coke and in general shows better reforming characteristic. A study on the utilisation of nickel oxide as an oxygen carrier (OC) concluded that its efficiency and capacity can be maintained while alternating between reactors [146].

Like the CLC-SR process, the first stage or Air-flow stage is the oxidation of the oxygen carrier notably nickel in the combustor with the view that the heat released can be utilised in the endothermic reactions in the other stage. The second stage which is the fuel flow stage entails the endothermic reforming reaction, the process may be followed by water gas shift reaction and amine scrubbing or pressure swing adsorption to reduce the formation of carbon monoxide, increase hydrogen production and capture carbon-dioxide respectively.

It is important to study the heat and mass balance of this process because the heat generated in the combustor must be enough to drive the endothermic reactions in the fuel reactor to have an efficient system. Studies on the thermodynamics and heat balance of the a-CLSR process indicates, the fraction of oxygen supplied by steam ideal must not exceed 0.3 of the total oxygen added to the fuel reactor and the O_2/CH_4 should be higher than 1.25 to ensure autothermality and maximise hydrogen production[147, 148] .

Many studies have shown that chemical looping steam reforming is a major improvement to the conventional stream reforming process as the reaction can take

place at lower temperatures reducing the amount of external heat needed, and also because it could potentially lead to a reduction of carbon deposits and other problems associated with the conventional process. Furthermore, a high conversion rate has been identified in various studies on biomass and model compounds representing them

The basis of chemical looping steam reforming is to maintain autothermality; it is reported that to attain an efficient autothermal system, the oxygen to fuel molar ratio should be more than 1.25. The air to fuel ratio must however remain low to maximise production of hydrogen and prevent complete oxidation in the fuel reactor. The basic reactions in the fuel reactor are summarised in Reaction 2.10;

Reaction 2.10: Reactions in the air and fuel reactors in CLSR

- Air reactor: $Me_yO_{x-1} + \frac{1}{2}O_2 \rightarrow Me_yO_x$
- Fuel Reactor:

$$(2n + 0.5m - y)Me_zO_x + C_nH_mO_y \rightarrow (2n + 0.5m - y)Me_zO_{x-1} + 0.5mH_2O + nCO_2$$

$$CO + Me_yO_x \leftrightarrow Me_yO_{x-1} + CO_2$$

$$H_2 + Me_yO_x \leftrightarrow Me_yO_{x-1} + H_2O$$

Many studies on the CLSR process has been conducted in two or more reactors with the fuel-steam feed stage and oxidation stage occurring in a separate reactor; however, the use of a single reactor for both stages of the CLSR process while alternating the flows between oxidation and reducing set conditions has also been investigated in a packed bed with high efficiency observed [144]. A single packed bed reactor as described in 3.3 is also utilised in this study for the CLSR experimental runs.

A combination of both sorption enhanced reforming and unmixed steam reforming or chemical looping steam reforming in a process called sorption enhanced chemical looping steam reforming has also been researched [149, 150]; the advantage of this is the in-situ carbon capture without the need for separation and water gas shift reactions. It tends to be a more self-sustaining process than the normal sorption enhancement

process particularly with heat required. It is also more straight-forward with high hydrogen yield and lesser problems when compared to the conventional steam reforming process[151]. Ryden et al. [151] proposed the SE-CLSR process using three interconnected reactors- a reforming reactor, an air reactor and a calcination reactor; this led to the production of H_2, CO_2 and N_2 in separate streams without the need of extra separation as is the case in conventional steam reforming. Dou et al. [152] investigated the SE-CLSR of glycerol in moving bed reactors and reported > 90 % hydrogen purity produced in an auto thermal process. Pimenidou et al. [150] also investigated the SE-CLSR process using waste cooking oil with the production of high purity hydrogen over 6 cycles of SE-CLSR.

In general, Process intensification is very important as it helps in ascertaining not only optimal conditions but provides an opportunity to improve the conversion of feedstock particularly through the reforming process to hydrogen. It is also a means to reduce the problems affecting the overall sustainability and efficiency of the reforming process, and furthermore could be a way to increase the competitiveness of smaller scale plants due to the economies of scale and reduction of process steps/additional steps. In general, it poses an opportunity for industrial commercialisation for sustainable hydrogen production. Process intensification could also help to reduce the amount of external heat duty required for the entire process as in the case of chemical looping combustion coupled with reforming and chemical looping steam reforming, and could help save the need for extra processes like gas purification, and carbon capture/ separation as in the case of sorption enhanced reforming. The effect of sorption enhancement and chemical looping steam reforming would be investigated in this study using acetic acid as a model compound of pyrolysis oils; both processes has been investigated on pyrolysis oils and have been reported to lead to an increased hydrogen yield efficiency [100, 101, 153]; However, in the present study, emphasis would also be placed on chemical looping steam reforming (CLSR) of acetic acid and sorption enhanced chemical looping reforming of acetic acid (SE-CLSR) with the view to also carry out studies on materials utilised (catalyst in the case of CLSR and catalyst plus sorbent in the case of SE-CLSR)

whilst comparing the process outputs with chemical equilibrium data and stoichiometric values.

Chapter 3 Materials and methods

3.1 General overview

The major aim of this work is to study the effect of process intensification measures as a means to improve the efficiency of the conventional steam reforming of biomass derived oils using acetic acid as a model compound; three basic processes were examined as follows;

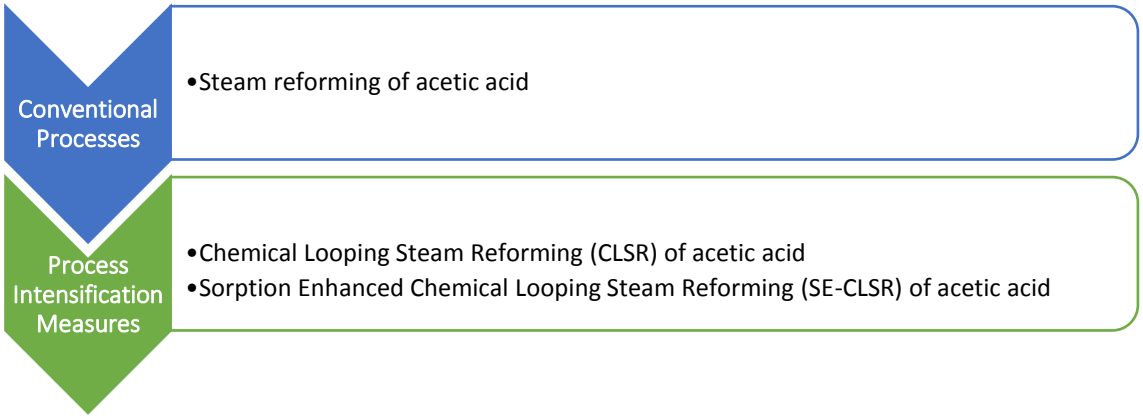

Figure 3.1 Process investigated and examined

This chapter details the materials utilised in the investigation of the processes as illustrated in Figure 3.1 in terms of material preparation and data source, it also details the reactor set-up and configuration used in this study, and the methods of characterisation of the materials utilised. The metrics for comparison of the examined processes with stoichiometric and thermodynamic equilibrium data are also discussed.

3.2 Materials

Acetic acid purchased from Sigma-Aldrich (≥99%) was utilised as the fuel feedstock in all experiments carried out in this study; its utilisation as a model compound of bio-derived oils is due to its high presence in most bio-oil compositions [74, 154].

Distilled water is also utilised in all experimental runs with the water utilised changed after every reforming cycle in the case of chemical looping steam reforming and sorption

enhanced chemical looping steam reforming. The overall quantity of distilled water utilised was dependent on the molar steam to carbon ratio required for the experimental run; it is important to reiterate that pure distilled water might not be required for mass commercialisation of all the processes studied as water reuse, and process integration could be utilised on a large-scale basis. However, in the base study, pure distilled water is utilised for all experimental runs for easier interpretation and elucidation of results.

3.2.1 Steam reforming catalysts

Two catalysts supplied by TST limited were utilised in this study; catalyst A (Figure 3.2A) contains 18wt% NiO on alpha-alumina support and has been utilised in previous work on steam reforming of bio-derived oils [100, 150, 153]. This catalyst has also been regarded as an ideal catalyst and oxygen carrier for looping processes due to little or no fluidisation problems encountered in its utilisation and its high durability [155]. Catalyst B (Figure 3.2B) is another commercial catalyst which has been utilised in previous studies on the steam reforming of bio-derived oils [156]; it contains 15wt% NiO on an calcium aluminate support; this is utilised to exemplify the advantages of alkali or alkali earth metals to the reforming process[12]. Catalyst B alone was utilised for sorption enhanced chemical looping steam reforming experiments with the addition of sorbent.

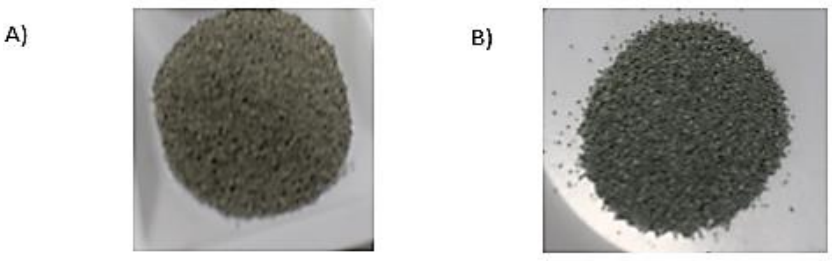

Figure 3.2 A) Catalyst A and B) catalyst B after crushing and sieving (250 µm -355µm)

[12] The presence of alkali metals like Ca, K, and Mg on the alumina support has been promoted as it helps to enhance adsorption of water and increases mobility on the surface of the catalyst; it also reduces potential catalyst deactivation and poisoning.

3.2.2 Sorbent

CaO based sorbent was used for sorption enhanced reforming experiments; the sorbent utilised (Figure 3.3A) was supplied by Longcliffe calcium carbonates, UK as high purity granular limestone (Longcal SP25SA) with granular size < 1.0mm. The sorbent utilised was pre-treated to form spent sorbent (Figure 3.3B) before use in all sorption enhanced chemical steam reforming experimental runs as described in 3.2.2.1.

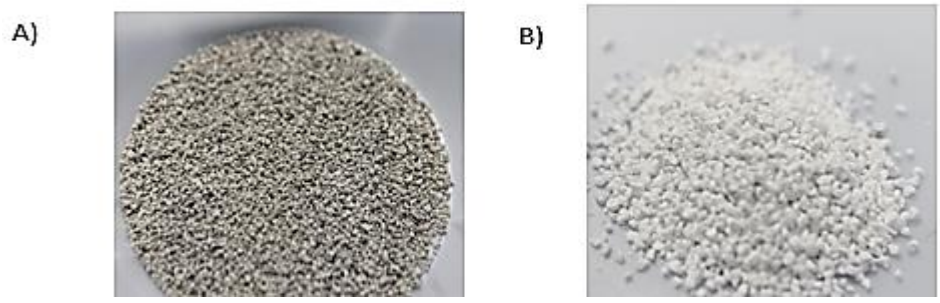

Figure 3.3 A) Longcal SP25SA B) Calcined spent sorbent

3.2.2.1 Generation of spent sorbent

Spent sorbent has been utilised in several studies investigating the cyclic stability and capabilities of CaO based sorbents [157, 158], this is because it has been reported that pre-treatment of CaO based sorbents to spent sorbent would stabilise the CO_2 carrying capacity of the sorbent [130].

The sorbent utilised in this study was subjected to 13 cycles of carbonation and calcination in a packed bed reactor similarly to that described in previous studies [123, 158]; calcination was carried out at 850 °C in the presence of nitrogen while carbonation was carried out at 650 °C in the presence of pure CO_2, these has been reported to be ideal for calcination and carbonation of CaO based sorbents [158].

The calcination step and carbonation step lasted for 30 – 45 minutes per step with the process output for both processes monitored from the micro-GC. Prior to the 13 cycles of carbonation and calcination, activation of the fresh sorbent (limestone) was done by calcining at 850 °C; the activating calcination step lasted longer than the other calcinations done during the generation of the spent sorbent. XRD patterns (Figure 3.4A)

indicate the presence of $CaCO_3$, when the limestone is calcined for 1hr in a furnace indicating partial calcination of the sorbent whereas full calcination was observed when the limestone was calcined and activated for 4 hours.

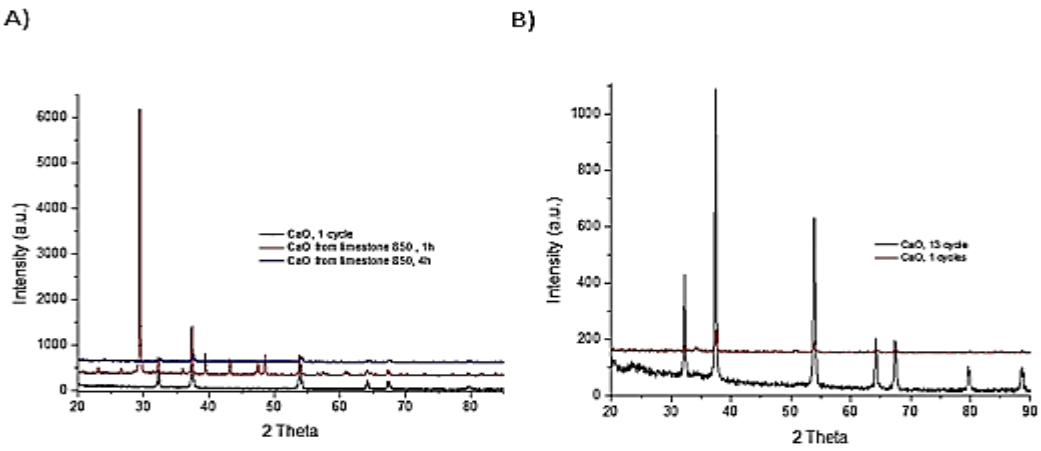

Figure 3.4 XRD Patterns of A) calcined fresh limestone b) spent sorbent

A comparison of the calcined sorbent after 1 cycle and 13 cycles of calcination can be seen in Figure 3.4B, XRD patterns with Reitveld refinement indicate that the calcined spent sorbent utilised in the experimental runs contains 4.5 % $CaCO_3$ and 95.5% CaO.

The major challenge associated with the use of natural CaO based sorbent is the loss of surface area during its utilisation particularly during cyclic processes; There is a clear similarity between the pore characteristics of the calcined spent sorbent which has undergone 13 cycles of calcination after activation and the sorbent which has gone through 1 cycle of calcination as seen in Table 3.1; this might indicate that there is no loss of porosity across the cycles with a little loss of surface area observed.

Table 3.1 BET surface area analysis of fresh and spent sorbent

	MBET surface area	**Pore volume**	**Pore radius**
	M^2/g	**Cc/g**	**nm**
Lime stone	0.495	0.004	1.105
1 cycle of Calcination	13.272	0.081	1.894
Spent sorbent (calcined)	11.421	0.08	1.893

There is however an increase in porosity and surface area when the un-calcined sorbent is compared to the sorbent after calcination as already reported in previous literature [130].

3.2.2.2 Hydration of the spent sorbent

Steam is then passed through the spent sorbent in the presence of nitrogen before it is utilised in sorption enhanced chemical looping reforming experiments; the utilisation of steam to hydrate the sorbent before utilisation in carbonation processes has also been promoted as a means of increasing the reactivity of the CaO based sorbent [158, 159]. The hydration was carried out at 250°C and 650°C depending on the set hydration temperature for the sorption enhanced chemical looping steam reforming process to be carried out.

3.3 Reactor set-up and experimental approach

As illustrated in earlier parts of this chapter, three basic experimental processes were investigated in this study using acetic acid as the fuel feed stock; the reactor set up system and configuration utilised in this study has already been described in previous literature [52, 156].

3.3.1 Reactor set-up

The system is a down flow system using a fully insulated packed bed reactor consisting of a stainless steel tube of 12.7 mm internal diameter (ID) and 25cm in length (1/2OD, SS310 tube); Fixed or packed bed reactors even though more economic and simplistic than the corresponding fluidised bed has been slated to be unsuitable for the reforming of bio-oil and its model compounds particularly when the lignin fraction of pyrolysis oils are also taken into account; this is due to increased coking noticed in this reactors during this process[160]; it is however important to reiterate that coking and attrition issues have also been identified in fluidised bed[161].

It is also essential to note that coking and attrition should be minimised with the advent of process intensification measures in this study; packed bed reactors have also been slated to be more efficient when compared to fluidized bed in sorption enhanced

processes due to increased efficiency of heat transfer and because sorption enhancement in a fluidized bed places extra demand and pressure on the mechanical strength and stability of the sorbent when compared to packed bed reactors [133].

The reactor system (Figure 3.5) was fully insulated to prevent heat losses from the system in all experimental runs. The flow rates of the fuel (water and acetic acid) is controlled by two programmable syringe New Era Syringe Pumps systems; with the flows rates determined by the S/C and the WHSV required. A gas tight 25 cm syringe from SGE which was connected to the pumps through drop injector connectors was utilised for all experimental runs in this study.

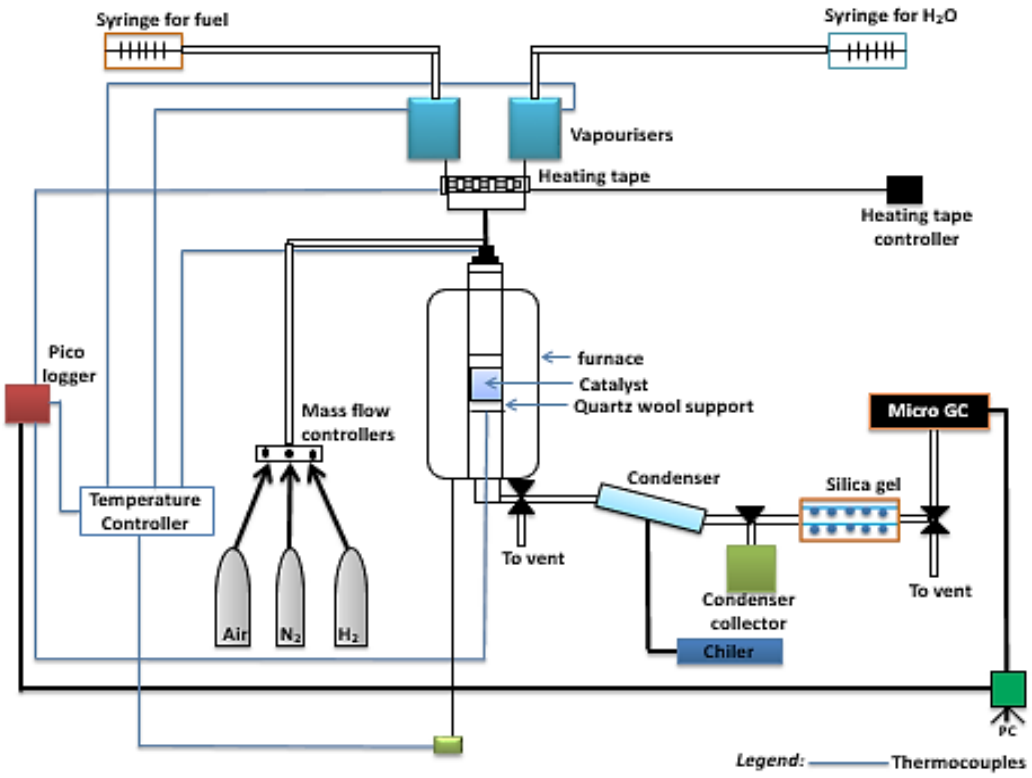

Figure 3.5 Reactor set-up for experimental runs

The flow of gasses into the system (N_2, H_2, CO_2 and Air) was regulated by mass flow controllers[13] supplied by MKS; the flows were set depending on the process to be carried out and the WHSV required for the process.

Two 180 mm long aluminium and stainless steel insulated vaporisers are utilised for each fuel (water and acetic acid) with the set point controlled by limit based Proportional Integral Derivative (PID) controllers manufactured by Watlow in the UK; the vaporisers were used to preheat the fuel (water and Acetic acid) separately before they are introduced into the reactor. Four dual junction thermocouples by TC direct UK and a heating tape were also used to monitor heat loss in the system using a TC-08 Pico log reader; two of the four thermocouples are set in the vaporisers to monitor while one is used in the reactor inlet and outlet respectively.

The product gasses are passed through a condenser and a silica gel trap before contact with the micro-Gas chromatogram; this is to cool the gasses and prevent moisture from getting in contact with the micro- gas chromatogram.

The micro gas chromatogram (Varian CP 4900) reads and measures the composition of hydrogen, oxygen, nitrogen and carbonaceous products notably CO, CH_4 and CO_2[14]. The Micro-GC consists of two columns which was operated to 100 °C at 100 kPa; column 1 which operates with a back flush of 13 seconds is a molecular sieve 5A column and was used to detect H_2, O_2, CO, N_2 while the second column is a Pora Plot Q column used to detect CO_2 and CH_4 It is however also set and has the capability to read other constituents like ethane, ethane, propane and butane etc. that could be formed from the reforming of higher hydrocarbons. The inlet sample line leading to the two pre-columns[15] installed before the columns in the Micro-GC was operated at 35 °C while the

[13] The MKS mass flow controller is poised to measure and control the mass flow rate of gasses with high accuracy (±1%)

[14] The micro gas chromatogram is set to read and take the composition of gasses present every 2 and half minutes.

[15] The installed pre-columns are pre-installed to ensure moisture do not enter into the column

pump injecting the sample into the micro-GC had a sampling time of 20 s. Conditioning of the micro-GC was carried out after every reforming run by heating the columns to 180 °C to remove any moisture and maintain the column's performance.

The micro-GC was fully calibrated to identify all potential products and reactants from all experimental processes to be conducted before utilisation (Appendix 1 Gas chromatograph calibration and method) and Galaxie software was used to observe the detected peaks and extract the data for further analysis (Sample detected peak at different retention time can be seen in Appendix 1 Gas chromatograph calibration and method).

3.3.2 Experimental procedures and approach

For all experimental runs, the reactor was set up as described in 3.3.1, after thorough cleaning with acetone and loading of the catalyst (catalyst and sorbent in the case of sorption enhanced processes); it is set up in a way to prevent severe pressure drops and leaks and an Agilent ADM 1000 flow meter is utilised to ensure no leaks or gas loss is apparent from the system. All catalyst utilised and the sorbent in the case of sorption enhanced processes was crushed and sieved to about 0.25 -2mm size particles depending on the particle size to be investigated. This is essential to prevent pressure drops and diffusion limitations that could arise from the use of large pellets. For all experimental runs, 2 grams of catalyst was utilised with the WHSV and reactor loading optimised by varying the flow rate of nitrogen and fuel supplied. In the case of sorption enhanced processes, 1 - 2g of sorbent was utilised depending on the parameter to be investigated.

The reducing stage for all experimental runs were carried out at temperatures between 550°C and 700 °C while the oxidation stage was carried out between 600 °C and 850 °C depending on the experimental run and parameter investigated. The S/C was set between 2 and 3 depending on the experimental run, with acetic acid supplied at 0.978 ml/hr for all experimental runs and water supplied at 1.23 ml/hr and 1.846 ml/hr for experiments with steam to carbon ratio set to 2 and 3 respectively; this is because

previous studies on pyrolysis oils and its model compounds conclude that the reforming process is optimal at this range without significant coking and attrition problems [95, 100, 162]. The vaporiser temperature to be utilised was varied between 50°C and 100°C for the fuel and between 120°C and 150°C for water; the vaporiser temperature was varied to ascertain the effect of pre-heating on the reaction kinetics. Nitrogen was utilised as an inert material in all experimental runs; this is essential to prevent any unwanted by-reactions and also flush the system in between each step and runs in the case of looping experimental runs.

Each experimental run basically consists of a reduction step and the reforming step; in the case of looping processes an oxidation step is also required for reuse of the catalyst for another run and in the case of sorption enhanced experiments the spent calcined sorbent is mixed and loaded with the catalyst into the reactor. The fresh catalyst which is majorly supplied as oxides was reduced and activated by subjecting through 5 % H_2/N_2. It is important to note that in industrial applications particularly middle to large-scale productions, ammonia, methane or other reducing agents could be utilised for reduction and catalyst activation depending on cost and availability[163]. The continuous utilisation of 5 % H_2/N_2 for catalyst reduction is also not required after the 1^{st} looping cycle for the looping processes as the fuel feed (acetic acid) is utilised in reducing the catalyst. The reduction of the catalyst is carried out at the same operating temperature utilised for the subsequent steam reforming or CLSR process in all experimental runs in this study; this is ≥ 550 °C for all experimental runs and has been reported to be adequate for full reduction of Ni based catalyst [164].

The reforming process is allowed to run for two hours after stable hydrogen production is observed. This equates to about thirty-eight injections and readings by the micro gas chromatogram; this is also enough to observe all stages and phases in sorption enhanced experimental runs.

The results as detected by the Micro-GC and extracted through the Galaxie software are then used in the definition of the process outputs and calculation of the conversions,

hydrogen yield and selectivity to hydrogen containing gases and carbon containing gases using elemental balances; these calculated parameters were compared against calculated stoichiometric and equilibrium values for all experimental runs.

3.4 Thermodynamic equilibrium calculations and stoichiometric values

The calculated values for the yield of hydrogen, hydrogen purity and conversions were compared with thermodynamic equilibrium values and stoichiometric data; thermodynamic equilibrium calculations in this study was done using a computer program by NASA Lewis Research centre called Chemical Equilibrium with Applications (CEA) (P=1 atm, T= 600°C ,650 °C, Omit= C(gr), H_2O(cr) H_2O(l)) [165, 166]; the program written in ANSI standard Fortran 77 takes in the input composition of reacting fuel in mole basis and gives the molar thermodynamic fractions of the products using equilibrium mixture properties like temperature ranges in this case of this study. Nitrogen was added to the fuel input composition in this study to act as an inert which helped in the calculation of the number of moles of the products using nitrogen balance. The following calculations were now carried out to ascertain thermodynamic relationships for the basis of comparison (Equation 3:1).

Equation 3:1 Equilibrium calculations

- Steam conversion at thermodynamic equilibrium (%) =

$$\frac{Initial\ moles\ of\ water - moles\ of\ water\ at\ equilibrium}{initial\ moles\ of\ water} \times 100$$

- Yield of hydrogen (wt. % of feedstock) =

$$\frac{2\ \times 1.01\ \times 100\ \times\ moles\ of\ Hydrogen\ at\ equilibrium}{molar\ mass\ feedstock * intial\ molesof\ feedstock}$$

- Hydrogen purity (% Dry basis) = $\frac{moles\ of\ hydrogen\ at\ equilibium}{total\ gas\ moles\ at\ equilibrium - moles\ of\ H2O\ and\ N2}$

- Selectivity of carbonaceous product (x)

$$= \frac{moles\ of\ C\ atoms\ in\ x\ at\ equilibrium}{moles\ of\ C\ atoms\ in\ all\ carbon\ containing\ compounds}$$

Stoichiometric calculations were also done using the maximum theoretical values for the reforming of acetic acid.

Asides from the comparison of the experimental data with thermodynamic and stoichiometric calculations, the used catalyst and sorbent (in the case of sorption enhanced experimental runs) are also characterised with the view to check changes in morphology, structure, and coking or carbon deposition that might have occurred. Condensate is also collected after every experimental run for further analysis and characterisation.

3.5 Characterisation and analysis methods

The characterisation of the materials (fresh and used) are very important in ascertaining the overall efficiency of the steam reforming process; The XRD pattern of the fresh and used calcined sorbent was utilised to study the crystallographic structure of the sorbent and in ascertaining full calcination of the sorbent, it was also used in determining constituent composition which was used in the overall carbon balance of the sorption enhanced process. BET surface analysis of the fresh and used catalyst and sorbent was used to check changes in surface area and was also used to infer pore characteristics after steam reforming, chemical looping steam reforming and sorption enhanced steam reforming experiments. CHN elemental analysis and TOC was used to quantify deposited carbon on the catalyst and sorbent (in the case of sorption enhanced processes), and collected condensate respectively. This was also essential in the calculation of the overall carbon balances of the chemical looping process and sorption enhanced chemical loping process. TGA-FTIR on the used catalyst was essential to check mass change in the catalyst and also infer the type of carbon deposited during the reforming process; while SEM-EDX and TEM images and diffraction patterns would help in studying carbon deposition on the surface of the catalyst in terms of morphology and the material phases. ICP-MS was also utilised to check potential leaching in the steam reforming process as already observed in previous studies[167].

3.5.1 X-Ray diffraction (XRD) and Rietveld refinement

XRD is widely used to extract and study crystallographic information regarding materials; this includes changes in the crystallite phase, size and phase quantification after utilization of materials. A diffracted beam is produced due to the constructive interference of X-rays from crystal planes; the diffraction angle and intensity distribution of the diffracted beams varies depending on the crystal planes but contains very important information on identifying the underlying crystal structure of materials.

XRD test were performed on calcined sorbent in this study to compare the crystal structure of the sorbent for freshly calcined sorbent and calcined sorbent after several cycles (spent sorbent); it was done using an X-ray diffractometer (Bruker D8) using Cu Kα radiation. The sample range (2Θ) of the X-rays was set at 20° - 100° with a speed of 0.7 second per step, steep size of 0.108 °/step and an increment of 0.0332 °/step.

Phase analysis and Reitveld analysis was obtained from the observed XRD patterns using the X'pert High Score Plus software; this was done by comparing the obtained patterns with known standard reference diffraction patterns from the International Centre for Diffraction Data (ICDD) database to ascertain the phases in the sorbent materials. The composition and quantification of the phases observed was done through Rietveld refinement as developed by Hugo Rietveld [168, 169] using PAnalytical's non-linear, least squares algorithm embedded in the X'pert High Score Plus software. The quantified composition was utilised when calculating the overall carbon balance of the sorption enhanced process.

3.5.2 Surface area analysis and pore characteristics of catalyst and sorbent

The multi-point BET surface area and pore characteristics of the fresh and used materials was done using adsorption/desorption isotherm analysis; the BET theory gives a mathematical model for physical gas adsorption on the surface of solid materials and was carried out in this study using a Quantachrome Nova 2200e instrument with nitrogen as the adsorbate gas.

The samples were vacuum degassed for 2 hours at 200 °C in a degasser to remove any moisture, contamination or trapped gasses on the solid material; the change in mass of the material is observed after degassing to ascertain the mass of the material before the start of the isothermal analysis. The isothermal adsorption of N_2 at 77.35 K occurs at different pressures; as the pressure increases, the nitrogen occupies the surface of the material and also fills the pores (physisorption); this enables the extrapolation and calculation of the surface area of the material.

The pore radius and volume are extrapolated using the BJH model [1] from the desorption branch of the isotherms. The surface area and pore characteristics is important to ascertain changes in open porosity after utilizing the materials; this is essential particularly for sorption enhanced processes as the surface area and porosity of CaO based sorbent has been linked to the apparent loss of sorbent efficiency during utilization of the materials.

3.5.3 Electron microscopy and energy dispersive X-ray (EDX)

Transmission electron microscopy (TEM) and scanning electron microscopy was used to check morphological changes in the fresh and used materials; SEM is based on the detection of scattered electrons produced from scanning sample materials with focused high energy electrons while TEM is based on transmitted electrons detected from electron beams on the material sample.

The SEM was conducted using a high resolution Hitachi SU8230 and Carl Zeiss EVO MA15 both coupled with an Oxford Instruments Aztec Energy EDX system while the TEM was conducted using a FEI Tecnai TF20. The samples were coated with 10 nm layer of gold or iridium before the SEM-EDX tests, while the samples were suspended in methanol and decontaminated in a treatment chamber before the TEM experiments.

The SEM-EDX images was used to observe the formation of carbon in chemical looping reforming and sorption enhanced processes; the coupling of the EDX with the SEM apparatus allowed for quantification of the different element observed in the electron image. TEM patterns was used to observe the structure and type of carbon formed, this

was also confirmed using the SAED diffraction patterns obtained for the used materials. The dispersion of elements in the materials were also observed and discussed (SEM-EDX result analysis of all investigated experimental runs can be found in the appendices: Appendix 4: SEM-EDX images).

3.5.4 CHN elemental analysis

CHN elemental analysis was used to quantify the deposited carbon on the used catalyst (and sorbent mix in the case of sorption enhanced processes); this is essential in comparison of the carbon deposited using different operating parameters and would also be vital in the overall carbon analysis of the process.

The CHN analysis was conducted in a Flash EA 2000 elemental analyser. About 15 mg of the used material was placed into a combustion reactor in folded tin capsules. A thermal conductivity detector in a chromatography column measures the composition of the constituent elements in the material after burning the samples at very high temperatures (1000-1800 C) in oxygen. Helium is used as a carrier gas for the equipment and the samples were done in duplicates to ensure repeatability, precision and accuracy.

3.5.5 Total organic carbon (TOC) analysis

The carbon in the collected condensate is also calculated to aid the overall carbon balance of the chemical looping process and the sorption enhanced processes; the TOC was derived using a Hach-Lange IL 550 analyser using the differential method. The differential method measures the total carbon and inorganic carbon present in materials separately, with the total organic carbon calculated by the difference in the total carbon and the total inorganic carbon.

The samples were diluted by 5 times with deionized water and placed in centrifugation tubes before the TOC analysis.

3.5.6 Inductively coupled plasma-mass spectrometry (ICP-MS)

Potential leaching has been inferred in previous studies on steam reforming of model compounds of biomass derived oils [167], hence, the presence and concentration of Ni ion in the condensate collected was also observed using ICP-MS.

The ICP-MS was conducted using a SCIEX Elan 900 by Perkin Elmer; the high temperature ICP converts elements in a material into ions which are then detected and quantified by a mass spectrometer.

ICP-MS analysis was conducted on condensates diluted by 100 times with deionised water which were collected in different cycles during chemical looping reforming and sorption enhanced chemical looping reforming to observe potential leaching across the cycles.

3.5.7 Thermal gravimetric analysis (TGA) coupled with Fourier transform infrared spectroscopy (FTIR)

TGA-FTIR was utilised in this study to enumerate on the type of carbon formed during the chemical looping steam reforming process through temperature programmed oxidation of used catalysts; the different peaks of CO_2 observed in the FTIR analysis when coupled with the mass loss observed from the TGA can be used to ascertain the type of carbon formed. This is because the peak at which the carbon is oxidised in the FTIR has been reported to indicate the type of carbon on the material [167].

A Stanton-Redcroft TGA connected to a FTIR (Nicolet iS10, Thermo scientific) was utilised in this study; 100 mg of the used samples was placed in the TGA and the change in mass of the sample is observed and recorded after the temperature is increased from room temperature at the rate of 10°C/min in 50 cm^3/min to 900 °C. The gas produced from the TGA is transferred via a transfer line heated to 170 °C into the FTIR spectrometer. The FTIR spectral scanning was repeated every 60 seconds from 4000 to 400 cm^{-1}. Chemigram for the evolution of CO_2 was obtained and compared to the mass loss from the TGA to ascertain the type of carbon formed.

Chapter 4 Acetic acid as a model compound of bio-derived oils

4.1 General overview

The steam reforming of acetic acid as a model component of bio-oil/pyrolysis oils has been studied due to its high presence in bio-oils particularly its aqueous fraction [170-175]. GC-MS studies on Bio-oils indicates that acetic acid is one of the major compounds in bio-oils with a detected percentage of 15% and 32% in Pine oil and PEFB oil respectively, this equates to about 24% and 43% of the oils respectively on a water free basis [154]. TGA analysis of both bio-oils [101] also indicates that two phases of pyrolysis takes place for both bio-oils, the first phase occurring at a lower temperature, which is mainly attributed to the loss of acetic acid from the bio-oils. This has prompted indications that acetic acid might be evaporated and potentially reacted first before the reforming of other components in bio-oils; hence study on the efficient reforming of acetic acid would play a pivotal role in the elucidation of the dynamics of the reforming of bio-derived oils.

Another school of thought is that acetic acid on its own can also be regarded as a renewable resource because it can be produced from the fermentation of biomass residues and as a by-product of other processes. Hence the study of its reforming efficiency and the effect of process intensification measures on conversion rates, catalyst life and other important factors to be considered for general sustainability and effectiveness are essential for easier understanding of how bio-oils would react under different conditions but also gives an opportunity to study the utilisation of acetic acid as a renewable resource for hydrogen production [176].

The reforming of acetic acid, like that of its parent mixture bio-oils, has also been characterised by many other side reactions particularly decomposition, methanation and ketonisation; this however is dependent on the operating parameters utilised [172]. Basagiannis and Verykios concluded that the reforming of acetic acid is complicated due to side reactions prominent at lower reforming temperatures, they also stipulated that

the rate of carbon deposition observed on the catalyst is generally determined on the reforming temperature, catalyst utilised and the feed to steam ratio[171, 172].

Graphitic carbon deposition has been particularly observed with the reforming of acetic acids particularly at temperatures below 650 ° C [177]. Amorphous carbon has also been found to inhibit the utilisation of acetic acid and bio-oil in general as they block the active sites of the catalyst preventing suitable reactions[178]. T_{SR} and the S/C also has an important role to play in terms of conversion as studies show a high obtained conversion rate of acetic acid reforming at 650°C and S/C of 3 [167].

In terms of the type of catalyst utilised, studies indicate that high conversion rates could be achieved for the reforming of acetic acid by using noble metals as catalysts; the utilisation of transition metals has also been studied, however lower efficiency has been identified from their utilisation when compared to noble metals due to their susceptibility to carbon deposition. Nickel is however a more stable transition metal that shows more activity, stability and selectivity when compared to other transition metals [179]. It is promoted to be as effective as noble metals with a reported high yield of hydrogen of about 80% [162].

4.2 Reaction mechanism for the steam reforming of acetic acid

The reaction path for the steam reforming of acetic acid is complex based on the several side reactions that potentially could occur simultaneously; Wang et al. [176] proposed a reaction pattern for the steam reforming of acetic acid (Figure 4.1), it was inferred that acetic acid is adsorbed and dissociated on the active sites of the catalyst. Decarboxylation of the adsorbed species then leads to the formation of methyl radicals which is then reformed in the same pattern as in the case of steam methane reforming, and water gas shift follows just as in the case of steam methane reforming

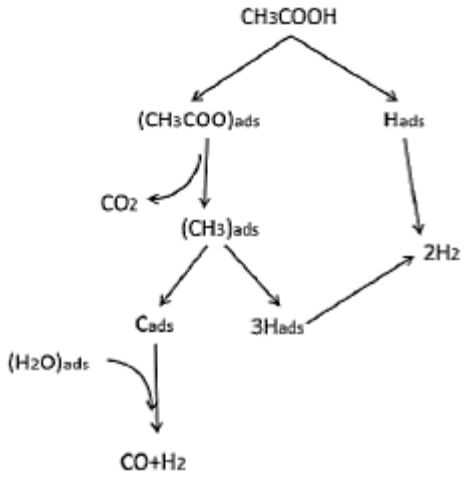

Figure 4.1 Schematic diagram of acetic acid steam reforming [176]

The overall acetic acid steam reforming reaction can be summarised as seen in Reaction 4.1;

Reaction 4.1 Acetic acid steam reforming and water gas reactions

Overall acetic acid steam reforming

$$CH_3COOH + 2H_2O \rightarrow 2CO_2 + 4H_2$$

Steam reforming

$$CH_4 + H_2O \rightarrow 3H_2 + CO$$

Water gas shift

$$CO + H_2O \leftrightarrow H_2 + CO_2$$

Several side reactions tend to occur during the steam reforming of acetic acid depending on the operating conditions utilized; it has been inferred that both homogenous decomposition which is always apparent in the steam reforming of acetic acid (Reaction 4.2) and the heterogeneous reforming reactions occur simultaneously during the steam reforming of acetic acid [176].

Reaction 4.2 Homogeneous thermal decomposition

$$CH_3COOH \rightarrow CH_4 + CO_2$$

$$CH_3COOH \leftrightarrow CH_2CO + 2H_2O$$

$$CH_3COOH \rightarrow 2CO + 2H_2$$

$$CH_3COOH \rightarrow C_2H_4, C_2H_6, C_3H_4, coke$$

The thermal decomposition of acetic acid has been studied extensively and two major competing reactions is said to occur; dehydration of acetic acid to ketene and water (first order >700°C and second order <600°C) [180, 181] and the first order decarboxylation to form carbon-dioxide [180], the ketene formed can then be further decomposed to CO, ethylene and methane or CO_2 and allene at low temperatures [182].

Ketonisation of acetic acid can also occur as already reported in previous literature (Reaction 4.3) [173]; it is said to occur at lower temperatures (250 °C - 450 °C) [183]. The ketonisation reaction can be suppressed by the active metal on the catalyst (nickel in the case of this study) and is affected by the acidity or basicity of the catalyst. The ketonisation reaction has been observed to occur on shift catalyst and support materials [184, 185]; it is more selective on acidic catalyst and the addition of basic oxides should lead to an improvement of the catalytic capabilities of reforming catalysts and the prevention of ketonisation reactions [173].

Reaction 4.3 Ketonisation of acetic acid

$$2CH_3COOH \rightarrow (CH_3)_2CO + CO_2 + H_2O$$

Another thermodynamically possible reaction is the de-carbonylation reaction of acetic acid (Reaction 4.4); this however has been reported to not occur thermally due to large energy barrier when compared to other homogenous cracking reactions [176].

Reaction 4.4 De-carbonylation of acetic acid

$$CH_3COOH \rightarrow CH_3OH + CO$$

Methanation (Reaction 4.5) and boudouard reaction (Reaction 2.4) can also occur during the reforming of acetic acid due to reverse steam reforming and inhibited water gas shift respectively;

Reaction 4.5 Methanation reactions

$$CO + 3H_2 \leftrightarrow CH_4 + H_2O$$

$$CO_2 + 4H_2 \leftrightarrow CH_4 + 2H_2O$$

Most of the side effects occurring can be suppressed depending on the operating conditions utilized; this is prominently and not limited to the type of catalyst utilized in terms of acidity and basicity, the reforming temperature employed and seam to carbon ratio utilized.

4.3 Thermodynamic equilibrium data of acetic acid

The thermodynamic equilibrium results calculated as described in Chapter 3, could help check the efficiency of the reforming process with the view of comparison; using different steam to carbon ratios, thermodynamic equilibrium is used to compare the purity, conversion and selectivity of carbonaceous product at different temperatures.

The hydrogen yield (wt. %) was compared using different steam to carbon ratios and at different temperatures as seen in Figure 4.2; the results indicate that the yield of hydrogen produced from the reforming of acetic acid is highest at 600°C- 650°C and decreases at temperatures higher than this range at atmospheric pressure. This is in accordance with previous results that indicate good yield and fuel conversion at 550°C - 650°C for model compounds of pyrolysis oils and pyrolysis oils [167]. Another conclusion that could be derived is that the yield of hydrogen increases as the steam to carbon ratio of increases; this is due to the increase in hydrogen that could be produced potentially from the increase of water molecules.

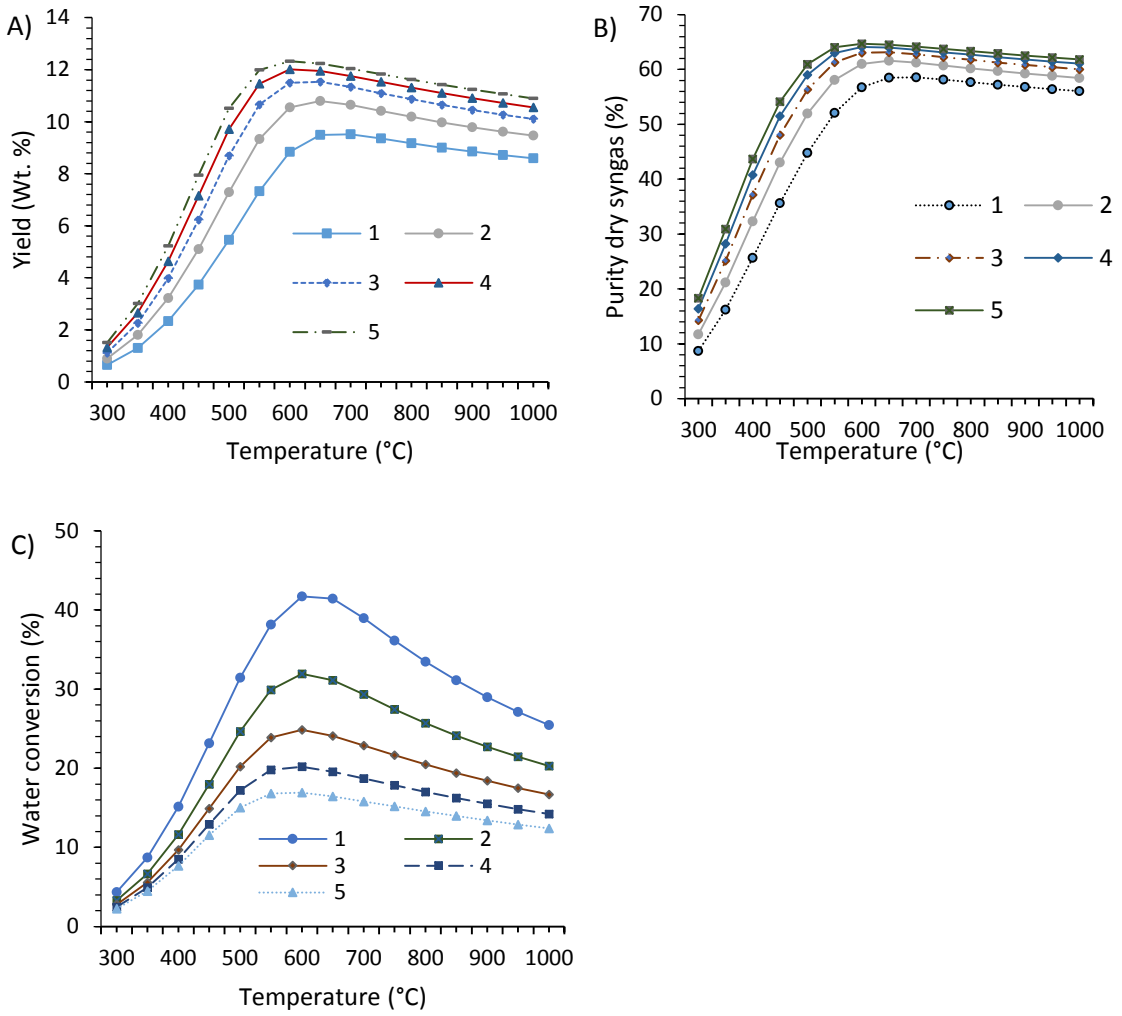

Figure 4.2 A) Hydrogen yield (wt. %), B) Hydrogen purity dry basis (%), C) water Conversion (%) at different T_{SR} and S/C (P=1 atm)

The steam conversion (%) also shows a similar trend across increasing temperatures and tend to peak at 600°C to 650°C just like the yield of hydrogen; the major difference however is that water conversion tends to decrease as the steam to carbon ratio increases; this is expected due to the increase in moles of water or steam of convertible steam as the steam to carbon ratio increases. As expected, the purity of hydrogen produced on a dry basis also increases as steam to carbon ratio increases, it also peaks around 550°C to 650°C.

In terms of selectivity, it is optimal to have low methane selectivity to carbonaceous products; this is because the production of methane inhibits the reforming reaction as

it is majorly formed from thermal decomposition of the feedstock or the reverse process of steam reforming, hence utilising the desired hydrogen.

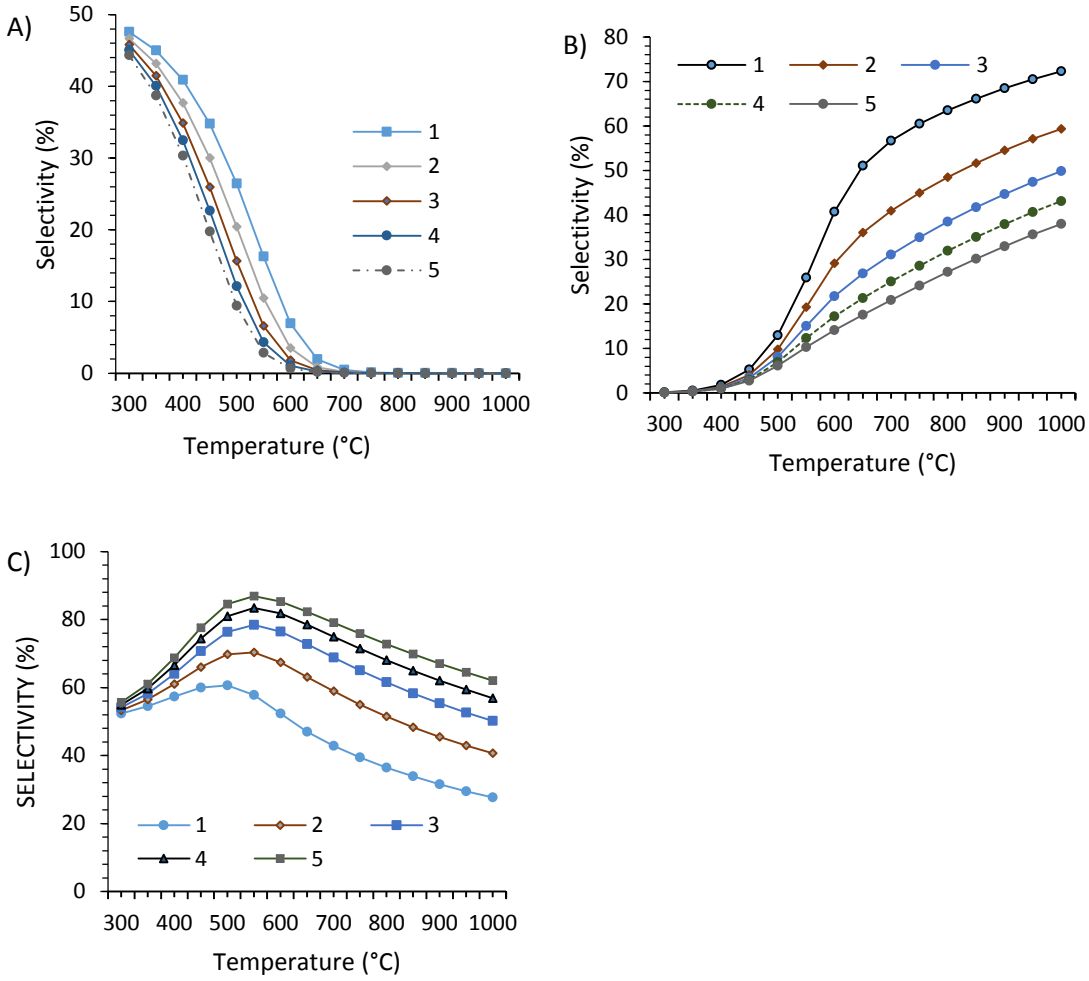

Figure 4.3 Selectivity to A) Methane B) CO C) CO_2 at different T_{SR} and S/C (P=1 atm)

It can be observed from Figure 4.3 that the selectivity of methane to other carbonaceous products decreases as the reacting temperature increases; it is also observed that the selectivity is lowest and optimal at temperatures above 650°C. The selectivity is also optimal at 450°C to 600°C for the selectivity of CO_2, this indicates the advent of the water gas shift, and for the selectivity of CO, the selectivity increases from 450°C to indicate the production of syngas beyond that temperature; it can thus be concluded that the reforming of acetic acid would not take place at temperatures below 450°C.

Another conclusion that could be detected especially when taking the yield and conversion into consideration is that the reforming reaction is optimal thermodynamically between 600°C and 650°C; it is also more sustainable not to increase the S/C significantly.

4.4 Methodology for determination of process outputs from elemental balances

Balances of the N, C, H, and O elements during the steam reforming process was used to determine in turn the conversion of fuel to gas products, water conversion, and yield of hydrogen whilst the gas compositions determined the selectivity to C-gases and H-gases; A nitrogen balance was used to calculate the total molar gas output flow rate ($\boldsymbol{n_{OUT,dry}}$) which in turn is used to calculate the conversion of the reactants; acetic acid conversion to gas products is calculated from a carbon balance as summarised in Equation 4:1 while the water conversion is also calculated from a hydrogen balance;

Equation 4:1 Fuel and water conversion calculation using elemental balances

$$X_{HAC}(\%) = 100 \times \frac{(n_{OUT,dry} \times (y_{CO} + y_{CO_2} + y_{CH_4} + 2y_{C_2H_6} + 2y_{C_2H_4} + 3y_{C_3H_6} + 3y_{C_3H_8}))}{2 \times n_{HAC,in}}$$

$$X_{H_2O}(\%) = 100 \times \frac{(n_{OUT,dry} \times (y_{H_2} + 2y_{CH_4} + 3y_{C_2H_6} + 2y_{C_2H_4} + 3y_{C_3H_6} + 4y_{C_3H_8}) - 2 \times n_{HAC,in} \times X_{HAC})}{n_{H_2O,in}}$$

The calculation of the acetic acid conversion to gases did not represent the conversions to solid carbon or organic condensate which were evaluated separately by CHNS analysis of the used catalyst and TOC analysis of the condensates after the experiments. A value of acetic acid conversion lower than 100 % denoted carbon deposition on the catalyst or in the condensate.

The hydrogen yield (wt. %) is defined as a ratio of the weight of hydrogen in the process output to the weight of acetic acid feedstock (no water) (Equation 4:2). According to

stoichiometry of, the maximum theoretical hydrogen yield is 13.45 wt. %. The hydrogen purity dry basis (%) was also calculated as indicated in Equation 4:3; the water conversion, hydrogen yield and hydrogen purity is compared with chemical equilibrium and stoichiometric values to ascertain the efficiency of the fuel feed stage.

Equation 4:2 Calculation of hydrogen yield (wt. %) using elemental balances

$$\frac{W_{H_2} \times 100 \times n_{OUT,dry} \times y_{H_2}}{W_{HAC} \times n_{HAC,in}}$$

$$= \frac{\mathbf{2} \times \mathbf{1.01} \times \mathbf{100} \times \boldsymbol{n_{OUT,dry}} \times \boldsymbol{y_{H_2}}}{\boldsymbol{n_{HAC,in}} \times \boldsymbol{W_{HAC,dry}}}$$

Equation 4:3 Hydrogen Purity (% Dry basis) =

$$\frac{moles\ of\ hydrogen\ \ detected\ in\ \ \ process\ gas\ output}{total\ gas\ moles\ detected\ \ -\ \ moles\ of\ N_2} \times 100$$

Selectivity to C- gases and H-gases was also calculated as described in Equation 4:4 with $y_{\boldsymbol{a}}$ representing all C-gases and H-gases in the outlet gas for the selectivity to C- gases and H-gases respectively;

Equation 4:4 Selectivity to C-gases ($sel_{i,C}$) and H-gases (sel_{i,H_2})

$$sel_{i,C}\% \ = 100 \times \frac{\alpha_i y_{i,C}}{\sum_j^n \alpha_{j,C} y_{j,C}}$$

$$sel_{i,H_2}\% \ = 100 \times \frac{\alpha_i y_{i,H_2}}{\sum_j^n \alpha_{j,H_2} y_{j,H_2}}$$

Where indices i and j represent gas species.

4.5 Experimental results and discussion

Steam reforming experimental runs using acetic acid as fuel feedstock was conducted at S/C set to 2 or 3 using the experimental approach and reactor design as described in chapter 3.3; this was done to ascertain optimal operating conditions for further experiments on CLSR and SE-CLSR of acetic acid using catalyst A and catalyst B. Table 4.1 shows the MBET analysis of the fresh catalyst before its utilisation in the steam reforming of acetic acid; it can be observed that the fresh catalyst B has an higher surface area and open porosity when compared to catalyst A; this might have an

important effect on its efficiency as a steam reforming catalyst. The basicity of its support when compared to Catalyst A might also play an important part in its overall efficiency; this is because it has been reported that the nickel content and nature of the support in regards to alkalinity would have a prominent effect on catalytic activity and also carbon deposition [186].

Table 4.1 BET analysis of as received fresh catalyst A and catalyst B before steam reforming experiments (catalyst particle size= 250 µm– 355 µm)

	MBET surface area	**Pore volume**	**Pore radius**
	M^2/g	**Cc/g**	**nm**
Fresh Catalyst A (oxidised form)	4.484	0.015	1.218
Fresh Catalyst B (oxidised form)	34.898	0.068	1.913

The gases detected by the micro GC from all steam reforming experiments carried out at different operating conditions in this study were H_2, CO, CO_2, CH_4, C_2H_6, and C_3H_8, (the last two always remaining below threshold of detection) (Figure 4.4); this indicates that sustained steam reforming and water gas shift has occurred. The detection of CH_4 in the experimental runs also indicates that thermal decomposition of acetic acid as supposed to methanation or reverse steam reforming might have occurred; this is confirmed by the higher selectivity to carbon-dioxide calculated when compared to chemical equilibrium values.

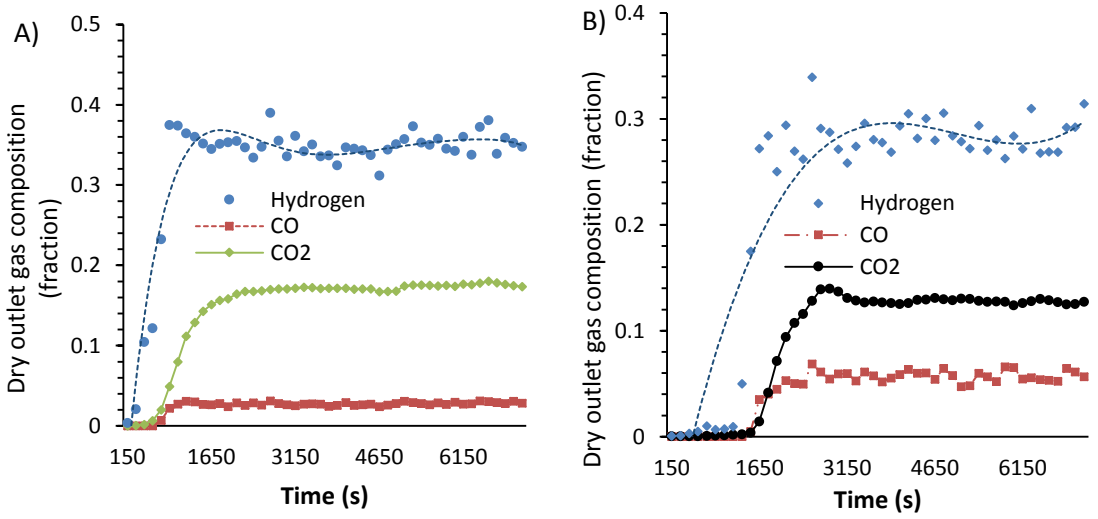

Figure 4.4 Dry outlet gas composition after steam reforming of acetic acid at A) S/C=3 B) S/C =2, (T_{SR}=600 °C, WHSV=2.5 hr^{-1})

As expected the hydrogen and carbon-dioxide detected in the experimental runs were higher whilst CO detected was lesser for those carried out at steam to carbon ratio set to 3 when compared to those carried with the S/C set to 2; this is due to additional steam present which would have favoured the water gas shift reaction and hence increase the conversion of CO formed to CO_2.

4.5.1 The steam reforming of acetic acid-Influence of different operating conditions on process efficiency (hydrogen yield, hydrogen purity, conversions and selectivity)

It is essential to ascertain and review optimal conditions for the conventional steam reforming of acetic acid using the reactor set up and experimental procedures as already discussed before process intensification measures are adopted. In this study, the effect of the temperature of pre-heating of the fuel before it is introduced to the reactor on process output, yield and conversions was observed. The effect of the reforming temperature and WHSV on the process output and conversion was also reviewed experimentally as they have been attributed to have a crucial and important effect on the efficiency of the steam reforming process [171, 172].

4.5.1.1 The effect of water and feedstock vaporisers temperatures on hydrogen yield, hydrogen purity, conversions and selectivity to C-gases

The steam reforming of acetic acid was carried using the reactor set up as described in chapter 3.3, using three different vaporiser temperatures for acetic acid (50°C, 70°C, 100°C); the pre-heat temperature for water added was set > 100 °C for all the experimental runs to ensure that water supplied is above its boiling point before it comes in contact with the fuel. The experimental runs were carried out at reforming temperature set at 600°C and WHSV set to 2.5 hr^{-1} at a S/C of 2 using catalyst A with catalyst particle size sieved to 1000 µm– 1400 µm. The catalyst was activated or reduced by 5 % H_2/N_2 as already described in 3.3.2.

Quantitative comparison of the results as seen in Figure 4.5 indicate that there are no direct significant difference in the hydrogen yield (calculated using Equation 4:2), water conversion (calculated using Equation 4:1) and hydrogen purity (Equation 4:3) impacted

by the increase of the temperatures of the vaporisers except a slight increase in the yield of hydrogen observed when the vaporiser temperature was set to 100°C; the selectivity of the carbonaceous product however shows a trend as CH_4 and CO selectivity reduces as the temperature of the vaporisers are reduced, an opposite relationship is observed for the selectivity of CO_2 as the selectivity increases as the vaporiser temperatures are reduced.

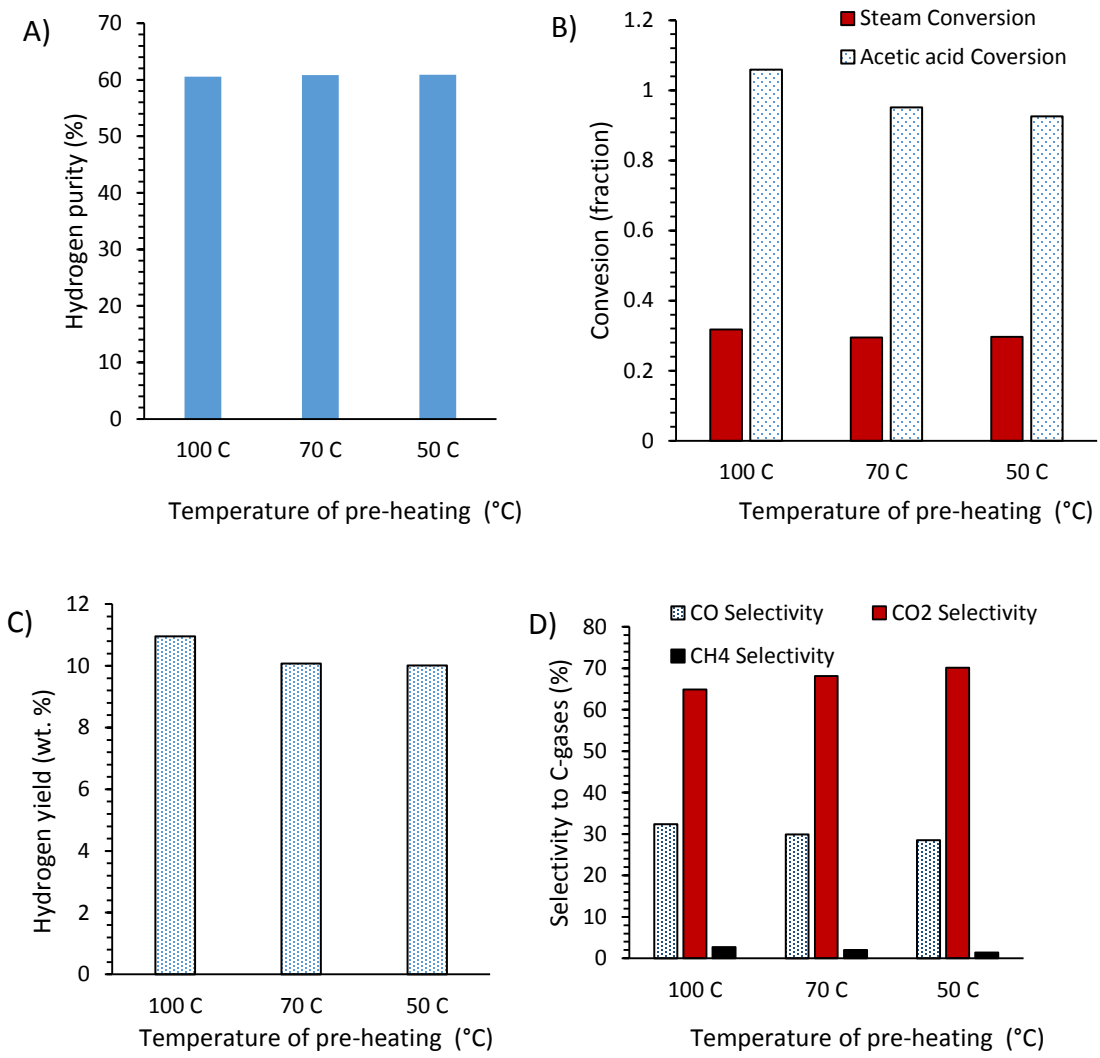

Figure 4.5 A) Hydrogen purity (%), B) conversions, C) hydrogen yield (wt. %) and D) selectivity to C-gases at different pre-heating temperature (T_{SR}=600 °C, WHSV = 2.5 hr^{-1}, S/C = 2)

The acetic acid conversion also increases as the temperature of the vaporizers are increased; this might indicate a slightly better steam reforming efficiency as the

temperature of vaporizer is increased, however, it is prudent to observe that care and caution must be taken for the increment of vaporizer temperatures due to the volatility of the feedstock. Qualitative study of the results also show that pyrolysis or thermal decomposition might have occurred at the beginning of the experiment when the vaporizer temperature was set at 100°C; this was evident by production of carbon-dioxide and methane in the process gas output with no hydrogen observed at the earlier stage of the experiment indicating no dominant steam reforming reaction at that stage.

It is evident that the increase in temperature of the vaporisers is beneficial for process efficiency, however the increase in fuel vaporiser temperatures is limited due to side reactions and pyrolysis that might occur. It is also important to reiterate that these side reactions would be more apparent in pyrolysis oils due to its instability and the presence of more compounds that would easily vaporise at lower temperatures.

4.5.1.2 The effect of reforming temperature (T_{SR}) on hydrogen yield, hydrogen purity, conversions and selectivity

The influence of T_{SR} on the efficiency of the reforming of acetic acid has been extensively discussed in previous literature [172, 173]; it is generally agreed that increase in temperature would lead to an increase in gas yields and hence acetic acid conversion [173].

4.5.1.2.1 The effect of T_{SR} on hydrogen yield, hydrogen purity and, conversion

A general increase in hydrogen yield and acetic acid conversion was observed for catalyst A as seen in Figure 4.6 after steam reforming at 550 °C, 600 °C and 650 °C (WHSV = $2hr^{-1}$, S/C = 2, catalyst particle size = 1000 µm– 1400 µm); this however did not denote an observable increase in water conversions and hydrogen purity for catalyst A. With regards to the calculated hydrogen purity for catalyst A, the indifference across all reforming temperature can be attributed to the high efficiency (>98%) of the calculated values when compared to equilibrium values for all reforming temperature utilised as seen in Table 4.2. The similar water conversion fractions for all experimental runs with catalyst A when discussed together with the increasing acetic acid conversion and

hydrogen yield indicates that the steam reforming reaction to syngas is favoured as the temperature is increased, this could also infer that carbon deposition reduces with increasing reforming temperature.

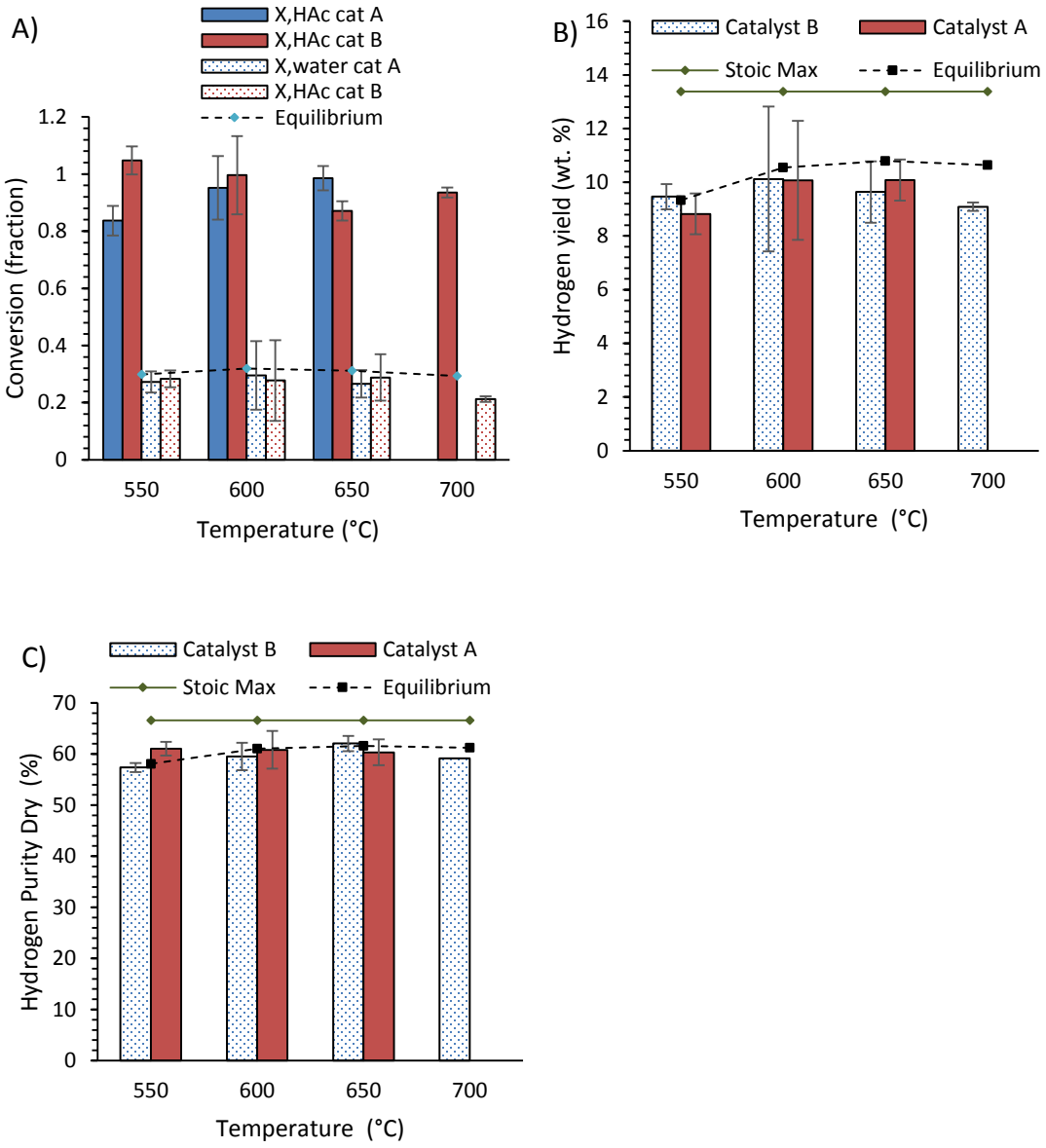

Figure 4.6 Conversion fraction, hydrogen yield (wt. %), hydrogen purity (%) at different reforming temperature (WHSV = 2.5 hr^{-1}, S/C = 2, catalyst particle size = 1000 µm– 1400 µm)

A different observation was observed for steam reforming experimental runs carried out using catalyst B as seen in Figure 4.6 after steam reforming at 550 °C, 600 °C, 650 °C and 700 °C (WHSV = 2hr^{-1}, steam to carbon ratio = 2, catalyst particle size = 1000 µm–

1400 µm); unlike catalyst A, there are no observed trend in conversions (water and acetic acid) and hydrogen yield across the reforming temperatures utilised. This might lead to an inference that the nature of the catalyst in regards to basicity of its support plays a more prominent role in ensuring its stability even at different reforming temperatures.

A comparison of the efficiency of conversions (water and acetic acid), hydrogen yield and hydrogen purity when compared to equilibrium values as seen in Table 4.2 shows that the increase observed for conversions and yield for catalyst A does not indicate a better efficiency when compared to equilibrium values. No trend can be observed for the efficiency of the conversions (water and fuel), hydrogen yield and hydrogen purity for both catalysts across the reforming temperatures utilised.

Table 4.2 Efficiency (%) of conversion (water and fuel), hydrogen yield, and hydrogen purity when compared to chemical equilibrium values (%) at different T_{SR} - (WHSV = 2.5 hr^{-1}, S/C = 2, catalyst particle size = 1000 µm– 1400 µm)

Temp(°C)	Fuel Conversion efficiency (%)		Water Conversion efficiency (%)		Hydrogen Yield (%)		Hydrogen Purity (%)	
	Cat. A	*Cat. B*	*Cat. A*	*Cat. B*	*Cat. A*	*Cat. B*	*Cat. A*	*Cat. B*
550	83.69	104.74	91.14	94.72	94.51	101.40	105.11	98.78
600	95.13	99.60	92.36	86.92	95.48	95.95	99.64	97.51
650	98.51	87.10	85.43	92.60	93.39	89.26	97.98	100.75
700		93.57		72.39		85.38		96.53

4.5.1.2.2 The effect of reforming temperature on selectivity to C- gases and H-gases

Previous studies indicate that the increase in the temperature of reforming should lead to an increase in CO gas composition and a corresponding reduction of CO_2 gas composition in the process gas output [173]; a similar trend was observed in this study for the selectivity to C-gases across the reforming temperatures utilised as seen in Table 4.3. The selectivity to methane also reduces as the reforming temperature is increased corresponding to the selectivity to CO for both catalysts; this confirms the inference that the production of syngas is enhanced as the temperature is increased, the reduction in the selectivity to CO_2 also indicates a reduction in water gas shift reactions as the temperature is increased.

Table 4.3 Selectivity to C-gases and H-gases at different reforming temperature (WHSV = 2.5 hr^{-1}, S/C = 2, catalyst particle size = 1000 µm– 1400 µm)

Temp (°C)	$sel_{i,C}\%$						$sel_{i,H_2}\%$			
	Selectivity to CO (%)		Selectivity to CO_2 (%)		Selectivity to CH_4 (%)		Selectivity to H_2 (%)		Selectivity to CH_4 (%)	
	Cat. A	*Cat. B*	*Cat. A*	*Cat. B*	*Cat. A*	*Cat. B*	*Cat. A*	*Cat. B*	*Cat. A*	*Cat. B*
550	16.90	18.10	79.20	72.30	3.90	9.60	97.50	93.30	2.50	6.70
600	29.90	30.00	68.10	67.90	2.00	2.00	98.70	98.70	1.30	1.30
650	35.30	35.50	64.00	63.90	0.60	0.60	99.60	99.60	0.40	0.40
700		41.60		58.10		0.30		99.80		0.20

In regards to the selectivity to H-gases an obvious increase in selectivity to hydrogen gas is observed as the reforming temperature is increased which subsequently leads to a decrease in the selectivity to methane. The high selectivity to hydrogen gas (>93%) for all experimental runs also affirms that the steam reforming is prominent and dominant in all experimental runs.

4.5.1.3 The effect of catalyst particle size on hydrogen yield, hydrogen purity, conversions and selectivity

The catalyst particle size has a prominent role in determining the efficiency of the steam reforming process; a smaller particle size should lead to an increase in steam reforming efficiency due to an increase in open porosity and active surface area for catalysis. Catalyst A and B were sieved into different sizes (> 1400 µm, 1000- 1400 µm, <1000 µm) before utilisation in steam reforming experiments; the experiments were carried out with the WHSV set to 2.5 hr^{-1}, using steam to carbon ratio of 2 or 3 and T_{SR} set to 600 °C.

It was observed as seen in Table 4.4 that there is an increase in hydrogen yield for the experimental runs carried out as the particle size is reduced; this corresponds to an increase in hydrogen yield efficiency from 86 % to 96 % observed after steam reforming at steam to carbon ratio set to 2 using catalyst B and an increase in hydrogen yield efficiency from 86% and 87% to 93% for catalyst A and catalyst B respectively when

compared to equilibrium values after steam reforming with steam to carbon ratio set to 3.

In regards to the conversion of acetic acid, there is also an increase realised as the particle size of the catalyst is reduced as also detailed in Table 4.4 after the experiments using both steam to carbon ratio set to 2 and 3; a short decline in conversion is however observed for catalyst A when the catalyst size is reduced to < 1000 with steam to carbon ratio set to 3, this can be attributed to the fact that the experimental run were carried out very close to equilibrium and is hence believed to be negligible.

Table 4.4 Conversion (water and fuel), hydrogen yield, and hydrogen purity at different catalyst particle size - (WHSV = 2.5 hr^{-1}, S/C = 2 or 3, T_{SR} =600 °C.)

Catalyst size (µm)	S/C	X_{HAC} (fraction)		X_{H_2O} (fraction)		Hydrogen yield (wt. %)		Hydrogen purity (%)	
		Cat. A	*Cat. B*	*Cat. A*	*Cat. B*	*Cat. A*	*Cat. B*	*Cat. A*	*Cat. B*
>1400	2	0.92	0.91	0.28	0.25	9.77	9.04	60.83	59.28
	3	0.87	0.92	0.20	0.20	9.83	10.01	62.44	61.76
1000 - 1400	2	0.95	1.00	0.27	0.28	9.83	10.12	60.51	59.52
	3	1.00	0.98	0.25	0.21	11.65	10.64	63.42	61.03
<1000	3	0.92	0.99	0.23	0.21	10.64	10.66	62.81	61.08

There was no obvious trend observed for the purity of hydrogen from all the experimental runs; this can be attributed to the high efficiency of the process (>97 % and > 89 % hydrogen purity efficiency when compared to equilibrium and stoichiometric values respectively observed for all experimental runs).

In regards to selectivity to C-gases (Table 4.5), there is also no observed trend identified when the experimental runs are compared; this once again can be attributed to the high efficiency of the process. A minimum of 98 % efficiency was achieved for the selectivity to CO_2 in all experimental runs conducted, while a minimum of 95% efficiency was achieved for the selectivity to CO in all experimental runs conducted when compared to equilibrium values; the exception to these was the selectivity to CO after reforming using steam to carbon ratio set to 3; an efficiency of >63% was achieved when compared to equilibrium values however, this correlates to an increase in the selectivity to CO_2 in the experimental runs.

Table 4.5 Selectivity to C-gases and H-gases at different catalyst particle size - (WHSV = 2.5 hr-1, S/C = 2 or 3, T_{SR} =600 °C.)

Catalyst size (µm)	S/C	Selectivity to C-gases						Selectivity to H-gases			
		Selectivity to CO (%)		Selectivity to CO_2 (%)		Selectivity to CH_4 (%)		Selectivity to H (%)		Selectivity to CH_4 (%)	
		Cat. A	*Cat. B*	*Cat. A*	*Cat. B*	*Cat. A*	*Cat. B*	*Cat. A*	*Cat. B*	*Cat. A*	*Cat. B*
>1400	2	27.80	30.70	70.70	66.60	1.50	2.70	99.00	98.20	1.00	1.80
	3	20.90	20.60	78.40	78.10	0.80	1.30	99.50	99.20	0.50	0.80
1000 - 1400	2	32.50	30.00	66.20	67.90	1.30	2.00	99.20	98.70	0.80	1.30
	3	13.80	23.30	85.90	75.70	0.40	1.00	99.80	99.30	0.20	0.70
<1000	3	17.90	21.20	81.50	77.40	0.60	1.40	99.60	99.10	0.40	0.90

In regards to selectivity to H-gases, all experimental runs exhibited high efficiency when compared to equilibrium values (>98%); this infers that the steam reforming process for the production of hydrogen was occurring and dominant in all experimental runs.

4.5.1.4 The effect of reaction time on hydrogen yield, hydrogen purity, conversions and selectivity

The WHSV (inverse of reaction time) utilised has also been attributed to have an adverse effect on the process analysis of steam reforming; an increase in reaction time leads to an increase in gas yields and conversions of feedstocks [173]. The increase in conversion is due to increase contact time between the reactants and the catalyst hence increasing the steam reforming efficiency. In this study, the effect of reaction or contact time was studied by varying the WHSV utilised between 2.1 and 2.8; the experiments were carried out at reforming temperature set to 600 °C, at steam to carbon ratio set to 3 and catalyst particle size <1000 µm.

The WHSV were varied by changing the nitrogen supplied to the system between 20 sccm and 40 sccm with acetic acid and water flow rates fixed at 0.98 ml/hr and 1.49 ml/hr respectively. The fuel conversion and hydrogen yield increased as the contact time was increased (Table 4.6), there is however no observed trend in the water conversion and hydrogen purity as the different WHSV utilised; the efficiency of the hydrogen purity for all the experimental runs was however >97% and >92% when compared to equilibrium and stoichiometric values respectively, this also equates to >85% water conversion across the experimental runs.

Table 4.6 Conversion (water and fuel), hydrogen yield, and hydrogen purity at different WHSV-(S/C = 3, T_{SR} =600 °C.)

WHSV (hr^{-1})	X_{HAC} (fraction)	X_{H_2O} (fraction)	Hydrogen yield (Wt. %)	Hydrogen purity (%)
2.1	1.01	0.21	10.72	61.73
2.3	1.00	0.21	10.64	61.17
2.5	0.92	0.23	10.64	62.81
2.8	0.82	0.22	9.91	64.27

In regards to selectivity to C-gases as observed in Table 4.7, there is no obvious trend in the selectivity of all carbon gasses observed; this however equates to 100% efficiency and > 92% efficiency for selectivity to CO_2 and CO respectively when compared to equilibrium values. The only exception was when the WHSV was set to 2.5 where the selectivity to CO was < 90% this however corresponds to a slight increase in the selectivity to CO_2 and hence is considered negligible.

Table 4.7 Selectivity to C-gases and H-gases -(S/C= 3, T_{SR} =600 °C.)

WHSV	Selectivity to CO (%)	Selectivity to CO_2 (%)	Selectivity to CH_4 (%)	Selectivity to H (%)	Selectivity to CH_4 (%)
2.1	20.00	79.20	0.9	99.50	0.50
2.3	20.00	78.30	1.6	99.00	1.00
2.5	17.90	81.50	0.6	99.60	0.40
2.8	20.00	79.30	0.7	99.60	0.40

In regards to selectivity to H-gases, all experimental runs had a high affinity towards hydrogen production with very little methane (<1%) produced in the process gas output.

4.5.2 The steam reforming of acetic acid- carbon deposition on the used catalyst and condensate

Carbon deposition has been attributed to be prominent in the reforming of acetic acid due to coking and several side reactions that could be occurring [178]; the type of carbon formed has however been a subject of debate in several studies. It is nevertheless agreed that the carbon deposited on the catalyst would lead pore blockage and deactivation of the active sites of the catalyst [187-190]. Carbon could also be found in the collected condensate due to unreacted feedstock or side reactions from the

reforming process; it is hence essential to also evaluate and quantify the carbon content in the condensate to ascertain the efficiency of the reforming process.

4.5.2.1 Carbon content in the collected condensate

The carbon in the condensate were quantified through TOC analysis as seen in Table 4.8; the experiments were carried out at a T_{SR} set to 600°C or 650°C, S/C set to 3 and using catalyst A and catalyst B (<1000 µm particle size). It has been previously reported that the carbon found in the condensate might be directly linked to the WHSV utilised [53]; it was inferred that an increase in the carbon content in the condensate would increase as the WHSV utilised is increased. This was not the case in the experimental runs as no trend was observed for all experimental runs conducted; the presence of organic carbon might suggest incomplete conversion of the feedstock or the advent of side reactions, however, the carbon found amounted to <0.2% of the carbon in the process after carbon balance analysis for all experimental runs conducted. This ascertains that majority of the carbon in the process is utilised for steam reforming and are either deposited on the catalyst or converted and released in the process gas output.

Table 4.8 Carbon content of the Condensate after steam reforming at different WHSV and T_{SR} using Catalyst A and B (S/C=3)

	T_{SR} (°C)	WHSV (hr^{-1})	Mol of carbon (mol)
Catalyst A	600	2.1	1.15×10^{-5}
		2.4	18.42×10^{-5}
Catalyst B	600	2.2	3.58×10^{-5}
		2.3	5.76×10^{-5}
		2.4	3.58×10^{-5}
		2.5	1.31×10^{-5}
	650	2.5	5.95×10^{-5}

4.5.2.2 Catalyst characteristics and carbon content in the used catalyst

Majority of the carbon from the feedstock in the steam reforming of acetic acid as already discussed are either utilised and converted to process gas output or deposited on the catalyst; SEM images of the used catalyst in all experimental runs investigated after steam reforming indicates the presence of filamentous carbon as seen in Figure 4.7. This is in accordance to previous suggestion from literature that filamentous carbon are formed after the steam reforming of acetic acid over Ni catalyst [186].

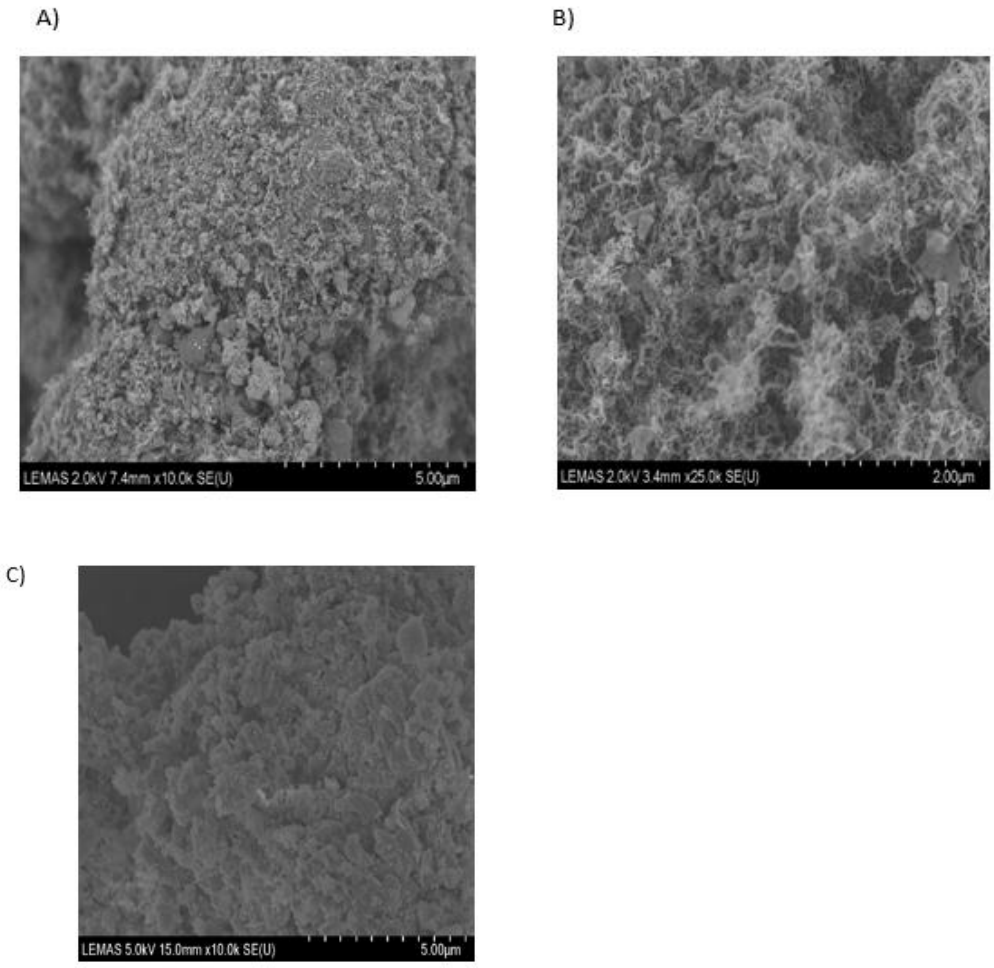

Figure 4.7 SEM images of A) and B) used reforming catalyst, and C) Fresh catalyst (T_{SR}= 600 °C, S/C =3, WHSV =2.5)

The nature of the carbon deposited has always been debated with several articles inferring that the carbon formed on the catalyst surfaces are majorly in the form of whiskers [191, 192], while others have argued that they are disordered polyaromatic carbonaceous deposits [193, 194].

TGA-FTIR analysis of the used catalysts after steam reforming (Figure 4.8) indicates the presence of two CO_2 peaks as already reported in previous studies [172, 194, 195]; it is generally agreed that the CO_2 peak formed at the lower temperature is majorly coke formed on the active surface of the catalyst while the more prominent peak at the higher temperature can be attributed to coke deposited on the catalyst support.

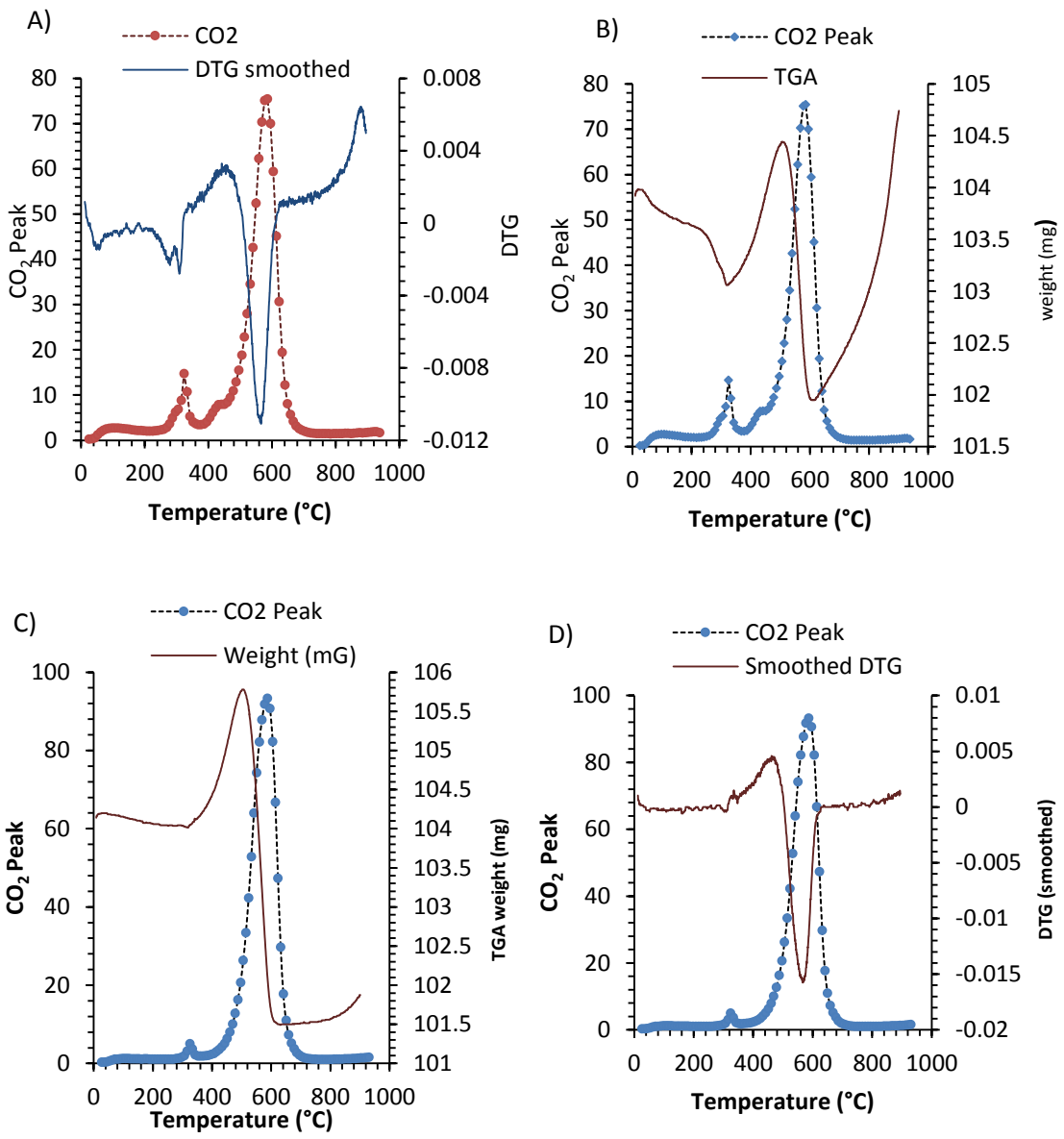

Figure 4.8 TGA FTIR analysis of used Catalyst A after steam reforming at A and B) S/C=2, C and D) S/C =3 (T_{SR} =600 °C and WHSV =2.5 hr^{-1})

As seen in Figure 4.8 C and D, the smaller peak formed in the lower temperatures are less prominent in the catalysts with reforming performed using S/C set to 3; these affirms that the coke deposited particularly on the active surfaces are influenced by the steam to carbon ratio utilised.

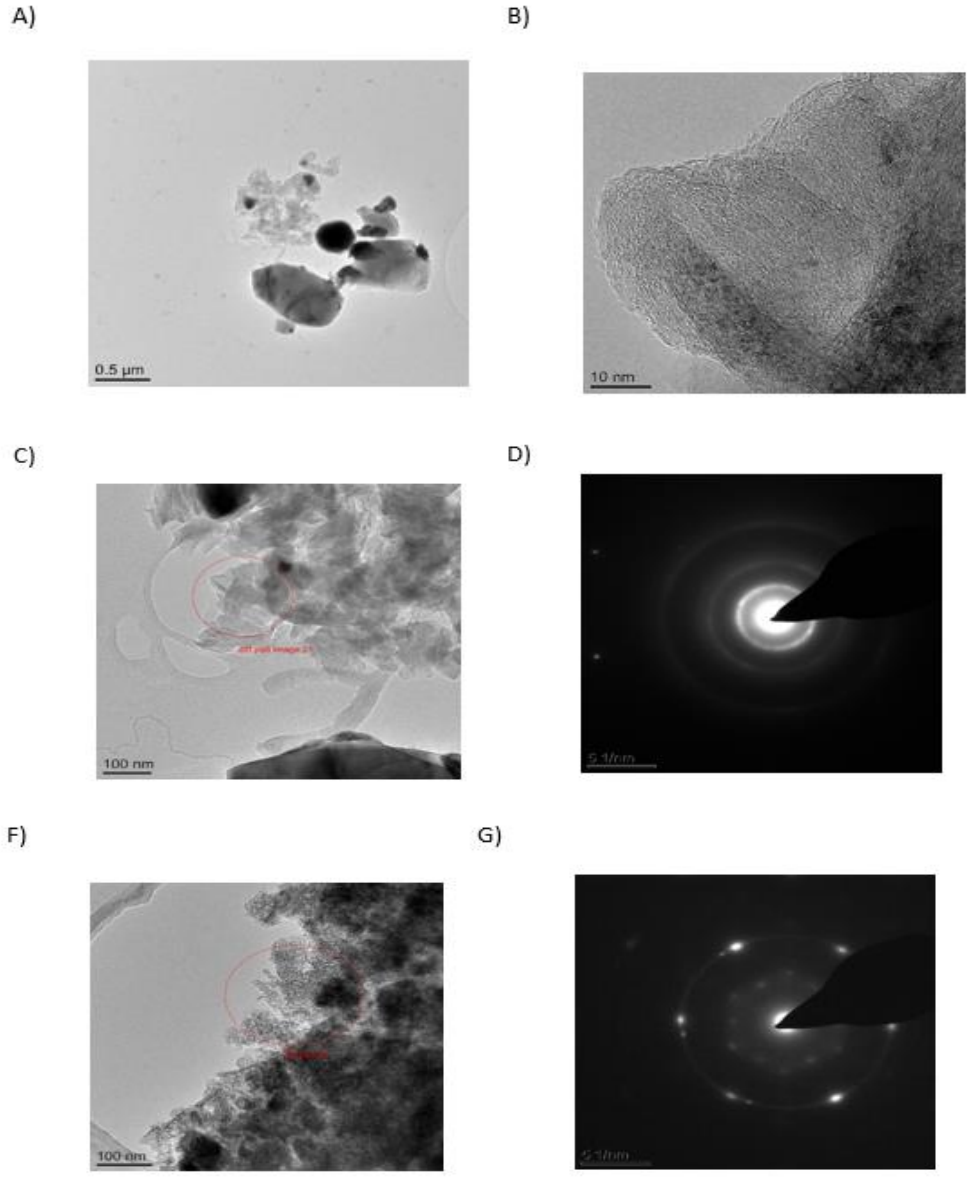

Figure 4.9 TEM images and diffraction patterns of used reforming catalysts 3 (T_{SR} =600 °C and WHSV =2.5 hr-1, S/C=3)

TEM images (Figure 4.9) of the used catalyst A after steam reforming at S/C set to 3 and T_{SR} set to 600 °C gives an indication of the types of carbon formed; it can be observed from Figure 4.9A that the carbon formed is dispersed and is not uniformly distributed across the catalyst. Figure 4.9B indicates a poly crystalline plane which infers that crystalline carbon is formed; It has been reported that the type of carbon formed in the catalyst support as indicated in the higher peaks of CO_2 in the FTIR chemigram are either poly aromatic or polycrystalline structures which are graphitic-like in nature [196], as

also confirmed from the diffraction pattern (Figure 4.9G) of the TEM image of Figure 4.9F. Amorphous carbon is also formed particularly on the active surface of the catalyst as indicated in which is the diffraction pattern of the TEM image seen in Figure 4.9C; this has also been reported in previous literature on the reforming of acetic acid [167] and can be Figure 4.9 attributed to be the CO_2 formed on the lower temperature on the FTIR chemigram.

4.6 Conclusion

The steam reforming of acetic acid was reviewed experimentally in this chapter with the view to ascertain the optimal conditions suitable for process intensification measures to be investigated and discussed in subsequent chapters. The steam reforming process was dominant and efficient in all experimental runs investigated with high yield of hydrogen with purity close to equilibrium values. It was also established that the T_{SR}, S/C, pre-heating temperature and WHSV has an influence on the efficiency of the process analysis particularly with respect to the yield of hydrogen, feedstock conversions and selectivity (C and H gases). It was also ascertained that the carbon found in the condensate can be said to be negligible after carbon balance as >99 % of the carbon in the fuel is converted to process gas outputs after steam reforming or deposited on the reforming catalyst in the form of poly crystalline aromatic structures or amorphous carbon.

In regards to optimality, the fuel pre-heating temperature is set <70°C while the water pre-heating temperature is set >120°C in further experiments (CLSR experiments and SE-CLSR experiments); this is done to prevent pyrolysis of the fuel and also ensure water is fed as steam. Subsequent experiments are also conducted at T_{SR} set to 600 °C or 650 °C at S/C set to 2 or 3 and WHSV set between 2.3 hr^{-1} to 2.5 hr^{-1} for CLSR and < 2 hr^{-1} for SE-CLSR experiments due to the additional presence of the sorbent.

Chapter 5 Chemical looping steam reforming of acetic acid

5.1 General overview

Chemical looping steam reforming has been promoted as a viable measure of improving the efficiency of the steam reforming process of biomass derived oils; as described in previous chapters, looping processes are important process intensification measures in dealing with the external heat demand of the reforming process. Chemical looping reforming is also regarded as an important and promising process intensification measure due to the in-situ CO_2 capture that is also possible particularly when a sorbent is also looped across the process, it also helps in the regeneration and longevity of steam reforming catalysts as carbon produced during the reforming step can be oxidised in the oxidation step. This is vital in the sustained reforming of feedstocks that are easily prone to thermal decomposition and coking like acetic acid as detailed in Chapter 4. It is therefore essential to study the redox cyclic ability of the oxygen carrier utilised particularly when a feedstock prone to coking and thermal decomposition like acetic acid is utilised; this would also give a basis to understand the process when bio-oils are utilised, given the high concentration of acetic acid in biomass pyrolysis oils generated via fast pyrolysis processes.

Previous work on the chemical lopping reforming of acetic acid and other liquids of biomass origin with or without sorption enhancement have been centred on the reactivity of the catalyst across looping cycles; it has been reported that the fuel conversion and consequently hydrogen yield reduces upon cycling for the CLSR of bio-diesel and scrap tyre pyrolysis oils [197, 198]. Other studies indicated that no deterioration occurs in fuel conversion and hydrogen yield from the CLSR of other liquids of biomass origins investigated [96, 99, 199]. Thus, the efficiency of the fuel conversion and hydrogen yield of CLSR is influenced by the feedstock and operating conditions utilised, and the deterioration of the reactivity of the catalyst is generally due to carbon deposition, sintering and thermal decomposition of the feedstock.

As detailed in previous chapters, the catalysts support may have an adverse effect on the reactivity and efficiency of looping catalysts; Luis et al. [200] in a study on the effect of the catalyst support on oxygen carriers in the chemical looping reforming process using Nickel-based oxygen carriers concluded that Nickel-based catalysts with α-alumina supports are more durable as oxygen carriers when compared to the corresponding catalyst with γ-alumina support, they however also stated that both catalysts behave consistently during oxidation runs in the looping process. The underperformance of nickel-based catalyst with γ-alumina support when compared to Nickel-based catalyst on α-alumina was also discussed and attributed to partial auto-reduction of the catalyst noticed in nickel-based catalyst with γ-alumina support in another study [201].

The auto-reduction capability of the catalyst by the fuel feedstock is another important part of the chemical looping process as it affects the overall efficiency of the process. A dead time has been identified in some studies which indicates that the auto-reduction process and the steam reformatting process can be mutually exclusive and occur independently, with reduction completing before full steam reforming is established [202, 203]. Partial auto-reduction and distinct intermediate sections where both reduction and reforming processes occur simultaneously have however been observed and identified in some studies [167, 201]; the competition between steam reforming and auto-reduction of the catalyst in the intermediate stages might lead to increased thermal decomposition of feedstock and hence enhanced coking. This prompted the need for the use of a multifunctional catalyst by the addition of Palladium (Pd) to a Nickel-cobalt catalyst to act as oxygen carrier in the chemical looping reforming of acetic acid in a study by Moulijn et al. [99], the addition of Pd was to ensure catalyst activation and reactivity was maintained without the need of extra reduction of the catalyst, it was generally assumed that reduction of the catalyst was done by produced hydrogen hence lowering the overall hydrogen yield and leading to thermal decomposition of acetic acid. It was however observed and concluded in other studies on bio-oil and acetic acid that auto-reduction of the catalyst can occur efficiently without maximal effect on the products in the reforming process [96, 167].

The auto-reduction capabilities of acetic acid have been investigated in great detail using nickel-based catalyst on α-alumina[167]; it was observed for the catalyst utilised that auto-reduction and steam reforming occur simultaneously with a short lag or dead period, it was also stipulated that the lowest auto-reduction temperature for this catalyst is 550° C. It was also highlighted that increasing steam to carbon ratio of the reforming process whilst having a positive effect on the reforming reaction had a negative effect on the auto-reduction potential of the feedstock. It was hence suggested that a changing steam to carbon ratio could be introduced with a lower steam to carbon ratio utilised for auto-reduction and a higher one utilised for steam reforming [167]. The challenge therein of using different steam to carbon ratio for the reduction and reforming process is the short time identified for dominant auto-reduction of acetic acid before reforming kicks in, another school of thought is the fact that the presence of additional steam could also lead to steam gasification of carbon deposited.

In this chapter the redox cyclic ability of the chemical looping reforming of acetic acid is investigated using catalyst A and B as described in chapter 3.2.1 , the influence of the oxidation temperature in regards to full oxidation of the nickel catalysts and carbon burning is also investigated for both catalyst, a full carbon balance is also carried out for the whole cyclic process over 5 reforming cycles to estimate the efficiency of the overall process. This would serve as a basis for ascertaining the stability of the catalyst for sorption enhanced chemical looping steam reforming which will be investigated in the next chapter.

5.2 Experimental approach and methods

5.2.1 Material for CLSR

Catalyst A and B as described in chapter 3.2.1 were crushed and sieved to 250-350 µm before utilization; Catalyst A was utilised in this study as it has been regarded to be very efficient for looping processes in regards to durability and low fluidization problems [155], Catalyst B was also utilised to exemplify the advantages of an alkali metal on the support of reforming catalysts in regards to increased mobility on the surface of catalyst

and the prevention of coking. The reactor system and configuration is the same as described in chapter 3.3 for chemical looping steam reforming and, acetic acid and distilled water utilised are also as described.

5.2.2 Experimental procedures for CLSR

Chemical looping steam reforming consists of two basic steps; the reducing or reforming step (fuel-steam feed) and the oxidation step (air feed). Both steps as carried out in this study are preceded by purging the reactor system with N_2 (200 sccm) and raising the temperature of the furnace to the required temperature for each phase. The reforming/reforming step was carried out at temperatures: 600°C and 650°C and at S/C set to 3 using the feed rates of water and acetic acid as already described in chapter 3.3; this is because previous studies on pyrolysis oils and their model compounds as reviewed and discussed in previous chapters indicate that the reforming process is optimal at this range [95, 100, 153, 162, 167].

Studies on the effect of water content on the auto-reduction rate of acetic acid also stipulates that auto-reduction is optimal at steam to carbon ratio of 2 however S/C set at 3 shows great promise [167].

The global reactions that are expected to occur in the fuel-feed step for the chemical looping reforming of acetic acid is summarised and expressed as follows;

Reaction 5.1 Stoichiometric reactions occurring in fuel feed stage of CLSR

$$C_2H_4O_2 + 4NiO \rightarrow 2CO_2 + 2H_2O + 4Ni \qquad \text{A}$$

$$C_2H_4O_2 + 2H_2O \xrightarrow{Ni} 2CO_2 + 4H_2 \qquad \text{B}$$

This includes the auto-reduction of the catalyst by acetic acid (Reaction 5.1A), and the complete steam reforming of acetic acid (Reaction 5.1B). The Sequence of reactions for the reducing or reforming phase is however more complex than what is described in Reaction 5.1 as other intermediate and side reactions might occur (discussed in chapter 4.2). Intermediate reactions might include NiO reduction by CO, H_2 and other hydrocarbon intermediates, side reactions include coking, formation and dissociation of

intermediates, decomposition of acetic acid, ketonisation and sometimes methanation reactions, and water gas shift [167].

The reducing step for all CLSR runs in this study was carried out for 2 hrs; using 2 grams of catalyst. The catalyst as prepared into granules is first reduced or activated by 5% H_2/N_2 (Reaction 5.2) at the temperature set for the reducing phase. Auto-reduction of the catalyst by acetic acid in subsequent cycles is also carried out after the oxidation step at the temperature set for the reducing step; this is ≥ 550°C for all experimental runs and has been reported to be adequate for full reduction of Ni based catalysts by acetic acid [164].

Reaction 5.2 Activation of catalyst by hydrogen

$$NiO + H_2 \rightarrow Ni + H_2O$$

The oxidation step was done at temperatures ranging between 600° C and 800° C with the view to evaluate the effect of the oxidation temperature (T_{OX}) on the overall process; air was passed through the reactor to re-oxidise the already utilised catalysts from the reducing/reforming step (Reaction 5.3A) while also gasifying carbon formed on the catalyst from the preceding fuel feed stage (Reaction 5.3B and 5.3 C). The air feed during the oxidation step was allowed to run until the concentration of oxygen detected in the micro-GC stabilised at 21 Vol%.

Reaction 5.3 Reactions in air feed stage

$$2Ni + O_2 \rightarrow 2NiO \quad \text{A}$$

$$C + O_2 \rightarrow CO_2 \quad \text{B}$$

$$2C + O_2 \rightarrow 2CO \quad \text{C}$$

Another set of chemical looping experimental runs were also conducted using 2 grams of catalyst and 2 grams of inert (sand) in the reactor bed; this was done with the basis of understanding the influence of an additional material on process output and overall efficiency. This would be vital in the next chapter where a sorbent would be added to the catalyst bed.

5.3 Process outputs and material balances

The process outputs as detected by the micro-GC was used to determine the yield of hydrogen, fuel conversion, water conversion and selectivity to carbon gases on the basis of elemental balance. The calculations for the process analysis are as described Chapter 4 for steam reforming of acetic acid, and just like in the steam reforming experiments the calculated results from each experimental run were also compared with stoichiometric and equilibrium values with the view to ascertain the efficiency of the process.

Further calculations using elemental balances were made particularly for the additional air feed stage which is not present in the steam reforming process; they were calculated with the view of ascertaining the efficiency of the oxidation of carbon and nickel in the air feed, and also for the calculation of a full carbon balance the process.

The total gas molar flow rate ($\dot{n}_{out,dry}$) was calculated using a nitrogen balance just like in the steam reforming process, however nitrogen flow-in during the air feed stage was calculated from the nitrogen already present in air as no extra nitrogen flow was passed through the system as in the case of steam reforming.

The molar flow rate calculated was used to calculate the rate of the oxidation of carbon deposited from the prior steam reforming phase ($\dot{n}_{c,gas}$) using a carbon balance as expressed in Equation 5:1; $\dot{n}_{c,gas}$ is then integrated over time to calculate the total number of moles of carbon gasified (n_{Cgas}) in the oxidation stage, this is paramount for calculating the overall carbon balance of the process and extrapolating the extent of carbon gasified (number of moles of carbon gasified at a time with respect to the total number of moles gasified at the air feed stage).

Equation 5:1 Rate of oxidation of Carbon

$$\left(\dot{n}_{c,gas}\right) = \dot{n}_{out,dry} \times (y_{CO} + y_{CO_2})$$

The rate of the oxidation of the reduced catalyst ($\dot{n}_{Ni \rightarrow NiO}$) was also calculated using the total gas molar flow rate via an oxygen balance as expressed in Equation 5:2 using

an oxygen balance; this rate is also integrated to calculate the number of moles of Nickel oxidised over time till a steady oxygen production was detected in the product gas composition from the micro-GC, which is then used to calculate the extent of Nickel conversion (Equation 5:3). The time for full Nickel oxidation was also estimated from the calculated extent of nickel oxide.

Equation 5:2: Ni Oxidation rate

$$(\dot{n}_{Ni\rightarrow NiO}) = 2\dot{n}_{O_2,in} - \dot{n}_{out,dry} \times (2y_{O_2} + y_{CO} + 2y_{CO_2})$$

Equation 5:3: Extent of Ni Oxidation, $X_{Ni\rightarrow NiO}$ (%)

$$X_{Ni\rightarrow NiO}\ (\%) = \frac{n_{Ni,t}}{n_{Ni(i)}} \times 100$$

The selectivity of the products in the oxidation phase was also calculated on two ways, on oxygen basis to take into account nickel oxidation as expressed in Equation 5:4 and also on carbon basis as calculated for in steam reforming experiments. This gave an indication of the efficiency of the oxidation process and the dynamics of the oxidation step.

Equation 5:4: Selectivity Oxygen basis

$$Sel_{CO\ or\ CO_2}\ (\%) = \frac{\left(y_{CO} \text{or } 2y_{CO_2}\right) \times \dot{n}_{out,dry}}{(y_{CO} + 2y_{CO_2}) \times \dot{n}_{out,dry} + \dot{n}_{Ni\rightarrow NiO}} \times 100$$

$$Sel_{NiO}\ (\%) = \frac{\dot{n}_{Ni\rightarrow NiO}}{(y_{CO} + 2y_{CO_2}) \times \dot{n}_{out,dry} + \dot{n}_{Ni\rightarrow NiO}} \times 100$$

Full carbon balance was done by calculating the total carbon output from the process; this is defined in the chemical looping reforming process as the addition of the total number of moles of carbon oxidised in the oxidation phase, plus the total number of moles of carbon detected in the received condensate for each cycle and the total carbon detected from the micro-GC in the product gas composition.

The total carbon detected in the condensate was extrapolated through TOC differential test analysis, the total number of moles of carbon from the air feed stage was calculated

by integrating the molar flowrate of carbon produced in the oxidation cycle (Equation 5:1), and the total number of moles of carbon from the product gas during the reduction can be calculated by multiplying the molar fractions of all carbon products detected by the total molar flowrate ($\dot{n}_{out,dry}$) in the reducing phase. More details in regards to the calculations for the carbon balance is giving in the appendices (Appendix 2 Carbon balance Calculation)

5.4 CLSR solids and condensates characterisation

Characterisation work was also carried out on the used catalyst and the collected condensate to analyse the amounts of carbon and hydrogen deposited over cycles and observe any changes in morphology after chemical looping steam reforming. CHN elemental analysis was utilised to calculate the carbon content of the utilised catalyst; this is essential to determine the number of moles of carbon present at the end of the last reducing step since it would not be oxidised as per previous cycles.

BET analysis was conducted using a Quantachrome Nova 2200e instrument to observe any changes in the open porosity and surface area of the used catalyst. ICP test and TOC tests were carried out on the collected condensate to determine the Ni ion content and carbon content respectively. SEM-EDX and TEM surface analysis were carried out on the used catalyst for surface topography analysis this is essential in determining carbon element distribution on the surface of the used catalyst, it also gives a clear description of the size of filamentous carbon formed, and EDX analysis can be used in estimating quantitatively the carbon present in the used catalyst.

TGA-FTIR was also carried out on the used looping catalysts under the same TPO conditions as described for steam reforming conditions; like the steam reforming runs, the CO_2 chemigram profile from the FTIR analysis is examined and compared to the loss of weight shown through the TGA analysis. This gives an estimation for the reason for the loss of weight in the TGA run and the type of carbon deposited.

5.5 Results and discussion

5.5.1 Process outputs with time on stream and upon redox cycling of CLSR-HAc

The gases detected by the micro-GC for all experimental runs in this study were CO, CO_2, CH_4, C_2H_6, C_3H_8, (the last two always remaining below threshold of detection), H_2, N_2, and O_2 (observed during the oxidation steps). In the event of acetone being a significant product of the process, it would have been detected by significant C content in the condensates. Ketonisation reactions are generally inhibited by nickel catalysts and are stipulated to occur during the reforming of acetic acid ideally at temperatures below 600°C [204, 205].

5.5.1.1 Process outputs with time on stream- fuel-water feed stage

The fuel-water feed stage was carried out at 600°C and 650°C for all experimental runs in this study, it was preceded either by catalyst activation/ reduction by hydrogen (1st Cycle) or by auto-reduction by acetic acid. A similar trend for the main output gas species molar fractions with time on stream was observed for the first cycle (H_2 reduced catalyst) and subsequent cycles (auto-reduced) for the experimental runs as shown in Figure 5.1 for catalyst B (T_{SR} =600°C, T_{OX} =600°C, S/C= 3, WHSV = 2.5hr^{-1}). This is similar to the product gas profile noticed during steam reforming experiments and is indicative that steam reforming of the feedstock occurred efficiently in all reduction phase runs.

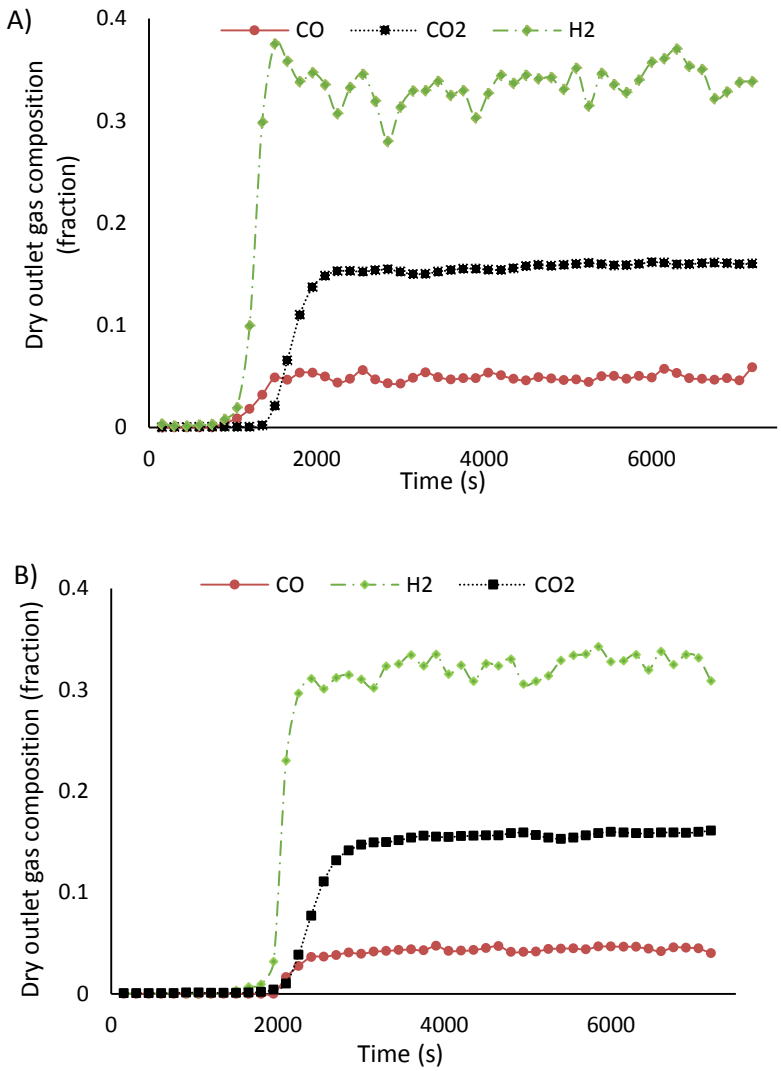

Figure 5.1: Dry outlet gas composition of products after reforming at (A) cycle one where the catalyst has been activated by reduction with hydrogen (b) Auto reduced catalyst (i.e. catalyst reduced with acetic acid) at the 5th reduction run (after four oxidation runs) (T_{SR}= 600 °C, T_{OX} =600 °C, catalyst B, WHSV=2.5 hr^{-1}, S/C=3)

In the H_2 reduced cycle, CO is detected ca. 500s earlier than CO_2 whereas in the autoreduced cycle, CO and CO are simultaneously detected. Similarly, the lag between H_2 and CO generation is increased by 250 s for the autoreduced cycle. This is consistent with a steam reforming reaction delayed by the consumption of the fuel to carry out the reduction of the nickel oxide to metallic nickel, with the steam reactant exhibiting temporary faster reactivity for dissociation to hydrogen on the reduced catalyst compared to the hydrocarbon reducing reactions and steam reforming. This has also been observed in previous studies where a short lag period or simultaneous partial auto

reduction and reforming reactions are observed [167]. A similar dry outlet gas composition profile was derived for the H_2 reduced cycle and auto reduced cycle when catalyst A was utilised with a slight increase in the lag (50s – 200s) between CO and H_2 generation in the auto reduced cycle.

The only exception to this stable trend of dry outlet gas composition in the reducing phase occurred during the 2nd reducing phase of the chemical looping reforming of acetic acid using catalyst A with T_{SR} set as 600° C and S/C set as 3. This experimental run was carried out with the oxidation temperature set at 600° C; the reason for this anomaly would be discussed in full detail in subsequent sections.

5.5.1.2 Process gas output (oxidation phase) and extent of oxidation

The oxidation phase in this study was carried out between 600°C and 800° by passing air through the reactor. An increase of approximately 30 – 50°C was observed at the beginning of all oxidation phase runs; this was due to the exothermic nature of the oxidation reactions.

The operating conditions at which the oxidation phase is conducted has an effect on the overall process efficiency; it is also fitting to check the extent of oxidation of carbon and nickel during the air feed stage with the view to ascertain the effectiveness of the air feed stage. Five chemical looping cycles (4 oxidation phase runs) were conducted on catalyst B at WHSV 1.18 hr^{-1} and S/C of 3 to check the oxidation effectiveness. Air was passed at 200 sccm and 2g of inert material (sand) were mixed with catalyst B (2g) in the reactor load, this is with the view to aid comparison with the SECLSR experimental runs as detailed in the next chapter (the effect of the inert material is also detailed in the next chapter). The oxidation temperature under air feed was also set at 800 °C while the reducing phase was carried out at 650 °C.

The process gas composition detected by the micro GC for all oxidation runs contained oxygen, CO and CO_2 as depicted in Figure 5.2;

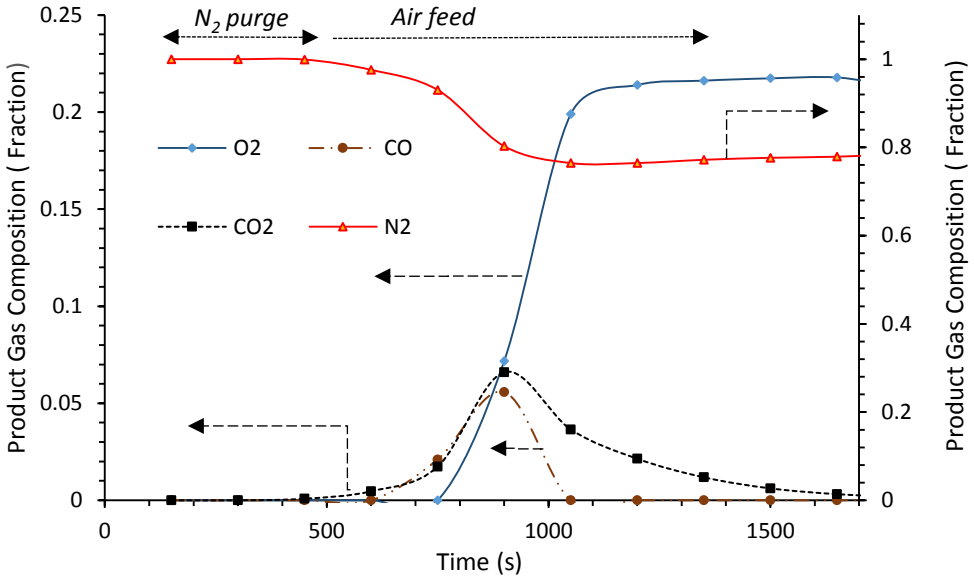

Figure 5.2: Product gas composition of oxidation phase for CLSR experiments (T_{SR}= 650 °C, T_{OX} =800 °C, catalyst B, WHSV=1.18 hr^{-1}, S/C=3)

The CO and CO_2 indicate the oxygen passed through air was utilised in oxidation of carbon that had been formed during the preceding fuel-steam feed stage; it is also expected as reported in several literature on CLSR that the catalyst is oxidised from its catalytically active nickel state to deactivated nickel oxide [167, 206].

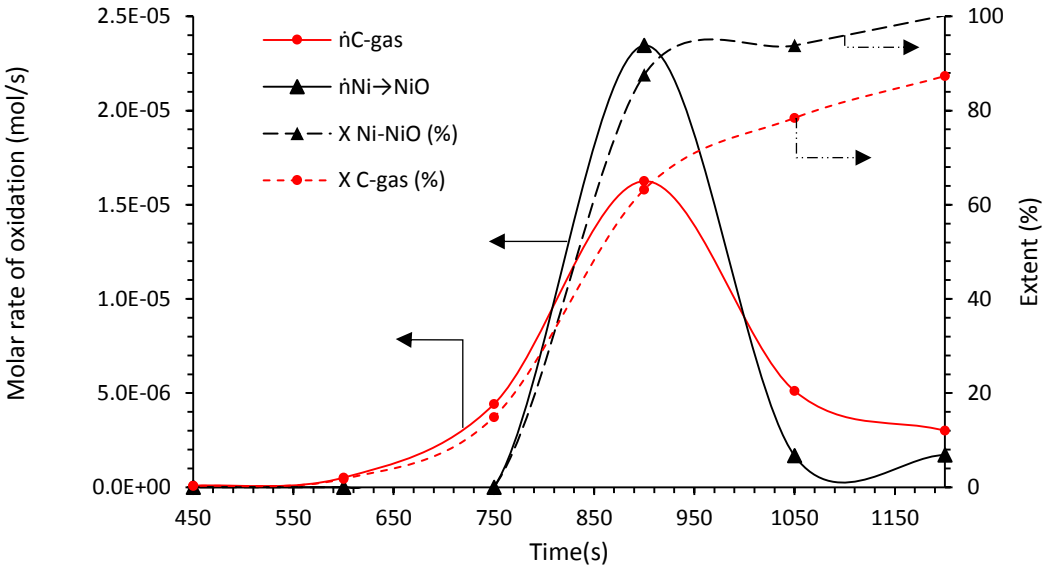

Figure 5.3: Rate of oxidation of carbon and nickel, and extent of nickel and carbon oxidised in oxidation step 1 (T_{SR}= 650 °C, T_{OX} =800 °C, catalyst B, WHSV=1.18 hr^{-1}, S/C=3)

Using the first air feed stage as a basis for comparison between the three oxygen product (CO, CO_2 and NiO), Figure 5.3 shows the rate of oxidation of carbon molecules ($\dot{n}_{c,gas}$) and the rate of oxidation of nickel ($\dot{n}_{Ni\rightarrow NiO}$) calculated using Equation 5:1 and Equation 5:2 Viewed together with the extent of nickel ($X_{Ni\rightarrow NiO}$) and extent of carbon gasified (X_{C-gas}) calculated by taking the percentage of the mol of carbon gasified per time against the total ammount of carbon gasified (mol) in the air feed stage, these confirm that the oxygen consumed was utilised for both nickel oxidation and gasification of carbon, with carbon gasification starting 300s before the nickel oxidation begins.

The selectivity to oxygen containing compounds with time on stream (Figure 5.4) calculated using Equation 5:4 also indicates, complete oxidation of accumulated carbon to CO_2 is the more prominent reaction for the carbon oxidation reactions in the air-feed stage. A similar profile was observed for the elemental analysis in the subsequent oxidation runs of the CLSR cycles.

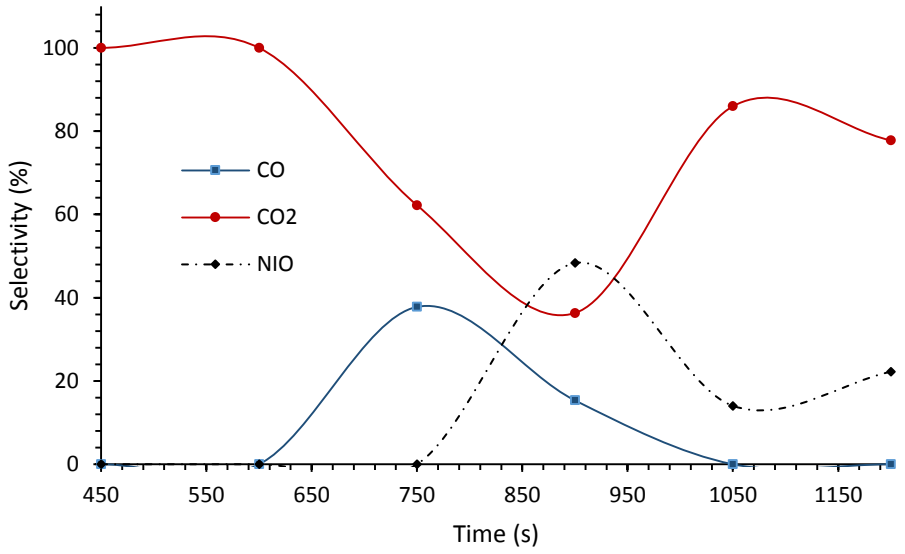

Figure 5.4: Selectivity oxygen basis for 1st air feed stage (T_{SR}= 650 °C, T_{OX} =800 °C, catalyst B, WHSV=1.18 hr^{-1}, S/C=3)

Review of the literature indicate that the oxidation of carbon may occur first before the diffusion controlled Nickel oxidation [101, 206]; however, it was observed in this study

that both reactions occur in parallel with carbon oxidation starting first and freeing up space on the nickel catalyst which is then oxidised whilst more carbon is burnt off.

A more accurate way of detecting the extent and nature of oxidation is by the use of the selectivity to Carbon gases, at the point of carbon peak for oxidation cycle 1 the selectivity to CO (Carbon basis) was 45 % while the selectivity of CO_2 was 55 %. Integrating the rates of the nickel oxidation ($\dot{n}_{Ni \rightarrow NiO}$) over time allows to determine whether the nickel redox extent ($X_{Ni \rightarrow NiO}$) are maintained at the same level from cycle to cycle.

The number of moles of nickel oxidised at steady oxygen output (evidencing the end of oxidation reactions) is shown in Table 5.1; there is a drop in the extent of nickel oxidised and an increase in the duration of Ni oxidation from the first oxidation cycle to subsequent oxidation cycles, however the extent of nickel oxidation remained >80% across the other cycles. This indicates that the oxidation of nickel can be maintained across the oxidation cycles.

Table 5.1: Nickel oxidised in CLSR oxidation stage (T_{SR}= 650 °C, T_{OX} = 800 °C, catalyst B, WHSV=1.18 hr^{-1}, S/C=3)

	$n_{Ni,t}$ (mol)	$X_{Ni \rightarrow NiO}$ (%) (Equation 5:3)	Duration of Ni Oxidation (s)
1	4.03×10^{-3}	100.22	449
2	3.80×10^{-3}	94.63	634
3	3.25×10^{-3}	80.83	557
4	3.37×10^{-3}	83.97	536

5.5.1.3 Overall carbon balance of CLSR process

An overall carbon balance was carried out on the CLSR process (using the set operating conditions as described in 5.5.1.2) as detailed in Table 5.2; an average of 1.3 % of the carbon calculated through the carbon balance was unaccounted for in the overall process across 5 cycles, indicating high accuracy of the carbon balance and distribution across products for the 5 cycles, as well as validating the methodology for their calculation.

Table 5.2: Overall carbon balance of CLSR process (T_{SR}= 650 °C, T_{OX} =800 °C, catalyst B, WHSV=1.18 hr^{-1}, S/C=3)

	C in feed (mol) During HAc/steam feed	X_{HAc} (%) (Equation 4:1)	C product during HAc/steam feed (mol)	n_{Cgas} (mol)	C in the condensate (mol)	Total carbon (gas + solid + condensate) (mol)
1	6.82×10^{-2}	93.1	6.35×10^{-2}	5.04×10^{-3}	1.99×10^{-5}	6.86×10^{-2}
2	6.82×10^{-2}	85.9	5.86×10^{-2}	6.19×10^{-3}	4.48×10^{-5}	6.49×10^{-2}
3	6.82×10^{-2}	85.7	5.86×10^{-2}	9.64×10^{-3}	3.39×10^{-5}	6.83×10^{-2}
4	6.82×10^{-2}	91.8	6.26×10^{-2}	7.19×10^{-3}	1.39×10^{-5}	6.98×10^{-2}
5	6.82×10^{-2}	84.5	5.76×10^{-2}	7.91×10^{-3}	0.10×10^{-5}	6.55×10^{-2}

The carbon share of the carbon in the product across the process cycles is illustrated in Table 5.3, The carbon distribution in the products across the process cycles indicates the major share of carbon was in the process gas (85%-92%) and as a solid on the oxidised catalyst (7% -14%) across all cycles, where n_{Cgas} represented deposited solid carbon from the previous cycle; these entail that most of the carbon in the feedstock is utilised in the process for auto-reduction and steam reforming, whilst approximately 10 % is deposited on the catalyst; it is essential to stress that the amount deposited on the catalyst must have been influenced by the presence of the inert material in the reactor load; these will be discussed in full details in the next chapter. Carbon in the condensates was negligible (<0.1%) in all the cases.

Table 5.3: Share of C-Out across the process cycle (Reforming temperature= 650 °C, oxidation temperature =800 °C, catalyst B, WHSV=1.18 hr^{-1}, S/C=3)

	C-in gas (%)	C oxidised/ on catalyst (%)	C- condensate (%)
1	92.61	7.36	0.03
2	90.39	9.54	0.07
3	85.82	14.13	0.05
4	89.69	10.29	0.02
5	87.92	12.07	0.02

5.5.2 Effect of oxidation temperature on process outputs

The effect of T_{OX} on chemical looping steam reforming of acetic acid was investigated by oxidising the used reforming catalyst (catalyst A) at 600 °C, 700 °C and 800 °C. T_{SR} was kept at 600 °C and the experiments were carried out at S/C of 3 and WHSV of 2.36 hr^{-1}. The effect of the catalyst utilised was also investigated by performing 5 reforming experimental cycles using catalyst B at the same operating conditions but oxidising only at 600°C.

5.5.2.1 Gas outputs in oxidation temperature study

A comparison of the selectivity to carbon gases and conversion fraction of acetic acid, and steam for the first reforming cycle which was preluded by activation of the catalyst with hydrogen indicates a similar profile for both catalysts as seen in Figure 5.5; the efficiency realised when compared to chemical equilibrium values indicate that the reforming process for both catalysts performed proficiently well with an steam conversion efficiency of 83 % observed for both catalyst. This is similar to the efficiency realised for the steam reforming runs already discussed in Chapter 4 using the same operating conditions.

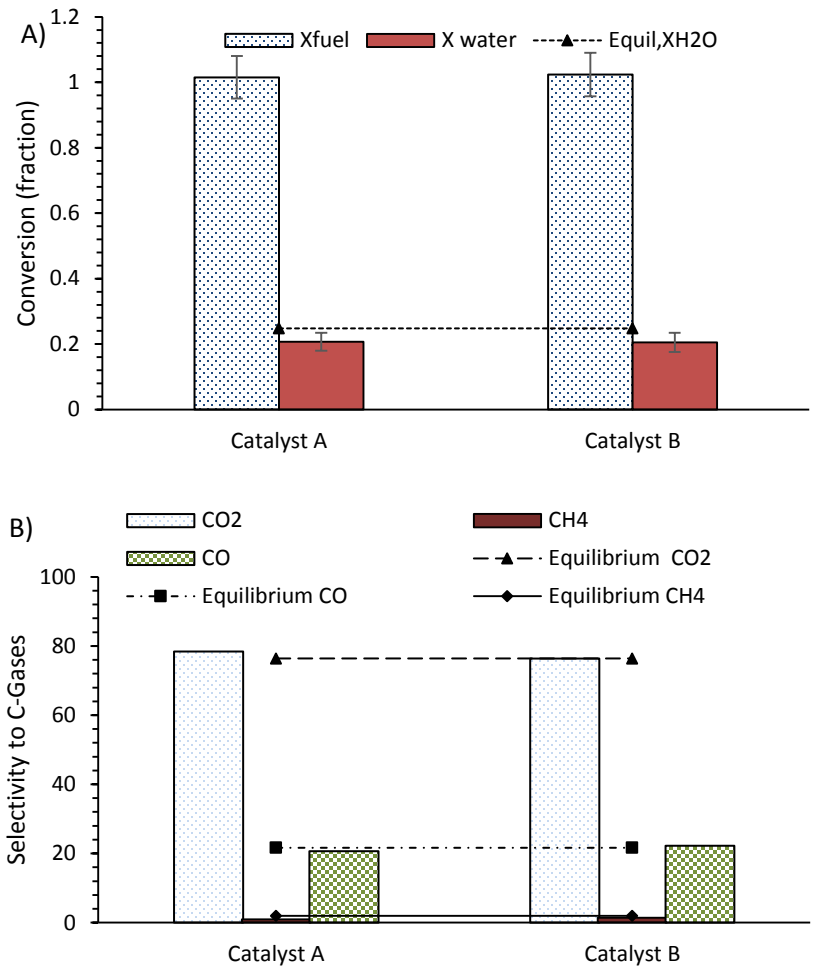

Figure 5.5: A) fuel and water Conversion Fraction B) selectivity to C-gases for hydrogen reduced catalyst (T_{SR}= 600 °C, T_{OX} =600 °C, WHSV=2.36 hr^{-1}, S/C=3)

The Hydrogen yield (wt.%) and hydrogen purity (%) as shown in Figure 5.6 also shows a great resemblance to those previously carried out during steam reforming of acetic acid showing great consistency and reproducibility for the experimental run. Both catalyst as observed performed well with a calculated hydrogen yield efficiency of 81% and 94% realised for both catalysts when compared with stoichiometric values and equilibrium values respectively.

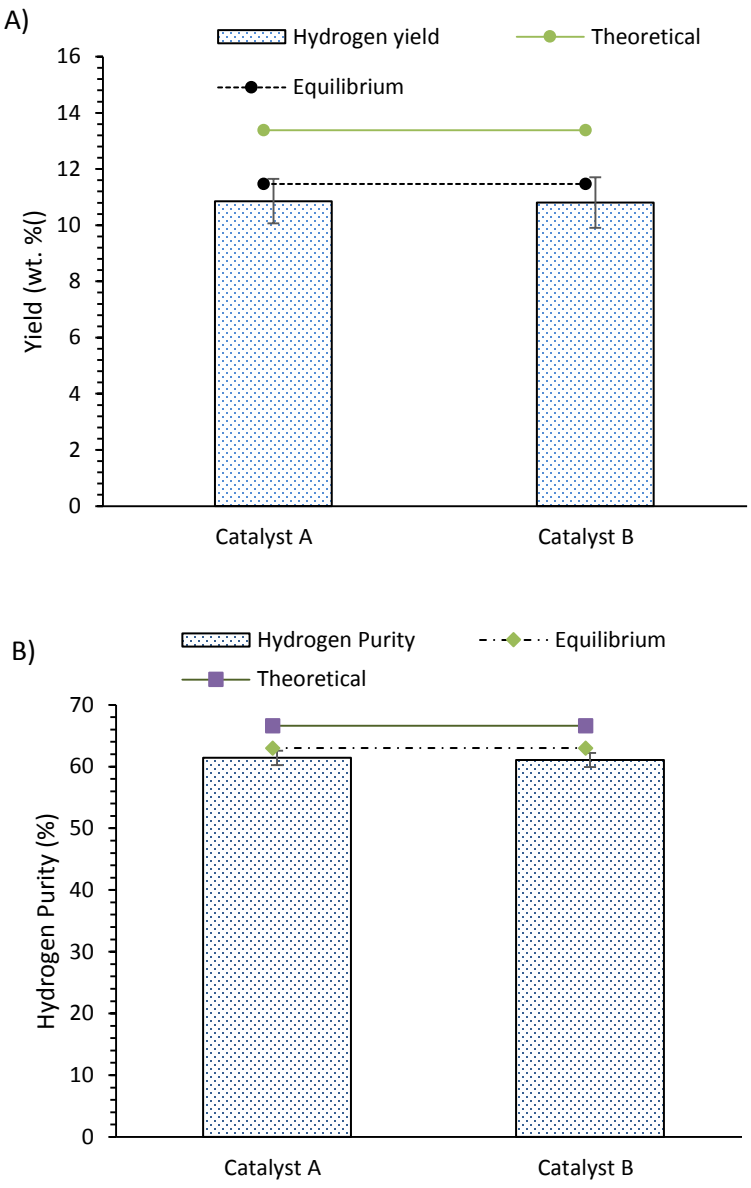

Figure 5.6: A) Hydrogen yield (wt. %) and B) purity of hydrogen (%) for hydrogen activated catalyst (T_{SR}= 600 °C, T_{OX} =600 °C, WHSV=2.36 hr^{-1}, S/C=3)

The major difference between the reactivity of both catalysts occurs after oxidation at 600 °C and at the beginning of the 2nd cycle; it is important to reiterate that oxidation of both catalysts during the oxidation phase was done till after steady oxygen gas flow (21% in output) was realised; for both catalysts at these point, no carbon products were formed at this time indicating that no carbon oxidation was occurring at the end of the oxidation phase.

There was no steady and sustained production of gases (H_2, CO_2, CO, CH_4) in the 2nd cycle for catalyst A after oxidation at 600 °C. This affirms that sustained steam reforming is not occurring in the second cycle; this could be due to increased side reactions and increased coking via thermal decomposition. Coking might have been enhanced by the acidic nature of the catalyst support in Catalyst A [171, 172, 207]. Acidic catalysts support increases the chances of thermal decomposition and other polymerisation reactions resulting in graphitic carbon decomposition on the acidic sites of the support[172].

Another probable cause could be that the auto-reduction of the catalyst could not occur efficiently at this temperature; this however would negate a previous study that states that the lowest auto-reduction temperature for acetic acid using Catalyst A is 550 °C [167].

Catalyst B showed a different trend to catalyst A and the product gas composition was stable as expected during the steam reforming process, it showed a similar profile as depicted in Figure 5.1 indicating that the auto-reduction and steam reforming occurred appropriately and consistently.

Sustained steam reforming was observed during the CLSR of acetic acid using catalyst A after oxidising at higher temperatures (700 °C and 800 °C) while leaving the temperature at the reducing phase at 600 °C over five cycles (Table 5.4). > 89% of the fuel was converted across all five cycles of CLSR when T_{OX} was set at 700 °C or 800 °C, corresponding to a water conversion efficiency > 73% across all the cycles. This also corresponded to hydrogen yield efficiencies >71% and >82% when compared to equilibrium and stoichiometric values respectively. High hydrogen purity efficiencies (> 97% when compared to equilibrium values and >91% when compared to stoichiometric calculations) were also achieved across all CLSR experimental runs.

The fuel conversion in some of the recycles tend to be slightly over 100%; this is not attributed to an increase in the active sites on the surface of the catalysts but is due to the blockage of the active sites hence promoting carbon gasification by steam and acetic

acid. This is more prominent in the recycles due to weaker bonds that exists between the support and metal cations from cycle to cycle [208].

Table 5.4 Conversion fraction, purity and hydrogen yield over 5 cycles (T_{SR} set to 600 ° C, WHSV set to 2.36 hr^{-1}, and S/C set to 3)

	Cycle	X_{HAc} (fraction) Equation 4:1		X_{H_2O} (fraction) Equation 4:1		Hydrogen purity (%) Equation 4:3		Hydrogen yield (wt. %) Equation 4:2	
Oxidation temperature		*700 °C*	*800 °C*	*700 °C*	*800 °C*	*700 °C*	*800 °C*	*700 °C*	*800 °C*
Reduced by Hydrogen	1	0.89	0.96	0.18	0.21	60.94	61.92	9.51	10.50
Auto reduced	2	0.90	1.00	0.19	0.21	61.86	61.55	9.80	10.72
	3	0.94	1.01	0.20	0.24	61.55	62.87	10.11	11.48
	4	1.00	1.06	0.21	0.23	61.46	61.74	10.80	11.63
	5	1.05	1.07	0.22	0.23	61.58	61.66	11.31	11.64
Equilibrium values		1.00		0.24		63.01		11.47	

A closer look at the selectivity to carbon gases as detailed in Table 5.5 indicates also a similar profile for the selectivity to C-gases across all CLSR cycles at both temperatures investigated.

Table 5.5: selectivity to C-gases over 5 cycles (T_{SR} set to 600 ° C, WHSV set to 2.36 hr^{-1}, and S/C set to 3)

Oxidation temperature	Cycle	Selectivity to C-gases					
		CO2		CO		CH_4	
		700	***800***	***700***	***800***	***700***	***800***
Reduced by Hydrogen	1	78.30	79.70	20.90	19.70	0.80	0.60
Auto reduced	2	79.70	78.90	19.70	20.20	0.6	0.9
	3	77.10	77.40	21.80	21.60	1	1
	4	76.40	77.80	22.50	21.20	1.20	1.00
	5	76.40	78.80	22.50	20.30	1.10	0.90

Catalyst B performed better even when oxidised at 600 °C in terms of process efficiency; 5 cycles of chemical looping reforming were carried out using the same operating conditions as catalyst A with an oxidation temperature set at 600 °C; a look at the conversion fractions (fuel and water) across the cycles indicates a steadier profile similar to that observed for the first cycle (Figure 5.7). An efficiency between 83% and 87 % was calculated and derived for water conversion when compared to equilibrium values for all 5 CLSR cycles, this is similar to values for efficiency derived for water conversion during steam reforming experiments as discussed in Chapter 4 for both catalysts; this

also infers high affinity of the process to steam reforming as already indicated in Chapter 4 (selectivity to hydrogen with respect to other H-gases >98%)

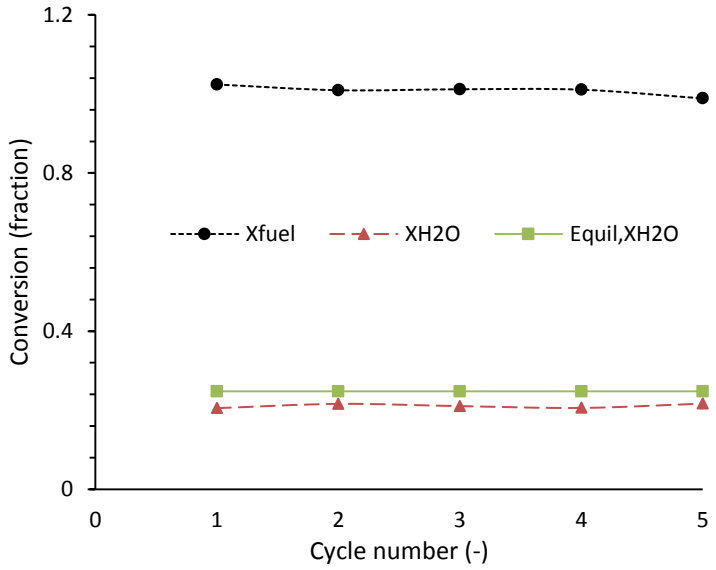

Figure 5.7: Conversion Fraction of CLSR across 5 cycles for catalyst B (T_{SR}= 600 °C, T_{OX} =600 °C, catalyst B, WHSV=2.36 hr^{-1}, S/C=3)

The purity of hydrogen produced and hydrogen yield (wt. %) as depicted in Figure 5.8 also indicates a similar trend across all 5 reducing or reforming phase experimental runs; hydrogen purity with an efficiency of 92 % and 97% was also derived when compared to equilibrium and theoretical or stoichiometric maximum respectively across the 5 cycles of CLSR using catalyst B. The efficiency of the hydrogen yield (wt. % of acetic acid) also showed great consistency when compared to steam reforming experiments with an efficiency between 81 - 82% noticed when compared to stoichiometric values and an efficiency of 94 - 95% observed when compared with equilibrium values.

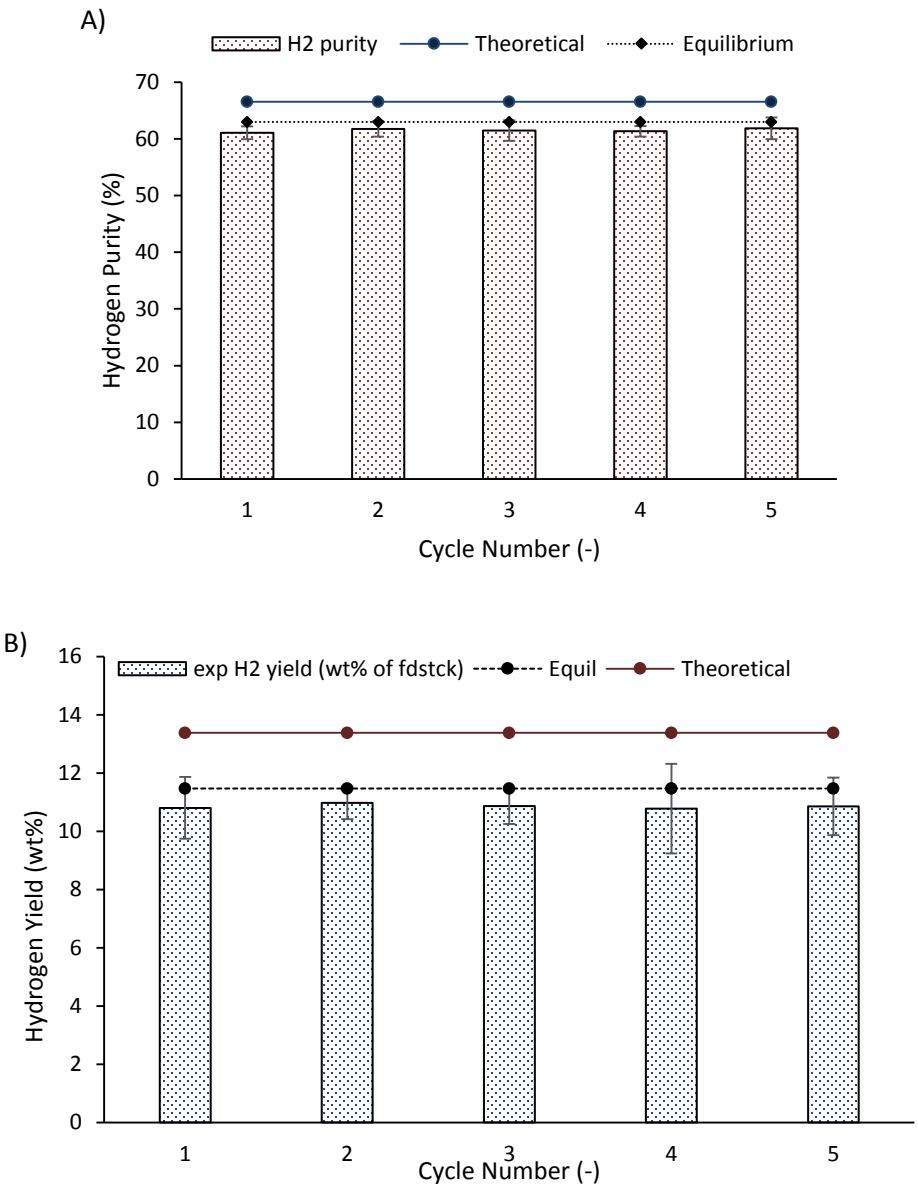

Figure 5.8: A) Hydrogen Purity (%) and B) Hydrogen Yield (wt. %) across 5 cycles of CLSR for catalyst B (T_{SR}= 600 °C, T_{OX} =600 °C, catalyst B, WHSV=2.36 hr^{-1}, S/C=3)

There was no obvious sign in the selectivity to carbon containing gases to indicate a reduction in steam reforming or water gas shift (there was a slight increase in the selectivity to CO_2 corresponding to a slight decrease in the selectivity to CO in cycles 2, 3 and 4, these observations had no bearing on the fuel conversion in these cycles and is considered negligible or insignificant to the process efficiency and stability).

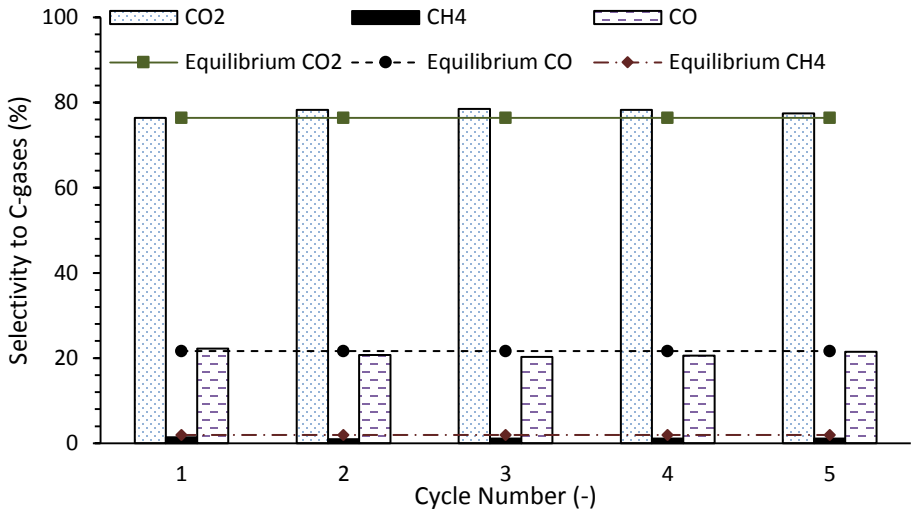

Figure 5.9: Selectivity to C-gases for CLSR using catalyst (T_{SR}= 600 °C, T_{OX} =600 °C, catalyst B, WHSV=2.36 hr^{-1}, S/C=3)

5.5.2.2 Solid carbon product in Tox study

There is an obvious decline in the carbon content (mol) of catalyst A as T_{OX} of catalyst A is increased as shown in Table 5.6; with a 68 % decrease in carbon content (mol) found for catalyst A when oxidised at 800 °C compared to oxidised catalyst A at oxidation temperature 600 °C.

Table 5.6: CHN elemental analysis on catalyst A and catalyst B at Different Oxidation Temperatures (T_{SR}= 600 °C, WHSV=2.36 hr^{-1}, S/C=3)

Catalyst, final state, cycle number	T_{Ox} (°C)	$C_{(s)}$ (mol)	Expressed as % of carbon in the feed
Used catalyst B, oxidised, 5 cycles	600	3.57×10^{-4}	0.52
Used catalyst A, oxidised, 5 cycles	600	8.32×10^{-4}	1.22
Used catalyst A, oxidised, 5 cycles	700	3.65×10^{-4}	0.54
Used catalyst A, oxidised, 5 cycles	800	2.68×10^{-4}	0.39
Used catalyst B, reduced, 5 cycles	800	55.6×10^{-4}	8.15
Used catalyst A, reduced, 5 cycles	800	79.1×10^{-4}	11.6

There is also a large difference in the carbon content (mol) when catalyst A and catalyst B are compared; the carbon present in catalyst A is much higher than that observed in catalyst B when oxidised at 600 °C (57% increase). CHN analysis of used CLSR catalyst A

after 5 cycles of CLSR also exhibits a higher carbon content when compared to the corresponding carbon content for catalyst B as seen in Table 5.6.

TGA coupled with FTIR was conducted on used Catalyst B after 5 chemical looping reforming cycles with oxidation at 800 °C; two CO_2 peaks were observed in the Chemigram profile as also identified during steam reforming experiments. This is already discussed in Chapter 4, the two CO_2 peaks which correspond to the DTG curve as seen in Figure 5.10A indicate that two types of carbon were formed on the catalyst. Previous studies indicate that CO_2 generated at the lower temperature is due to coking on the active sites of the surface of the catalyst while the other carbon formed is pseudo-graphitic in structure and contains poly aromatic compounds, these are most likely formed in the catalyst support or in some cases at the interface between the catalyst supports and the active sites [167, 172, 209, 210].

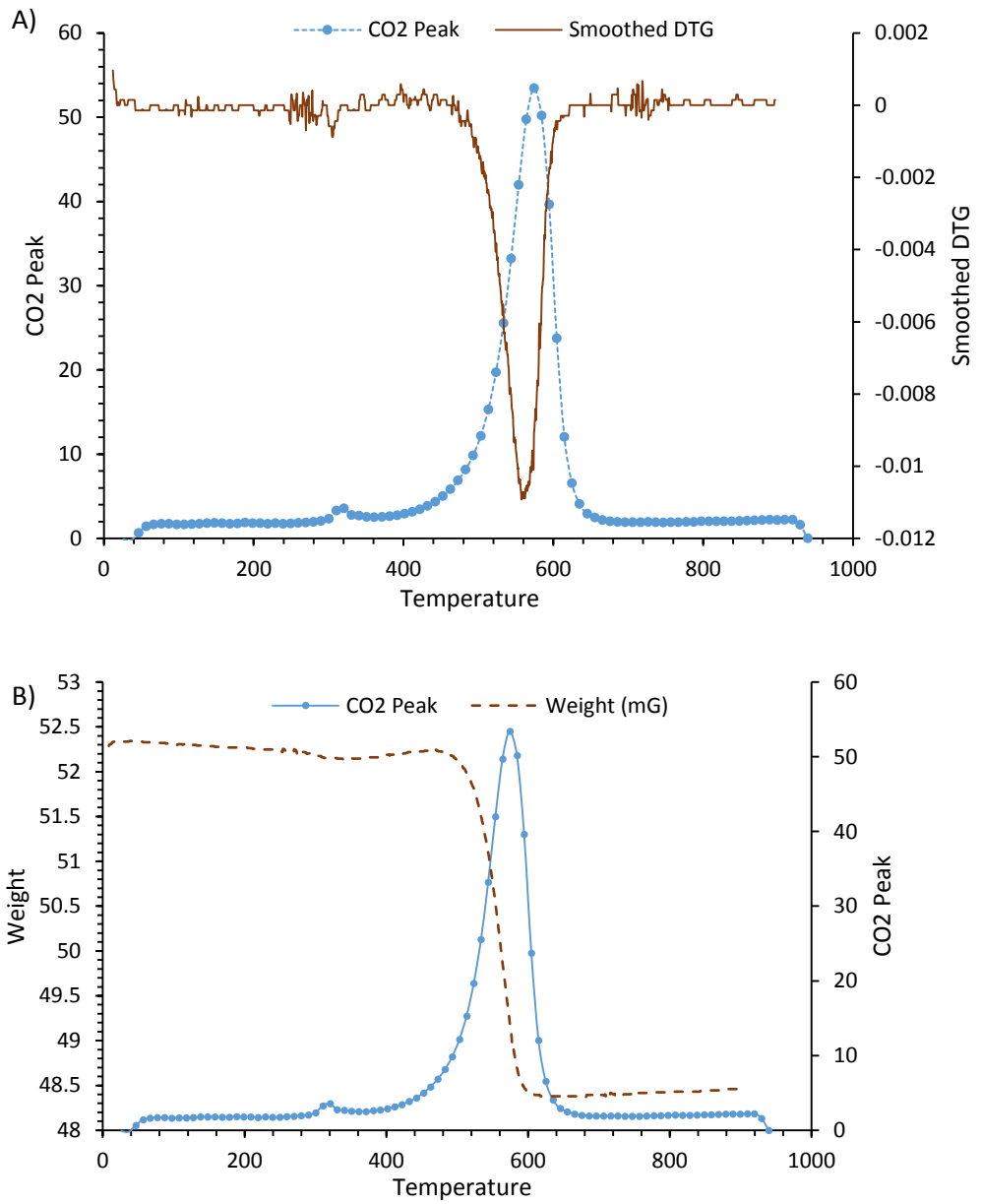

Figure 5.10: TGA FTIR analysis of used Catalyst B for CLSR A) CO_2 peak against DTG curve B) CO_2 peak against Weight (T_{SR}= 600 °C, T_{OX} =800 °C, catalyst B, WHSV=2.36 hr^{-1}, S/C=3)

The increase in T_{OX} alone does not alleviate all challenges highlighted in catalyst A because incomplete gasification of the carbon deposited in the acidic sites might subsequently occur during the oxidation stage, which would prompt further gasification required in the next reforming or reducing cycle. This phenomenon would affect the efficiency of the CLSR process as the potential of thermal decomposition and cracking reactions might increase particularly at the beginning of the reducing phase where auto-

reduction or dominant auto-reduction plus suppressed steam reforming are occurring [99, 167].

The addition of promoters or doping of the catalyst has been shown to improve the stability and selectivity of steam reforming catalysts [211]; they are promoted to increase the reforming process by enhancing water gas shift and catalyst reduction [212]. A more pressing advantage of a promoter as seen in the more performant catalyst B, which is doped with CaO, when compared with the un-doped catalyst A is its ability to inhibit coke deposition. This makes it easily reusable and better suited for chemical looping steam reforming. It has also been reported that catalysts with less acidic supports such as catalyst B would have a higher ability to promote gasification and complete oxidation of deposited carbon, and hence promotes a better efficiency for auto-reduction and reforming in subsequent reducing phase [213].

5.5.2.3 Catalysts characteristics after CLSR-HAc use in TOX study

SEM images (Figure 5.11A) of used catalyst A taken after a few minutes into the reforming phase after oxidation at 600 °C shows the presence of filamentous carbon formed at the beginning of the second reforming cycle; this filamentous carbon was not present after oxidation as seen in Figure 5.11C, hence must have been formed in the earlier part of reducing stage.

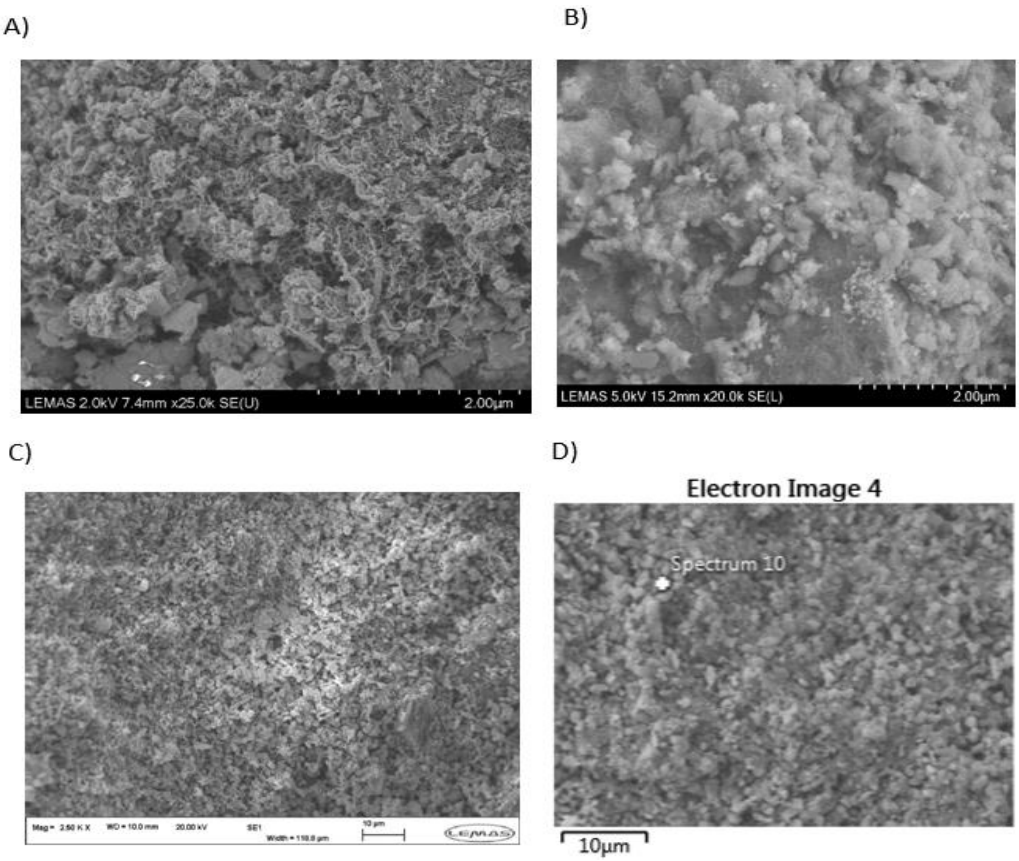

Figure 5.11A) SEM image for used catalyst A after a few minutes into the 2nd cycle after 1st cycle of CLSR B) Fresh catalyst A C) SEM image for oxidised catalyst A and D) EDX electron image for oxidised catalyst A after 1st cycle of CLSR (TSR = 600 °C, TOX=600 °C, WHSV=2.36 hr-1, S/C=3)

EDX profiling and composition of the oxidised catalyst coated in gold as seen in Figure 5.11D and Table 5.7 indicate the presence of carbon in the oxidised catalyst A which further confirms the presence of additional carbon black asides the filamentous carbon which has been oxidised.

Table 5.7: EDX composition for electron image

Element	Wt.%	Wt.% Sigma
C	5.66	0.40
O	35.03	0.28
Al	37.43	0.25
Ni	11.29	0.19
Au	10.58	0.25

The graphitic carbon deposited on the acidic sites of the support of the steam reforming catalyst would be more prominent in the reforming of feedstocks susceptible to coking and thermal decomposition like acetic acid; oxidation of the carbon formed would be

more difficult when compared to those formed on the surface of the catalyst but as seen in the case of catalyst A, this could be improved by the increase in the temperature of oxidation.

Surface area analysis of the catalysts is also important as it has been associated with the efficiency of the reforming process; the surface area analysis of CLSR is difficult to elucidate due to the several reactions occurring at the same time, it has been reported that the reduced catalyst (after reforming in a looping cycle) would have a higher surface area than its subsequent oxidised form [130, 203]. The increase in the surface area and pore volume in the reduced catalysts is due to the formation of smaller pores caused by openings of the pore mouths plugged with the oxidised form of the catalyst and/or the different molar volume of the Ni particle when compared to its oxidised form.

Table 5.8 details results from the BET analysis of catalyst B before and after CLSR (5 cycles, S/C=3, T_{SR} = 600 °C, WHSV=2.5 hr^{-1}); a loss of surface area and an increase in porosity was observed during catalyst activation and reduction using hydrogen. Nevertheless, comparison of the used reduced catalyst after several cycles indicates a higher surface area and pore volume in the reduced used catalysts when compared to the used oxidised catalyst.

Table 5.8 BET surface analysis of fresh and used catalyst for CLSR process (S/C=3, T_{SR} = 600 °C, WHSV=2.5 hr^{-1})

	MBET surface area (m^2/g)	Pore volume (cc/g)	Pore radius (nm)
Fresh Catalyst B (oxidised form)	34.9	0.068	1.9
Reduced fresh catalyst	28.8	0.114	2.4
Used oxidised Catalyst B (oxidised at 600°C after 1 cycle)	20.9	0.084	1.9
Used oxidised catalyst B (oxidised at 800 °C after 1 cycle)	8.6	0.058	1.9
Used Reduced Catalyst after cycles of CLSR with oxidation carried out at 600°C	26.5	0.131	1.9
Used Reduced Catalyst after cycles of CLSR with oxidation carried out at 800°C	13.9	0.072	1.9

In regards to oxidation of the catalysts, it was observed that the effect of sintering during oxidation is dependent on the temperature of oxidation; higher temperature of

oxidation leads to higher level of sintering and a further loss in surface area and open porosity as observed in Table 5.8.

It can be postulated that two major phases would occur in the oxidation step; an increase of surface area and porosity would be achieved due to the opening of pores blocked by carbon deposition from the subsequent reforming step and a more pronounced reduction of porosity observed due to the oxidation to NiO and sintering particularly at higher oxidation temperature.

It is nevertheless reported that the overall surface area and porosity of the chemical looping catalyst is expected to stabilise due to the Red-Ox cycle of chemical looping reforming [203].

It is obvious that the oxidation temperature in the oxidation phase run has a bearing effect on the process stability at the subsequent auto-reduction and steam reforming run as seen in catalyst A; however, the catalyst support in the catalyst utilised for the CLSR process is also very essential.

It is important to note, the consistent and stable profile with time on stream observed in the CLSR using catalyst B even after oxidation is carried out at 600 °C means that acetic acid decomposition to solid carbon and subsequent carbon gasification reactions are suppressed and minimised due to its non-acidic support and higher surface area compared to catalyst A. As already discussed, acidic supports increase the chances of sintering, cracking reactions, thermal decomposition and other polymerisation reactions which would naturally result to more graphitic carbon deposition and eventually the deactivation of the catalyst [171, 172]. The graphitic carbon deposited on the acidic sites of the support of the steam reforming catalyst would be more prominent in the reforming of feedstocks susceptible to coking and thermal decomposition like acetic acid. Oxidation of the carbon formed would be more difficult when compared to those formed on the surface of the catalyst. As seen in the case of catalyst A, this could be improved by the increase in the temperature of oxidation.

5.5.3 Optimised chemical looping cycling stability for catalyst B at T_{SR} 650 °C and T_{OX} 800°C

Ten CLSR cycles were conducted at 650 °C (T_{SR}) using catalyst B which as promoted in the previous section is a more effective chemical looping reforming catalyst when compared to catalyst A; these were done at a WHSV of 2.5 hr^{-1} and oxidation carried out at 800°C.

5.5.3.1 Gas outputs in CLSR cycling stability study

A similar product gas profile as identified in Figure 5.1B with hydrogen, CO, CO_2 and CH_4 as the main product was observed in all CLSR runs, while in the oxidation run O_2, CO and CO_2 were the major products. Table 5.9 shows the results derived from elemental analysis during the fuel on feed stage; the conversion fraction (X_{HAc} and X_{H2O}) calculated using Equation 4:1, hydrogen yield (wt. %) calculated using Equation 4:2and hydrogen purity (%) calculated using Equation 4:3 were consistent over the 10 cycles of CLSR, these indicated no obvious loss in the catalyst activity down to coking or catalyst deactivation.

Table 5.9 Conversion Fraction, Hydrogen purity and hydrogen yield (wt. %) (T_{SR}= 650 °C, T_{OX}=800 °C, catalyst B, WHSV=2.5 hr^{-1}, S/C=3)

	Cycle	X_{HAc} (fraction)	X_{H2O} (fraction)	Hydrogen purity (%)	Hydrogen yield (wt. %)
Reduced by Hydrogen	1	1.00	0.21	61.77	10.92
Auto reduced	2	0.95	0.20	61.71	10.31
	3	0.98	0.20	61.63	10.56
	4	0.98	0.21	62.04	10.75
	5	0.97	0.20	61.73	10.52
	6	0.98	0.20	61.69	10.63
	7	0.96	0.21	61.99	10.51
	8	0.95	0.20	61.87	10.40
	9	1.05	0.22	61.88	11.38
	10	1.03	0.22	61.90	11.23
Equilibrium		1.00	0.24	63.14	11.53

In terms of efficiency the water conversion efficiency and fuel conversion are shown in Figure 5.12; the minimum water conversion efficiency when compared to equilibrium was 83 % with the maximum efficiency at the 9th reforming cycle of 92 % when

compared to equilibrium values. The water conversion fraction and efficiency increased as the fuel conversion increased but no obvious trend which might indicate catalyst deterioration was observed in all 10 reforming/ reducing cycle; this entails that stable steam reforming with high affinity towards the production of hydrogen was apparent in all 10 reforming cycles. This is similar to a study on the chemical looping reforming of pyrolysis oils which concluded that auto-reduction of acetic acid and subsequent reforming of acetic acid and pyrolysis oil can be potentially done efficiently without obvious deterioration in its feedstock conversion [96, 167].

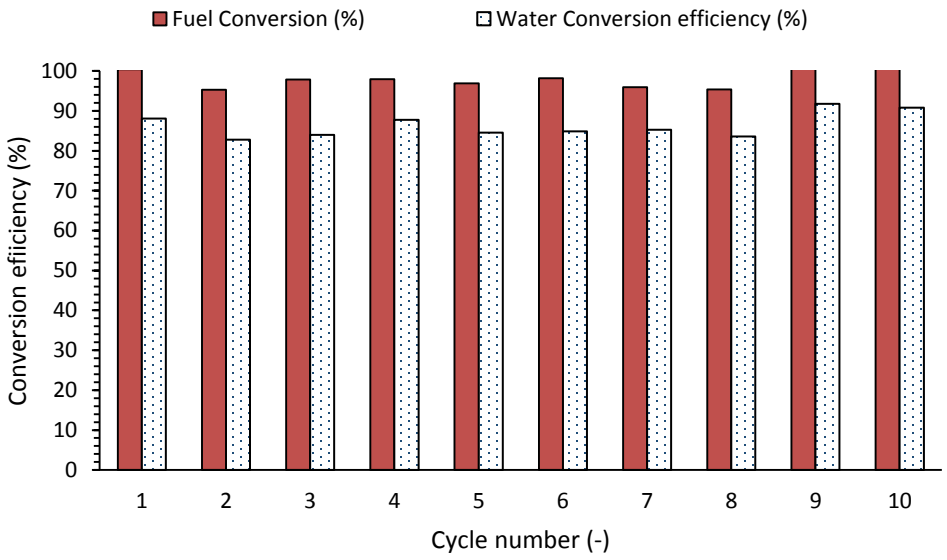

Figure 5.12: Conversion fraction across 10 cycles of CLSR using catalyst B (T_{SR}= 650 °C, T_{OX}=800 °C, catalyst B, WHSV=2.5 hr^{-1}, S/C=3)

As seen in Table 5.10, the selectivity to H-gases ($\mathrm{Sel\,H_{2,H_2}}$ and $\mathrm{Sel\,CH_{4,H_2}}$) shows no disparity across all 10 CLSR cycles. CH_4 is an intermediate by-product formed from methanation reactions (prominent at lower temperatures) and homogenous cracking of acetic acid which is promoted on nickel catalysts due to its high affinity towards breaking C-C bonds [214-216]; its decomposition has been attributed as one of the major routes of catalyst deactivation for the steam reforming of acetic acid [195]. The $\mathrm{Sel\,CH_{4,H_2}}$ is primarily determined by the S/C, catalyst loading and T_{SR}; nevertheless, high selectivity to methane ranging from 4% to ca15% has been reported

in previous studies on nickel catalysts[186, 217]. The obtained Sel CH_{4,H_2} and Sel H_{2,H_2} in this study are relatively close to equilibrium values and consistent across all 10 cycles of CLSR. This strongly indicate, the rate of reaction of the process is primarily determined by the thermodynamics of the reaction system. It also indicates, no loss of activity in the efficiency of the reforming catalyst towards efficient steam reforming and hydrogen production across all 10 cycles of CLSR. In regards to selectivity to C-gases, there is no major change identified for selectivity to $CH_{4,C}$. The selectivity to CO_2 increased sparingly from the first cycle (H_2-reduced catalyst) to the subsequent cycles, which were auto-reduced by the feedstock; this also corresponded to a decrease in the selectivity to CO from the first cycle to subsequent cycles, for the auto-reduced catalyst. This observation coupled with the stable water conversion fraction indicates improved water gas shift in the reducing-stream reforming stage and could also indicate less carbon gasification.

Table 5.10: Selectivity's to C-gases and H-gases across 10 cycles (T_{SR}= 650 °C, T_{OX} =800 °C, catalyst B, WHSV=2.5 hr^{-1}, S/C=3)

		Selectivity to C-gases			Selectivity to H-gases	
	Cycle	Sel $CO_{2,C}$	Sel $CO_{,C}$	Sel $CH_{4,C}$	Sel H_{2,H_2}	Sel CH_{4,H_2}
Reduced by Hydrogen	1	75.9	23.5	0.6	99.6	0.4
Auto reduced	2	77.6	21.8	0.7	99.6	0.4
	3	77.5	22	0.5	99.7	0.3
	4	78.5	20.9	0.5	99.7	0.3
	5	78.4	21.1	0.5	99.7	0.3
	6	77.8	21.7	0.5	99.7	0.3
	7	78.4	21.2	0.4	99.7	0.3
	8	78.2	21.4	0.4	99.8	0.2
	9	78.1	21.4	0.5	99.7	0.3
	10	78.2	21.4	0.5	99.7	0.3

The Hydrogen yield (wt. %) and the purity of hydrogen produced also showed high consistency across all cycles; the efficiency of the yield across all 10 cycles of chemical looping reforming was between 89 % and 97 % when compared to equilibrium (H_2 yield eff (equi)) and 77% and 85% when compared to theoretical maximum (H_2 yield eff (stoic)). The trend in the hydrogen yield also corresponds to the fuel conversion of the reducing -steam reforming stage (Figure 5.13). The hydrogen purity (%) was also

consistent across all 10 cycles in the reducing phase with an efficiency of 93% observed across all cycles when compared to equilibrium calculations (H_2 purity eff (equi)), this is equivalent to 98% compared to theoretical maximum or stoichiometric values (H_2 purity eff (stoic)).

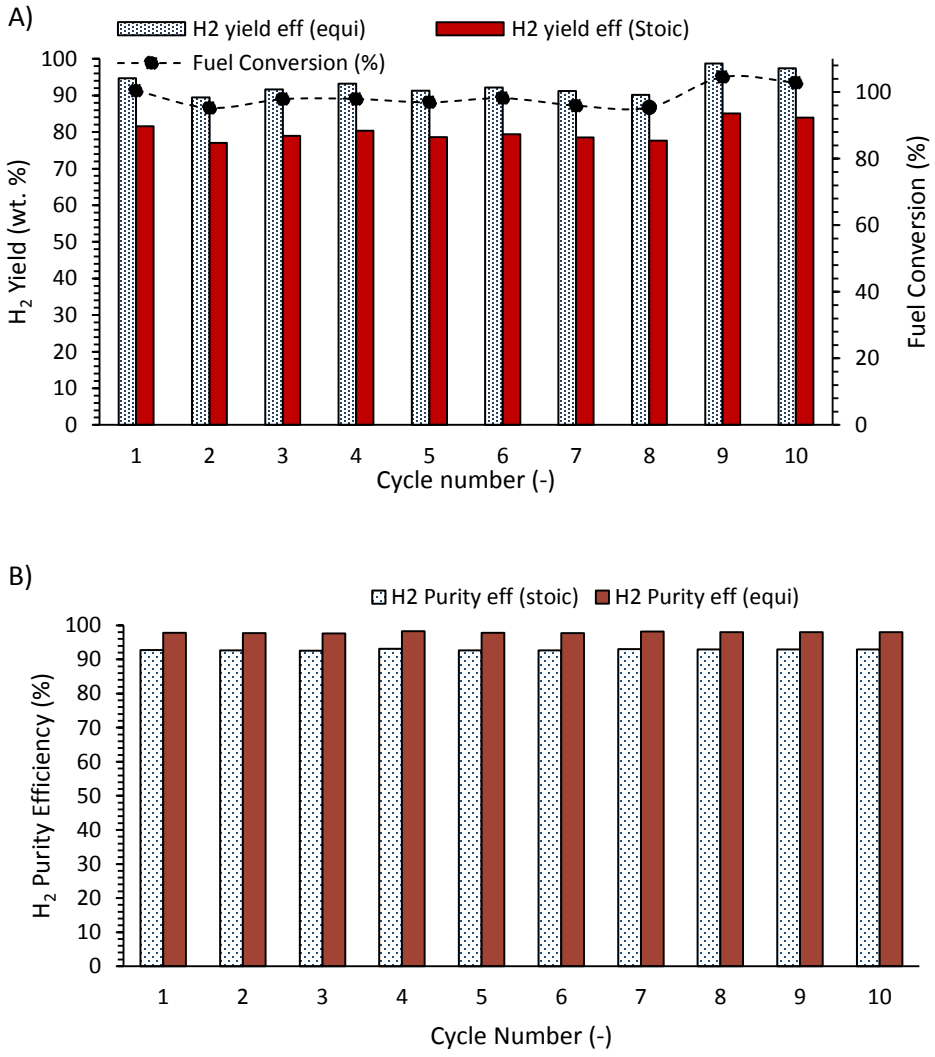

Figure 5.13: A) Hydrogen Yield Efficiency B) Hydrogen purity efficiency across all 10 cycles of CLSR (T_{SR}= 650 °C, T_{OX} =800 °C, catalyst B, WHSV=2.5 hr^{-1}, S/C=3)

5.5.3.2 Solid carbon product in redox cycling stability study

Post experimental analysis on the used chemical looping reforming catalyst and condensates samples collected over 10 cycles were also conducted; the possibility of leaching of nickel catalyst has been postulated for steam reforming of acetic acid[167],

hence to check the extent of leaching, ICP-MS testing was carried out on the condensate collected after the 10^{th} chemical looping cycle. 0.0819 mg/L of Nickel was detected through ICP-MS which indicated potential leaching of the catalyst into the condensate, these however corresponded to about 0.0001% of the nickel originally present in the catalyst and is therefore taken as insignificant (details of calculation of Nickel content calculation is found in the appendices (Appendix 3: Ni content in condensate). Total organic carbon analysis of the condensates collected after the reducing-steam reforming phase of the CLSR experimental runs using catalyst B indicates there was no obvious trend or relationship across the cycles. The carbon (mol) found in the condensate constituted less than 0.1 % of all carbon formed for each experimental run with the majority share of carbon formed either present in the product gas as CO_2, CO and CH_4 formed during oxidation or auto-reduction/reforming or deposited as solid on the catalyst.

TGA-FTIR analysis was also conducted on the used CLSR catalyst after 10 cycles of chemical looping steam reforming cycles. The evolution of CO_2 from the FTIR chemigram was plotted against the weight loss of catalyst from the TGA (Figure 5.14); Two CO_2 peaks were identified which is similar to those found in used CLSR catalyst utilised in experimental runs conducted at a T_{SR} of 600 °C; the major difference in these case is the greater influence of the CO_2 peak evolving at the lower temperature. As detailed in earlier sections, the carbon formed at lower temperature(360°C) was due to coking on the active sites of the surface of the catalyst while the other type of carbon formed (544°C) was pseudo-graphitic in structure and contains poly aromatic compounds. These are most likely formed in and on the catalyst support or in some cases at the interface between the catalyst supports and the active sites [167, 172, 209, 210].

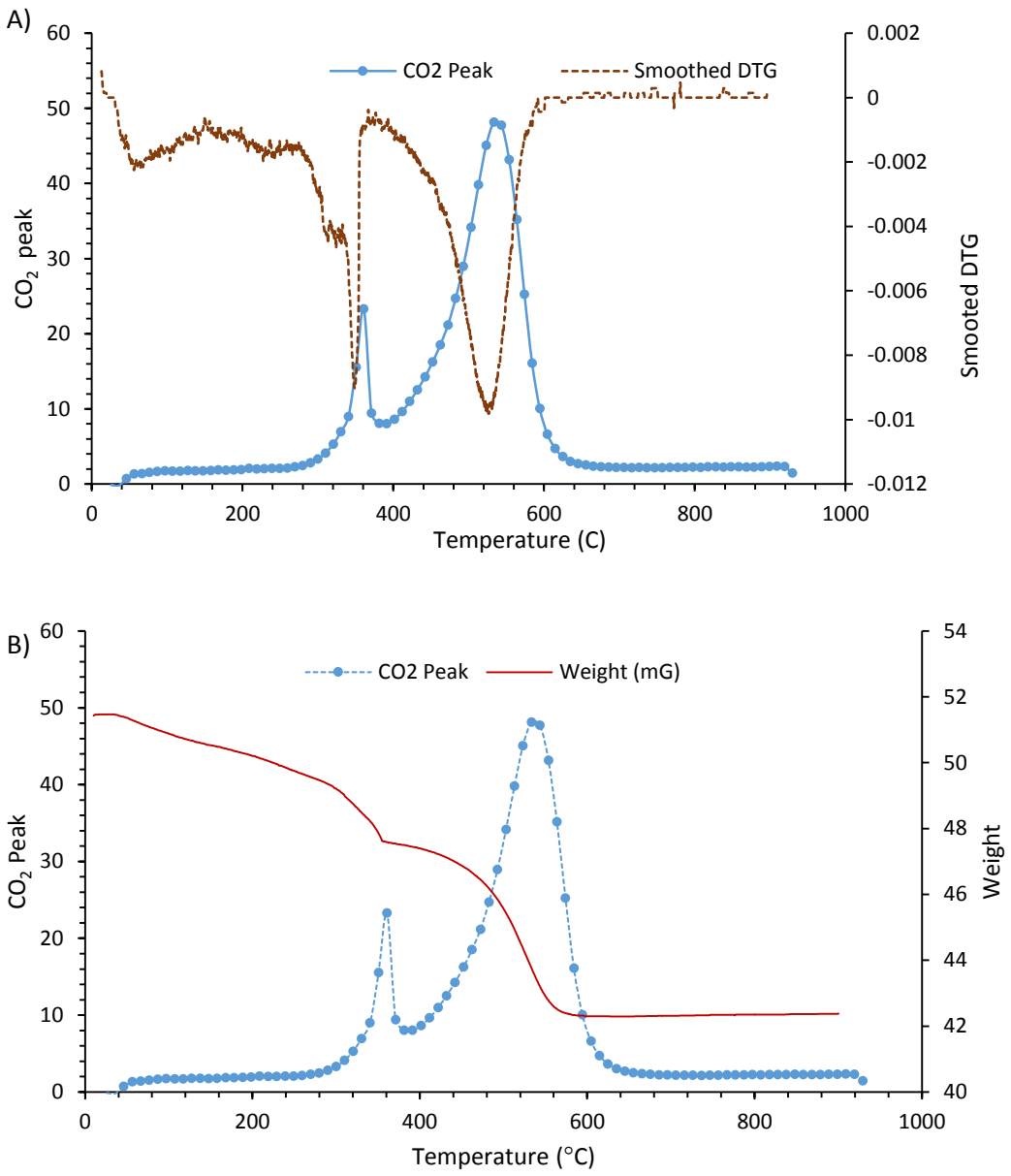

Figure 5.14:TGA FTIR analysis of used CLSR catalyst B A) CO_2 against smoothed DTG B) CO_2 against weight loss of catalyst (T_{SR}=650 °C, T_{OX}=800 °C, S/C= 3 and WHSV=2.36 hr^{-1})

5.5.3.3 Catalysts characteristics after CLSR-HAc use in redox stability study

SEM images of the used CLSR catalyst (Figure 5.15) shows the presence of filamentous carbon as identified in previous CLSR experiments; in higher magnification, it is observed that two types of carbon filaments were formed in regards to size of the carbon filaments. Denser and larger carbon filaments with a diameter of 51nm were identified,

and shorter and smaller filaments with diameter between 14nm to 18 nm which formed the major share of carbon filaments were also observed.

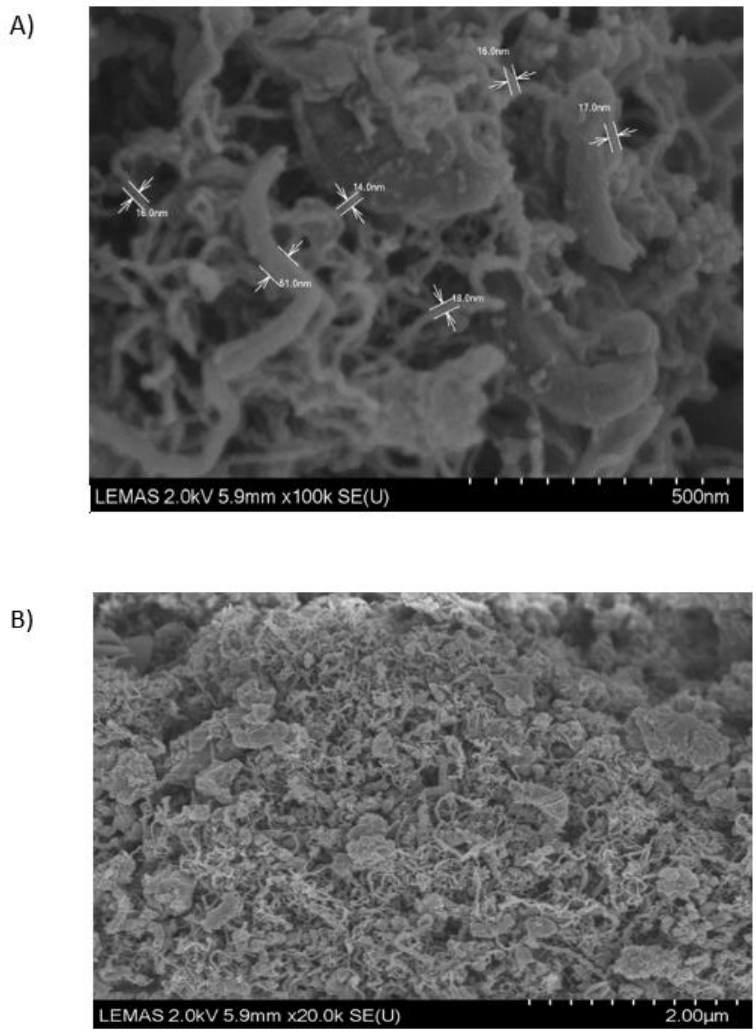

Figure 5.15: SEM images of the Used CLSR catalyst B (A-100k mag and B-20k mag) after 10 CLSR cycles (Reforming temperature= 650 °C, oxidation temperature =800 °C, catalyst B, WHSV=2.5 hr^{-1}, S/C=3)

It has been suggested in a previous study that the size of the carbon filaments formed on the surface of the catalyst might have an effect on the process efficiency [167]; the presence of more dense or larger carbon filaments would make it more difficult for the fuel and steam reacting molecules to reach the active sites of the catalyst thus introducing a larger external mass transfer barrier and hence reducing the rate of reaction and catalytic activity. The oxidation of shorter and smaller carbon filaments

which are prominent on catalyst B is also easier when compared to oxidation of larger and denser carbon filaments.

It was also noted through EDX profiling at different points or spectrum of the catalyst surface that the deposited carbon might be evenly distributed across the catalyst surface (Table 5.11)

Table 5.11: EDX profile of Used CLSR catalyst B after 10 cycles

	Spectrum 11	Spectrum 12	Spectrum13
Element	Wt.%	Wt.%	Wt.%
C	11.47	12.02	14.16
O	30.98	32.60	32.26
Al	25.88	29.27	25.16
Ca	9.80	8.26	6.30
Ni	10.22	5.13	5.45
Au	11.65	12.73	16.67

TEM images and SAED diffraction patterns of the used CLSR catalyst can be seen in Figure 5.16; the images in Figure 5.16(A) and the diffraction pattern in Figure 5.16(B) indicates and confirms the presence of amorphous carbon across the catalyst; these carbon spots are not evenly distributed across the catalyst but are dispersed. The different intensity in the colours in Figure 5.16C also indicates that the level of carbon deposition varies across different point of the catalyst. A poly-crystalline structure Figure 5.16(E,F, and G) was also observed in higher magnification of the catalyst which as expected represents the pseudo graphitic carbon formed as already reported for the steam reforming of acetic acid [167].

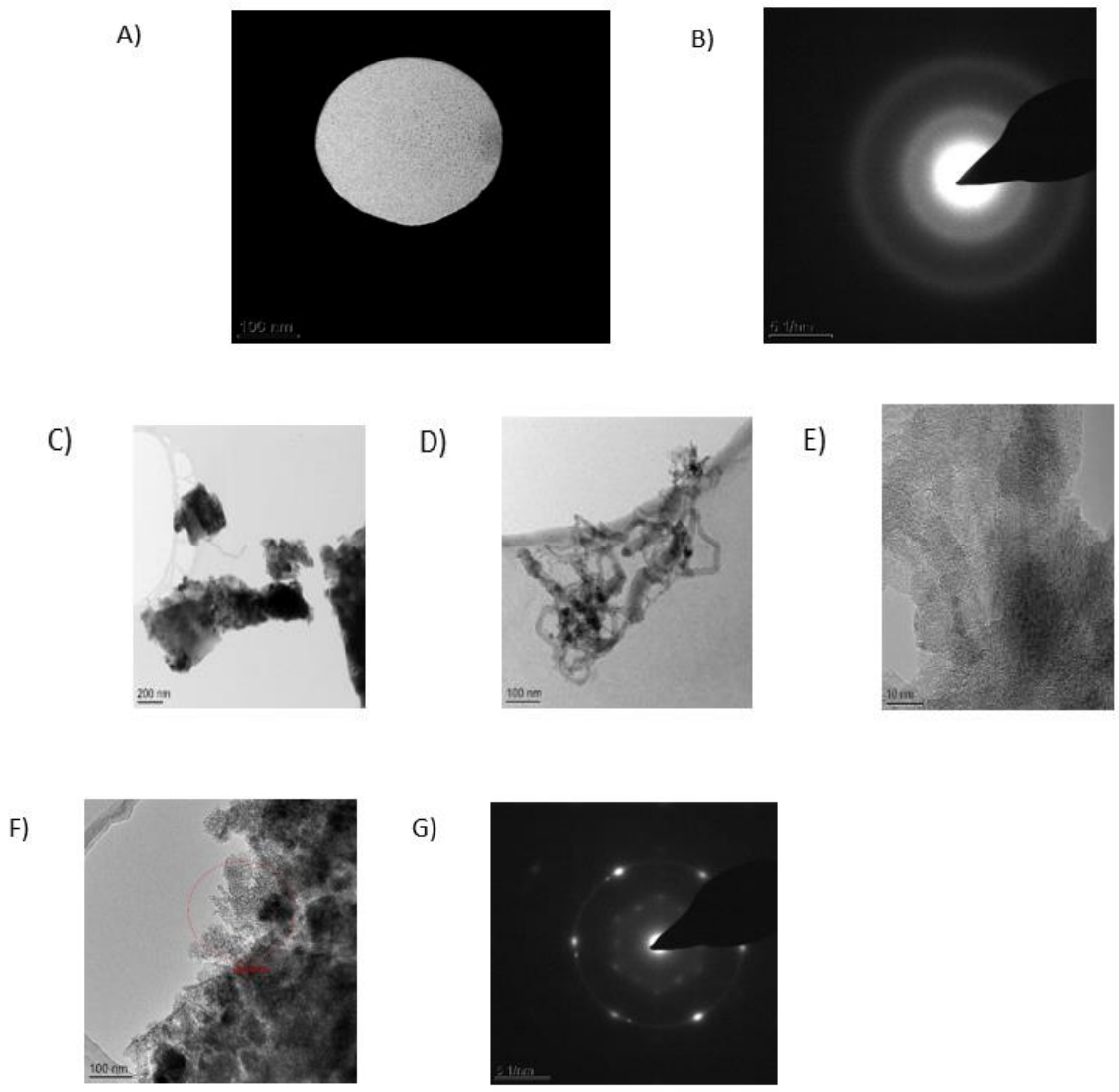

Figure 5.16 TEM images and Diffraction patterns of used chemical looping steam reforming catalysts (after 10 cycles of reforming) (T_{SR}= 650 °C, T_{OX} =800 °C, catalyst B, WHSV=2.5 hr^{-1}, S/C=3)

The poly crystalline structure as observed in the SAED diffraction patterns (Figure 5.16G) corresponds to CO_2 peak observed at higher temperatures in the chemigram obtained from TGA-FTIR analysis as detailed in Figure 5.14 while the amorphous carbon corresponds to the carbon filaments as observed in SEM images (Figure 5.15) and the lower CO2 peak in the TGA-FTIR chemigram (Figure 5.14).

Total organic carbon analysis of the condensates collected after the reducing phase of the CLSR experimental runs also confers the high efficiency of the process across all

cycles with carbon (mol) detected in the condensate constituting less than 0.1 % of the carbon share distribution for all cycles. This indicates that major share of carbon formed is either present in the product gas as CO_2, CO and CH_4 during the fuel feed stage, or is oxidised during the air feed stage.

5.6 Conclusion

The feasibility and efficiency of the chemical looping steam reforming of acetic acid was investigated taking into consideration the catalyst redox cycling ability, the effect of the oxidation temperature and elemental analyses of process outputs using catalyst A. It was established that the oxidation temperature has a substantial effect on the effectiveness of the catalyst in the subsequent reducing phase.

It was also stipulated that catalyst B, which contains calcium aluminate, would be a more suitable oxygen carrier and chemical looping reforming catalyst when compared to catalyst A due to its less acidic sites on the catalyst support; the advantage of additives and promoters was also enumerated. Catalyst B also showed great efficiency in terms of redox cycling ability without any apparent loss in catalytic activity, which suggests it would be suitable also for sorption enhanced chemical looping steam reforming runs. The high efficiency of hydrogen yields and water conversion across the 10 cycles of chemical looping steam reforming investigated also indicates that steam reforming was prominent and maintained across all 10 cycles.

An overall carbon balance also indicated that in the overall cyclic process, the majority of the carbon from the feedstock is converted efficiently to the product gas with no apparent loss of activity in the cycles.

It can then be concluded that chemical looping steam reforming of acetic acid can be carried out successfully and efficiently with a high fuel conversion and hydrogen yield across several cycles at a stable and sustainable rate as long as the operating parameters in regards to catalyst type, reforming and oxidising temperature, and steam to carbon ratio are taken into account.

Chapter 6 Sorption enhanced chemical looping steam reforming of acetic acid

6.1 General overview

Sorption enhanced chemical looping reforming incorporates in-situ carbon capture or sorption enhancement within the CLSR process. It has an advantage over conventional steam reforming systems as the equilibrium of the process is shifted into production of hydrogen higher than the thermodynamic limits for conventional steam reforming. This shift in equilibrium is crucial particularly when steam reforming oxygenates like acetic acid and bio-oils which are prone to coking; this is because both the steam reforming and water gas shift reactions as already described in previous chapters are equilibrium limited.

It is also reported that it is impossible to achieve optimal feed conversion in a single reactor for the conventional reforming process of complex bio-oils and its model compounds due to product dilution and reduced fuel conversion caused by the complexity of its reactions pathways and side reactions that naturally occur during its reforming [218]; the shift in equilibrium also entails that some of these side reactions are averted or minimised during the SE-CLSR process. The SE-CLSR process is also stipulated to be self-sufficient or auto thermal depending on the operating conditions utilised; this is attributed to the heat transfer between endothermic and exothermic reactions occurring in the reactors employed.

Another essential advantage of sorption enhancement as reviewed in previous chapters is the cost and energy savings derived when compared to conventional processes; it has been promoted to potentially lead to a reduction of capital and operational costs, this is due to process intensification, decreased heat exchangers unit sizes and reduced purification costs required[219].

It also has an advantage when compared to chemical looping steam reforming process without in-situ sorption enhancement as the oxidation step of chemical looping can be

used to regenerate the sorbent. SE-CLSR could help alleviate some of the problems associated with conventional steam reforming particularly catalyst deactivation and sintering and would lead to the production of high concentration hydrogen with a reduced purification requirements which can be utilised in fuel-cells.

Sorption enhanced steam reforming of biomass derived compounds[150, 209, 220-227], pyrolysis oils [153]and its model compounds[228, 229] has been studied previously with the view of optimising the steam reforming of bio-oils; it was reported that sorption enhanced steam reforming of PEFB and pine pyrolysis oils could potentially lead to an increase in hydrogen purity from 68 % and 54 % from conventional steam reforming to 96% and 87% for both pyrolysis oils respectively, an increase in the hydrogen yield (wt. %) from 9.5 wt. % and 9.9 wt. % to 10.4 wt. % and 13.9 wt. % was also reported for PEFB and pine oil respectively [153].

The sorption enhanced steam reforming of acetic acid has also been investigated in previous studies with the view to ascertain optimal conditions for the process; it was inferred in a study by Gill et al. [218] that the reforming temperature has more influence on process outputs than the operating steam to carbon ratio and weight hourly space velocity utilised in sorption enhanced steam reforming of acetic acid, they recorded a hydrogen yield of 92% when compared to stoichiometric values when acetic acid is steam reformed at a reforming temperature of 560 °C, and they concluded that ideal sorption enhanced steam reforming of acetic acid should be conducted at steam reforming temperature between 400 °C and 650 °C with equilibrium attained at steam reforming temperature between 550 °C and 650 °C, at atmospheric pressure, steam to carbon ratio between 1.5 to 4.5 and WHSV set below 2 hr^{-1} [218].

The effect of T_{SR} on Sorption enhanced reforming of acetic acid shows the same trend as the corresponding Steam reforming process without the use of a sorbent with regards to the hydrogen yield, hydrogen purity and hydrogen concentration; the hydrogen yield and hydrogen concentration tends to increase with an increase in T_{SR} until an optimal point is reached from where a decrease in hydrogen yield and concentration is observed

as the temperature increases. Also, the hydrogen yield and purity is generally favoured with a high S/C and low WHSV values similar to steam reforming of acetic acid as already reviewed in previous chapters. Another study on the sorption enhanced steam reforming of model oxygenates of bio-oils indicates that hydrogen yield from the sorption enhanced steam reforming of acetic acid is optimal between 575 °C and 675 °C at atmospheric pressure, they also concluded that SE-SR of most model compounds of bio-oils and mixed blends of model compounds would attain equilibrium between steam reforming temperature of 525 °C and 725 °C at 1 atm [228]. Poor hydrogen yield which was attributed to the slow rate of CO_2 capture and poor steam reforming was also observed at lower reforming temperatures for the SE-SR of acetic acid [228] whilst a further reduction in hydrogen purity, hydrogen yield and hydrogen selectivity was observed at reforming temperatures higher than 675 °C after observing hydrogen concentration > 99% evolved at atmospheric pressure between reforming temperature 525 °C and 675 °C [230].

The major challenge encountered in the SE-CLSR process has been attributed to the cyclic ability and efficiency of regenerated materials; obvious deterioration or decay of Ni based catalyst and CaO sorbent was not observed in the continuous sorption enhanced reforming of glycerol when reformed at 500 °C and 600 °C with regenerative temperature set at 900 °C [222], however, loss of sorbent activity has been reported in several literature on the SE-CLSR process; a loss of sorbent activity was observed over three cycles when glycerol was steam reformed with in-situ sorption enhancement [224], this was attributed to a loss of CO_2 capture capacity as observed in SE-SR of methane [231, 232]. It has also been shown that the observed decay in the sorbent has no effect on the process outputs and efficiency after evolution and stable CO_2 production which occurs after saturation of the sorbent during the SE-SR process (post-breakthrough phase) [220], this indicates that the sorbent has no bearing on the steam reforming process after saturation. The sorbent nevertheless acts an inert after saturation and has a diluting effect on the catalyst bed leading to a decrease in the conversions as in the case with the CLSR experiments with sand. It has also been

reported that this dilution acts as a heat sink and unfavourably affects the heat demand of the looping process[233]. This loss of efficiency has also been postulated to occur after the first sorption enhanced reforming phase [150]; it was calculated that the carbonation efficiency of the sorbent dolomite in this case, reduced from 100 % in the first cycle to between 46 % and 64 % in cycle 2 to cycle 6 with no apparent pattern or trend observed.

The major cause of the sorbent deterioration particularly in CaO based sorbent has been attributed to the inability of the CaO to re-carbonate fully from cycle to cycle after calcining at a high temperature; this is largely due to ash fouling, mass loss, and reduced porosity which might arise through accelerated sintering which prevents diffusion of CO_2 into the sorbent material due to the collapse of pore particles [221, 234-237]; Noor et al. [238] also indicated in a study on the production of fuel-cell grade hydrogen by sorption enhanced water gas shift reaction that the loss of CO_2 capacity across cycles could be attributed to sintering and a decrease in the surface area of the sorbent.

Nevertheless, CaO based sorbent are promoted as suitable adsorbents for the SE-CLSR process due to their low cost, easy availability and their adequate adsorption capacities at high temperatures; hence, suggested techniques for improving their cyclic stability and efficiency is being investigated. These techniques include sorbent modification, steam hydration and obtaining CaO from precursors [239]; doping of the sorbent might help to increase the sorbent's resistance to attrition and reduce the decay of its capacity that might arise through sintering [240], the use of thermal pre-treatment and self-reactivation [241], and the use of synthetic sorbent are all being investigated to improve the cyclic stability of CaO based sorbent [99, 201, 219].

Direct and indirect hydration of CaO based sorbents has been shown to effectively improve the cyclic stability of sorbents; the process of indirect hydration for reactivation of CaO sorbents has been investigated in several studies [126, 242], it entails dehydrating the hydrated calcined sorbent after hydration before introducing the sorbent into the carbonator; these has been shown to lead to an increase in the surface

area of the sorbent but might also lead to cracking and the production of fragile materials [126]. Materic et al. [243] proposed that the attrition rate and fragile materials observed due to steam hydration could be avoided through superheated dehydration, this is done by dehydrating the calcined sorbent in a CO_2 environment. More interest has however been directed towards direct hydration; this is because it has inferred that it leads to higher carrying capacity, higher carbonation efficiency with less attrition [157, 158].

In this chapter, the performance of the SE-CLSR of acetic acid; a major model compound of volatile bio-derived feedstocks was examined over 20 reduction-oxidation (redox) cycles in a fixed bed reactor with the view of checking the viability and efficiency of the process. Emphasis is centred on the cyclic stability of the sorbent and oxygen transfer material; the process outputs are compared with those observed in chemical looping reforming without in-situ CO_2 sorption. The effect of direct steam hydration of the sorbent and catalyst before steam reforming are also examined for SE-CLSR of acetic acid.

6.2 Experimental approach, procedure and methods

A similar experimental approach to that utilised in the chemical looping reforming of acetic acid as detailed in chapter 3.3 was utilised in this study with the extra addition of the calcined spent sorbent generated as described in chapter 3.2.2.1; catalyst B, as already described in previous chapters is utilised in this study, it was crushed and sieved to 250 – 350 µm before utilisation as was the case in chemical looping reforming experiments without in-situ sorption enhancement. 2 grams of crushed catalyst were mixed with varying weight of the calcined spent sorbent depending on the calculated operating WHSV; this particles mixture was then transferred into the reactor system before experimentation. The reactor system and configuration were the same as described in previous chapters and, acetic acid and distilled water utilised are also as described in earlier chapters.

Similarly, to chemical looping steam reforming without in-situ CO_2 sorption, there were two basic stages of operation; the reducing or reforming stage under acetic acid and steam feed, and the oxidation stage under air feed. The major difference is that the reducing/reforming stage would also be used for the carbonation of the sorbent whilst calcination of sorbent would also occur during the oxidation stage. Both stages as carried out in this study were preceded by purging the reactor system with N_2 (200 sccm) and raising the temperature of the furnace to the required temperature for each stage. The reforming stage was carried out at temperature set to 650 °C, this is within the range observed for carbonation of CaO [158] and optimal sorption activity for the sorption enhanced steam reforming of acetic acid [228] whilst the oxidation phase was carried out at 850 °C, this was done to ensure adequate calcination of the sorbent before re-use.

Steam hydration of the sorbent and catalyst material was carried out for 30 minutes before each reforming phase using two hydration temperatures; the hydration temperature influences the hydration extent and degree of hydration; it has been reported that high hydration temperatures would lead to less hydration conversion. However, another advantage of steam hydration in the system would be the steam gasification of any remaining carbon deposited which has not been oxidised in the oxidation phase, this occurs prominently at higher temperatures. The steam hydration was conducted setting the temperature at 250 °C and 650 °C in the presence of nitrogen flow (50 sccm); it is expected that steam hydration of the sorbent would occur effectively at the lower temperature whilst steam gasification would occur more prominently at the higher temperature, the downside nevertheless of this reactor system is the fact that steam hydration of sorbent is more effectively carried out in a pressurised system, it is however assumed that partial hydration would occur efficiently at the lower temperature set.

The general stoichiometric reactions that occur in the reforming and carbonation phase including hydration are summarised in Reaction 6.1;

Reaction 6.1 Reactions occurring the fuel feed stage for SE-CLSR

$$C_2H_4O_2 + 4NiO \rightarrow 2CO_2 + 2H_2O + 4Ni \quad \text{A}$$

$$C_2H_4O_2 + 2H_2O \xrightarrow{Ni} 2CO_2 + 4H_2 \quad \text{B}$$

$$CaO + H_2O \leftrightarrow Ca(OH)_2 \quad \text{C}$$

$$Ca(OH)_2 + CO_2 \leftrightarrow CaCO_3 + H_2O \quad \text{D}$$

$$CaO + CO_2 \leftrightarrow CaCO_3 \quad \text{E}$$

This basically includes the auto-reduction of the catalyst by acetic acid Reaction 6.1A), complete steam reforming including water gas shift reaction (Reaction 6.1B), hydration and carbonation of sorbent (Reaction 6.1C, D, E). The overall reaction considering Reaction 6.1 B, C,D and E can therefore be written as follows (Reaction 6.2);

Reaction 6.2 Overall reaction

$$C_2H_4O_2 + 2H_2O + 2CaO \rightarrow 4H_2 + 2CaCO_3$$

The reducing stage for all SE-CLSR runs in this study was carried out for 2 hrs; using 2 grams of catalyst B. The catalyst as supplied was first reduced or activated by 5% H_2/N_2 (reaction 5) at the temperature set for the reducing phase just like in steam reforming and chemical looping reforming experiments.

The oxidation stage was performed at 850 °C, this ensures full and adequate calcination of the sorbent (Reaction 6.3) [158] whilst oxidising the catalyst and gasifying additional deposited carbon (Reaction 5.3); air (200 sccm) was passed through the reactor to re-oxidise the already utilised catalysts from the reforming phase; the air feed stage or oxidation phase was allowed to run until the concentration of oxygen detected in the micro-GC stabilised at 21 Vol% with no CO_2 formation detected and recorded by the micro-GC.

Reaction 6.3 Full calcination of CaO sorbent

$$CaCO_3 \rightarrow CaO + CO_2$$

6.3 Methodology for determination of process outputs from elemental balances

The process outputs as detected by the micro-GC was used to determine the yield of hydrogen, fuel conversion, water conversion and selectivity to carbon gases based on elemental balance. The calculations for the process analysis are as described in previous chapters for chemical looping reforming and steam reforming of acetic acid, and just like in the steam reforming experiments the calculated results from each experimental run were also compared with stoichiometric and equilibrium values with the view to ascertain the efficiency of the process. Due to the presence of additional material in the reactor load (sorbent), new thermodynamic equilibrium parameters were calculated and derived using CEA, this was used for comparison and determination of process efficiency particularly during periods of sorption activity.

Further calculations were done to ascertain the cyclic stability and efficiency of the sorbent; the rate of adsorption of CO_2 and maximum conversion of sorbent per cycle deactivation were calculated through elemental balance, nickel oxidation rate and time to complete reduction of nickel in the presence of the sorbent was also calculated.

The extrapolation to determine the efficiency and stability of the sorbent during the reforming stage was facilitated by observing the different phases occurring during the SE-CLSR process; the phases are all linked to CO_2 adsorption and hence the production of CO_2 was used to easily identify, monitor and analyse the process and sequence of reaction [117, 150]. Three distinct time phases could be identified for all SE-CLSR reforming phase as described in Figure 6.1;

- Pre-Breakthrough Phase (PB): This stage also called prior to breakthrough phase is the phase at which carbonation of the sorbent occurs fully with little or no CO_2 present in the product gas; other carbonaceous products like CO and CH_4 are also expected to have negligible concentrations at this phase.
- Breakthrough phase (BT): The breakthrough phase occurs as the sorbent saturates and loses some of its adsorbing capabilities. At this phase, it is triggered

by the detection of CO_2 from the process outputs, the level of CO and CH_4 tends to increase gradually in the product gas.

- Post breakthrough or steady state phase (SS): At this phase the sorbent is fully saturated and the constant level of CO_2 would be noticed at the product gas to indicate that sorption enhancement is not occurring in the process.

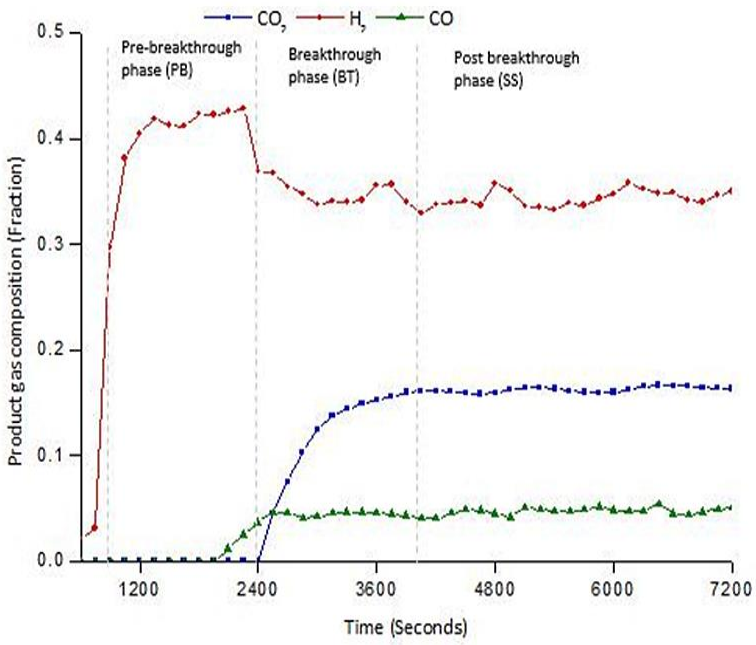

Figure 6.1: Different phases of SE-CLSR of acetic acid process (T_{SR}= 650 °C, S/C=3, sorbent mass= 2g at 1 atm)

The phases can also be distinguished by the output hydrogen purity as the % output hydrogen purity for the pre-breakthrough phase tends to be very high and close to 100% which gradually decreases in the breakthrough phase and becomes constant at the post breakthrough phase to indicate no sorption enhancement. As there are little or no carbon products formed in the pre-breakthrough phase due to sorption activity, calculation of acetic acid conversion through elemental balance as described in previous chapters and detailed in Equation 4:1 could not be ascertained.

A similar challenge was encountered in the breakthrough phase due to partial sorption activity occurring in this phase, this was not the case with the post breakthrough phase as no sorption activity occurred in this phase. Nevertheless, it is generally agreed that

the fuel conversion would be higher in the pre-breakthrough and breakthrough phase when compared to the post breakthrough phase because of the shift in equilibrium caused by sorption activity [150, 153]; hence, a minimum fuel conversion can be assumed for the breakthrough and pre-breakthrough phase using the fuel conversion calculated for the post breakthrough phase.

$$X_{Hac,PB-min} = X_{Hac,BT-min} \approx X_{Hac,SS}$$

The fuel conversion for the post breakthrough phase can be calculated similarly as calculated for chemical looping experiments and steam reforming experiments using Equation 4:1.

The carbonation rate or rate of adsorption of CO_2 ($\check{n}_{CO_{2,CARB}}$) can easily be calculated using Equation 6:1 after the fuel conversion is calculated; the rate of carbonation is calculated through a carbon balance and would aid discussion on the capabilities of the sorbent and help in calculation of its conversion and efficiency.

Equation 6:1 Molar rate of carbonation

$$\check{n}_{CO_{2,CARB}} = (X_{Hac,ss} \times n \times \check{n}_{Hac,in}) - (\frac{\check{n}_{N_{2,in}}}{y_{N_{2,}}}(y_{CH_4} + y_{CO_2} + y_{CO})$$

(For acetic acid, the value of n, the carbon atoms in the organic feedstock is 2)

As there are little or no carbon products in the pre-breakthrough phase, the carbonation rate tends to be relatively constant as it is mainly just an expression of the first part of Equation 6:1, this however changes as the carbon products evolves.

An integration of the carbonation rate was used to calculate the number moles of carbon products adsorbed which then is used to calculate the conversion of the sorbent material. The conversion of the sorbent is calculated using the number of moles of CaO in the sorbent per Equation 6:2 and an efficiency of the sorbent conversion is then extrapolated for the different phases using Equation 6:3;

Equation 6:2 Maximum conversion of sorbent per cycle of SE-CLSR

$$Max\ Conversion\ (\%) = \frac{\int_{t_0}^{t_{ss}} \check{n}_{CO_{2,CARB}} dt}{n_{CaO_{in}}} X\ 100$$

Equation 6:3: Efficiency of conversion per cycle of SE-CLSR

$$Efficiency\ at\ duration\ x\ (\%) = \frac{conversion\ of\ Cao\ for\ duration\ x}{Maximum\ conversion\ of\ CaO\ for\ cycle} \times 100$$

The total carbonation time is also calculated for each phase in the SE-CLSR reducing phase; T_0 which indicates the beginning of the pre-breakthrough phase is taken from the onset of high hydrogen amount as detected by the micro –GC, whilst T_{BT} and T_{SS} are taken from the time of the onset of CO2 production and stable CO2 production respectively as indicted in Figure 6.2.

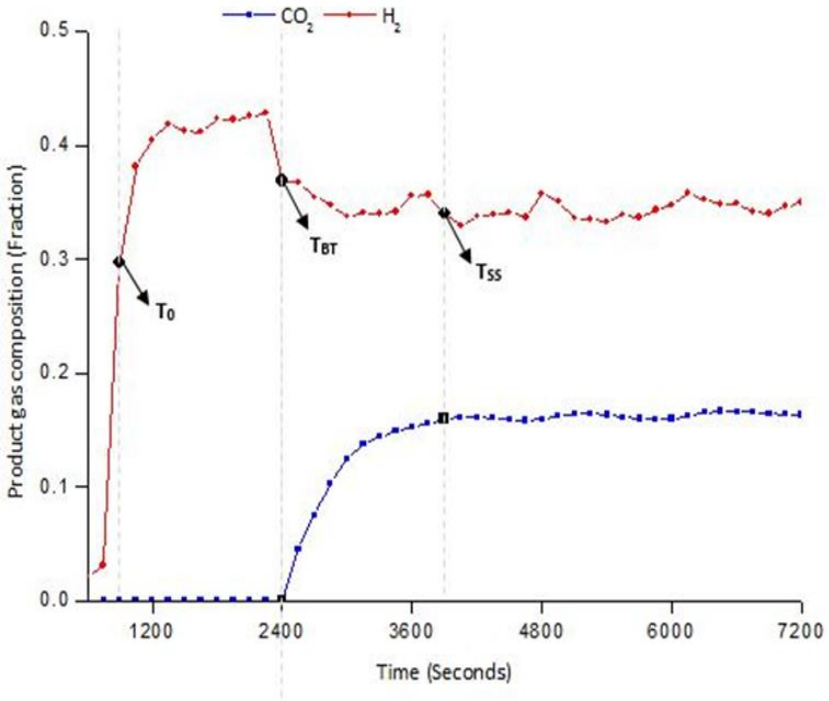

Figure 6.2: Carbonation time for each phase in SE-CLSR (T_{SR}= 650 °C, S/C=3, sorbent mass= 2g at 1 atm)

The molar rate of NiO reduction which occurs mainly in the pre-breakthrough phase can be calculated using estimates of the steam conversion and fuel conversion as described earlier; this is essential to verify that the catalyst was reduced and helps in

determining the extent of reduction of the catalyst. As detailed in Chapter 5 during the discussion for chemical looping experiments, the reduction rate of the catalyst is difficult to calculate due to the quick nature of the reduction process and also due to the fact the micro–GC detects process outputs every 2.5 minutes; However, using the assumption of minimum conversion for the pre-breakthrough phase and carbonation rate, the rate of reduction can be estimated using Equation 6:4 [150] where the first part of the equation corresponds to the maximum stoichiometric value when only hydrogen is produced and the second part of the equation corresponds to the molar rate of produced hydrogen;

Equation 6:4 Reduction rate of catalyst for SE-CLSR process

$$\check{n}_{NiO\rightarrow Ni,ss} = \check{n}_{Hac,in}X_{Hac,SS}(2n + 0.5m - k) - y_{H_2,SS}\frac{\check{n}_{N_{2,in}}}{(1 - y_{H_2,SS})}$$

(The stoichiometric value 2n + 0.5m – k for acetic acid =4)

The time for full nickel reduction ($\boldsymbol{T_{FR}}$) was also calculated using the number of moles of nickel present in the catalyst and the calculated molar reduction rate as described in Equation 6:5;

Equation 6:5 Time for full reduction of Catalyst

$$T_{FR} = \frac{n_{ni}}{\hbar_{NiO\rightarrow NiPB}}$$

Another parameter calculated was the % R_{red} (Equation 6:6); these is the ratio of the rate of reduction of nickel to the maximum stoichiometric reduction rate attainable, it aids the discussion of the dominant reaction during the pre-breakthrough phase.

Equation 6:6 Ratio of NiO reduction (%)

$$R_{red} = 100 \times \frac{\check{n}_{NiO\rightarrow Ni,PB}}{\check{n}_{Hac,in}X_{Hac,SS}(2n + 0.5m - k)}$$

Post experimental quantitative analysis of the process outputs during the oxidation/calcination phase could not be achieved as was done during chemical looping

experiments without in-situ sorption enhancement; this is because elemental balance could not be used to ascertain the oxidation rate of the catalyst/carbon or sorbent calcination rate due to the difficulty in differentiating the different occurring reactions.

6.4 Results and discussion

6.4.1 Thermodynamics equilibrium Data for SE-CLSR of acetic acid

The thermodynamic data utilised for comparison of the process analysis during the pre-breakthrough phase was obtained using the Chemical Equilibrium with Application (CEA) software just as in the case of steam reforming experiments; the hydrogen yield (wt. %), hydrogen purity and steam conversion was calculated using Equation 3:1 respectively and taking into consideration the presence of the sorbent in the input for the CEA software. The input of CaO in the CEA software for the pre-breakthrough phase was calculated from the overall stoichiometric equation (reaction 6.2) on mol basis ($1C_2H_4O_2 = 2CaO$) with the general assumption that all CO_2 produced in the reforming and auto-reduction reactions would be adsorbed by the CO_2 sorbent and converted into $CaCO_3$ in the pre-breakthrough phase. The selectivity to carbon gases was also calculated as in the case of steam reforming experiments using Equation 3:1.

Additionally, Equation 3:1 was modified to Equation 6:7 to calculate the selectivity to calcium containing compounds at different temperatures and steam to carbon ratio, and finally the CO_2 capture efficiency of the sorbent was calculated using the calculated number of moles of carbon in CO_2 and the calculated number of moles of carbon in the $CaCO_3$ material as described in Equation 6:8;

Equation 6:7 Selectivity to calcium components

$$sel_{individual\ calcium\ constituent}\% = \frac{mol\ fraction\ \ individual\ calcium\ constituent}{sum\ of\ all\ molar\ fractions\ of\ all\ constituent\ calcium\ gasses} \times 100$$

Equation 6:8CO_2 capture efficiency (%)

$$Capture\ efficiency\ = \frac{C_{moles\ in\ CO_2}}{C_{moles\ in\ CO_2} + C_{moles\ in\ CaCO_3}} \times 100$$

6.4.1.1 Hydrogen yield (wt. %), purity (%) and water conversion (%)

The hydrogen yield and hydrogen purity at different T_{SR} and S/C are represented in Figure 6.3; just as in the case of steam reforming experiments, there is an observed increase in the hydrogen yield and hydrogen purity as the S/C increases. This, as explained for steam reforming experiments, is due to the presence of available steam that can be converted to hydrogen. With reference to the operating temperature, there is a steep increase in the hydrogen yield and purity when the operating temperature is set between 300 °C and 400 °C, and a more stable and constant optimal hydrogen yield between 400 °C and 650 °C except at steam to carbon ratio set at 1, a stable hydrogen purity is also observed between 400 °C to 600 °C; this is in accordance with previous literature that has stipulated that SE-SR of acetic acid is optimal between this temperatures [229]. There is a general decrease in hydrogen purity and yield above these stable conditions to imply less reforming reactions occurring.

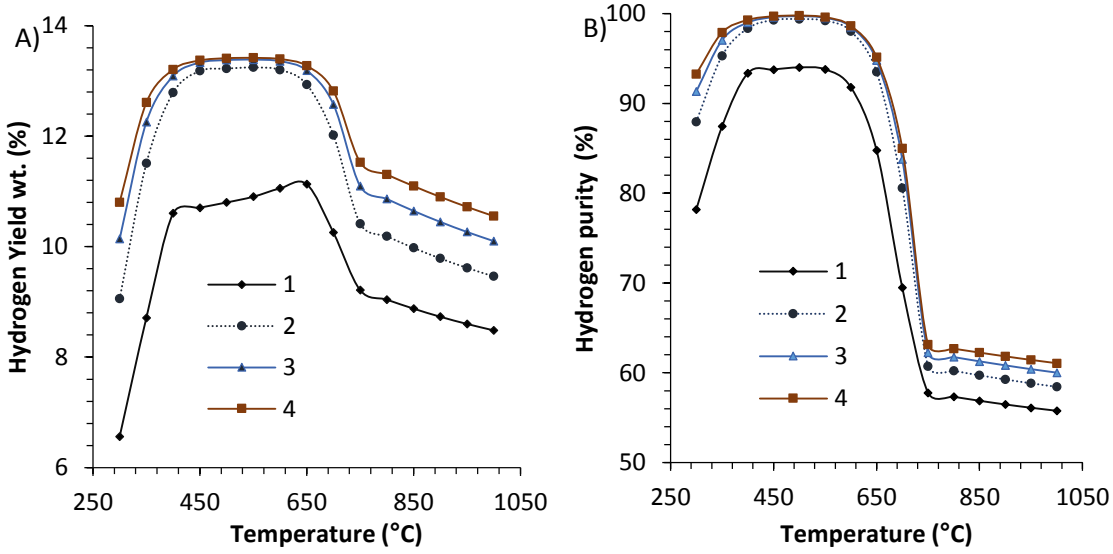

Figure 6.3 A) Hydrogen yield (wt. %) and B) purity (%) at different S/C and T_{SR} at 1 atm

The water conversion across different T_{SR} and S/C is represented in Figure 6.4; there is slight increase in water conversion as the operating temperature increases until the

optimal temperature between 500°C and 650°C just as in the case of steam reforming experiments, there is negative effect on the water conversion as the S/C ratio is increased, this is simply due to the fact that excess steam to the stoichiometric requirement is available as the S/C is increased and hence less conversion of the steam is attained.

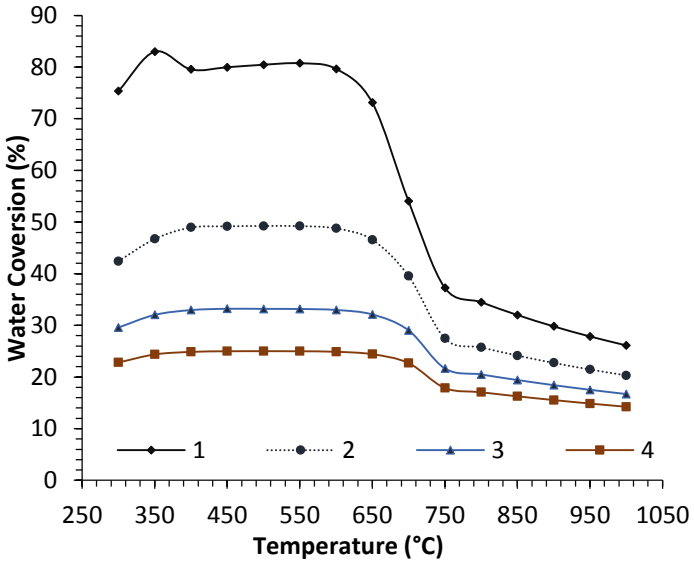

Figure 6.4 Water conversion (%) at different S/C and T_{SR}

A comparison of the water conversion, hydrogen yield and hydrogen purity of the SE-CLSR of acetic acid was compared with its corresponding values without sorption enhancement at steam to carbon ratio 2 and 3; a look at the hydrogen yield and purity illustrates the advantages of SE-CLSR when compared to conventional steam reforming (Figure 6.5); a higher hydrogen yield (wt. %) and purity can be clearly seen for the points with sorption enhancement when compared to the points without sorption enhancement, these trends continued for operating temperatures until 750 °C where there is no apparent difference between the sorption enhanced process and the non-enhanced process. This indicates that the sorption activity would not occur above 750°C and can be attributed to the fact that CaO conversion to $CaCO_3$ is not favoured above this temperature [158].

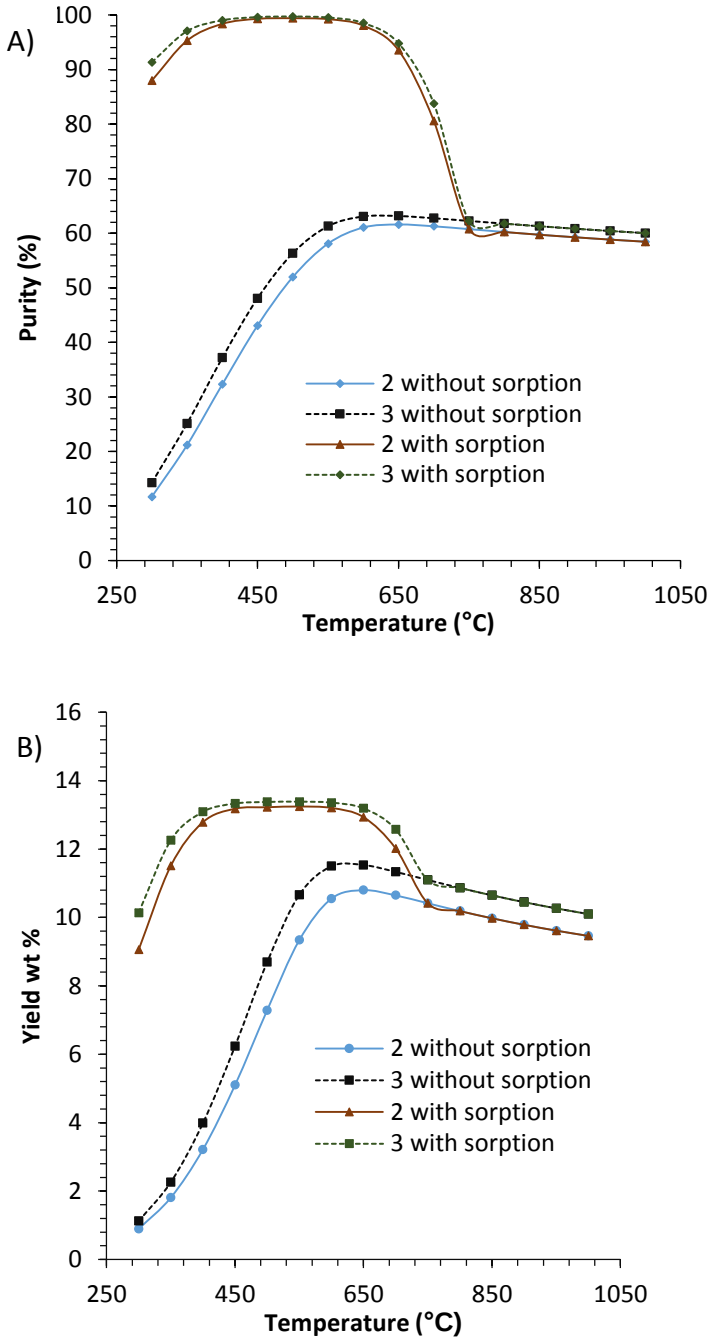

Figure 6.5 Comparison of A) Hydrogen purity (%) B) Hydrogen yield (wt. %) with or without sorption enhancement of the steam reforming of acetic acid at S/C= 2 and 3 (1 atm)

The comparison of the steam conversion of the SE-CLSR process with steam reforming with in-situ sorption enhancement can be seen in Figure 6.6; similarly to the hydrogen yield and hydrogen purity plots, the water conversion for the SE-CLSR process is much higher than the corresponding one without sorption enhancement, this is due to the

shift of equilibrium attained because of the presence of the sorbent which entails that more fuel can be converted hence more steam required for the fuel conversion. There is also no difference between both processes for both steam to carbon ratio at temperatures above 750 °C.

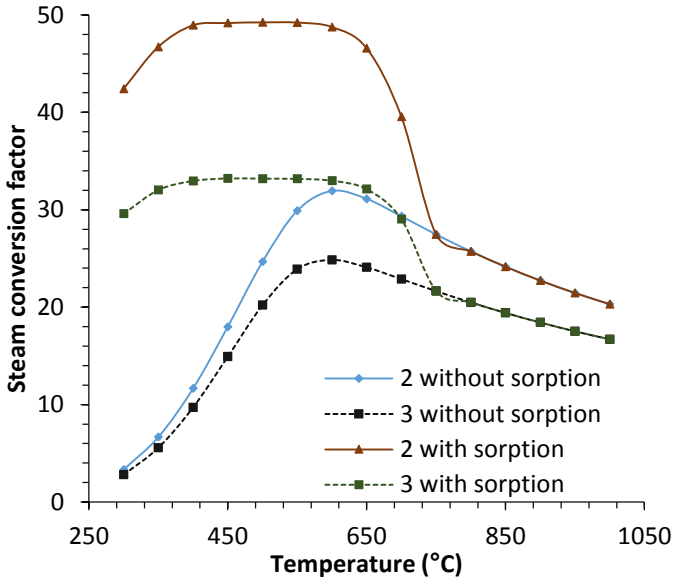

Figure 6.6 Comparison of water conversion (%) with or without sorption enhancement of the steam reforming of acetic acid at S/C= 2 and 3 (p=1atm)

6.4.1.2 Selectivity to carbon gasses and calcium containing components

The selectivity to carbon gases can be seen in Figure 6.7; just as in the case of steam reforming experiments, there is an increase in the selectivity of CO as the temperature of operation increases, there is however a dip between 650 °C and 750 °C except at steam to carbon ratio 4 where the dip in selectivity is not apparent. The selectivity to CO_2 and CH_4 also shows a similar trend to the steam reforming experiments; an increase in selectivity of CO_2 is observed as the steam to carbon ratio and temperature is increased until an optimal temperature from which it starts to drop. A reverse relationship is also observed in the selectivity to CH_4 as the selectivity reduces as the steam to carbon ratio and temperature are increasing.

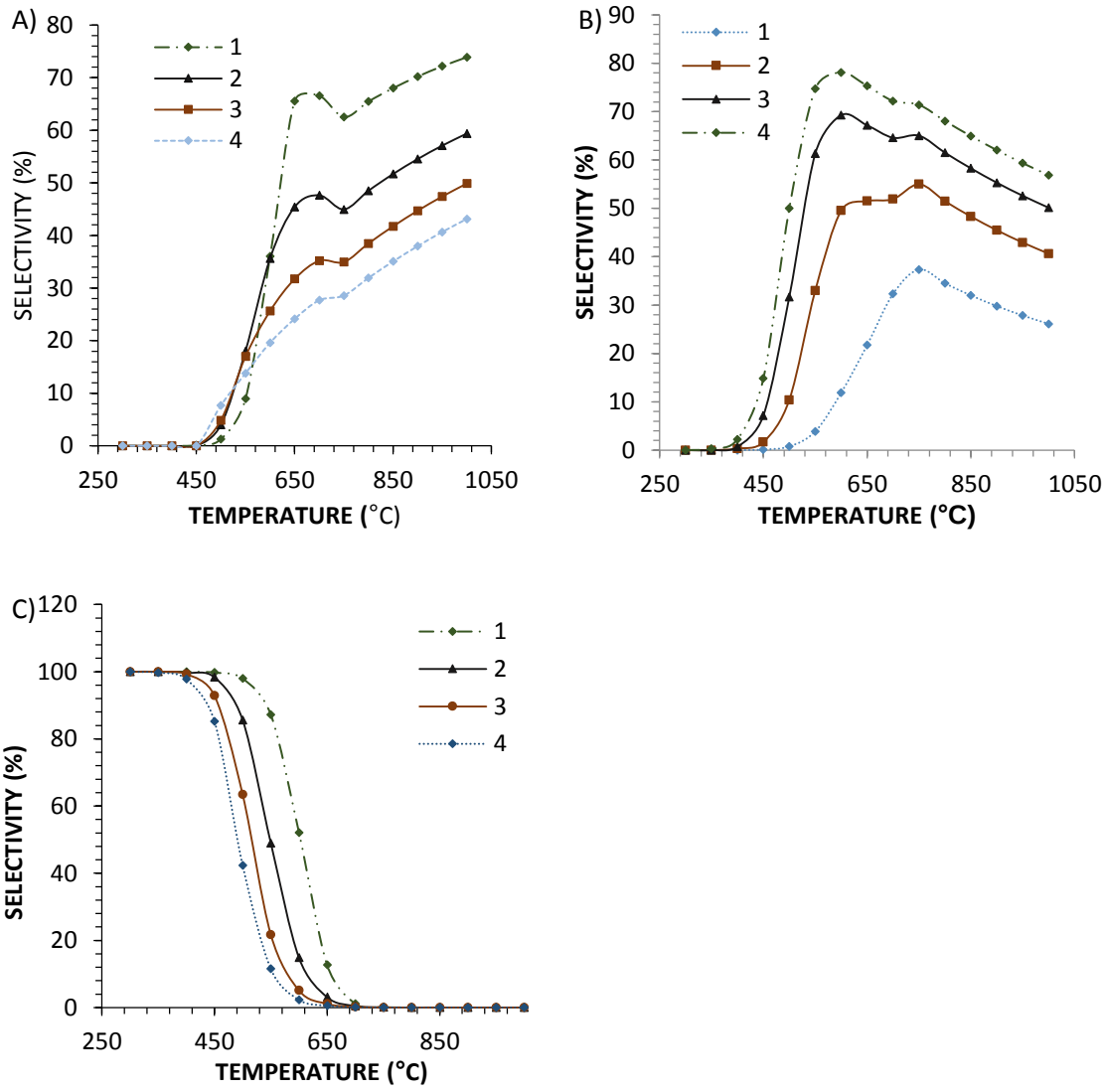

Figure 6.7 Selectivity to A) CO, B) CO_2 and C) Methane for SE-CLSR of acetic acid at different T_{SR} (P= 1 atm)

The selectivity to calcium containing products are indicated in Figure 6.8; a slight increase in the selectivity to $CaCO_3$ is observed as the steam to carbon ratio is increased while a slight decrease in noticed in the selectivity to CaO and $Ca(OH)_2$ as the steam to carbon ratio is increased. This indicates increased sorption activity as the steam to carbon ratio is increased due to the presence of more CO_2 as the steam to carbon ratio increases. Figure 6.8 also indicates that sorption activity for the CaO sorbent is optimal between 450 °C and 600 °C for steam to carbon ratio 1 and 400 °C to 600 °C for higher steam to carbon ratios, although a high selectivity to $CaCO_3$ (>95%) is also observed at

350 °C and 650 °C for steam to carbon ratios > 1. The selectivity to $Ca(OH)_2$ also confirms that competition between steam reforming reactions and sorbent hydrolysis would not occur above 450 °C.

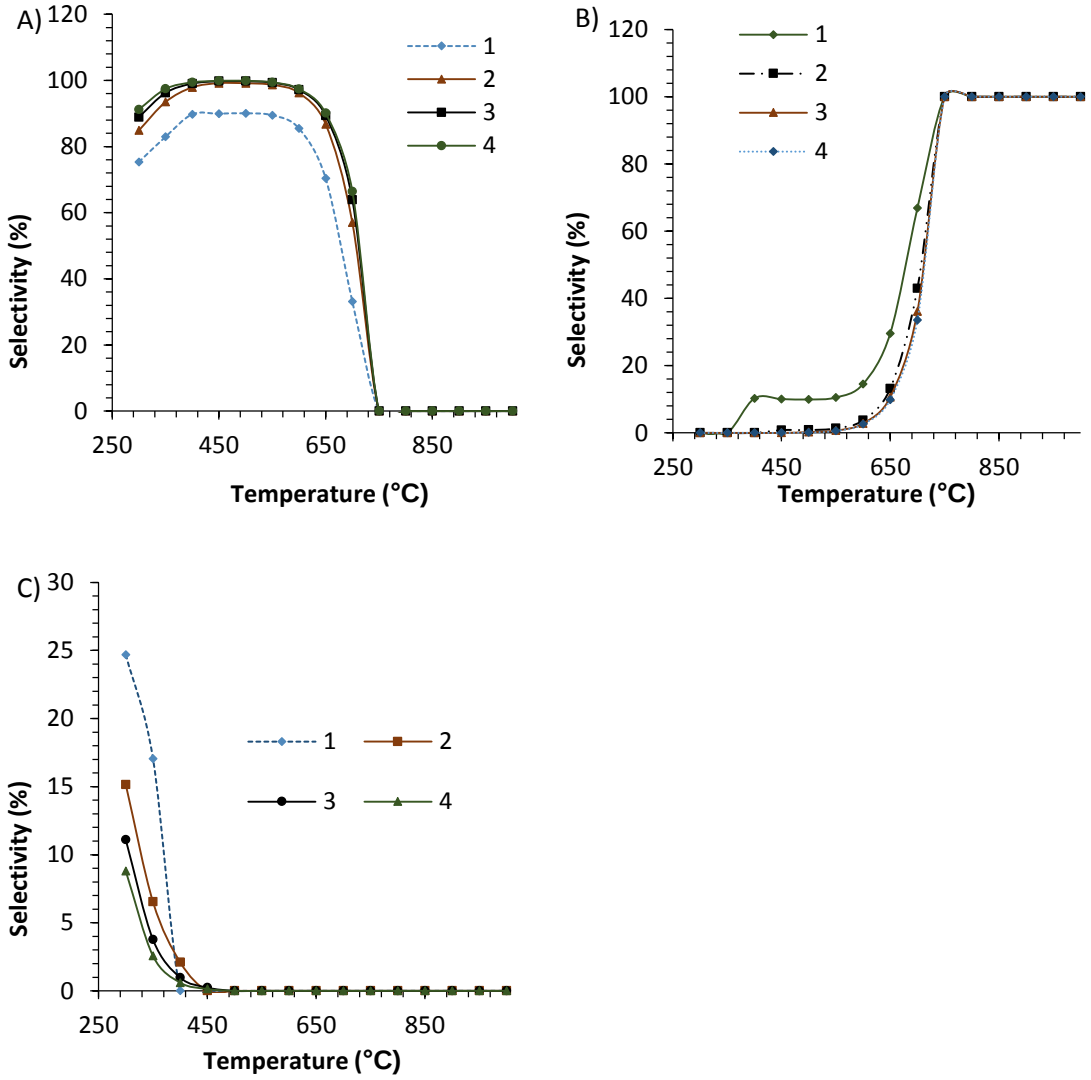

Figure 6.8 Selectivity to A) $CaCO_3$, B) CaO and C) $Ca(OH)_2$ for SE-CLSR of acetic acid at different T_{SR} (p=1 atm)

A comparison of the selectivity to carbon compounds of the steam reforming of acetic acid with in-situ sorption against those without in-situ sorption activity was done using steam to carbon ratio 2 and 3 as shown in Figure 6.9;

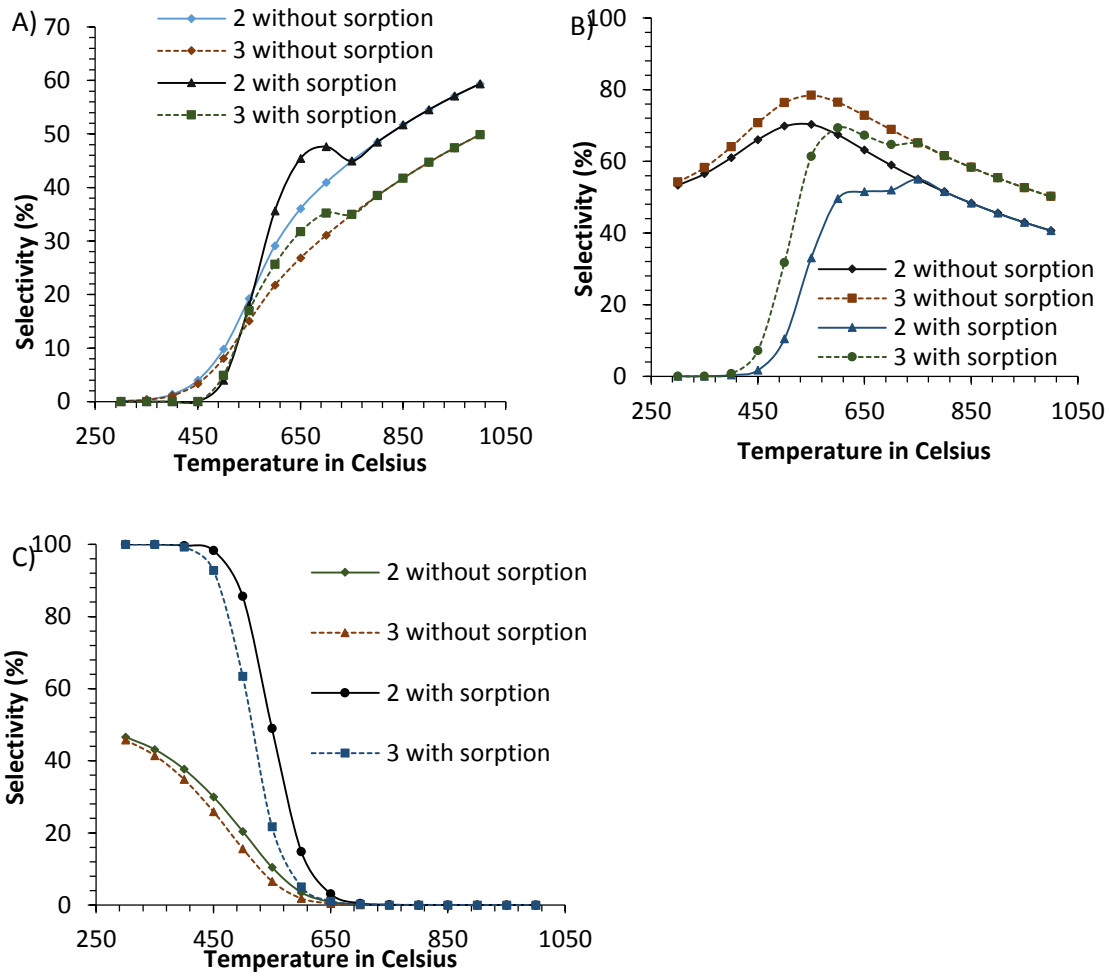

Figure 6.9 Comparison of Selectivity to A) CO, B) CO_2 and C) Methane for SE-CLSR of acetic acid at S/C= 2 and 3 (p=1atm)

As expected there is no difference between with and without sorption processes in the selectivity to carbon products above 750 ° to indicate no sorption activity, the selectivity to CO between 450 °C and 550 °C is higher for the reforming experiments without sorption enhancement as the shift caused due to sorption enhancement would ensure that CO formed are converted to CO_2.

A summary of the thermodynamic equilibrium data indicates that SE-SR of acetic acid is optimal between 400°C and 650°C with steam to carbon ratios set above the stoichiometric limits for the process. It can also be concluded that there would be no sorption enhancement effect at temperatures set above 750 °C at 1 atm.

6.4.2 Effect of the mass of sorbent on the process output analysis

The mass of the sorbent has a huge effect in the material balance on material loading and the operating WHSV; sorption enhanced steam reforming was carried out experimentally at 650°C using different sorbent mass[16] whilst leaving the mass of the catalyst constant with the view to ascertain the effect of the mass of the sorbent on the carbonation or sorption efficiency and process output efficiency. Three experiments (A, B, and C) with 2g of catalyst B were conducted; experiment A was conducted with sand (2g) in addition to the catalyst whilst experiment B and C were conducted with 1g and 2g of sorbent respectively.

6.4.2.1 Post breakthrough phase process analysis

The three phases for SE-SR process (pre-breakthrough, breakthrough and post breakthrough phase) was observed for the sorption enhanced experiments (B and C) whilst one phase was observed for the steam reforming run with sand (A); analyses of the post- breakthrough phase in experiment B and C were compared with the results obtained in experiment A as detailed in Table 6.1;

Table 6.1 Post breakthrough process analysis of experiment B and C compared against experiment A

	Sorbent Mass (g)	**Catalyst Mass (g)**	**X_{HAc} (fraction)**	**X-H_20 (faction)**	**Sel CO_2 (%)**	**SEL CO (%)**	**SEL CH_4 (%)**	**Hydrogen purity (%)**	**Hydrogen yield (wt. %)**
			Equation 4:1		Equation 4:4			Equation 4:3	Equation 4:2
A	0	2	0.93	0.22	76.10	23.30	0.60	62.96	10.63
B	1	2	0.91	0.22	72.75	26.50	0.60	63.15	10.45
C	2	2	0.92	0.20	77.10	22.40	0.50	61.93	10.02

There is no apparent or significant difference in the conversion (acetic acid and steam), hydrogen yield (wt. %), hydrogen purity (%) and selectivity to carbon gases observed when all three experimental runs are observed and compared; this indicates that the sorbent has no effect on process analysis after the saturation of the sorbent. All three

[16] The maximum material loading weight that could be effectively utilised for this set of experiments was 4 grams due to limitations set by the size of the reactor

experimental runs had a hydrogen purity efficiency >98% and 92% when compared to equilibrium and stoichiometric values respectively. They also have a hydrogen yield efficiency >87% and 74% when compared with equilibrium and stoichiometric values respectively, indicating a process close to equilibrium.

6.4.2.2 Process output analysis during carbonation period

A more explicit difference in the experimental runs can be seen by comparing the process outputs during the period where sorption enhancement is effective or carbonation period[17] (PB and BT phase). The process CO_2 output fraction as detected by the micro-GC can be seen in Figure 6.10; it takes a longer time for CO_2 to evolve when experiment A is compared to experiment B and C, the delay in the detection of CO_2 in the process output is due to sorption activity occurring. It can also be inferred that the carbonation period is directly linked to the mass of sorbent utilised as an increase in carbonation period is observed for experimental run C when compared to experimental run B.

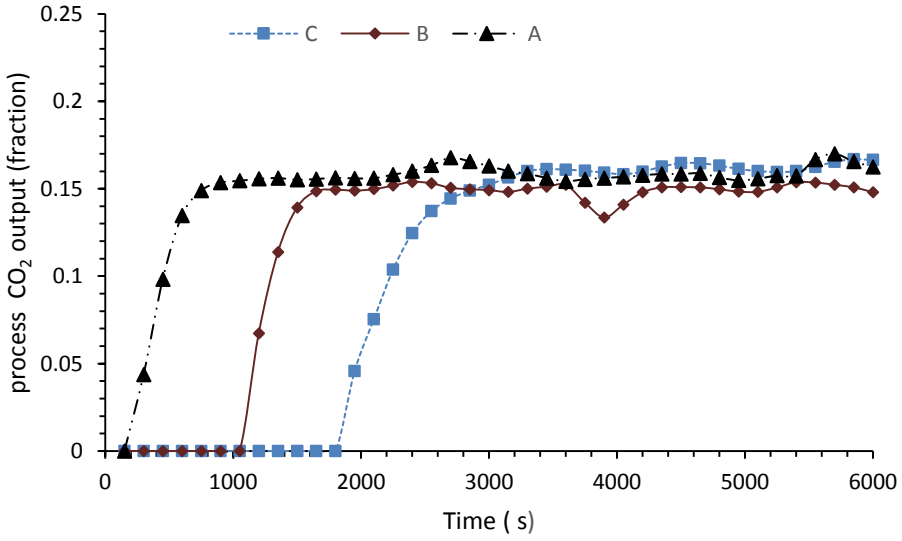

Figure 6.10 Process CO_2 output fraction for experimental runs A, B and C performed at S/C 3 and T_{SR} of 650 C°

[17] The carbonation period is defined as the difference in time from the onset of hydrogen (when compared to hydrogen produced during steam reforming) and time of steady CO2 production.

The total carbonation period was calculated to be 22.5 mins and 52.5 mins for experiment B and C respectively as seen in Table 6.2 with 44% and 52% of the total carbonation period attained in the pre-breakthrough phase where full sorption activity was occurring.

Table 6.2 Carbonation time and rate, and hydrogen purity during carbonation (S/C 3 and T_{SR} of 650 C°)

Experiments	Time (PB) (s)	Time (BT) (s)	Total Carbonation period (s)	Hydrogen Purity [18] (%) (Equation 4:3)	NCO_2 (mol/s) (Equation 6:1)
a	0	0	0	62.96	-
b	600	750	1350	97.77	8.57E-6
c	1650	1500	3150	98.39	8.70E-6

The calculated rate of carbonation or CO_2 adsorption indicates that there is no apparent difference on the rate of sorption activity caused be the change in mass of the sorbent, there is also no identified significant difference in the hydrogen purity obtained during the pre-breakthrough period for experiment B and C. However, there is a significant difference in the hydrogen purity of the experiments with sorption enhancement (experiment B and C) when compared to the one without sorption enhancement; as expected there is an increase in hydrogen purity for experiments with sorption enhancement due to sorption activity.

The sorbent conversion for the experimental runs are depicted in Table 6.3; there is a higher sorbent conversion in experimental run C when compared to experimental run B, these can be attributed to the increased mass of sorbent in the catalyst plus sorbent bed in experimental run C which would allow more carbonation time and hence more sorbent conversion.

[18] Values recorded for hydrogen purity for experimental runs B and C are for the pre-breakthrough phase only

Table 6.3 Sorbent conversion and efficiency for experiment A, B and C (S/C 3 and T_{SR} of 650 C°)

Experiment	Total conversion	Conversion efficiency PB (%)	Conversion Efficiency BT (%)	Total Efficiency at beginning of SS (%)
	Equation 6:2	Equation 6:3		
A	-	-	-	-
B	35.48	77.64	18.88	96.52
C	48.81	80.33	17.71	98.67

In regards to the overall sorbent conversion efficiency (conversion at the end of each time phase (PB, BT and SS) when compared to the overall maximum conversion) as expected a major share of the sorbent conversion was converted during the pre-breakthrough phase (>75% for experimental run A and B) with very little sorption activity (<4% of sorbent conversion) observed at the beginning of the post breakthrough phase.

In summary, it can be concluded from the comparison of experiment B and C that the change in mass of the sorbent affects proportionately the carbonation time which consequently causes a change in the total conversion measured. It however does not have any major effect on the share of sorption activity or efficiency of the sorbent converted during each carbonation phase or the extent of conversion in each phase. Such effects on the process material balance of course do not take into account the effects that sorbent amount may have on the energy balance related to the exothermicity/endothermicity of carbonation/calcination, and heat sink effect of deactivated sorbent.

6.4.3 Optimised cycling stability of SE-CLSR of acetic acid for catalyst B at T_{SR} 650 °C and T_{OX} 850°C

Twenty SE-CLSR cycles were conducted at 650 °C (T_{SR}) and T_{OX} set to 850 °C using catalyst B with steam to carbon ratio set to 3 and WHSV set to 1.18; the operating parameters utilised is within the range stated to be optimal for the SE-CLSR of acetic acid [218, 230].

The three phases of the SE-CLSR reducing run as illustrated in Figure 6.11 was observed and could be easily identified for all 20 cycles conducted;

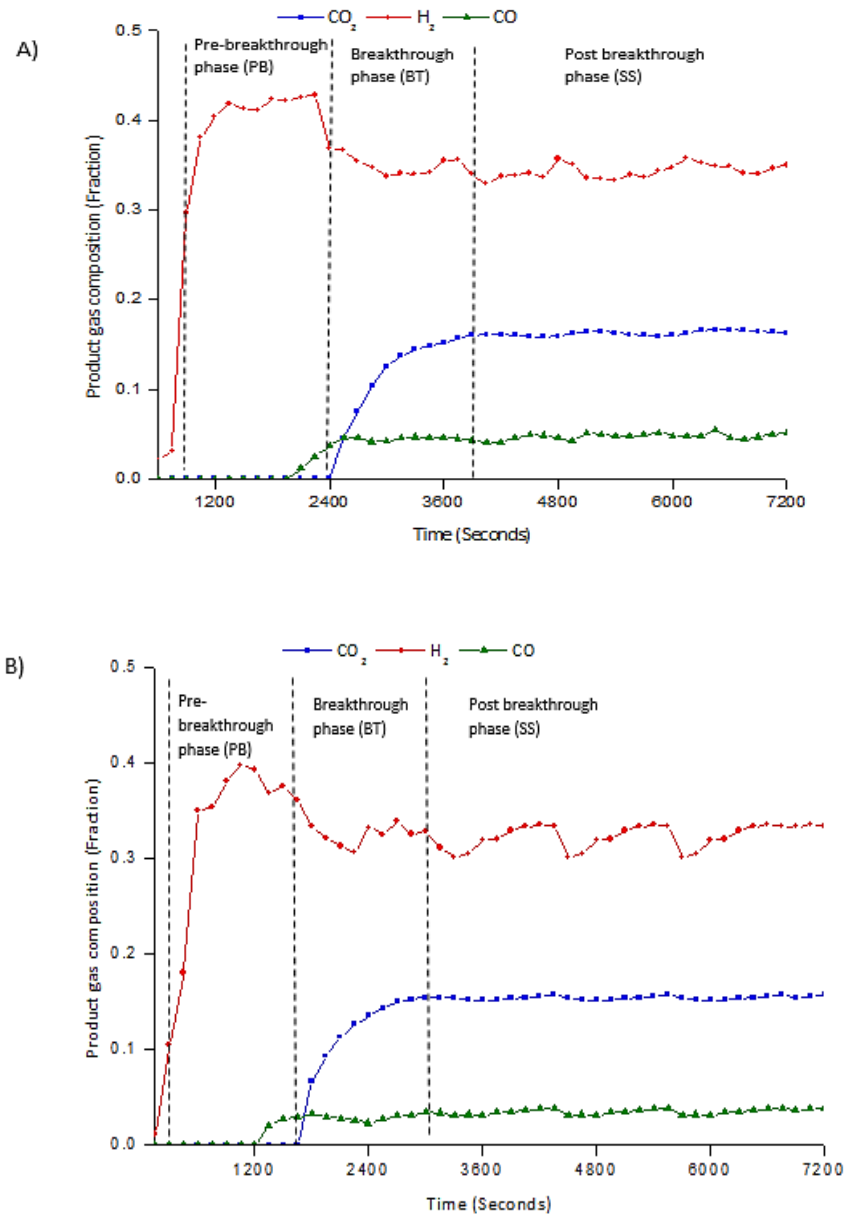

Figure 6.11 Dynamic profile of process gas composition (dry basis) on A) hydrogen reduced catalyst B) auto reduced catalyst cycle 5- (T_{SR}=650°C, WHSV=1.18 hr^{-1},S/C=3,T_{OX}=850 °C)

The easy identification of the three phases after twenty cycles of reforming indicates sorption activity in the reducing phase of all cycles of SE-CLSR; however, analysis of the process output was still essential to determine the extent of the sorption activity and process efficiency.

6.4.3.1 Process outputs with time on stream and upon redox cycling of SE-CLSR-HAc at steady state (fuel-feed stage)

The process gas output observed and detected by the micro- GC for all reducing run was the same detected in the CLSR runs as described in Chapter 5 and consist of CO_2, CO, H_2 and CH_4; elemental analysis of the process outputs was used to calculate the acetic acid conversion, water conversion and hydrogen yield (wt. %) as depicted in Table 6.4;

Table 6.4 Process analysis at steady state or post breakthrough phase (T_{SR}=650°C, WHSV=1.18 hr^{-1}, S/C=3, T_{OX}=850 °C)

cycle number	X_{HAc} (fraction)	X-H_20 (faction)	Hydrogen Purity (%)	Hydrogen Yield (Wt. %)
	Equation 4:1		Equation 4:3	Equation 4:2
1	0.92	0.20	61.93	10.02
2	0.81	0.18	63.14	8.93
3	0.81	0.19	62.48	9.09
4	0.84	0.18	61.77	9.10
5	0.83	0.20	63.12	9.52
6	0.87	0.20	62.38	9.71
7	0.92	0.20	61.64	9.90
8	0.90	0.19	61.34	9.54
9	0.87	0.20	62.58	9.73
10	0.86	0.19	62.07	9.42
11	0.85	0.20	62.71	9.56
12	0.86	0.19	62.30	9.71
13	0.88	0.20	62.29	9.80
14	0.88	0.19	62.03	9.60
15	0.91	0.20	63.14	9.92
16	0.90	0.21	62.81	10.25
17	0.86	0.19	62.27	9.62
18	0.92	0.19	61.57	9.90
19	0.90	0.21	62.71	10.23
20	0.94	0.21	63.14	10.39

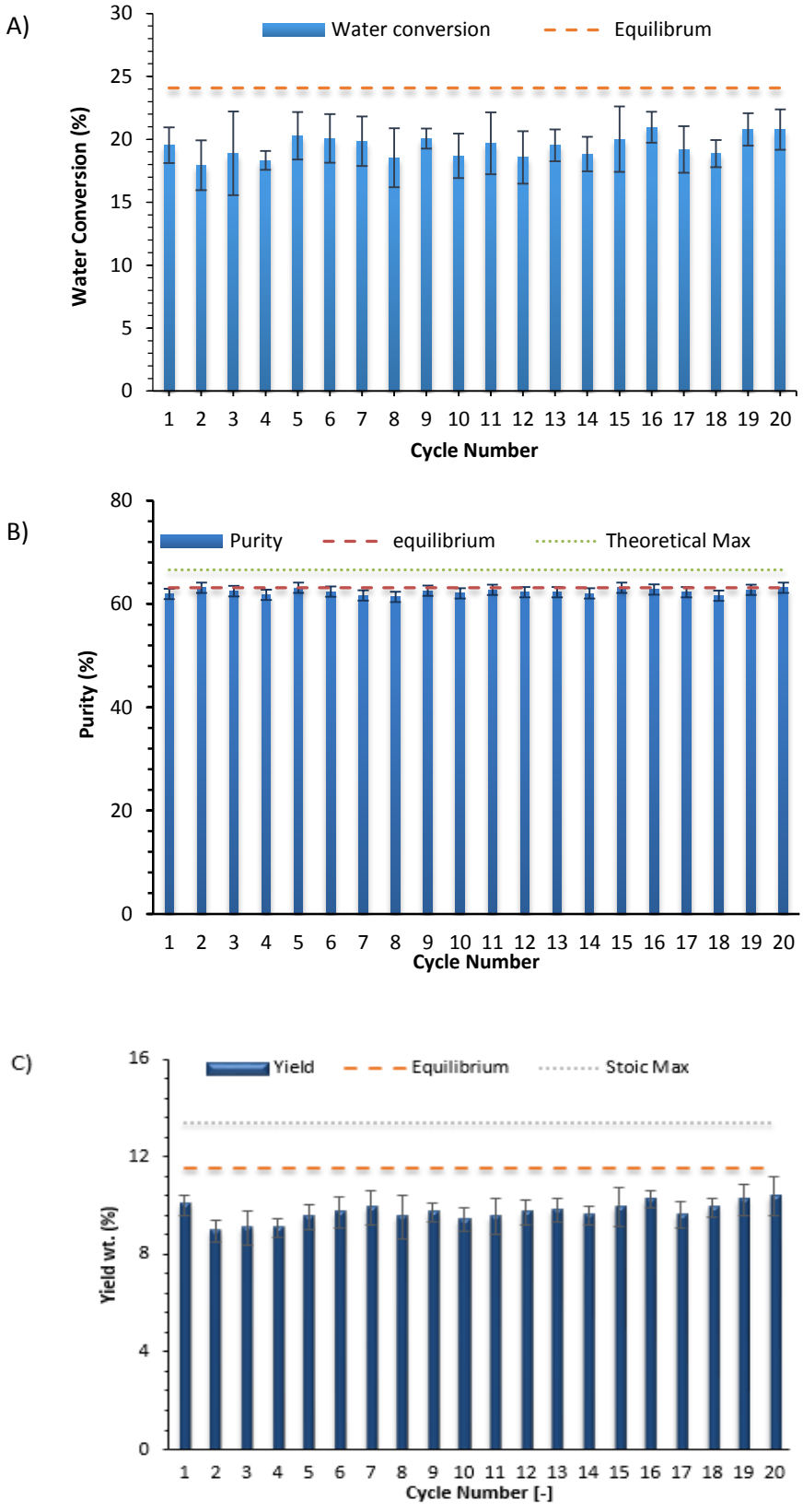

Figure 6.12 Water conversion %%), hydrogen purity (%) and hydrogen yield (wt. %) of 20 cycles of SE-CLSR (T_{SR}=650°C, WHSV=1.18 hr^{-1}, S/C=3, T_{OX}=850 °C)

The fuel conversion at steady state as depicted in Table 6.4 indicates that steam reforming occurred effectively in all 20 cycles; an average fuel conversion of 88 % was obtained across the 20 cycles which compares effectively to those obtained during CLSR experiments.

Figure 6.12 indicates the performance of the process with regards to water conversion, hydrogen purity and hydrogen yield (wt. %) when compared to equilibrium and stoichiometric values; the water conversion at steady state was between 75% - 87% of the equilibrium values across the reducing phase of all SE-CLSR cycles, while the purity of hydrogen across the reducing phase of all cycles of SE-CLSR was between 92%-95% of the calculated stoichiometric or theoretical maximum which equates to >97% of equilibrium values. The hydrogen yield (wt. %) was also > 78% of the equilibrium values across all cycles of SE-CLSR which equates to >67% efficiency when compared to stoichiometric values. The values calculated in regards to efficiency are like those deduced for chemical looping reforming experiments which indicates that the presence of the sorbent has not reduced or affected the catalytic activity of the catalyst across all 20 cycles.

The selectivity to carbon gases at steady state over 20 cycles of SE-CLSR can also be seen in Table 6.5; the major share of carbon (gas) formed is in the form of CO_2 (68% - 81% across all 20 cycles) which indicates that steam reforming and effective water gas reactions are dominant, with very little CH_4 (< 2% of the carbon share for all 20 cycles) formed. The selectivity of carbon gases when compared to equilibrium data shows a high consistency with those formed in CLSR experiments with no sorption enhancement.

Table 6.5 Selectivity to Carbon gases of 20 cycles of SE-CLSR of acetic acid (T_{SR}=650°C, WHSV=1.18 hr^{-1}, S/C=3, T_{OX}=850 °C)

cycle number	Selectivity to CO2 (%)	Selectivity to CO (%)	Selectivity to CH4 (%)
	Equation 4:4		
1	77.10	22.40	0.50
2	80.60	18.40	0.90
3	81.00	17.60	1.40
4	79.70	18.40	1.90
5	81.10	17.80	1.10
6	80.00	18.45	1.55
7	78.90	19.10	2.00
8	78.80	19.60	1.60
9	80.50	18.40	1.00
10	79.30	20.00	0.80
11	80.30	19.00	0.70
12	76.10	23.30	0.60
13	78.50	21.10	0.50
14	76.90	22.60	0.50
15	68.10	30.20	1.70
16	79.90	19.80	0.30
17	76.60	22.80	0.60
18	74.40	25.10	0.60
19	80.30	19.50	0.30
20	75.00	24.40	0.60

In respect to selectivity to hydrogen containing gases; the greater of share of hydrogen formed was in the form of hydrogen gas (>99.6 % selectivity observed across all cycles) with a very little proportion of CH_4 formed (<0.4% selectivity observed across all cycles).

There is no apparent reduction in the process output analysis over twenty cycles which indicates no loss of catalytic activity across the cycles, this is in accordance and is similar to results from other studies on the SE-CLSR of bio-oils, acetic acid and other model oxygenates of bio-oil [101, 150, 229].

6.4.3.2 SE-CLSR oxidation stage process outputs with time on stream

The air feed step in the SE-CLSR process was used to burn off carbon deposits, oxidise the catalyst (Ni to NiO) and regenerate the sorbent as already discussed; just like in the case of chemical looping reforming experiments, the product gas composition as detected by the micro-GC for all 19 SE-CLSR air feed stage contained majorly oxygen, CO and CO_2 as depicted in Figure 6.13;

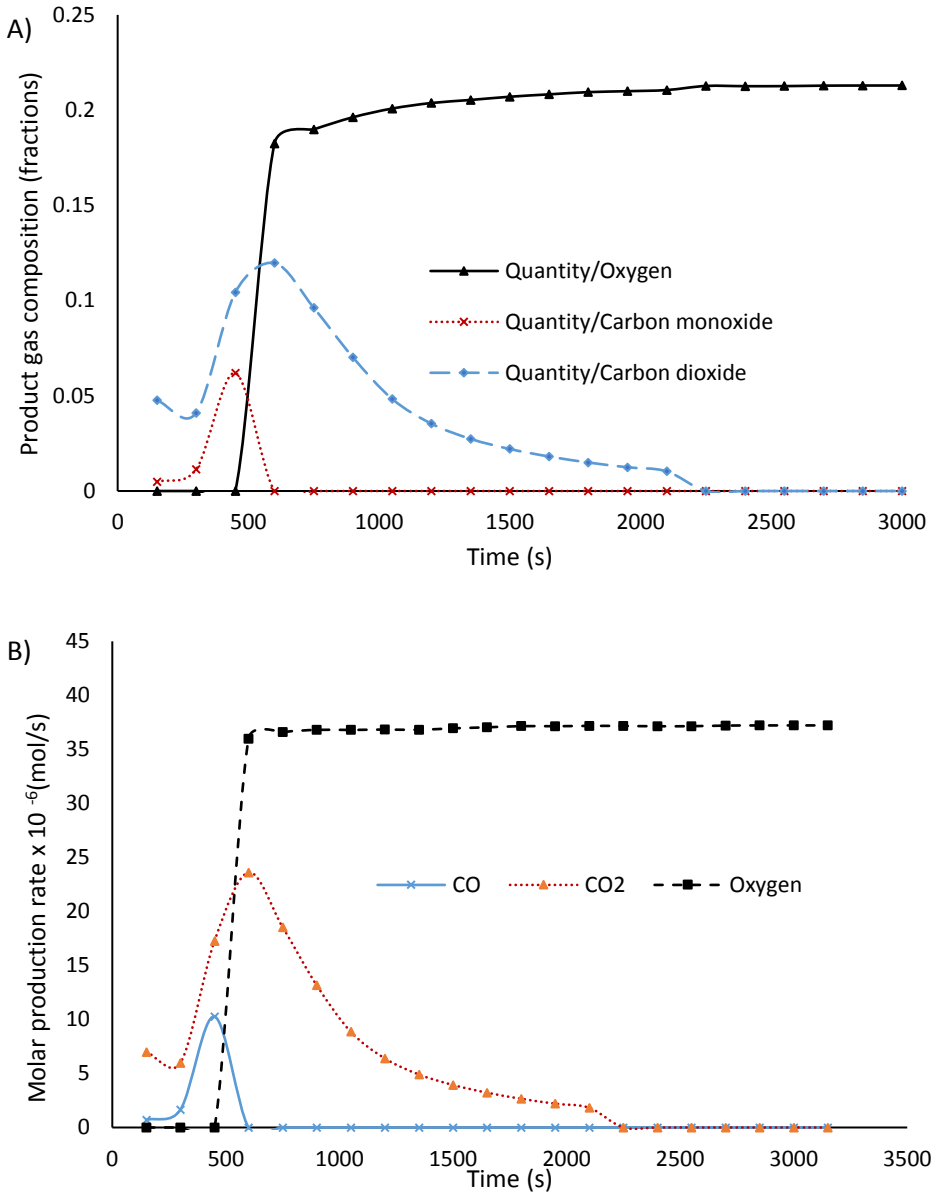

Figure 6.13 A) Product gas composition and B) Molar production rate of products at the air feed for SE-CLSR experiments (T_{SR}=650°C, WHSV=1.18 hr^{-1},S/C=3,T_{OX}=850 °C)

Similarly, to chemical looping experiments, the carbon derived gas products are evolved first for the 19 oxidation phase of SE-CLSR; this indicates the utilisation of the air in oxidation of the catalyst and burning of carbon deposits on the surface of the catalyst and sorbent. The exothermic nature of the oxidation process also led to an increase in temperature observed from the Pico log reader at the beginning of the air feed stage for all 19 cycles; the increase in temperature varied from cycle to cycle but was within 25°C to 45°C for all 19 cycles. The endothermic calcination process occurring simultaneously during the oxidation phase should naturally mean that the increase in temperature observed should be less than those observed in chemical looping reforming experiments; however, a further increase in temperature was observed for SE-CLSR than CLSR in a previous study. They attributed this to more active Ni sites available during the SE-CLSR oxidation phase due to carbon deposition on the surface of the sorbent instead of the surface of the catalyst [101]. In this study, however, there is no apparent difference in the increase in temperature averagely across the SE-CLSR cycles when compared to those observed during chemical looping reforming.

Other calculations derived through elemental analysis of the oxidation phase in chemical looping reforming experiments could not be calculated in the SE-CLSR process as the origin of the evolved gases could not be ascertained from the reactions occurring in this phase. Nevertheless, an overall carbon balance was calculated and was used as a basis for comparison with chemical looping reforming experiments without sorption enhancement.

6.4.3.3 Overall carbon balance of SE-CLSR process

An overall carbon balance was carried out on the SE-CLSR process across 20 cycles of reforming as detailed in Table 6.6; as an average, 3.7% of the carbon feed was unaccounted for through the carbon balance across 20 cycles of SE-CLSR (full details of the overall carbon balance is given in Appendix 2 Carbon balance Calculation). This means the remainder was accounted for in either the carbon gases evolved during reduction/reforming phase, or carbon gases evolved during the oxidation phase (equal

to the solid carbon deposited in the preceding reduction/reforming phase), or the carbon present in the condensate.

Table 6.6 Overall carbon balance of the SE-CLSR process across 20 cycles (T_{SR}=650°C, WHSV=1.18 hr^{-1}, S/C=3, T_{OX}=850 °C)

	C- in (feed) (Mol) ×10^2	Fuel Conversion (%)	C- out Process (mol) ×10^2	C –oxidation run (mol) × 10^2	C- condensate (mol) ×10^5	Total carbon out (mol) ×10^2	Balance × 10^3
1	6.91	91.76	3.91	3.09	5.13	7.00	-0.88
2	6.91	80.90	3.13	3.51	2.00	6.65	2.66
3	6.91	81.10	3.15	3.56	0.849	6.71	2.01
4	6.91	83.91	3.74	2.87	1.86	6.61	3.05
5	6.91	82.89	3.84	4.31	1.94	8.15	-12.4
6	6.91	87.35	3.26	3.54	1.87	6.80	1.13
7	6.91	91.81	4.20	2.71	1.98	6.92	-0.02
8	6.91	89.56	3.58	3.15	1.42	6.73	1.80
9	6.91	86.72	3.24	2.93	2.29	6.17	7.44
10	6.91	85.77	4.11	2.81	1.90	6.92	-0.08
11	6.91	84.62	3.56	2.98	1.54	6.54	3.71
12	6.91	86.01	3.87	3.24	2.75	7.12	-2.04
13	6.91	88.44	3.61	2.82	1.69	6.44	4.78
14	6.91	87.58	3.82	2.64	1.95	6.46	4.51
15	6.91	91.24	3.91	2.17	1.98	6.08	8.37
16	6.91	90.45	4.71	1.67	3.81	6.38	5.28
17	6.91	86.84	4.77	1.94	3.66	6.71	1.98
18	6.91	92.06	3.57	2.43	2.61	6.00	9.10
19	6.91	90.68	4.43	1.81	3.06	6.25	6.64
20	6.91	93.69	5.60	0.877	2.90	6.48	4.35

The carbon realised out of the process gas was between 0.03 to 0.06 mol, this amounted to 47% to 86.4% of the total carbon share in the process with the remaining carbon particularly burnt off during oxidation as detailed in Table 6.7. Just like in the case of chemical looping reforming, the carbon in the condensate can be considered to be

insignificant as it amounts to an average of 0.04% of the total carbon product share of the overall process across the cycles.

Table 6.7 Percentage share of carbon out in overall SE-CLSR process across 20 cycles (T_{SR}=650°C, WHSV=1.18 hr^{-1}, S/C=3, T_{OX}=850 °C)

	C-Out Process gas SECLSR (%)	C-during oxidation (SECLSR) (%)	C- condensate (%)	Total
1	55.83	44.10	0.07	100
2	47.13	52.84	0.03	100
3	46.99	53.00	0.01	100
4	56.59	43.39	0.03	100
5	47.14	52.84	0.02	100
6	47.87	52.10	0.03	100
7	60.79	39.18	0.03	100
8	53.13	46.85	0.02	100
9	52.45	47.51	0.04	100
10	59.42	40.55	0.03	100
11	54.44	45.54	0.02	100
12	54.43	45.53	0.04	100
13	56.09	43.89	0.03	100
14	59.14	40.83	0.03	100
15	64.33	35.63	0.03	100
16	73.84	26.10	0.06	100
17	71.11	28.84	0.05	100
18	59.44	40.52	0.04	100
19	70.94	29.01	0.05	100
20	86.42	13.53	0.04	100

The percentage carbon share across the cycles of SE-CLSR were compared against the total carbonation time as seen in Figure 6.17; a general increase in the process carbon gas during the reduction/reforming phase is observed which corresponds to a decrease in the carbon produced during oxidation (CO and CO_2 evolved by calcination). This supports a gradual decrease in the CO2 captured during the reduction/reforming phase.

A comparison of the share of carbon out in the overall process of the CLSR experiments and the SE-CLSR experiments was done as seen in Figure 6.14; the carbon content from the process gas has more influence in the CLSR experiments where it averaged 89% when compared to SE-CLSR experiments where it averaged 53% across the first 5 cycles. This is basically attributed to sorption activity in the SE-CLSR experiments which ensures that part of the carbon generated during the reforming phase would be captured by the sorbent (pre-breakthrough and breakthrough phase) as carbonate. This led to an increase in the carbon gases generated in the oxidation phase in SE-CLSR due to the release of the captured carbon during calcination of the sorbent as expected.

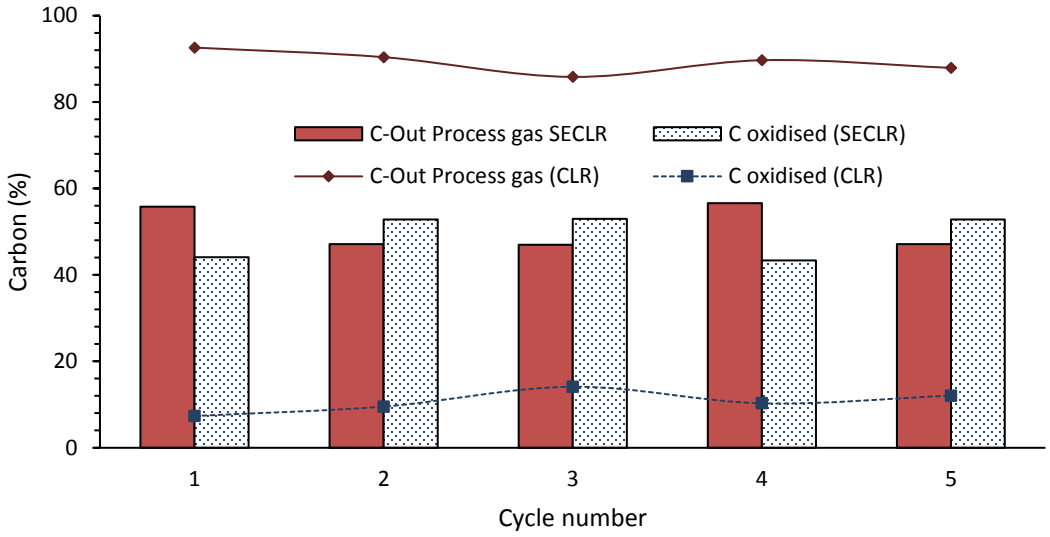

Figure 6.14 Comparison of the percentage carbon share in CLSR and SE-CLSR experiments across 5 cycles (T_{SR}=650°C, WHSV=1.18 hr^{-1}, S/C=3, T_{OX}=850 °C)

The duration of carbon detection in the oxidation phase in SE-CLSR experimental runs when compared to CLSR runs can be seen in Figure 6.15; as expected the duration of carbon detection is higher for sorption enhanced experiments due to carbon generated from calcination of the sorbent which is also occurring.

The observed decline in the duration of carbon detection in SE-CLSR can also be attributed to the loss of sorbent efficiency in the subsequent reforming step (discussed in subsequent sections); this decline is not observed in the chemical looping experiments due to lack of sorption activity.

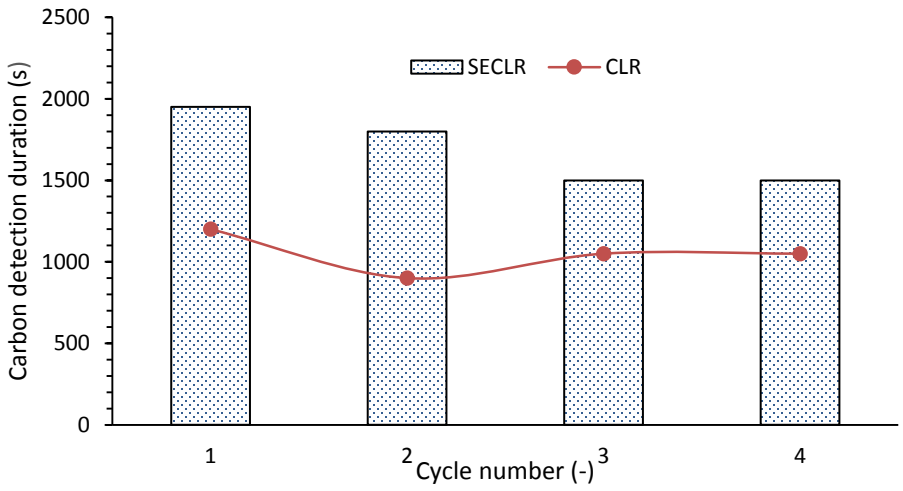

Figure 6.15 Duration of Carbon detection in the oxidation phase of Chemical looping reforming experiments and SE-CLSR experiments (T_{SR}=650°C, WHSV=1.18 hr^{-1}, S/C=3, T_{OX}=850 °C)

6.4.3.4 Carbonation time and carbonation rate of the sorbent across 20 cycles of SE-CLSR

It is widely reported that the carbonation of the sorbent starts with a fast chemical carbonation reaction which is then followed by a slower diffusion controlled phase reaction caused by the presence of $CaCO_3$ [229, 234, 244, 245].The rate and extent of carbonation during the carbonation period (pre-breakthrough and breakthrough phase) is essential to ascertain efficient sorbent activity during the SE-CLSR process; the three phases identified for each experimental run are thus divided into three time zones as depicted in Figure 6.2 where T_0 depicts the start of the pre-break period, T_{BT} depicts the beginning of the break through and T_{SS} depicts the start of the steady state. The time zones are then used to determine the carbonation time and extrapolate the carbonation rate using Equation 6:1 as seen in Table 6.8;

Table 6.8 Carbonation time and rate across 20 cycles of SECLSR

cycle number	Pre- Break Duration (T_{BT}-T_0) (s)	Breakthrough Duration (T_{SS}-T_{BT}) (s)	Total Carbonation Time before sorbent saturation (s)	$Nco_{2,\ CARB,PB}$ (mol/ s) × 10^6 (Equation 6:1)
1	1650	1650	3300	8.70
2	1650	1050	2700	7.67
3	1350	1500	2850	7.66
4	1200	1500	2700	7.88
5	1200	1350	2550	7.82
6	1050	1500	2550	8.05
7	900	1800	2700	8.70
8	900	1800	2700	8.45
9	750	1500	2250	8.19
10	750	1650	2400	8.12
11	600	1200	1800	8.00
12	600	1350	1950	8.15
13	750	600	1350	7.88
14	750	750	1500	8.29
15	750	750	1500	8.65
16	600	1050	1650	8.56
17	600	1050	1650	8.22
18	600	1200	1800	8.67
19	600	1350	1950	8.59
20	600	1200	1800	8.87

There is no apparent change or trend observed in the carbonation rate observed in the pre-breakthrough phase which indicates that the sorbent has the capabilities to operate with the same intensity for that phase across multiple cycles; the carbonation rate for all 20 cycles was between 7.7 × 10^{-6} mol/s to 8.87 × 10^{-6} mol/s, and it can also be observed that there is no obvious relationship between the carbonation time and the rate of carbonation across the cycle. There is however a relationship between the rate of carbonation and the number of moles of CO_2 produced in the product output; it can be observed in Figure 6.16 that the rate of carbonation is optimal at the pre-breakthrough phase where no CO_2 is produced but reduces steadily as the production of CO_2 increases in the breakthrough phase.

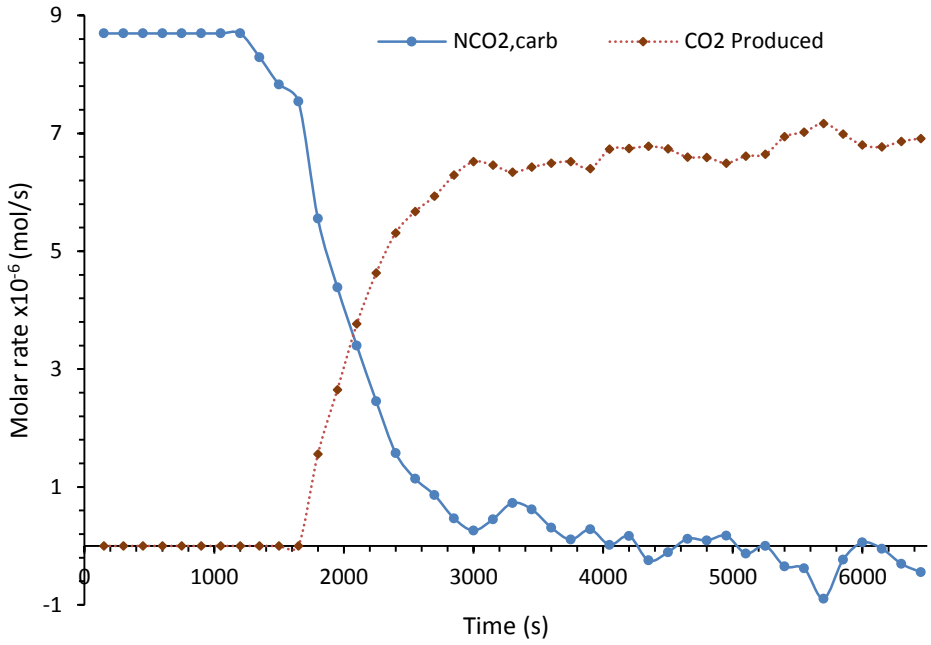

Figure 6.16 Molar production rate and rate of sorbent carbonation process (T_{SR}= 650 °C, S/C=3, at 1atm)

The carbonation time has a huge effect on the overall sorbent conversion and efficiency; as observed in Table 6.8, there is a decrease in the total carbonation time from the 1st cycle to the 2nd cycle, however a steady carbonation time between 38 minutes to 48 minutes, can be observed between cycle 2 and 10 while the total carbonation time after cycle 11 was also steady but below 33 minutes; the steady total carbonation time across cycle 2 and 10 can be attributed to an increase in the breakthrough duration which offsets the reduction in the pre-breakthrough duration. There is a steady reduction in the pre-breakthrough duration until the 9th cycle before a stable pre-breakthrough duration is observed between cycle 9 and cycle 20; the reduction in the pre-breakthrough phase can be attributed to a change in kinetics and CO_2 capture capacity in the pre-breakthrough phase which would have an effect on the full efficiency of the sorbent and its enhancement capabilities[229].

The general increase of the C- out process gas output and the decrease of carbon oxidised from cycle to cycle as detailed in Table 6.6 is due to the reduction of carbon retaining capacity of the sorbent in regards to the sorbent efficiency and the

carbonation time. It can be observed in Figure 6.17 that the carbonation duration reduces steeply in accordance with the carbon produced in the oxidation run; there is however a trend change from cycle 15 when the carbonation time increases while the carbon produced from oxidation still decreases, this trend change is attributed to the reduced influence of the pre-breakthrough phase during these cycles as already discussed.

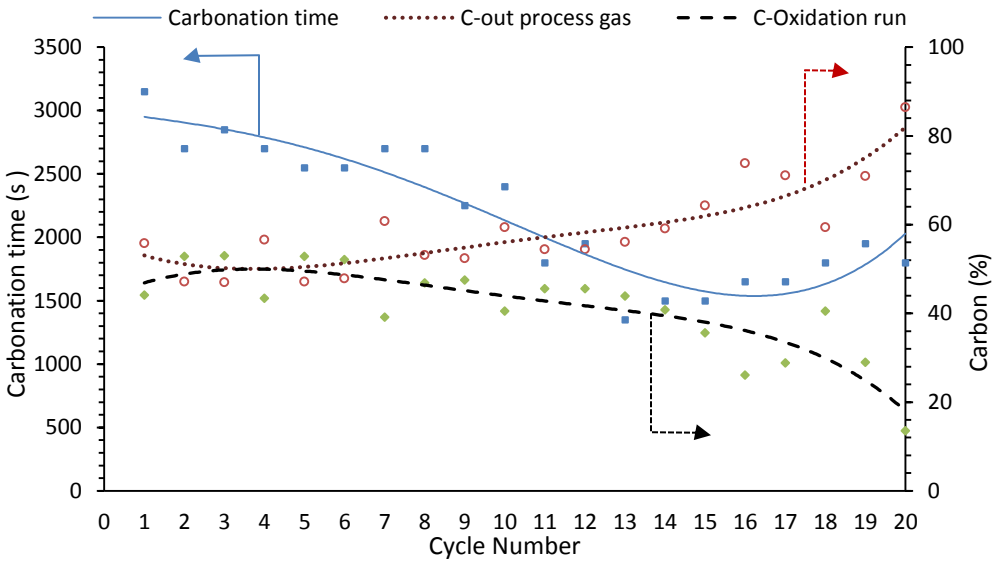

Figure 6.17 Comparison of the total carbonation duration during the reforming phase of SE-CLSR and the share of carbon across the cycles of SE-CLSR. Lines are polynomial fits applied to relevant experimental data. (T_{SR}=650°C, WHSV=1.18 hr^{-1}, S/C=3, T_{OX}=850 °C)

6.4.3.5 Sorption enhancement capacity at Pre-Breakthrough phase (PB) across 20 cycles of SE-CLSR

The SE-CLSR process has been promoted to improve the yield, concentration and purity of hydrogen when compared to conventional steam reforming and chemical looping reforming due to its sorption activity; the hydrogen purity calculated and deduced for the pre-breakthrough phase for all 20 cycles of SE-CLSR was compared against the corresponding hydrogen purity without sorption enhancement as seen in Figure 6.18;

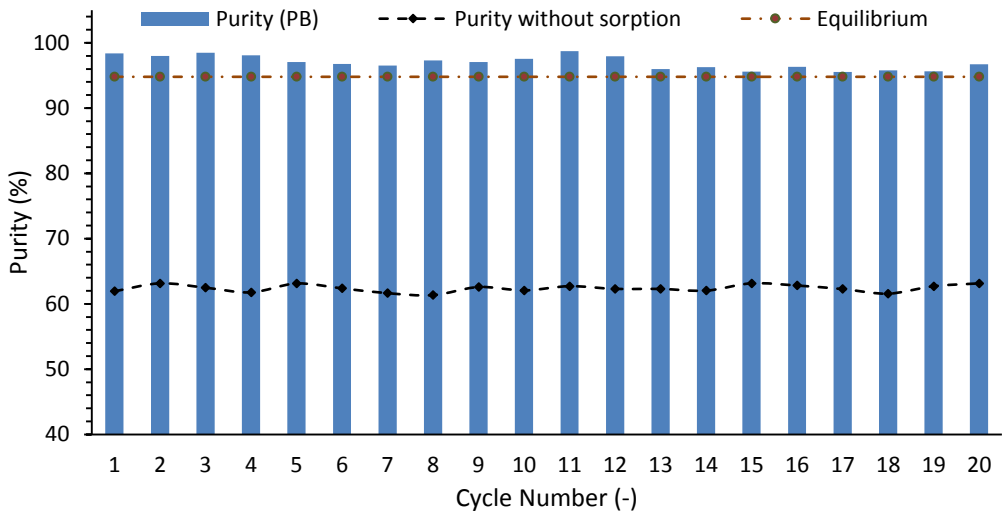

Figure 6.18 Hydrogen purity (%) of 20 cycles of SE-CLSR against the hydrogen purity without sorption enhancement (T_{SR}=650°C, WHSV=1.18 hr^{-1}, S/C=3, T_{OX}=850 °C)

The hydrogen purity for all 20 cycles of SE-CLSR of acetic acid was > 96 % which attains to approximately 101 % efficiency when compared to equilibrium data for all 20 cycles; this is way higher than values realised after the saturation of the sorbent which was in average 62% across all cycles. The dry outlet gas composition of hydrogen also showed a significant increase when the hydrogen obtained at the carbonation phase is compared to the hydrogen produced after sorbent saturation as observed in Figure 6.19;

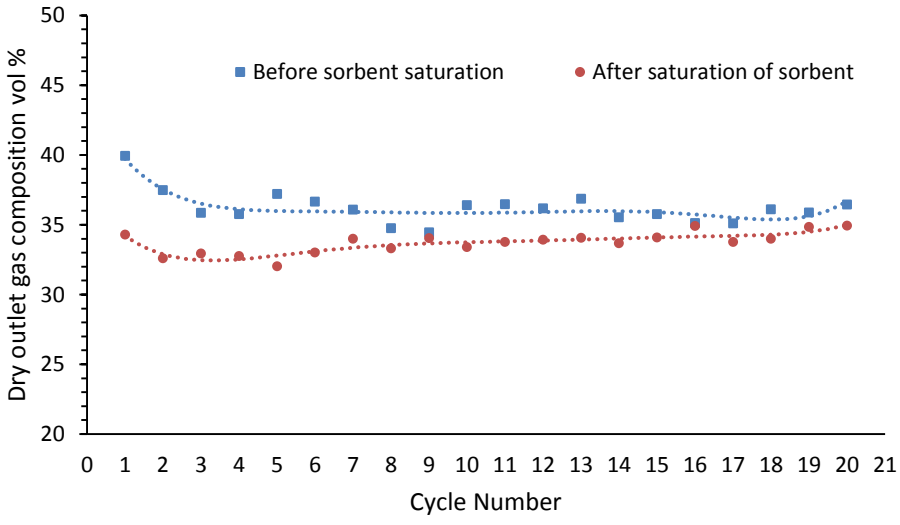

Figure 6.19: Dry outlet gas composition (%) of hydrogen before sorbent saturation and after saturation of sorbent across 20 cycles of SE-CLSR of acetic acid (T_{SR}=650°C, WHSV=1.18 hr^{-1}, S/C=3, T_{OX}=850 °C)

The increased dry outlet gas composition particularly in the first 5 cycles of SE-CLSR indicates that more hydrogen gas was produced during the pre-breakthrough phase, hence it can be inferred that there was a higher yield of hydrogen even at that phase, this would also mean a higher fuel and steam conversion during the carbonation phase.

Another parameter of interest is the effect of sorption activity on the reduction of the catalyst during the fuel feed stage as detailed in Table 6.9; sorption enhancement has been promoted to improve the efficiency of the steam reforming process, as already discussed it leads to higher hydrogen yield and concentration in the product. It can however be inferred that sorption enhancement would also improve the reduction of the catalyst as well because the CO_2 produced during the auto-reduction of the catalyst would also be adsorbed by the sorbent (sorption enhanced reduction).

Table 6.9 Nickel reduction rate, time to maximum reduction and % ratio of NiO reduction (T_{SR}=650°C, WHSV=1.18 hr^{-1}, S/C=3, T_{OX}=850 °C)

cycle number	NiO-Ni rate (mol/s) ×10^6	Time to max red (s)	% R_{red} (%)
	Equation 6:4	Equation 6:5	Equation 6:6
2	6.22	645.69	40.70
3	6.26	641.66	40.85
4	6.79	591.51	42.83
5	6.18	649.83	39.47
6	7.02	580.24	42.41
7	7.87	510.64	45.35
8	7.86	511.15	46.44
9	6.90	581.72	42.14
10	7.14	562.51	44.06
11	6.51	617.24	40.70
12	6.77	593.25	41.66
13	7.23	555.59	43.26
14	7.07	568.30	42.71
15	7.76	517.65	45.01
16	7.18	559.36	42.02
17	6.93	579.75	42.22
18	7.91	507.54	45.50
19	7.22	556.03	42.16
20	7.79	515.45	44.02

The process sequence and auto–reduction capabilities of the catalyst have been discussed in Chapter 5, it was generally agreed that there is a short dead time where steam reforming and auto-reduction of the catalyst occur independently before both

processes occur simultaneously. In this study, it can be observed from Figure 6.20 that the auto-reduction of the catalyst occurs prominently in the pre-breakthrough phase; it can be seen the maximum time required for full reduction of the catalyst for 19 of the 20 SE-CLSR cycles was within the pre –breakthrough phase where all the CO_2 produced are adsorbed by the sorbent. The maximum time estimated for the nickel oxide reduction was between 8 -11 minutes across all 20 cycles with no apparent trend observed across the cycles, there is also no observed trend in the reduction rate across the SECLSR cycles.

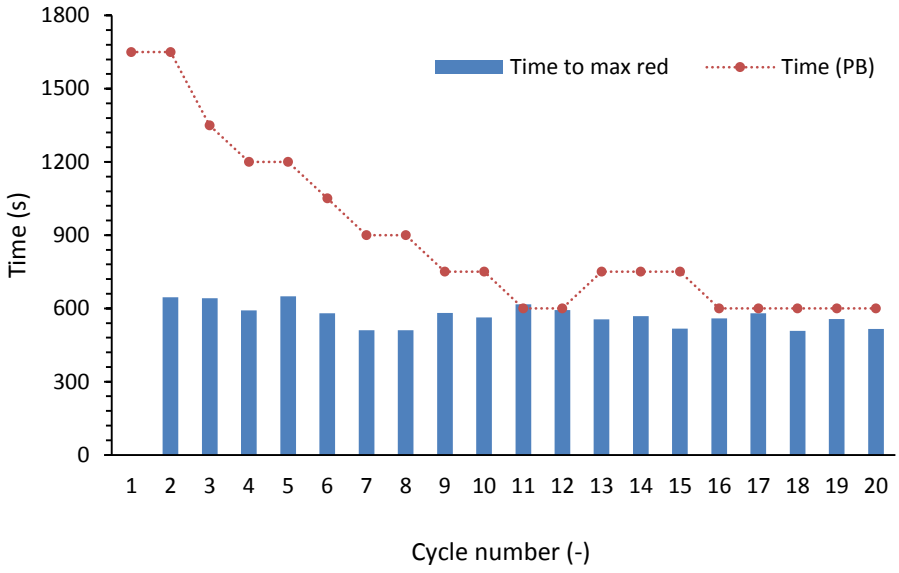

Figure 6.20 Time to maximum NIO reduction and the Pre-breakthrough time (T_{SR}=650°C, WHSV=1.18 hr^{-1}, S/C=3, T_{OX}=850 °C)

The $\%R_{red}$ was in average 39% to 46% across the cycles which confirms that sorption enhanced steam reforming reactions was prominent alongside NiO reduction during the pre-breakthrough phase.

6.4.3.6 Sorbent conversion and efficiency across 20 cycles of SE-CLSR of acetic acid

As highlighted previously, one of the major challenges associated with sorption enhanced processes is the sorbent deactivation that occurs across the cycles, the deactivation of the sorbent can be monitored by observing the sorbent conversion and its efficiency across the SE-CLSR cycles. Table 6.10 shows the maximum sorbent conversion per cycle and its efficiency and share in each carbonation phase;

Table 6.10 Conversion and efficiency of the sorbent across 20 cycles of SE-CLSR (T_{SR}=650°C, WHSV=1.18 hr^{-1}, S/C=3, T_{OX}=850 °C)

Cycle number	Maximum conversion of CaO per cycle (%)	Efficiency PB duration (% of max conversion)	Efficiency BT duration (% of max conversion)	Efficiency at end of BT (% of max conversion)
	Equation 6:2	Equation 6:3		
1	48.81	80.33	17.71	98.67
2	41.07	83.65	14.45	98.09
3	41.24	68.98	24.98	93.96
4	46.38	56.17	27.07	83.24
5	36.59	68.99	22.59	91.58
6	33.69	66.85	26.41	93.27
7	35.72	58.56	32.07	90.63
8	35.30	54.92	30.84	85.76
9	28.05	59.17	34.68	93.85
10	25.99	63.26	29.02	92.28
11	25.49	52.13	35.19	87.32
12	25.05	53.07	36.68	89.75
13	27.27	60.77	24.18	84.95
14	28.63	57.64	32.11	89.75
15	29.70	57.60	25.61	83.21
16	26.84	51.07	35.45	86.52
17	22.17	58.55	30.71	89.26
18	23.46	58.95	33.06	92.01
19	24.69	55.16	37.82	92.99
20	24.85	57.23	35.63	92.86

The maximum conversion for each cycle was calculated using Equation 6:2; it was observed from that full conversion or the highest attainable conversion for each cycle occurred during the post breakthrough phase after sorbent saturation; this as seen in Figure 6.21 indicates that little sorbent activity occurs after the saturation of the sorbent. However, the sorbent activity identified during the post-breakthrough phase amounts to < 2% of the total sorbent conversion in the first two cycle but amounted to < 10 % of the total sorbent conversion for all cycles.

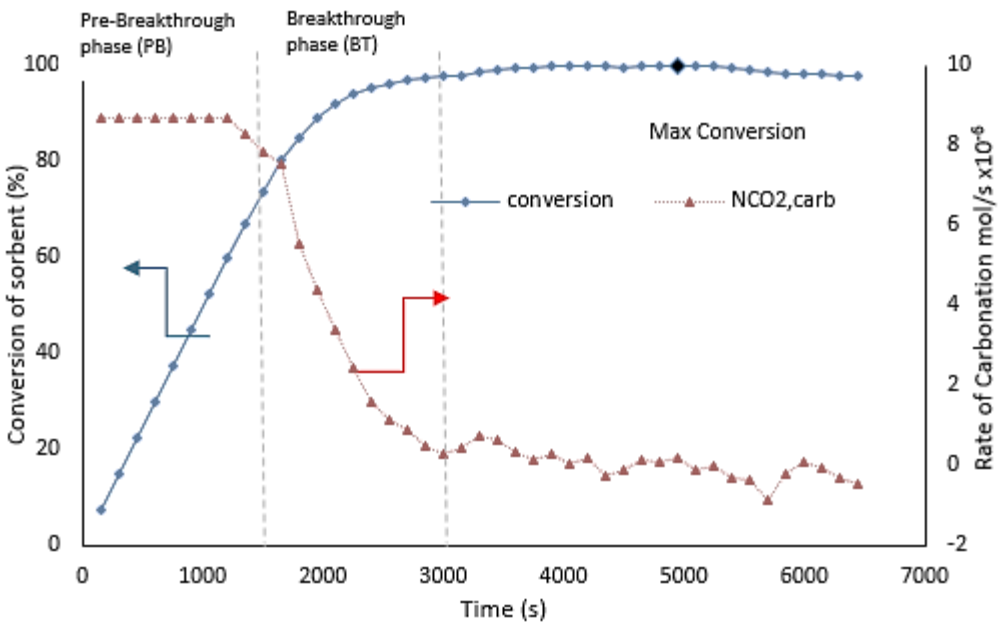

Figure 6.21 Sorbent conversion (%) and carbonation rate (mol/s) during the first cycle of SE-CLSR of acetic acid (T_{SR}=650°C, WHSV=1.18 hr^{-1}, S/C=3,T_{OX}=850 °C)

The major share of sorbent conversion occurred in the pre-breakthrough phase across all 20 cycles of SE-CLSR of acetic acid; results from Table 6.10 shows that 61% of the sorbent was converted in the pre-breakthrough phase across all 20 cycles with over 80% sorbent conversion occurring in the first two SE-CLSR cycles. This indicates that majority of the sorbent converted would have efficiently occurred during the production of high purity hydrogen (>96% dry basis for all 20 cycles).

The conversion efficiency is not dependent on the duration of the pre-breakthrough phase as seen in Figure 6.22 as it stabilises at the 3rd cycle where an efficiency of 51% to 69 % was deduced, whereas the pre-breakthrough phase duration does not stabilise and continues to reduce until the end of the 9th cycle.

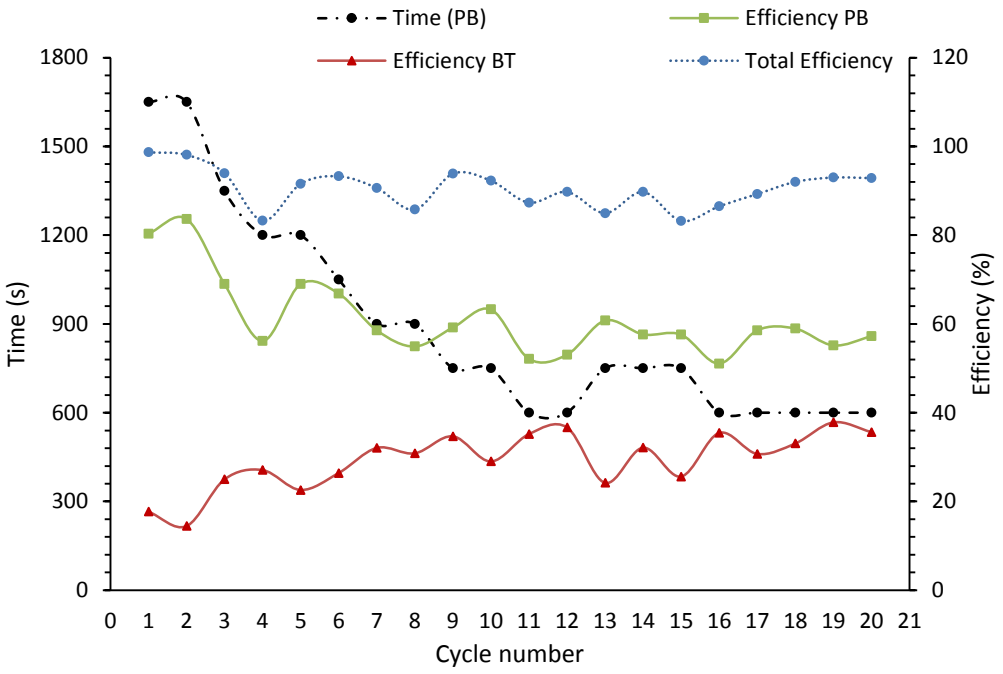

Figure 6.22 Sorbent Efficiency (%) and pre-breakthrough duration (T_{SR}=650°C, WHSV=1.18 hr^{-1}, S/C=3, T_{OX}=850 °C)

The conversion efficiency of the breakthrough phase however continues to rise till the 9th cycle where it stabilises to indicate an increasing sorption activity during the breakthrough phase from cycle 3 to cycle 9 due to the reduction of the pre-breakthrough duration.

There is a steady drop in the maximum conversion of the sorbent across the cycles till the 9th cycle, then a stable maximum conversion (24 % to 27%) is observed for the remaining SE-CLSR cycles. The drop-in conversion coincides with the drop in the pre-breakthrough phase mainly which indicates that the increase in the breakthrough duration which occurred to offset the drop in the pre-breakthrough duration as earlier discussed in 6.4.3.4 has no effect on the conversion of the sorbent.

It can also be observed from Figure 6.23, which shows the fuel conversion, steam conversion and conversion of the sorbent across the 20 cycles of SE-CLSR that the reduction in the sorbent conversion had no bearing with the conversion of the fuel or the steam conversion of the process which indicates that the catalyst operated efficiently across the cycles even as deactivation of the sorbent occurred.

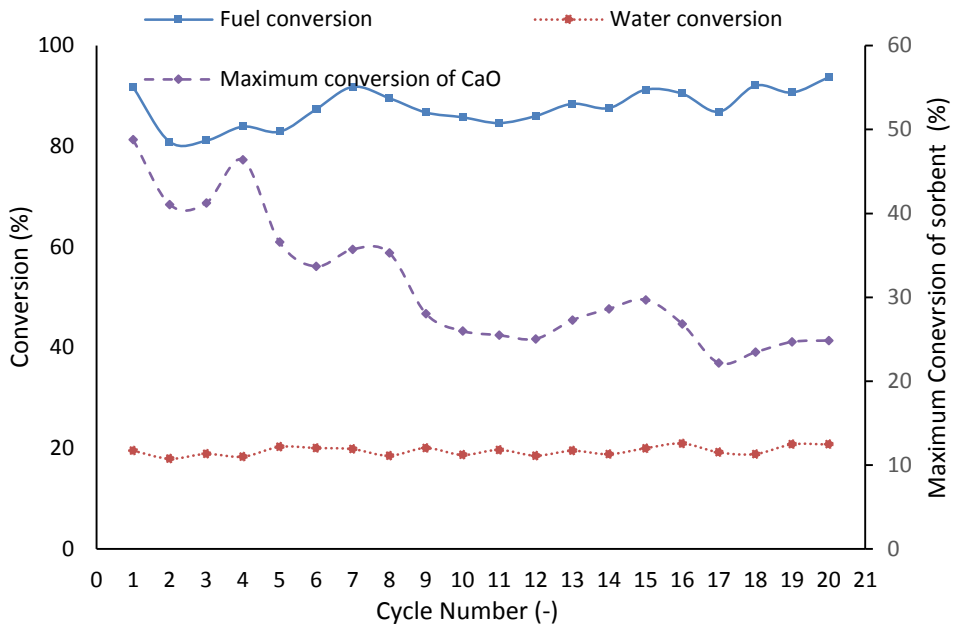

Figure 6.23 Fuel conversion (%), water conversion (%) and conversion of sorbent (%) (T_{SR}=650°C, WHSV=1.18 hr^{-1}, S/C=3,T_{OX}=850 °C)

An overall conversion efficiency was calculated to have a more concise idea of the deactivation of the sorbent across the SE-CLSR cycles as depicted in Figure 6.24; the maximum conversion fraction theoretically for CaO is 0.786, however, it is generally agreed and reported that the conversion fraction is realistically optimal between 0.45 - 0.50 due to conversion limitations caused by pore filling and pore blockage of calcined limestone which is microporous in nature [246]. The overall efficiency for this study was calculated on the assumption that efficient maximum conversion occurs and is optimal at the first SE-CLSR cycle (0.48) using Equation 6:9;

Equation 6:9 Overall conversion of sorbent

$$Overall\ conversion\ efficiency\ at\ cycle\ X = \left(\frac{\text{conversion fraction at cycle X}}{maximum\ conversion\ fraction}\right) \times 100$$

The decay in the conversion fraction across the 20 cycles of SE-CLSR can be seen in Figure 6.24; it can be observed that the overall conversion efficiency or sorption activity for the spent sorbent declines steadily till it stabilises from the 11th cycle. A similar trend for maximum conversion fraction has been observed in previous work on the cyclic ability

or stability of CaO sorbent [124]; at the end of the 20th cycle the sorbent conversion efficiency has dropped to approximately 50 % of the overall conversion efficiency obtained at the end of the first cycle. This corresponds to 26 % – 34 % conversion efficiency obtained at the pre-breakthrough phase from the end of the 9th cycle to the 20th cycle from 80 % obtained at the end of the 1st cycle.

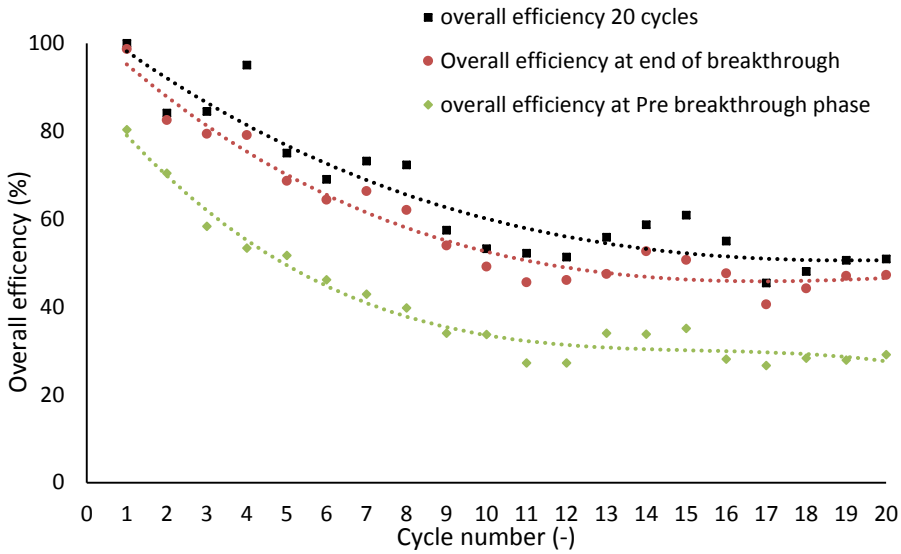

Figure 6.24 Decay in Overall Conversion efficiency across 20 cycles

6.4.3.7 SE-CLSR solids and condensates characterisation

The surface area and pore characteristics of sorbents utilised in cyclic processes has been a major research interest as the cyclic stability of sorbent has been associated with a loss of surface area across cycles; It is difficult to elucidate the surface area analysis of the SE-CLSR process due to the complexity of reactions occurring and the presence of materials with different surface area kinetics in the material bed. It has been previously reported that the surface area of the CaO sorbent would reduce whilst its particle density would increase during carbonation and sorption activity [130]; however, as already discussed in previous chapters, the surface area of the Ni catalyst increased during the reducing phase in chemical looping reforming due to the reduction of the catalyst.

The major reactions occurring at the reducing phase are carbonation of the calcined sorbent, auto-reduction of catalyst and enhanced steam reforming; the overall surface area and pore radius of the materials increased slightly after enhanced steam reforming as indicated in Table 6.11, these give an indication that there is no loss of surface area due to carbonation of the sorbent in the first cycle. A loss in overall surface area and porosity is however observed when the materials from steam reforming is compared to those cycled during SE-CLSR; this is attributed to loss of surface area and porosity due to sorbent decay and might affirm that the loss of sorbent conversion realised across the cycles might be related to the loss of surface area and pore characteristics as already inferred in previous studies [229], the high loss of surface area and porosity in the cycled materials might have also been caused by sintering during the oxidation phase which was carried out at 850 °C to ensure optimal calcination of the sorbent.

Table 6.11 BET surface area analysis of SE-CLSR process (T_{SR} at 650 °C, T_{OX} 850 °C, S/C =3)

	MBET surface area	**Pore volume**	**Pore radius**
	M^2/g	**Cc/g**	**nm**
Catalyst (Red) + spent sorbent (calcined) Fresh	17.480	0.097	1.905
Catalyst (Red) + sorbent ($CaCO_3$) after SE-Steam Reforming	20.271	0.067	1.913
Catalyst (Red) + sorbent ($CaCO_3$) after 10 cycles of SE-CLSR	10.68	0.054	1.899
Catalyst (Red) + sorbent ($CaCO_3$) after 20 Cycles of SE-CLSR	13.428	0.055	0.949

The effect of the loss in surface area and porosity in the oxidation phase is evidenced in Table 6.12 which indicates a 71 % loss in surface area and a 24% loss of pore volume when the fresh catalyst is compared to the oxidised catalyst; the loss of surface area and porosity is attributed to both catalysts and sorbent activities in the oxidation phase.

Table 6.12 BET surface area analysis of SE-CLSR process (oxidation at 850 °C)

	MBET surface area	Pore volume	Pore radius
	M^2/g	Cc/g	nm
Fresh Catalyst (oxidised form) + spent sorbent (calcined)	33.714	0.076	1.919
Oxidised catalyst + calcined sorbent (after 8 cycles of SE-CLSR)	9.623	0.058	1.861

The advantage of SE-CLSR can be inferred through observation and comparison of the surface area and open porosity of the oxidised catalyst plus sorbent and the surface area of the used catalyst (reduced) plus un-calcined sorbent in SE-CLSR. As observed, there appears to be a similar pore volume and surface area observed. This is because as already discussed for chemical looping reforming, the Red-Ox cycles would ensure stability of the Ni particle size and activity [203], and the loss in surface area and porosity of the sorbent is linked and associated to its overall conversion efficiency, which as detailed in this chapter, remained relatively stable after the 9^{th} cycle. It can therefore be inferred and assumed from the comparison of the surface area that there would be a reduction in the MBET surface area of the sorbent plus catalyst across the cycles which would affect the sorbent conversion in the next cycle until a certain point when the surface area becomes steady due to the Red-Ox cycling just as observed in the overall efficiency of the sorbent. There is however, a reduction in the pore radius of the used catalyst and sorbent mix from cycle to cycle which indicates the formation of smaller pores from cycle to cycle.

SEM images of the fresh and used catalyst plus sorbent can be seen in Figure 6.25; a similar image can be seen for the oxidised and fresh catalyst plus sorbent, filamentous carbon cannot be noticed in the oxidised material when compared to the used catalyst and sorbent. Just as in the case of chemical looping reforming two types of carbon filaments were observed, a large carbon filaments of about 139 nm and a short carbon filaments between 19-35nm; it has been inferred that the carbon formed particularly could also be deposited on the surface of the sorbent [101], these, as seen in the SEM images of the oxidised materials, would be burnt off during oxidation.

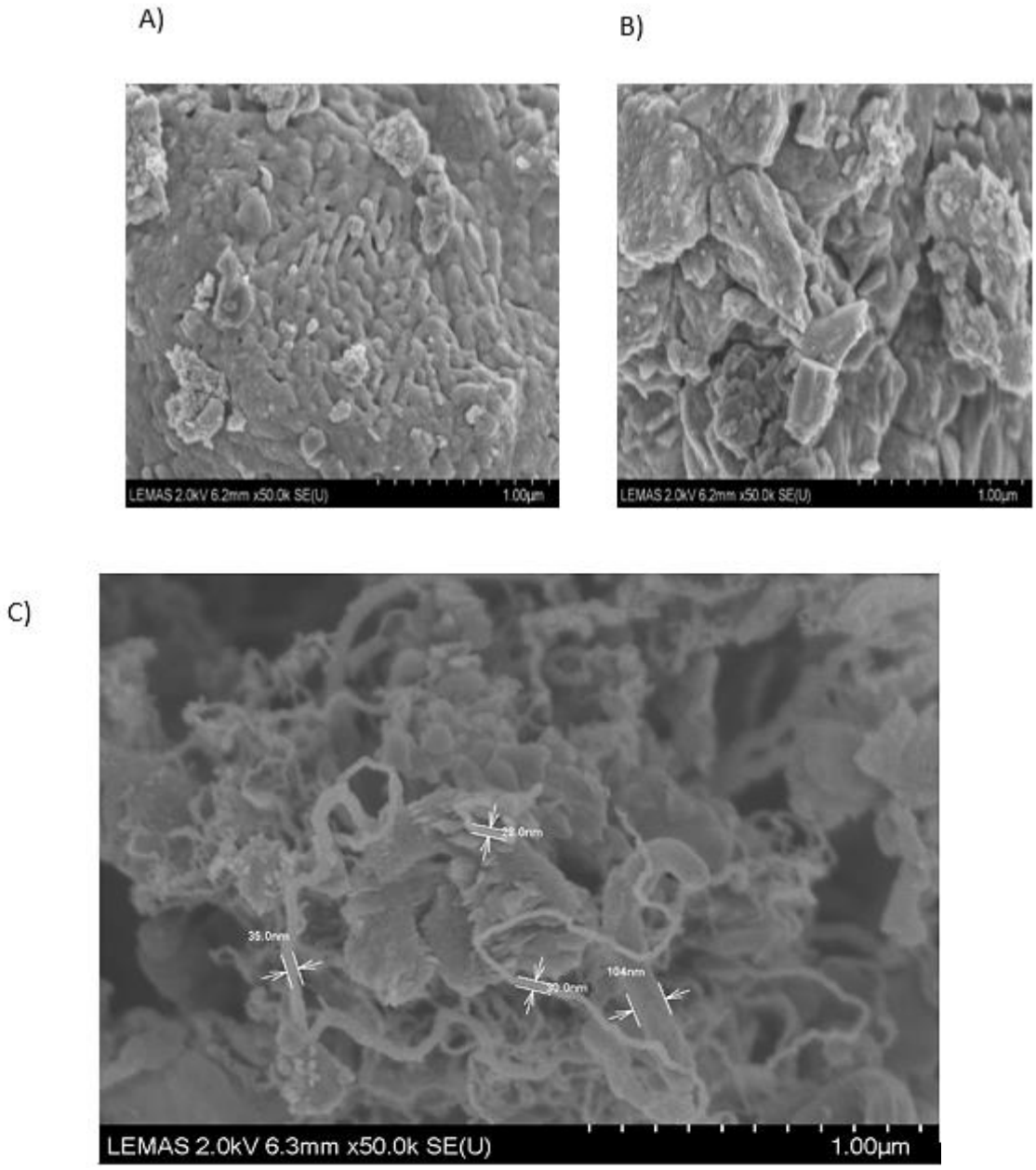

Figure 6.25 SEM images of the A) fresh catalyst (oxidised) plus spent calcined sorbent B) oxidised used catalyst plus calcined sorbent C) used catalyst (reduced) and sorbent ($CaCO_3$) after 20 cycles of SE-CLSR of acetic acid (T_{SR}: 650 °C, T_{OX}: 850 °C, S/C:3)

TEM images and SAED diffraction patterns of the used CLSR catalyst can be seen in Figure 6.26, a similar pattern to those observed in chemical looping reforming can be seen in the TEM images; the observed TEM and SEM images for the used catalyst and sorbent after SE-CLSR gives an impression that more carbon has been deposited due to the presence of more dispersed filamentous carbon, this can be attributed to the higher

number of reforming cycles which the SE-CLSR catalyst and sorbent has been exposed to. Figure 6.26 (A and B) clearly shows the filamentous carbon formed on the materials, with a poly crystalline structure just as in the case of chemical looping reforming catalysts observed in below C, the diffraction of Figure 6.26D as seen in Figure 6.26E shows a ring like structure with crystal spots clearly seen.

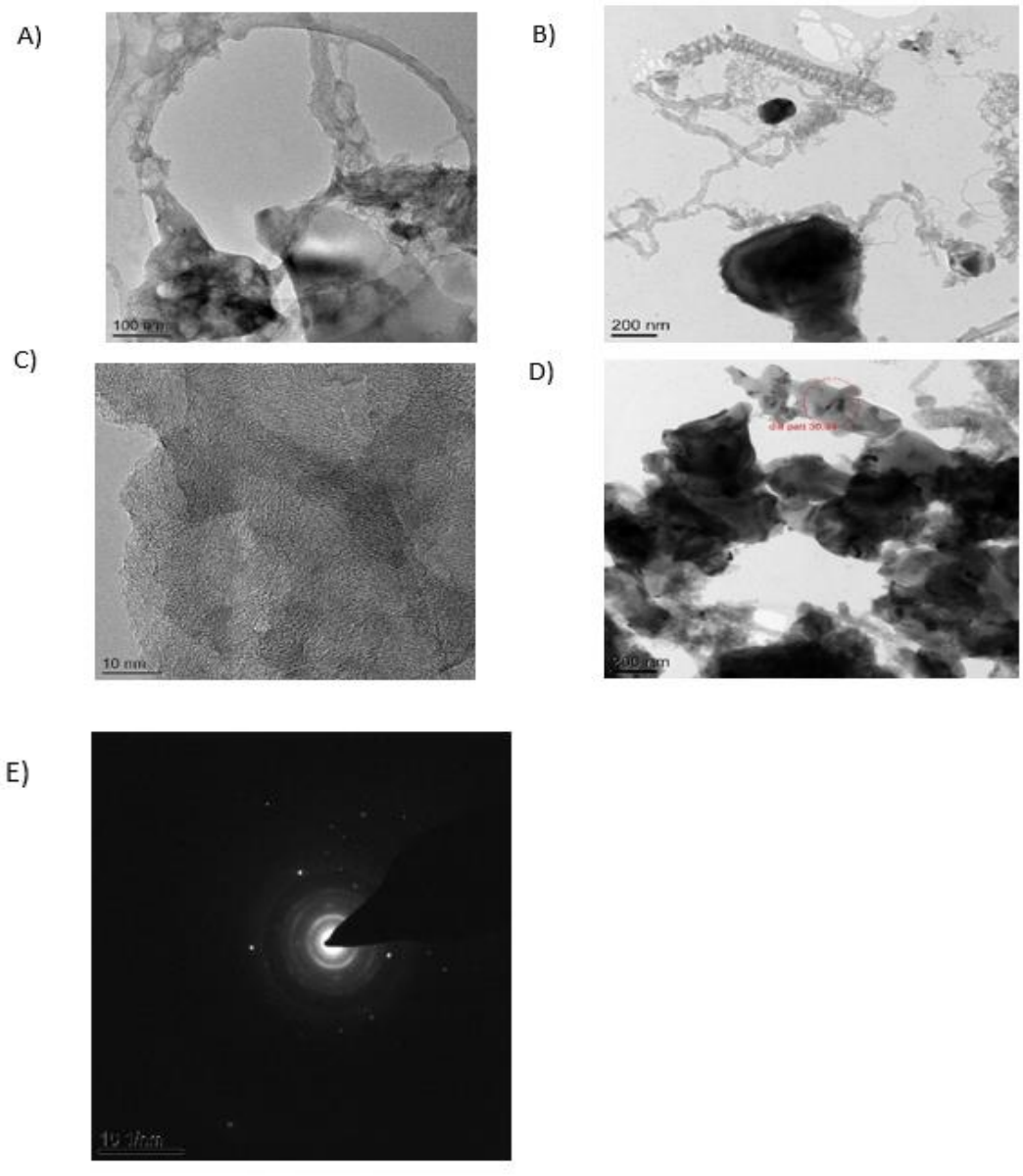

Figure 6.26 TEM images (A-D) and SAED diffraction pattern (E) of used SE-CLSR catalyst (reduced) plus sorbent ($CaCO_3$) after 20 cycles of SE-CLSR (T_{SR}=650°C, WHSV=1.18 hr^{-1}, S/C=3, T_{OX}=850 °C)

A similar carbon profile was attained through EDX profiling of the fresh and oxidised catalyst just as in the case of chemical looping reforming experiments, this indicates that the oxidised catalyst and sorbent have been fully oxidised and calcined respectively at the temperature of oxidation. The weight percentage of carbon in the used catalyst and sorbent is higher than those obtained in the oxidised or fresh catalyst; this is due to carbon deposited as already observed through SEM and TEM images, and unlike the EDX profile of the used catalyst in the chemical looping reforming experiments, the weight percentage of carbon varies in different points or spectra as observed in Table 6.13. This might indicate that the carbon is more dispersed after the SE-CLSR as already inferred from the TEM and SEM images.

Table 6.13 Carbon present through EDX profiling of Fresh, Oxidised and used catalyst and sorbent during the SE-CLSR process (T_{SR}=650°C, WHSV=1.18 hr^{-1}, S/C=3, T_{OX}=850 °C)

	Fresh catalyst and sorbent	Oxidised catalyst and sorbent after 8 cycles of steam reforming	Used catalyst and sorbent after 20 cycles of SE-CLSR (Point 1)	Used catalyst and sorbent after 20 cycles of SE-CLSR (Point 2)
	Wt. %	Wt. %	Wt. %	Wt. %
Carbon Present	4.85	5.75	14.38	21.47

The metal ion concentration of the collected condensate indicates the presence of Ni in the condensate, which might suggest potential leaching during the SE-CLSR runs as indicated in Table 6.14; It can be observed that the Ni concentration present in the condensates collected after 20 cycles of sorption enhanced reforming is higher than that present in the other tested condensates however, this amounts to 0.06% of the nickel present in the cycle and is therefore taken as insignificant.

Table 6.14 Nickel ion concentration in the collected condensate (T_{SR}=650°C, WHSV=1.18 hr^{-1}, S/C=3, T_{OX}=850 °C)

	NI concentration (mg/L)	**Efficiency (%) (x 10^{-2})**
SE-steam reforming	0.01869861	2.78
SECLSR after 7 cycles	0.01661576	2.47
SECLSR after 20 cycles	0.04048991	6.01

6.4.3.8 SE-CLSR with pre-hydration at 250 °C

Pre hydration of sorbents has been promoted to increase the reactivity of the CaO sorbents and improve its conversion [157]; the hydration temperature utilised alongside the calcination temperature has also been promoted to have a huge impact on the hydration extent of the sorbent particularly in cases where carbonation of the sorbent occurs immediately after hydration (direct hydration)[158]. In previous SE-CLSR runs already discussed, steam was introduced into the catalyst plus sorbent mix at 650 °C before acetic acid was introduced. This was done with the intent to further gasify any additional carbon that was not oxidised in the oxidation phase; 5 SE-CLSR cycles were conducted using the same condition utilised for the previous SE-CLSR runs as already discussed except with the pre-hydration temperature set to 250 °C with nitrogen utilised as inert gas.

The change in the hydration temperature did not affect the process gas composition as detected by the micro-GC when compared to previously discussed SE-CLSR experimental runs and the three identified phases for SE-CLSR as previously described could also be identified easily across all 5 cycles of SE-CLSR. Table 6.15 shows the process gas analysis at the post breakthrough phase for the SE-CLSR cycles with hydration temperature set to 250 °C; it can be observed the fuel was converted totally in all 5 cycles of SE-CLSR conducted which also corresponds to 100 % efficiency when the steam conversion fraction is compared to thermodynamic equilibrium values across the 5 cycles of SE-CLSR. In regards to hydrogen yield (Wt. %), an efficiency >97% and >83.7% was realised when the experimental yield of hydrogen was compared to equilibrium values and stoichiometric values respectively across the 5 cycles of SE-CLSR. The efficiency of the purity of hydrogen was also >93% and 98% when experimental results were compared against equilibrium and stoichiometric values respectively.

Table 6.15 Post-breakthrough process gas analysis of SE-CLSR with hydration temperature 250 °C (T_{SR}=650°C, WHSV=1.18 hr^{-1}, S/C=3, T_{OX}=850 °C)

cycle	**X_{HAc} (fraction)**	**X-H_20 (faction)**	**Selectivity to CO_2 (%)**	**Selectivity to CO (%)**	**Selectivity to CH_4 (%)**	**Hydrogen Purity (%)**	**Hydrogen Yield (Wt. %)**
	Equation 4:1		Equation 4:4			Equation 4:3	Equation 4:2
1	1.02	0.26	76.30	22.80	0.90	63.63	11.96
2	1.02	0.25	73.90	20.50	5.60	62.01	11.20
3	1.02	0.26	76.40	17.60	6.00	62.39	11.36
4	1.04	0.27	76.00	21.10	2.90	63.27	11.96
5	0.97	0.31	78.30	20.60	1.10	65.85	12.54

A comparison of the process gas analysis of the post breakthrough phase of the SE-CLSR experiments using a hydration temperature of 250°C was done against the corresponding values at SE-CLSR with hydration temperature set to 650°C as seen in Figure 6.27; an increase in hydrogen yield and hydrogen purity can be observed in the SE-CLSR experiments with hydration temperature set to 250 °C at the post breakthrough phase across all cycles. It is important to reiterate that the conversion realised at the post breakthrough phase is a minimum estimate of the conversion realised during the pre-breakthrough and breakthrough phase. In regards to hydrogen purity (%), there was no difference in the values realised when the hydration temperature is set to 250°C and those realised in previous SE-CLSR experiments; this is basically because the hydrogen purity realised was close to equilibrium in all SE-CLSR experimental runs compared. Nevertheless, the hydrogen purity and the hydrogen composition output realised at the pre-breakthrough phase showed an average increase of 50 % and 29% respectively when compared to those realised in steam reforming without sorption enhancement.

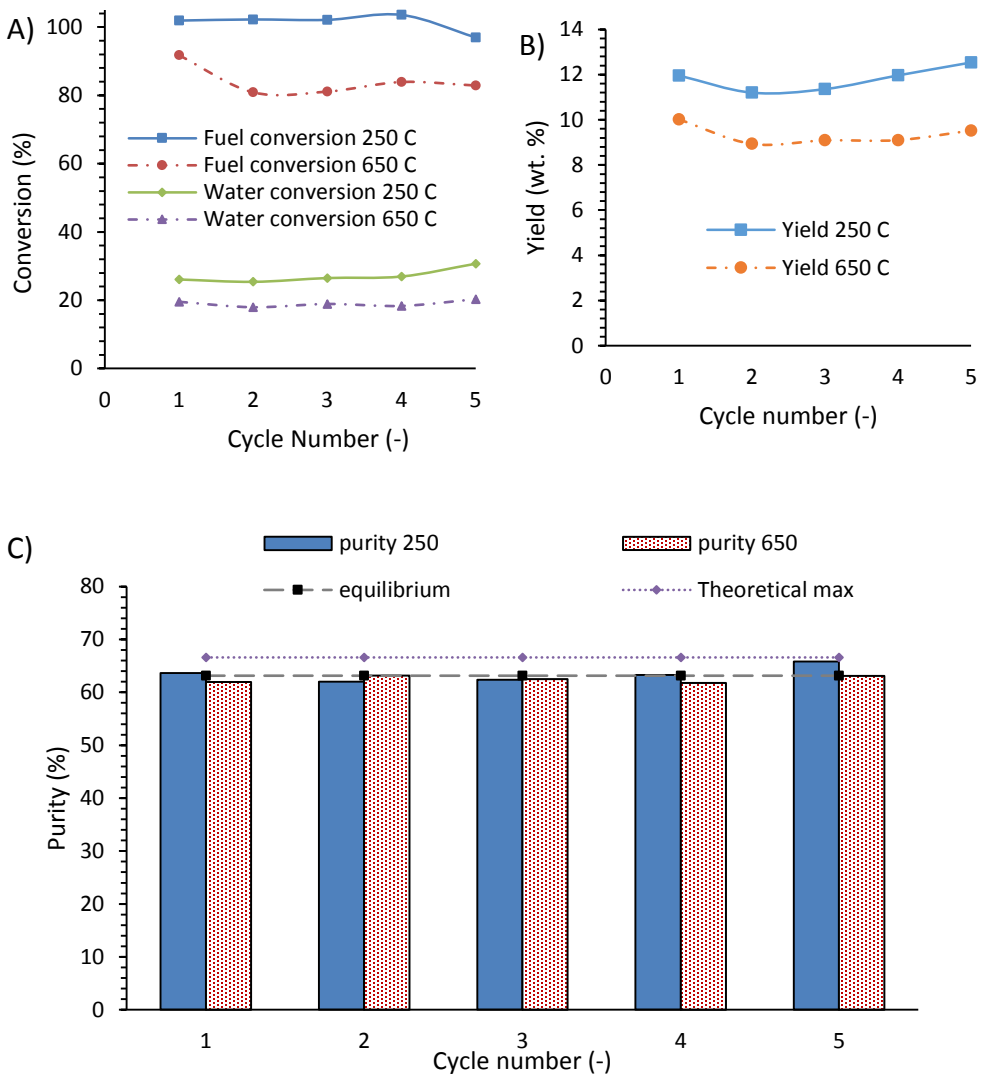

Figure 6.27 Comparison of the A) Conversion (%), B) Hydrogen yield and C) hydrogen purity of SE-CLSR experimental runs with pre-hydration set at 250 °C and 650 °C (T_{SR}=650°C, WHSV=1.18 hr^{-1},S/C=3,T_{OX}=850 °C)

The increase in the efficiency of the observed hydrogen yield and conversion in the cycles with hydration temperature set to 250 °C can be attributed to increased sorption activity; just like in the case of cycles with hydration temperature set to 650 °C, the sorbent was still active even in the early stages of the post breakthrough phase where little sorbent conversion was observed across the cycles of SE-CLSR. The increased sorption activity in this set of experiments would have led to an increase in the dynamics of reactions producing carbon-dioxide which is not limited to steam reforming and water gas shift reactions alone but also include side reactions like carbon gasification

and acetic acid decomposition. This might explain the increase in selectivity to methane and carbon-dioxide as seen in Figure 6.28 when the experiments with hydration temperature set to 250 °C is compared to those with done at 650 °C.

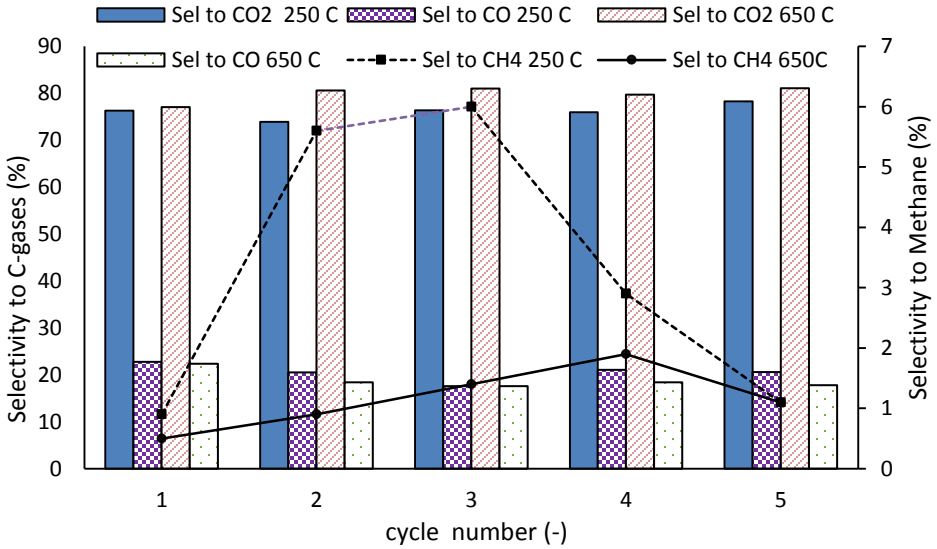

Figure 6.28 Comparison of the selectivity to carbon gases at the post breakthrough phase of SE-CLSR experimental runs with pre-hydration set at 250 °C and 650 °C (T_{SR}=650°C, WHSV=1.18 hr^{-1},S/C=3,T_{OX}=850 °C)

The carbonation duration and carbonation rate of the SE-CLSR cycles with hydration set to 250 °C are tabulated in Table 6.16; unlike previously discussed SE-CLSR experiments, there are no observed trend or reduction in the duration of the pre-breakthrough phase. It can also be observed that the total carbonation time in this set of experiments (1800s – 2550s) are lower than those observed in the first five cycles of previously discussed SE-CLSR experiments with hydration carried out at 650 °C (2550s-3150s); this does not necessarily mean a loss of the sorbent activity but can be attributed to the increase in the carbonation rate observed in the cycles with hydration set to 250°C. An average pre-breakthrough carbonation rate of 9.46 x 10^{-6} mol/s was derived across the SE-CLSR cycles with hydration temperature set to 250 °C which is way higher than 7.94 x 10^{-6} mol/s calculated for the first 5 SE-CLSR cycles with hydration temperature set to 650°C. The increased rate would have led to a quicker saturation of the sorbent which consequently would reduce the carbonation duration.

Table 6.16 Carbonation duration and carbonation rate during SE-CLSR with hydration temperature 250 °C (T_{SR}=650°C, WHSV=1.18 hr^{-1}, S/C=3, T_{OX}=850 °C)

cycle number	Pre- Break Duration (T_{BT}-T_0) (s)	Breakthrough Duration (T_{SS}-T_{BT}) (s)	Total Carbonation Time before sorbent saturation (s)	Nco_2 (carb) (mol/s) ×10^6 Equation 6:1
1	1050	750	1800	9.66
2	1200	1200	2400	9.57
3	1050	1500	2550	9.33
4	900	1650	2550	9.61
5	1050	1500	2550	9.14

The increase in the carbonation rate corresponds to a stable sorbent conversion in the cycles with hydration set to 250 °C as detailed in Table 6.17;

Table 6.17 Conversion and efficiency of sorbent during SE-CLSR with hydration temperature 250 °C (T_{SR}=650°C, WHSV=1.18 hr^{-1}, S/C=3, T_{OX}=850 °C)

cycle number	Max conversion of CaO per cycle (%)	Efficiency PB duration (% of max conversion)	Efficiency BT duration (% of max conversion)	Efficiency at end of BT (% of max conversion)
	Equation 6:2	Equation 6:3		
1	44.22	82.40	13.83	96.23
2	44.60	85.10	13.53	98.63
3	44.70	74.50	22.00	96.51
4	42.67	73.39	24.66	98.04
5	45.53	74.36	24.99	99.35

The maximum conversion of CaO remained relatively stable between 43% and 46% across the 5 cycles of SE-CLSR cycles; this corresponds to a stable overall efficiency at the end of the breakthrough phase as observed in Figure 6.29;

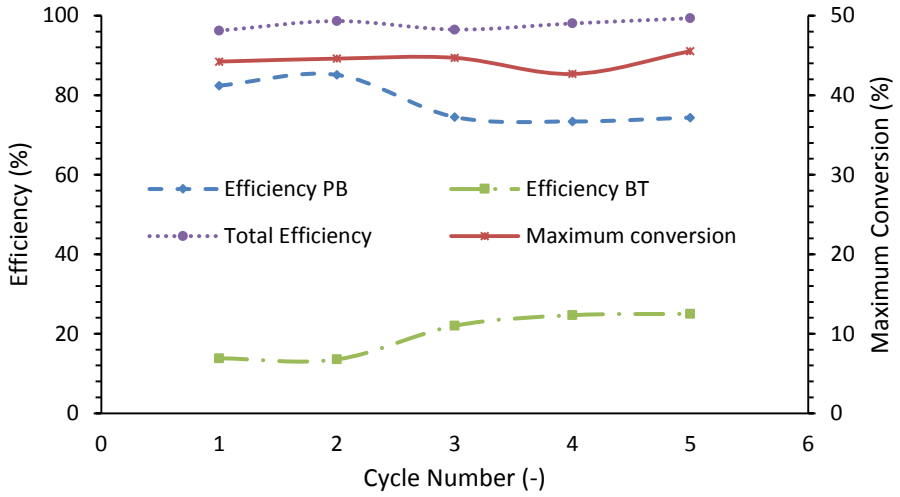

Figure 6.29 maximum conversion and conversion efficiency across SE-CLSR cycles with hydration temperature 250 °C (T_{SR}=650°C, WHSV=1.18 hr^{-1}, S/C=3, T_{OX}=850 °C)

There is an observed decrease in the efficiency of the pre-breakthrough phase similarly to those observed in previously discussed SE-CLSR cycles with hydration set to 650 °C. However, the extent of the decrease in the pre-breakthrough efficiency is higher in the experiments with hydration temperature set to 650 °C (19%) when compared to the extent of decrease in the pre-breakthrough efficiency higher in the experiments with hydration temperature set to 250 °C (10%). The decrease in the pre-breakthrough phase efficiency is however compensated with a corresponding increase in the efficiency in the breakthrough phase as indicated in Figure 6.29. Figure 6.30 compares the overall conversion efficiencies of SE-CLSR experimental runs with pre-hydrations set at 250 °C and 650 °C with the view to observe sorbent decay; it can be observed the SE-CLSR runs with hydration temperature set to 250 °C has a higher efficiency when compared to their counterparts with hydration temperature set to 650 °C. The same trend is observed for overall efficiencies at the pre-breakthrough phase and the end of the breakthrough phase; the increase in the efficiency is due to the stability of the sorbent capacity and capabilities across the 5 cycles of SE-CLSR observed with hydration set at 250 °C.

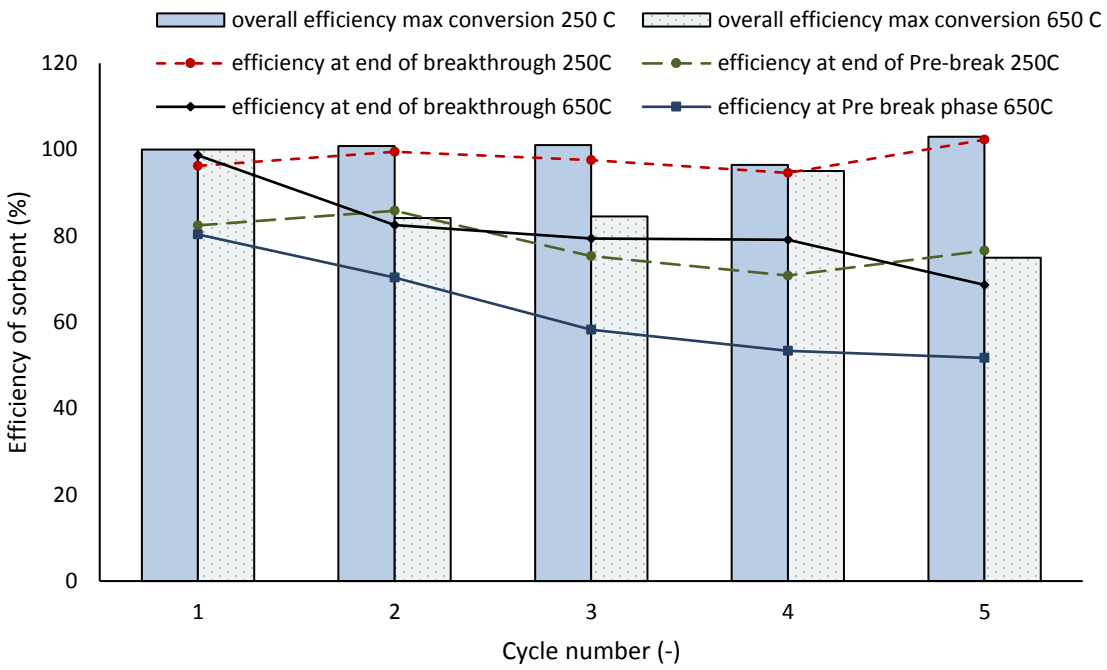

Figure 6.30 Comparison of the conversion efficiencies of SE-CLSR experimental runs with pre-hydration set at 250 °C and 650 °C (T_{SR}=650°C, WHSV=1.18 hr^{-1},S/C=3,T_{OX}=850 °C)

The catalyst reduction rate and time to maximum reduction was also calculated for the SE-CLSR runs with hydration temperature 250 °C as was previously done for SE-CLSR with hydration temperature 650 °C as depicted in Table 6.18; the reduction rate for cycle 2 to cycle 4 is higher than those observed in SE-CLSR with hydration temperature 650 °C, this leads to a reduction of the time required for full reduction of the catalyst. This is basically attributed to increased sorption enhanced reduction in the SE-CLSR runs with hydration temperature 250 °C when compared to the SE-CLSR runs with hydration temperature 650 °C. The 5th cycle however shows resemblance to the SE-CLSR runs with hydration temperature 650 °C which indicates that the improved sorbent enhanced reduction might be suppressed at this cycle.

Table 6.18 catalyst reduction rate, time to maximum reduction and efficiency of catalyst reduction during SE-CLSR with hydration temperature 250 °C (T_{SR}=650°C, WHSV=1.18 hr^{-1}, S/C=3, T_{OX}=850 °C)

cycle number	NiO-Ni rate (mol/s) x 10^6	Time to max red (S)	% Red (%)
2	8.97	448	46.4
3	8.94	449	46.3
4	8.76	459	44.8
5	6.56	612	35.8

It can also be ascertained from Table 6.18 that reduction of the catalyst occurred completely in the pre-breakthrough phase with a similar % Red observed for the SE-CLSR runs with hydration temperature 250 °C when compared to the SE-CLSR runs with hydration temperature 650 °C. This indicates that sorption enhanced steam reforming and auto-reduction would have occurred concurrently in the pre-breakthrough phase.

6.5 Conclusion

The efficiency of sorption enhanced chemical looping reforming of acetic acid was investigated with the view to ascertain the cyclic ability and stability of CaO based sorbents and the overall effect of sorption enhancement on the chemical looping steam reforming of acetic acid. It was inferred that the sorbent to catalyst mass ratio is important and must be selected cautiously to maximise sorbent performance; this must be done with the minimum requirements of all three phases of the SE-CLSR process fully identified during the experimental run [229]. It can be concluded that the sorption capacity of the sorbent would increase with an increase in the sorbent/catalyst mass ratio as discussed in 6.4.2.

It can also be concluded from the process gas analysis obtained from the SE-CLSR of acetic acid after 20 cycles that sorption activity occurred in all 20 cycles of SE-CLSR; this led to an increased hydrogen production, yield and purity particularly during the carbonation period. Sorption enhanced auto-reduction of the catalyst was also observed during the 20 cycles of SE-CLSR with the auto-reduction occurring predominantly in the pre-breakthrough phase where the sorbent is very active. A carbon balance of the overall process also indicates that more percentage of the carbon share is attributed to the oxidation phase due to the calcination of the sorbent therein.

Sorbent deactivation as already discussed in previous studies was also observed across the 20 cycles of SE-CLSR.

The effect of steam hydration on the overall process with the view to improve the cyclic stability of the sorbent was also investigated by hydrating the catalyst and sorbent mix at 250 °C before introducing acetic acid at 650 °C; it was inferred that the hydration of the sorbent at lower temperatures would deter the added advantage of gasification of carbon that would occur. However, SEM images and EDX profiling shows that the oxidised catalyst and sorbent shares a resemblance to the fresh catalyst and sorbent indicating the all carbon deposited was oxidised during the oxidation phase. A higher sorption activity and stability was observed for the experiments with hydration set at 250 °C; this led to an increase in hydrogen in the output gas composition, hydrogen yield and hydrogen purity to the equilibrium values when compared to experiments with hydration set at 650°C. It also led to a reduction in the time required for maximum reduction of the catalyst and an improvement in the nickel reduction rate and sorbent carbonation rate in the experiments with hydration set at 250 °C.

Chapter 7 Conclusion and future work

The major aim of this study was to investigate process intensification measures notably chemical looping steam reforming and sorption enhanced chemical looping steam reforming on the steam reforming of acetic acid as a model compound of volatile liquid products of biomass origin. An experimental review of the conventional steam reforming of acetic acid was conducted and discussed in Chapter 4; it was deduced the process outputs in terms of fuel and steam conversion, yield of hydrogen and selectivity's to carbon gases are influenced by the reforming temperature, steam to carbon ratio, pre-heat temperature and WHSV utilised. It was also agreed that the steam reforming process was dominant and efficient in all experimental runs investigated when compared with equilibrium values; this consequently entails high yield of hydrogen and efficient fuel and water conversions for the experimental runs conducted. In regards to optimality for process intensification measures to be investigated, it was concluded that a preheat temperature < 70 °C for acetic acid and > 120 °C for water with reforming temperature set at 600 °C or 650 °C, WHSV set between 2.3 hr^{-1} to 2.5 hr^{-1} and steam to carbon ratio set to 2 or 3 was ideal for efficient hydrogen production for the steam reforming of acetic acid using the methods as described in Chapter 3.

Characterisation of the catalyst after steam reforming indicates carbon formation with two types of carbon formed similar to those observed in previous studies [167]; the oxidation phase in chemical looping steam reforming investigated in this study efficiently oxidised the carbon deposited with sustained steam reforming and efficient production of hydrogen obtained, this is however dependent on the oxidation temperature utilised, operation conditions and type of catalyst utilised.

The efficiency of the chemical looping reforming was investigated taking into consideration the ideal operating conditions deduced for the steam reforming of acetic acid from Chapter 4; it was deduced that the oxidation temperature has a crucial effect on the efficiency of the subsequent steam reforming phase, this is due to the increased sintering of the catalyst as the temperature of oxidation is increased. Catalyst B also

showed great promise with no apparent loss of catalytic activity observed during its redox cycling in chemical looping steam reforming investigated. An overall carbon balance of the chemical looping steam reforming process using catalyst B also indicates that sustained seam reforming occurs with the major share of carbon converted into process gas output with efficient hydrogen production when compared to equilibrium and stoichiometric data.

Enhanced steam reforming was observed with the addition of the prehydrated CaO sorbent with an increased hydrogen concentration observed particularly during the pre-breakthrough duration; this was sustained for all 20 cycles of sorption enhanced chemical looping steam reforming performed; however, there is an observed decrease in sorbent conversion identified as more cycles of sorption enhanced chemical looping steam reforming, these has been observed in several literature utilising CaO based sorbent and has been attributed to reduced porosity and sintering of the material [221, 234]. Steam hydration of the sorbent before the fuel feed step led to an increase in the concentration of hydrogen produced and facilitated increased sorption enhanced auto-reduction. There is also an observed stable sorbent conversion across the cycles of sorption enhanced chemical looping reforming with steam hydration at 250 °C; this exemplifies the assertion that steam hydration is an effective reactivation technique to ensure efficient sorption capabilities and conversion of CaO based sorbents during looping cycles[157, 158].

Further work on the effect of steam hydration and other sorbent reactivation techniques on the efficiency of the sorption enhanced chemical looping steam reforming must be carried out monitoring the sorbent conversion over several cycles; this is paramount particularly for CaO based sorbent to improve the efficiency of the overall process and sustain the benefits of the utilised process intensification measures. Further studies on the operating temperatures utilised for both calcination and carbonation for the sorption enhanced chemical looping reforming process also needs to be carried out with the view of reducing the inherent sintering of materials that occurs at higher temperatures.

Finally, full scale modelling of the process with process intensification measures need to be carried out to investigate the potential advantages in terms of economics, kinetics and process flow dynamics when the process intensification measures are applied.

REFERENCES

1. Ramage, M.P., *Transitions to Alternative Transportation Technologies—A Focus on Hydrogen.* US National Research Council, National Academies Press, Washington, DC, 2008.
2. Sutton, D., B. Kelleher, and J.R. Ross, *Review of literature on catalysts for biomass gasification.* Fuel Processing Technology, 2001. **73**(3): p. 155-173.
3. Kothari, R., D. Buddhi, and R. Sawhney, *Comparison of environmental and economic aspects of various hydrogen production methods.* Renewable and Sustainable Energy Reviews, 2008. **12**(2): p. 553-563.
4. Das, D., N. Khanna, and N.T. Veziroğlu, *Recent developments in biological hydrogen production processes.* Chemical Industry and Chemical Engineering Quarterly/CICEQ, 2008. **14**(2): p. 57-67.
5. Hwang, J.-J., *Sustainability study of hydrogen pathways for fuel cell vehicle applications.* Renewable and Sustainable Energy Reviews, 2013. **19**: p. 220-229.
6. Ogden, J., et al., *The Hydrogen Fuel Pathway*, in *SUSTAINABLE TRANSPORTATION ENERGY PATHWAYS*, J.O.a.L. Anderson, Editor. 2011, Institute of Transportation Studies, University of California,: Davis. p. 64-95.
7. PATH, *Annual Report on World Progress in Hydrogen*. 2011, Partnership for Advancing theTransition to Hydrogen (PATH): Washington, D.C.
8. Konieczny, A., et al., *Catalyst development for thermocatalytic decomposition of methane to hydrogen.* International Journal of Hydrogen Energy, 2008. **33**(1): p. 264-272.
9. Chaubey, R., et al., *A review on development of industrial processes and emerging techniques for production of hydrogen from renewable and sustainable sources.* Renewable and Sustainable Energy Reviews, 2013. **23**: p. 443-462.
10. Veziroglu, T.N. and F. Barbir, *Hydrogen energy technologies.* Emerging Technology Series, prepared for the United Nations Industrial Development Organization, Vienna, 1998.

11. Yamin, J.A., *Heat losses minimization from hydrogen fueled 4-stroke spark ignition engines.* Journal of the Brazilian Society of Mechanical Sciences and Engineering, 2007. **29**: p. 109-114.
12. Shinnar, R., *Demystifying the hydrogen myth.* Chem. Eng. Prog, 2004: p. 5-6.
13. Milbrandt, A. and M.K. Mann, *Potential for hydrogen production from key renewable resources in the United States*. 2007: National Renewable Energy Laboratory.
14. Herzog, H., B. Eliasson, and O. Kaarstad, *Capturing greenhouse gases.* Scientific American, 2000. **282**(2): p. 72-79.
15. S. A. Sherif, F.B., T. N. Veziroglu, M. Mahishi, S. S. Srinivasan, *Hydrogen Energy Technologies*, in *Handbook of Energy Efficiency and Renewable Energy*, F.K.a.D.Y. Goswami, Editor. 2007, CRC Press. p. 27-1–27-16.
16. Siegel, A. and T. Schott, *Optimization of photovoltaic hydrogen production.* International Journal of Hydrogen Energy, 1988. **13**(11): p. 659-675.
17. Carpetis, C., *An assessment of electrolytic hydrogen production by means of photovoltaic energy conversion.* International Journal of Hydrogen Energy, 1984. **9**(12): p. 969-991.
18. Hancock Jr, O.G., *A photovoltaic-powered water electrolyzer: its performance and economics.* International Journal of Hydrogen Energy, 1986. **11**(3): p. 153-160.
19. Fouchard, S., et al., *Investigation of H< sub> 2</sub> production using the green microalga< i> Chlamydomonas reinhardtii</i> in a fully controlled photobioreactor fitted with on-line gas analysis.* International Journal of Hydrogen Energy, 2008. **33**(13): p. 3302-3310.
20. Melis, A. and M.R. Melnicki, *Integrated biological hydrogen production.* International Journal of Hydrogen Energy, 2006. **31**(11): p. 1563-1573.
21. Ghirardi, M.L., et al., *Microalgae: a green source of renewable H< sub> 2</sub>.* Trends in biotechnology, 2000. **18**(12): p. 506-511.

22. Fedorov, A., et al., *Hydrogen photoproduction by Rhodobacter sphaeroides immobilised on polyurethane foam.* Biotechnology letters, 1998. **20**(11): p. 1007-1009.
23. Basu, P., *Biomass gasification and pyrolysis: practical design and theory*. 2010: Academic press.
24. UNFCCC, *Clarifications of definition of biomass and consideration of changes in carbon pools due to a CDM project activity*. 2005. p. Appendix 8.
25. Eastman, D., *Synthesis Gas by Partial Oxidation.* Industrial & Engineering Chemistry, 1956. **48**(7): p. 1118-1122.
26. Wilhelm, D., et al., *Syngas production for gas-to-liquids applications: technologies, issues and outlook.* Fuel processing technology, 2001. **71**(1): p. 139-148.
27. Bharadwaj, S. and L. Schmidt, *Catalytic partial oxidation of natural gas to syngas.* Fuel Processing Technology, 1995. **42**(2): p. 109-127.
28. Tindall, B. and A. Crews, *Natural gas reforming technologies.* Gas-to-Liquids Processing: Bringing Clean Fuels to Market, San Antonio, TX, 1998.
29. Miller, B.G., *Coal energy systems*. 2004: Academic Press.
30. Kohl, A.L. and R. Nielsen, *Gas purification*. 1997: Gulf Professional Publishing.
31. GHG, I., *Opportunities for early application of CO2 sequestration technology.* Report Ph4/10. IEA Greenhouse Gas R&D Programme, Cheltenham, UK, 2002.
32. Hendriks, C., *Carbon dioxide removal from coal-fired power plants.* 1994.
33. Eliasson, B., P. Riemer, and A. Wokaun, *Greenhouse gas control technologies*. 1999: Elsevier.
34. Kobayashi, N. and L.-S. Fan, *Biomass direct chemical looping process: A perspective.* Biomass and Bioenergy, 2011. **35**(3): p. 1252-1262.
35. Hoogwijk, M., et al., *Exploration of the ranges of the global potential of biomass for energy.* Biomass and bioenergy, 2003. **25**(2): p. 119-133.
36. Heracleous, E., *Well-to-Wheels analysis of hydrogen production from bio-oil reforming for use in internal combustion engines.* International Journal of Hydrogen Energy, 2011. **36**(18): p. 11501-11511.

37. Bartels, J.R., M.B. Pate, and N.K. Olson, *An economic survey of hydrogen production from conventional and alternative energy sources.* International journal of hydrogen energy, 2010. **35**(16): p. 8371-8384.

38. Navarro, R., et al., *Hydrogen production from renewable sources: biomass and photocatalytic opportunities.* Energy & Environmental Science, 2009. **2**(1): p. 35-54.

39. Zygarlicke, C., *Renewable Hydrogen: Biomass for Sustainable Hydrogen Transportation Fuel*, in *Biomass Magazine*. 2014, BBI International: Grand Forks.

40. Milne, T.A., C.C. Elam, and R.J. Evans, *Hydrogen from Biomass: State of the Art and Research Challenges*. 2001, International Energy Agency: USA.

41. Balat, M., *Gasification of biomass to produce gaseous products.* Energy Sources, Part A, 2009. **31**(6): p. 516-526.

42. Ogwo, P., L. Obasi, and D. Okoroigwe, *Strategies for Converting Biomass Materials to Generate Energy and Power in Nigeria.*

43. Iye, E.L. and P.E. Bilsborrow, *Assessment of the availability of agricultural residues on a zonal basis for medium-to large-scale bioenergy production in Nigeria.* Biomass and Bioenergy, 2013. **48**: p. 66-74.

44. Sambo, A.S. *The place of renewable energy in the Nigerian energy sector*. in *World Future Council Workshop on Renewable Energy Policies, Energy Commission of Nigeria, Addis Ababa, October*. 2009.

45. Mohammed, Y., et al., *Renewable energy resources for distributed power generation in Nigeria: A review of the potential.* Renewable and Sustainable Energy Reviews, 2013. **22**: p. 257-268.

46. Nadabo, S.L., *Renewable Energy as a Solution to Nigerian Energy Crisis*. 2010, Vaasa University of Applied Sciences. p. 69 + 6 Appendix.

47. Cooper, C. and C. Laing, *A macro analysis of crop residue and animal wastes as a potential energy source in Africa.* Journal of Energy in Southern Africa, 2007. **18**(1): p. 11.

48. Koopmans, A. and J. Koppejan, *Agricultural and forest residues-generation, utilization and availability.* Paper presented at the Regional Consultation on Modern Applications of Biomass Energy, 1997. **6**: p. 10.
49. Demirbas, A., *Biohydrogen*. 2009: Springer.
50. Demirbas, A., *Competitive liquid biofuels from biomass.* Applied Energy, 2011. **88**(1): p. 17-28.
51. Cai, W., P.R.d.l. Piscina, and N. Homs, *Hydrogen production from the steam reforming of bio-butanol over novel supported Co-based bimetallic catalysts.* Bioresource technology, 2012. **107**: p. 482-486.
52. Nahar, G.A., *Hydrogen production by steam reforming of biodiesel*. 2014, University of Leeds.
53. Nahar, G., et al., *Feasibility of hydrogen production from steam reforming of biodiesel (FAME) feedstock on Ni-supported catalysts.* Applied Catalysis B: Environmental, 2015. **168–169**: p. 228-242.
54. Klass, D.L., *Biomass for renewable energy, fuels, and chemicals*. 1998: Academic press.
55. Bridgwater, A., *Progress in thermochemical biomass conversion*. 2008: John Wiley & Sons.
56. Kersten, S., et al., *Experimental fact-finding in CFB biomass gasification for ECN's 500 kWth pilot plant.* Industrial & engineering chemistry research, 2003. **42**(26): p. 6755-6764.
57. Bridgwater, A., *Renewable fuels and chemicals by thermal processing of biomass.* Chemical Engineering Journal, 2003. **91**(2): p. 87-102.
58. Balat, H. and E. Kırtay, *Hydrogen from biomass–present scenario and future prospects.* International Journal of Hydrogen Energy, 2010. **35**(14): p. 7416-7426.
59. Garcıa-Ibanez, P., A. Cabanillas, and J. Sanchez, *Gasification of leached orujillo (olive oil waste) in a pilot plant circulating fluidised bed reactor. Preliminary results.* Biomass and Bioenergy, 2004. **27**(2): p. 183-194.

60. Arvelakis, S. and E. Koukios, *Physicochemical upgrading of agroresidues as feedstocks for energy production via thermochemical conversion methods.* Biomass and Bioenergy, 2002. **22**(5): p. 331-348.
61. Hong, G. and M. Spritzer. *Supercritical water partial oxidation*. in *Proceedings of the 2002 US DOE Hydrogen Program Review NREL/CP-610-32405*. 2002.
62. Chornet, E., et al., *Biomass to hydrogen via pyrolysis and reforming.* Proceedings of the 1994 DOE/NREL Hydrogen Program Review, 1994: p. 407-432.
63. Bridgwater, A., D. Meier, and D. Radlein, *An overview of fast pyrolysis of biomass.* Organic Geochemistry, 1999. **30**(12): p. 1479-1493.
64. Czernik, S., et al. *Production of hydrogen from biomass-derived liquids*. in *DOE Hydrogen Program Review*. 2001.
65. Medrano, J., et al., *Hydrogen from aqueous fraction of biomass pyrolysis liquids by catalytic steam reforming in fluidized bed.* Energy, 2011. **36**(4): p. 2215-2224.
66. Beis, S., Ö. Onay, and Ö. Koçkar, *Fixed-bed pyrolysis of safflower seed: influence of pyrolysis parameters on product yields and compositions.* Renewable Energy, 2002. **26**(1): p. 21-32.
67. Özçimen, D. and F. Karaosmanoğlu, *Production and characterization of bio-oil and biochar from rapeseed cake.* Renewable Energy, 2004. **29**(5): p. 779-787.
68. Zhang, Q., et al., *Review of biomass pyrolysis oil properties and upgrading research.* Energy Conversion and Management, 2007. **48**(1): p. 87-92.
69. Boucher, M., A. Chaala, and C. Roy, *Bio-oils obtained by vacuum pyrolysis of softwood bark as a liquid fuel for gas turbines. Part I: Properties of bio-oil and its blends with methanol and a pyrolytic aqueous phase.* Biomass and Bioenergy, 2000. **19**(5): p. 337-350.
70. Elliott, D.C., *Historical developments in hydroprocessing bio-oils.* Energy & Fuels, 2007. **21**(3): p. 1792-1815.
71. Shihadeh, A. and S. Hochgreb, *Impact of biomass pyrolysis oil process conditions on ignition delay in compression ignition engines.* Energy & fuels, 2002. **16**(3): p. 552-561.

72. Yaman, S., *Pyrolysis of biomass to produce fuels and chemical feedstocks.* Energy conversion and management, 2004. **45**(5): p. 651-671.

73. Jahirul, M.I., et al., *Biofuels production through biomass pyrolysis—a technological review.* Energies, 2012. **5**(12): p. 4952-5001.

74. Sipilä, K., et al., *Characterization of biomass-based flash pyrolysis oils.* Biomass and Bioenergy, 1998. **14**(2): p. 103-113.

75. Zhang, L., et al., *Upgrading of bio-oil from biomass fast pyrolysis in China: A review.* Renewable and Sustainable Energy Reviews, 2013. **24**: p. 66-72.

76. Wang, J.-j., J. Chang, and J. Fan, *Catalytic esterification of bio-oil by ion exchange resins.* Journal of Fuel Chemistry and Technology, 2010. **38**(5): p. 560-564.

77. Tang, Y., et al., *One-Step Hydrogenation− Esterification of Aldehyde and Acid to Ester over Bifunctional Pt Catalysts: A Model Reaction as Novel Route for Catalytic Upgrading of Fast Pyrolysis Bio-Oil.* Energy & Fuels, 2008. **22**(5): p. 3484-3488.

78. Xiu, S. and A. Shahbazi, *Bio-oil production and upgrading research: A review.* Renewable and Sustainable Energy Reviews, 2012. **16**(7): p. 4406-4414.

79. Wang, D., S. Czernik, and E. Chornet, *Production of hydrogen from biomass by catalytic steam reforming of fast pyrolysis oils.* Energy & Fuels, 1998. **12**(1): p. 19-24.

80. Garcia, L.a., et al., *Catalytic steam reforming of bio-oils for the production of hydrogen: effects of catalyst composition.* Applied Catalysis A: General, 2000. **201**(2): p. 225-239.

81. Kechagiopoulos, P.N., et al., *Hydrogen production via reforming of the aqueous phase of Bio-Oil over Ni/Olivine catalysts in a spouted bed reactor.* Industrial & Engineering Chemistry Research, 2008. **48**(3): p. 1400-1408.

82. Wang, D., et al., *Biomass to hydrogen via fast pyrolysis and catalytic steam reforming of the pyrolysis oil or its fractions.* Industrial & Engineering Chemistry Research, 1997. **36**(5): p. 1507-1518.

83. Molburg, J.C. and R.D. Doctor. *Hydrogen from steam-methane reforming with CO2 capture*. in *20th Annual international Pittsburgh coal conference*. 2003.

84. Beyer, F. and J. Brightling, *Steam Reforming-50 years of Development and the challenges for the Nerxt 50 years*, in *AIChe 50th Annual Safety in Ammonia Plants and Related Facilities Symposium*. 2005, Uhde GmbH, Germany: Toronto,Canada.

85. Blythe, B.M. and R.W. Sampson, *Very large steam reformers. [Alternative to liquefied natural gas].* Journal Name: Am. Chem. Soc., Div. Fuel Chem., Prepr.; (United States); Journal Volume: 18:3, 1973: p. Medium: X; Size: Pages: 84-99.

86. Steynberg, A. and M. Dry, *Fischer-Tropsch Technology*. 2004: Access Online via Elsevier.

87. Dybkjær, I., *Tubular reforming and autothermal reforming of natural gas—an overview of available processes.* Fuel Processing Technology, 1995. **42**(2): p. 85-107.

88. Strait, M., A. Glenda, and G. Nisha. *Synthesis Gas Reformers*. 1997; Available from: http://www.owlnet.rice.edu/~ceng403/nh3ref97.html.

89. Wagner, A.L., R.S. Osborne, and J.P. Wagner, *Prediction of deactivation rates and mechanisms of reforming catalysts.* Prepr. Pap.-Am. Chem. Soc., Div. Fuel Chem, 2003. **48**(2): p. 748.

90. Rostrupnielsen, J. and J.B. Hansen, *CO< sub> 2</sub>-Reforming of Methane over Transition Metals.* Journal of Catalysis, 1993. **144**(1): p. 38-49.

91. Froment, G.F., K.B. Bischoff, and J. De Wilde, *Chemical reactor analysis and design*. Vol. 2. 1990: Wiley New York.

92. Sehested, J., *Four challenges for nickel steam-reforming catalysts.* Catalysis Today, 2006. **111**(1): p. 103-110.

93. Rostrup-Nielsen, J.R., J. Sehested, and J.K. Nørskov, *Hydrogen and synthesis gas by steam-and C0< sub> 2</sub> reforming.* Advances in Catalysis, 2002. **47**: p. 65-139.

94. Rostrup-Nielsen, J. and L.J. Christiansen, *Concepts in syngas manufacture*. Vol. 10. 2011: World Scientific.

95. Kechagiopoulos, P.N., et al., *Hydrogen production via steam reforming of the aqueous phase of bio-oil in a fixed bed reactor.* Energy & fuels, 2006. **20**(5): p. 2155-2163.

96. Lea-Langton, A., et al., *Biomass pyrolysis oils for hydrogen production using chemical looping reforming.* International Journal of Hydrogen Energy, 2012. **37**(2): p. 2037-2043.

97. Stankiewicz, A.I. and J.A. Moulijn, *Process intensification: transforming chemical engineering.* Chemical Engineering Progress, 2000. **96**(1): p. 22-34.

98. Cheng, F., V. Dupont, and M.V. Twigg, *Temperature-programmed reduction of nickel steam reforming catalyst with glucose.* Applied Catalysis A: General, 2016. **527**: p. 1-8.

99. Moulijn, J.A., M. Makkee, and A.E. Van Diepen, *Chemical process technology*. 2013: John Wiley & Sons.

100. Zin, R.M., *Advanced Steam Reforming of Pyrolysis Oils and their aqueous phase*, in *School of Process, Environmnetal and Materials Engineering*. 2012, University of Leeds: Energy and Research Institute.

101. Pimenidou, P., *Novel Process of Hydrogen Production from Liquids of Biomass Origin*, in *School of Process, Environmmental and Material Engineering*. 2010, University of Leeds.

102. Manzolini, G., D. Jansen, and A. Wright, *Sorption-Enhanced Fuel Conversion*, in *Process Intensification for Sustainable Energy Conversion*. 2015, John Wiley & Sons, Ltd. p. 175-208.

103. Gallucci, F. and M. van Sint Annaland, *Process intensification for sustainable energy conversion*. 2015: John Wiley & Sons.

104. Spallina, V., et al., *Chemical Looping Combustion for Power Production*, in *Process Intensification for Sustainable Energy Conversion*. 2015, John Wiley & Sons, Ltd. p. 117-174.

105. Kuusik, R., et al., *High temperature behavior of NiO-based oxygen carriers for chemical looping combustion.* Energy Procedia, 2009. **1**(1): p. 3885-3892.

106. Leion, H., T. Mattisson, and A. Lyngfelt, *Use of ores and industrial products as oxygen carriers in chemical-looping combustion.* Energy & Fuels, 2009. **23**(4): p. 2307-2315.

107. Lewis, W., E. Gilliland, and W. Glass, *Solid-catalyzed reaction in a fluidized bed.* AIChE Journal, 1959. **5**(4): p. 419-426.

108. Lewis, W., E. Gilliland, and R. Paxton, *Low-Temperature Oxidation of Carbon.* Industrial & Engineering Chemistry, 1954. **46**(6): p. 1327-1331.

109. Hurst, S., *Production of hydrogen by the steam-iron method.* Journal of the American Oil Chemists' Society, 1939. **16**(2): p. 29-35.

110. Gasior, S., et al., *Production of Synthesis Gas and Hydrogen by the Steam-Iron Process.* Bureau of Mines Report of Investigation, 1961. **5911**.

111. *Chemical Looping*. Available from: http://www.chemical-looping.at/start.asp?Seite=1.

112. Satrio, J.A., B.H. Shanks, and T.D. Wheelock, *Development of a novel combined catalyst and sorbent for hydrocarbon reforming.* Industrial & engineering chemistry research, 2005. **44**(11): p. 3901-3911.

113. Carvill, B., et al., *Sorption-enhanced reaction process.* AIChE Journal, 1996. **42**(10): p. 2765-2772.

114. Di Giuliano, A., et al., *Sorption enhanced steam methane reforming by Ni–CaO materials supported on mayenite.* International Journal of Hydrogen Energy, 2017. **42**(19): p. 13661-13680.

115. Roger, W., *Hydrogen production*. 1933, Google Patents.

116. Rostrup-Nielsen, J.R., *Catalytic Steam Reforming*, in *Catalysis- Science and Technology*, Dr. John R. Anderson and P.M. Boudart, Editors. 1984, Springer: Berlin. p. 1 -117.

117. Balasubramanian, B., et al., *Hydrogen from methane in a single-step process.* Chemical Engineering Science, 1999. **54**(15): p. 3543-3552.

118. Silaban, A., M. Narcida, and D. Harrison, *Characteristics of the reversible reaction between CO2 (g) and calcined dolomite.* Chemical Engineering Communications, 1996. **146**(1): p. 149-162.

119. Herzog, H.J., *Peer Reviewed: What Future for Carbon Capture and Sequestration?* Environmental science & technology, 2001. **35**(7): p. 148A-153A.

120. Yancheshmeh, M.S., H.R. Radfarnia, and M.C. Iliuta, *High temperature CO 2 sorbents and their application for hydrogen production by sorption enhanced steam reforming process.* Chemical Engineering Journal, 2016. **283**: p. 420-444.

121. Ochoa-Fernández, E., et al., *Process design simulation of H 2 production by sorption enhanced steam methane reforming: evaluation of potential CO 2 acceptors.* Green Chemistry, 2007. **9**(6): p. 654-662.

122. Feng, B., H. An, and E. Tan, *Screening of CO2 adsorbing materials for zero emission power generation systems.* Energy & Fuels, 2007. **21**(2): p. 426-434.

123. Blamey, J., et al., *The calcium looping cycle for large-scale CO 2 capture.* Progress in Energy and Combustion Science, 2010. **36**(2): p. 260-279.

124. Abanades, J.C. and D. Alvarez, *Conversion limits in the reaction of CO2 with lime.* Energy & Fuels, 2003. **17**(2): p. 308-315.

125. Sun, P., et al., *Investigation of attempts to improve cyclic CO2 capture by sorbent hydration and modification.* Industrial & Engineering Chemistry Research, 2008. **47**(6): p. 2024-2032.

126. Fennell, P., et al., *Regeneration of sintered limestone sorbents for the sequestration of CO2 from combustion and other systems.* Journal of the Energy Institute, 2007. **80**(2): p. 116-119.

127. Rout, K. and H. Jakobsen, *A numerical study of pellets having both catalytic-and capture properties for SE-SMR process: kinetic-and product layer diffusion controlled regimes.* Fuel processing technology, 2013. **106**: p. 231-246.

128. Aloisi, I., et al., *Hydrogen by sorption enhanced methane reforming: A grain model to study the behavior of bi-functional sorbent-catalyst particles.* Chemical Engineering Science, 2016. **149**: p. 22-34.

129. Broda, M., et al., *High-purity hydrogen via the sorption-enhanced steam methane reforming reaction over a synthetic CaO-based sorbent and a Ni catalyst.* Environmental science & technology, 2013. **47**(11): p. 6007-6014.

130. García-Lario, A.L., et al., *Experimental study of the application of a NiO/NiAl 2 O 4 catalyst and a CaO-based synthetic sorbent on the Sorption Enhanced Reforming process.* International Journal of Hydrogen Energy, 2015. **40**(1): p. 219-232.

131. Reijers, H.T.J., et al. *Hydrogen production through sorption enhanced reforming*. in *1st European Hydrogen Energy Conference, Grenoble*. 2003.

132. Reijers, H.T.J., et al., *Hydrotalcite as CO2 sorbent for sorption-enhanced steam reforming of methane.* Industrial & engineering chemistry research, 2006. **45**(8): p. 2522-2530.

133. Tzanetis, K., C. Martavaltzi, and A. Lemonidou, *Comparative exergy analysis of sorption enhanced and conventional methane steam reforming.* International Journal of Hydrogen Energy, 2012. **37**(21): p. 16308-16320.

134. Mayorga, S.G., et al., *Sorption enhanced reaction process for production of hydrogen. Phase 1 final report*. 1997, Air Products and Chemicals, Inc., Allentown, PA (United States).

135. Ortiz, M., et al., *Hydrogen production with CO< sub> 2</sub> capture by coupling steam reforming of methane and chemical-looping combustion: Use of an iron-based waste product as oxygen carrier burning a PSA tail gas.* Journal of Power Sources, 2011. **196**(9): p. 4370-4381.

136. Gupta, P., L.G. Velazquez-Vargas, and L.-S. Fan, *Syngas redox (SGR) process to produce hydrogen from coal derived syngas.* Energy & Fuels, 2007. **21**(5): p. 2900-2908.

137. Rydén, M., A. Lyngfelt, and T. Mattisson. *Two novel approaches for hydrogen production; chemical-looping reforming and steam reforming with carbon dioxide capture by chemical-looping combustion*. in *Proceedings of the 16th World Hydrogen Energy Conference, Lyon, France, June 2006.* 2006.

138. Rydén, M. and A. Lyngfelt, *Using steam reforming to produce hydrogen with carbon dioxide capture by chemical-looping combustion.* International Journal of Hydrogen Energy, 2006. **31**(10): p. 1271-1283.

139. Lyon, R.K. and J.A. Cole, *Unmixed combustion: an alternative to fire.* Combustion and Flame, 2000. **121**(1): p. 249-261.

140. Lyon, R.K., *Methods and systems for heat transfer by unmixed combustion*. 1998, Google Patents.

141. Galvita, V., et al., *Production of hydrogen with low CO x-content for PEM fuel cells by cyclic water gas shift reactor.* International Journal of Hydrogen Energy, 2008. **33**(4): p. 1354-1360.

142. Hacker, V., et al., *Hydrogen production by steam–iron process.* Journal of Power Sources, 2000. **86**(1): p. 531-535.

143. Bohn, C.D., et al., *Production of very pure hydrogen with simultaneous capture of carbon dioxide using the redox reactions of iron oxides in packed beds.* Industrial & Engineering Chemistry Research, 2008. **47**(20): p. 7623-7630.

144. Dupont, V., et al., *Unmixed steam reforming of methane and sunflower oil: A single-reactor process for H2-rich gas.* International journal of hydrogen energy, 2007. **32**(1): p. 67-79.

145. Adanez, J., et al., *Progress in Chemical-Looping Combustion and Reforming technologies.* Progress in Energy and Combustion Science, 2012. **38**(2): p. 215-282.

146. Kumar, R.V., J.A. Cole, and R.K. Lyon. *Unmixed reforming: an advanced steam reforming process*. in *Preprints of Symposia*. 1999.

147. Mattisson, T., et al. *Integrated hydrogen and power production from natural gas with CO2 capture*. in *15th World Hydrogen Energy Conference, Yokohama, 27th June-2 July, 2004.* 2004.

148. Ortiz, M., et al., *Optimization of hydrogen production by chemical-looping auto-thermal reforming working with Ni-based oxygen-carriers.* international journal of hydrogen energy, 2011. **36**(16): p. 9663-9672.

149. Ni, Y., et al., *High purity hydrogen production from sorption enhanced chemical looping glycerol reforming: Application of NiO-based oxygen transfer materials and potassium promoted Li2ZrO3 as CO2 sorbent.* Applied Thermal Engineering, 2017. **124**: p. 454-465.

150. Pimenidou, P., et al., *High purity H 2 by sorption-enhanced chemical looping reforming of waste cooking oil in a packed bed reactor.* Bioresource technology, 2010. **101**(23): p. 9279-9286.

151. Rydén, M. and P. Ramos, *H< sub> 2</sub> production with CO< sub> 2</sub> capture by sorption enhanced chemical-looping reforming using NiO as oxygen carrier and CaO as CO< sub> 2</sub> sorbent.* Fuel Processing Technology, 2012. **96**: p. 27-36.

152. Dou, B., et al., *Hydrogen production by enhanced-sorption chemical looping steam reforming of glycerol in moving-bed reactors.* Applied Energy, 2014. **130**: p. 342-349.

153. Zin, R.M., et al., *High hydrogen yield and purity from palm empty fruit bunch and pine pyrolysis oils.* International Journal of Hydrogen Energy, 2012. **37**(14): p. 10627-10638.

154. Pimenidou, P. and V. Dupont, *Characterisation of palm empty fruit bunch (PEFB) and pinewood bio-oils and kinetics of their thermal degradation.* Bioresource technology, 2012. **109**: p. 198-205.

155. de Diego, L.F., et al., *Hydrogen production by chemical-looping reforming in a circulating fluidized bed reactor using Ni-based oxygen carriers.* Journal of Power Sources, 2009. **192**(1): p. 27-34.

156. Nahar, G., et al., *Feasibility of hydrogen production from steam reforming of biodiesel (FAME) feedstock on Ni-supported catalysts.* Applied Catalysis B: Environmental, 2015. **168**: p. 228-242.

157. Blamey, J., et al., *Reactivation of CaO-based sorbents for CO2 capture: Mechanism for the carbonation of Ca (OH) 2.* Industrial & Engineering Chemistry Research, 2011. **50**(17): p. 10329-10334.

158. Blamey, J., et al., *On steam hydration of CaO-based sorbent cycled for CO 2 capture.* Fuel, 2015. **150**: p. 269-277.

159. Li, Z., et al., *Novel CO 2 sorbent: Ca (OH) 2 with high strength.* Fuel Processing Technology, 2015. **131**: p. 437-442.

160. Abedi, J., et al., *An integrated approach to hydrogen production from agricultural residues for use in urban transportation.* Proceedings of the 2001 DOE Hydrogen Program Review, NREL/CP —, 2001: p. 570-30535.

161. Czernik, S., et al., *Hydrogen by catalytic steam reforming of liquid byproducts from biomass thermoconversion processes.* Industrial & Engineering Chemistry Research, 2002. **41**(17): p. 4209-4215.

162. Vagia, E.C. and A.A. Lemonidou, *Hydrogen production via steam reforming of bio-oil components over calcium aluminate supported nickel and noble metal catalysts.* Applied Catalysis A: General, 2008. **351**(1): p. 111-121.

163. Goodman, D.R., *Handling and using catalysts in the plant*, in *Catalyst handbook*, M.V. Twigg, Editor. 1996, Manson Publishing Ltd: London. p. 161.

164. Cheng, F., V. Dupont, and M.V. Twigg, *Direct reduction of nickel catalyst with model bio-compounds.* Applied Catalysis B: Environmental, 2017. **200**: p. 121-132.

165. McBride, B.J. and S. Gordon, *Computer Program for Calculation of Complex Chemical Equilibrium Compositions and Applications II. Users Manual and Program Description. 2; Users Manual and Program Description.* 1996.

166. Gordon, S. and B.J. McBride, *Computer program for calculation of complex chemical equilibrium compositions and applications. Part 1: Analysis.* 1994.

167. Cheng, F. and V. Dupont, *Nickel catalyst auto-reduction during steam reforming of bio-oil model compound acetic acid.* International Journal of Hydrogen Energy, 2013. **38**(35): p. 15160-15172.

168. Rietveld, H., *Line profiles of neutron powder-diffraction peaks for structure refinement.* Acta Crystallographica, 1967. **22**(1): p. 151-152.

169. Rietveld, H., *A profile refinement method for nuclear and magnetic structures.* Journal of applied Crystallography, 1969. **2**(2): p. 65-71.

170. Wu, C., M. Sui, and Y.J. Yan, *A Comparison of Steam Reforming of Two Model Bio‐Oil Fractions.* Chemical engineering & technology, 2008. **31**(12): p. 1748-1753.

171. Basagiannis, A. and X. Verykios, *Catalytic steam reforming of acetic acid for hydrogen production.* International journal of hydrogen energy, 2007. **32**(15): p. 3343-3355.

172. Basagiannis, A. and X. Verykios, *Reforming reactions of acetic acid on nickel catalysts over a wide temperature range.* Applied Catalysis A: General, 2006. **308**: p. 182-193.

173. Bimbela, F., et al., *Hydrogen production by catalytic steam reforming of acetic acid, a model compound of biomass pyrolysis liquids.* Journal of Analytical and Applied Pyrolysis, 2007. **79**(1): p. 112-120.

174. Takanabe, K., et al., *Catalyst deactivation during steam reforming of acetic acid over Pt/ZrO< sub> 2</sub>.* Chemical Engineering Journal, 2006. **120**(1): p. 133-137.

175. Takanabe, K., et al., *Sustainable hydrogen from bio-oil—Steam reforming of acetic acid as a model oxygenate.* Journal of catalysis, 2004. **227**(1): p. 101-108.

176. Wang, D., D. Montane, and E. Chornet, *Catalytic steam reforming of biomass-derived oxygenates: acetic acid and hydroxyacetaldehyde.* Applied Catalysis A: General, 1996. **143**(2): p. 245-270.

177. Marquevich, M., et al., *Hydrogen from biomass: steam reforming of model compounds of fast-pyrolysis oil.* Energy & Fuels, 1999. **13**(6): p. 1160-1166.

178. Iwasa, N., et al., *Hydrogen production by steam reforming of acetic acid: comparison of conventional supported metal catalysts and metal-incorporated mesoporous smectite-like catalysts.* International journal of hydrogen energy, 2010. **35**(1): p. 110-117.

179. Hu, X. and G. Lu, *Comparative study of alumina-supported transition metal catalysts for hydrogen generation by steam reforming of acetic acid.* Applied Catalysis B: Environmental, 2010. **99**(1): p. 289-297.

180. Blake, P. and G. Jackson, *High-and low-temperature mechanisms in the thermal decomposition of acetic acid.* Journal of the Chemical Society B: Physical Organic, 1969: p. 94-96.

181. Mackie, J. and K. Doolan, *High‐temperature kinetics of thermal decomposition of acetic acid and its products.* International journal of chemical kinetics, 1984. **16**(5): p. 525-541.

182. Guenther, W. and W. Walters, *The Thermal Decomposition of Ketene1.* Journal of the American Chemical Society, 1959. **81**(6): p. 1310-1315.

183. Rajadurai, S., *Pathways for carboxylic acid decomposition on transition metal oxides.* Catalysis Reviews, 1994. **36**(3): p. 385-403.

184. Furimsky, E., *Chemistry of catalytic hydrodeoxygenation.* Catalysis reviews science and engineering, 1983. **25**(3): p. 421-458.

185. Nguyen, M.T., et al., *Theoretical study of the thermal decomposition of acetic acid: decarboxylation versus dehydration.* The Journal of Physical Chemistry, 1995. **99**(31): p. 11883-11888.

186. Thaicharoensutcharittham, S., et al., *Hydrogen production by steam reforming of acetic acid over Ni-based catalysts.* Catalysis today, 2011. **164**(1): p. 257-261.

187. Trimm, D.L., *Coke formation and minimisation during steam reforming reactions.* Catalysis Today, 1997. **37**(3): p. 233-238.

188. Trimm, D.L., *Catalysts for the control of coking during steam reforming.* Catalysis Today, 1999. **49**(1): p. 3-10.

189. Bartholomew, C.H., *Mechanisms of catalyst deactivation.* Applied Catalysis A: General, 2001. **212**(1): p. 17-60.

190. Rostrup-Nielsen, J.R., *Industrial relevance of coking.* Catalysis Today, 1997. **37**(3): p. 225-232.

191. Pen, M., J. Gomez, and J.G.a. Fierro, *New catalytic routes for syngas and hydrogen production.* Applied Catalysis A: General, 1996. **144**(1-2): p. 7-57.

192. Alstrup, I., *A new model explaining carbon filament growth on nickel, iron, and Ni ・ Cu alloy catalysts.* Journal of Catalysis, 1988. **109**(2): p. 241-251.

193. Chang, T., N. Rodriguez, and R. Baker, *Carbon deposition on supported platinum particles.* Journal of Catalysis, 1990. **123**(2): p. 486-495.

194. Guisnet, M. and P. Magnoux, *Organic chemistry of coke formation.* Applied Catalysis A: General, 2001. **212**(1): p. 83-96.

195. Nabgan, W., et al., *Production of hydrogen via steam reforming of acetic acid over Ni and Co supported on La 2 O 3 catalyst.* International Journal of Hydrogen Energy, 2017. **42**(14): p. 8975-8985.

196. Duprez, D., et al., *Deactivation of steam-reforming model catalysts by coke formation: I. Kinetics of the Formation of Filamentous Carbon in the Hydrogenolysis of cyclopentane on Ni/Al2O3 Catalysts.* Journal of Catalysis, 1990. **124**(2): p. 324-335.

197. Jiang, B., et al., *Hydrogen production from chemical looping steam reforming of glycerol by Ni-based oxygen carrier in a fixed-bed reactor.* Chemical Engineering Journal, 2015. **280**: p. 459-467.

198. Giannakeas, N., et al., *Hydrogen from scrap tyre oil via steam reforming and chemical looping in a packed bed reactor.* Applied Catalysis B: Environmental, 2012. **126**: p. 249-257.

199. Zin, R.M., et al., *Hydrogen from ethanol reforming with aqueous fraction of pine pyrolysis oil with and without chemical looping.* Bioresource technology, 2015. **176**: p. 257-266.

200. Luis, F., et al., *Synthesis gas generation by chemical-looping reforming in a batch fluidized bed reactor using Ni-based oxygen carriers.* Chemical Engineering Journal, 2008. **144**(2): p. 289-298.

201. Liu, W., et al., *Performance enhancement of calcium oxide sorbents for cyclic CO2 capture ・ A review.* Energy & Fuels, 2012. **26**(5): p. 2751-2767.

202. Dupont, V., et al., *Production of hydrogen by unmixed steam reforming of methane.* Chemical Engineering Science, 2008. **63**(11): p. 2966-2979.

203. Lysikov, A., A. Okunev, and O. Netskina, *Study of a nickel catalyst under conditions of the SER process: Influence of RedOx cycling.* International Journal of Hydrogen Energy, 2013. **38**(25): p. 10354-10363.

204. Lemonidou, A.A., E.C. Vagia, and J.A. Lercher, *Acetic acid reforming over Rh supported on La2O3/CeO2–ZrO2: catalytic performance and reaction pathway analysis.* ACS Catalysis, 2013. **3**(9): p. 1919-1928.

205. Khan, M.N. and T. Shamim, *Investigation of hydrogen production using chemical looping reforming.* Energy Procedia, 2014. **61**: p. 2034-2037.

206. Pimenidou, P., et al., *Chemical looping reforming of waste cooking oil in packed bed reactor.* Bioresource technology, 2010. **101**(16): p. 6389-6397.

207. Goicoechea, S., et al., *Support effect on structure and performance of Co and Ni catalysts for steam reforming of acetic acid.* Applied Catalysis A: General, 2016. **514**: p. 182-191.

208. Hoang, T., et al., *Steam reforming of acetic acid–A major component in the volatiles formed during gasification of humin.* Applied catalysis B: environmental, 2015. **163**: p. 74-82.

209. Cunha, A., et al., *Sorption enhanced steam reforming of ethanol on hydrotalcite-like compounds impregnated with active copper.* Chemical Engineering Research and Design, 2013. **91**(3): p. 581-592.

210. Barbier, J., *Deactivation of reforming catalysts by coking-a review.* Applied catalysis, 1986. **23**(2): p. 225-243.

211. Lisboa, J.d.S., et al., *Influence of the addition of promoters to steam reforming catalysts.* Catalysis today, 2005. **101**(1): p. 15-21.

212. Kousi, K., et al., *Glycerol steam reforming over modified Ni-based catalysts.* Applied Catalysis A: General, 2016. **518**: p. 129-141.

213. Nichele, V., et al., *Ni/ZrO 2 catalysts in ethanol steam reforming: inhibition of coke formation by CaO-doping.* Applied Catalysis B: Environmental, 2014. **150**: p. 12-20.

214. Sinfelt, J., *Specificity in catalytic hydrogenolysis by metals.* Advances in catalysis, 1973. **23**: p. 91-119.

215. Davda, R., et al., *Aqueous-phase reforming of ethylene glycol on silica-supported metal catalysts.* Applied Catalysis B: Environmental, 2003. **43**(1): p. 13-26.

216. Mizuno, S.C.M., et al., *Steam reforming of acetic acid over MgAl2O4-supported Co and Ni catalysts: Effect of the composition of Ni/Co and reactants on reaction pathways.* Catalysis Today.

217. Li, Z., et al., *Steam reforming of acetic acid over Ni/ZrO 2 catalysts: effects of nickel loading and particle size on product distribution and coke formation.* Applied Catalysis A: General, 2012. **417**: p. 281-289.

218. Gil, M.V., et al., *H 2 production by sorption enhanced steam reforming of biomass-derived bio-oil in a fluidized bed reactor: An assessment of the effect of operation variables using response surface methodology.* Catalysis Today, 2015. **242**: p. 19-34.

219. Harrison, D.P., *Sorption-enhanced hydrogen production: a review.* Industrial & Engineering Chemistry Research, 2008. **47**(17): p. 6486-6501.

220. He, L., H. Berntsen, and D. Chen, *Approaching Sustainable H2 Production: Sorption Enhanced Steam Reforming of Ethanol†.* The Journal of Physical Chemistry A, 2009. **114**(11): p. 3834-3844.

221. Olivas, D.A., et al., *Enhanced ethanol steam reforming by CO 2 absorption using CaO, CaO* MgO or Na 2 ZrO 3.* International Journal of Hydrogen Energy, 2014. **39**(29): p. 16595-16607.

222. Dou, B., et al., *Continuous sorption-enhanced steam reforming of glycerol to high-purity hydrogen production.* International Journal of Hydrogen Energy, 2013. **38**(27): p. 11902-11909.

223. He, L., et al., *Towards efficient hydrogen production from glycerol by sorption enhanced steam reforming.* Energy & Environmental Science, 2010. **3**(8): p. 1046-1056.

224. Fermoso, J., L. He, and D. Chen, *Production of high purity hydrogen by sorption enhanced steam reforming of crude glycerol.* international journal of hydrogen energy, 2012. **37**(19): p. 14047-14054.

225. Dou, B., et al., *Hydrogen production by sorption-enhanced steam reforming of glycerol.* Bioresource Technology, 2009. **100**(14): p. 3540-3547.

226. He, L. and D. Chen, *Hydrogen Production from Glucose and Sorbitol by Sorption‐Enhanced Steam Reforming: Challenges and Promises.* ChemSusChem, 2012. **5**(3): p. 587-595.

227. Han, L., et al., *H 2 rich gas production via pressurized fluidized bed gasification of sawdust with in situ CO 2 capture.* Applied energy, 2013. **109**: p. 36-43.

228. Esteban-Díez, G., et al., *Effect of operating conditions on the sorption enhanced steam reforming of blends of acetic acid and acetone as bio-oil model compounds.* Applied Energy, 2016. **177**: p. 579-590.

229. Fermoso, J., et al., *Multifunctional Pd/Ni–Co Catalyst for Hydrogen Production by Chemical Looping Coupled With Steam Reforming of Acetic Acid.* ChemSusChem, 2014. **7**(11): p. 3063-3077.

230. Gil, M.V., et al., *Production of fuel-cell grade H 2 by sorption enhanced steam reforming of acetic acid as a model compound of biomass-derived bio-oil.* Applied Catalysis B: Environmental, 2016. **184**: p. 64-76.

231. Lopez Ortiz, A. and D.P. Harrison, *Hydrogen production using sorption-enhanced reaction.* Industrial & Engineering Chemistry Research, 2001. **40**(23): p. 5102-5109.

232. Johnsen, K., et al., *Sorption-enhanced steam reforming of methane in a fluidized bed reactor with dolomite as -acceptor.* Chemical Engineering Science, 2006. **61**(4): p. 1195-1202.

233. Adiya, Z.I.S., V. Dupont, and T. Mahmud, *Chemical equilibrium analysis of hydrogen production from shale gas using sorption enhanced chemical looping steam reforming.* Fuel Processing Technology, 2017. **159**: p. 128-144.

234. Alvarez, D. and J.C. Abanades, *Pore-size and shape effects on the recarbonation performance of calcium oxide submitted to repeated calcination/recarbonation cycles.* Energy & Fuels, 2005. **19**(1): p. 270-278.

235. Mess, D., A.F. Sarofim, and J.P. Longwell, *Product layer diffusion during the reaction of calcium oxide with carbon dioxide.* Energy & Fuels, 1999. **13**(5): p. 999-1005.

236. Manovic, V. and E.J. Anthony, *CO2 carrying behavior of calcium aluminate pellets under high-temperature/high-CO2 concentration calcination conditions.* Industrial & Engineering Chemistry Research, 2010. **49**(15): p. 6916-6922.

237. Broda, M., A.M. Kierzkowska, and C.R. Müller, *Influence of the calcination and carbonation conditions on the CO2 uptake of synthetic Ca-based CO2 sorbents.* Environmental science & technology, 2012. **46**(19): p. 10849-10856.

238. Noor, T., M.V. Gil, and D. Chen, *Production of fuel-cell grade hydrogen by sorption enhanced water gas shift reaction using Pd/Ni–Co catalysts.* Applied Catalysis B: Environmental, 2014. **150**: p. 585-595.

239. Wu, G., et al., *Sorption enhanced steam reforming of ethanol on Ni–CaO–Al 2 O 3 multifunctional catalysts derived from hydrotalcite-like compounds.* Energy & Environmental Science, 2012. **5**(10): p. 8942-8949.

240. Salvador, C., et al., *Enhancement of CaO for CO 2 capture in an FBC environment.* Chemical Engineering Journal, 2003. **96**(1): p. 187-195.

241. Manovic, V. and E.J. Anthony, *Thermal activation of CaO-based sorbent and self-reactivation during CO2 capture looping cycles.* Environmental science & technology, 2008. **42**(11): p. 4170-4174.

242. Manovic, V. and E.J. Anthony, *Steam reactivation of spent CaO-based sorbent for multiple CO2 capture cycles.* Environmental science & technology, 2007. **41**(4): p. 1420-1425.

243. Materić, V., et al., *Ca (OH) 2 superheating as a low-attrition steam reactivation method for CaO in calcium looping applications.* Industrial & Engineering Chemistry Research, 2010. **49**(24): p. 12429-12434.

244. Bhatia, S. and D. Perlmutter, *Effect of the product layer on the kinetics of the CO2 -lime reaction.* AIChE Journal, 1983. **29**(1): p. 79-86.

245. Sun, P., et al., *A discrete-pore-size-distribution-based gas–solid model and its application to the CaO+ CO2 reaction.* Chemical Engineering Science, 2008. **63**(1): p. 57-70.

246. Gupta, H. and L.-S. Fan, *Carbonation-calcination cycle using high reactivity calcium oxide for carbon dioxide separation from flue gas.* Industrial & engineering chemistry research, 2002. **41**(16): p. 4035-4042.

Appendices

Appendix 1 Gas chromatograph calibration and method

All the gases detected by the micro-GC was identified and calibrated using different external standards gotten from BOC gases; the calibration point was taken as an average of a few constant readings from the micro-GC for each gas after passing the external standards through the micro-GC. The gases calibrated are Hydrogen, nitrogen, oxygen, methane and CO for channel 1 of the micro G-C and carbon-dioxide, propane, air, methane, ethane, ethylene and propylene for the 2nd channel; the correlation coefficient of all calibrated gas was >0.9.

Channel 1 calibrations

- ***Hydrogen calibration***

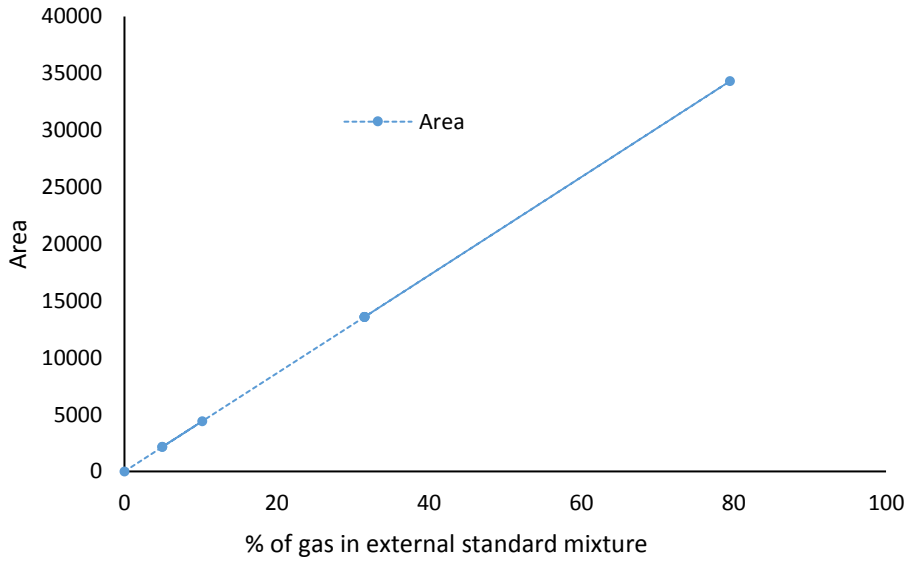

Appendix 1. 1 calibration of Hydrogen gas, Correlation Coefficient: 1.0000

- ***Nitrogen calibration***

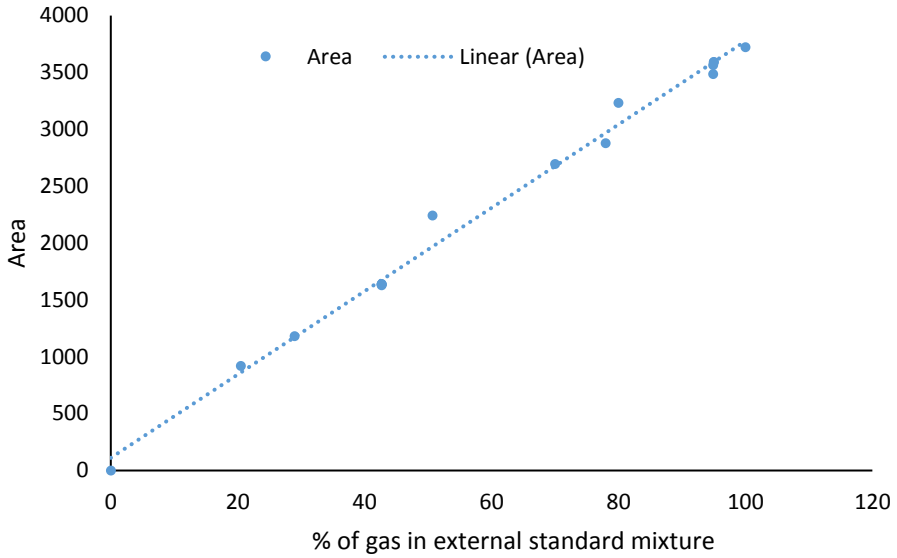

Appendix 1. 2 calibration of Nitrogen gas, Correlation Coefficient: 0.9994

- ***Methane***

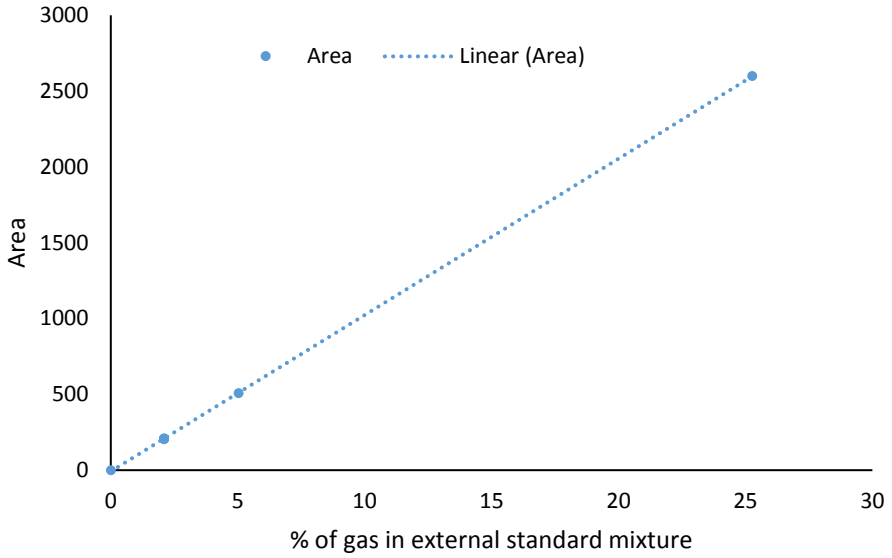

Appendix 1. 3 calibration of methane gas, Correlation Coefficient: 0.9999

- ***Carbon monoxide***

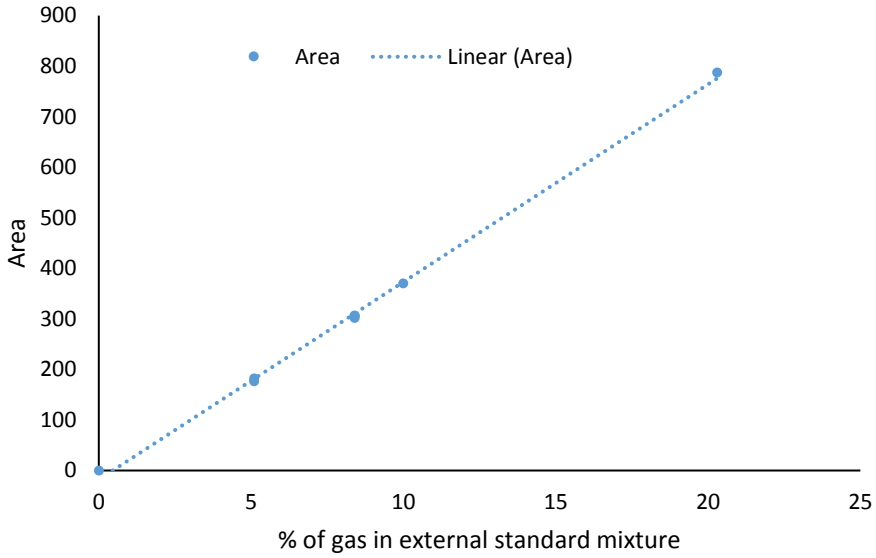

Appendix 1. 4 calibration of CO gas, Correlation Coefficient: 0.9957

- ***Oxygen***

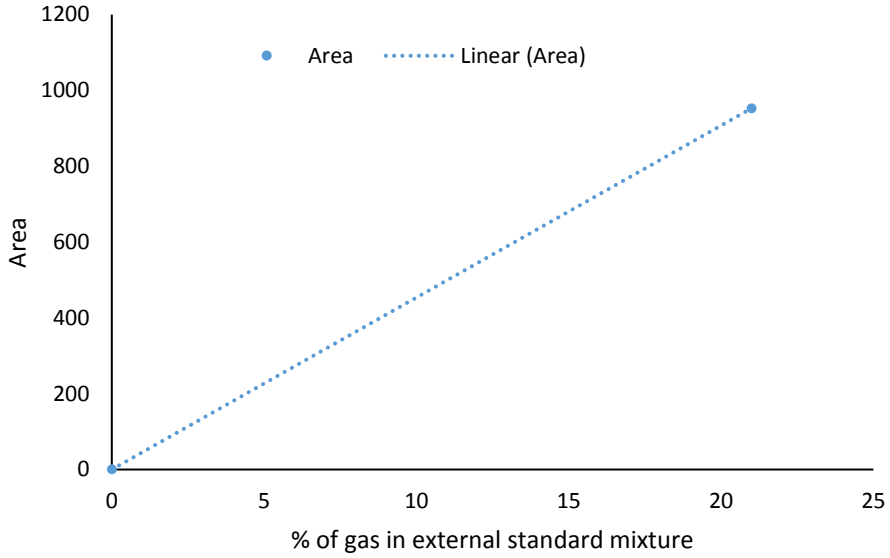

Appendix 1. 5 calibration of oxygen gas, Correlation Coefficient: 1.0000

Channel 2 calibrations

- ***Methane***

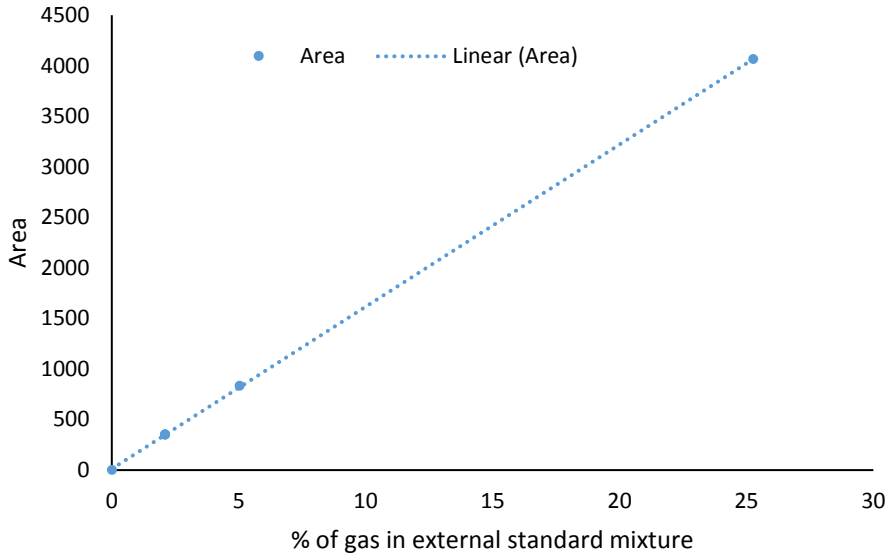

Appendix 1. 6 calibration of methane gas, Correlation Coefficient: 0.9999

- ***Carbon-dioxide***

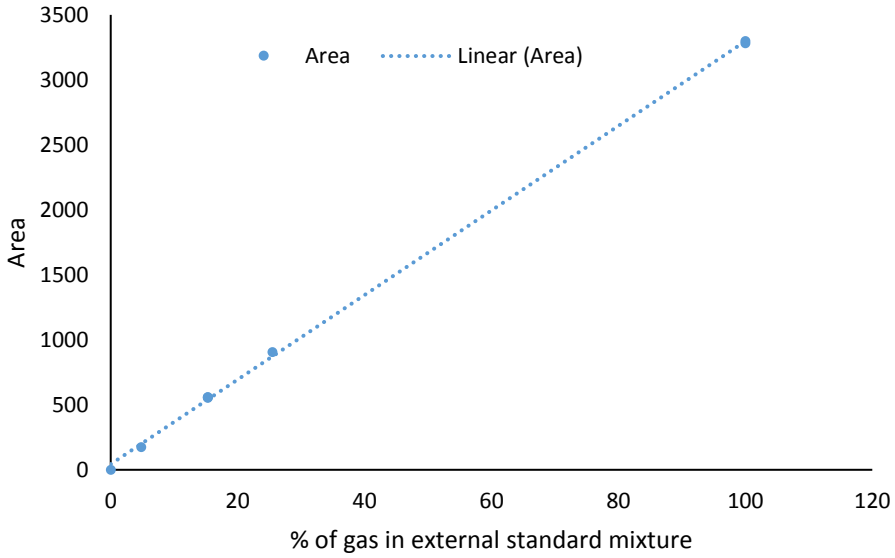

Appendix 1. 7 calibration of carbon-dioxide, Correlation Coefficient: 0.9992

- Ethane

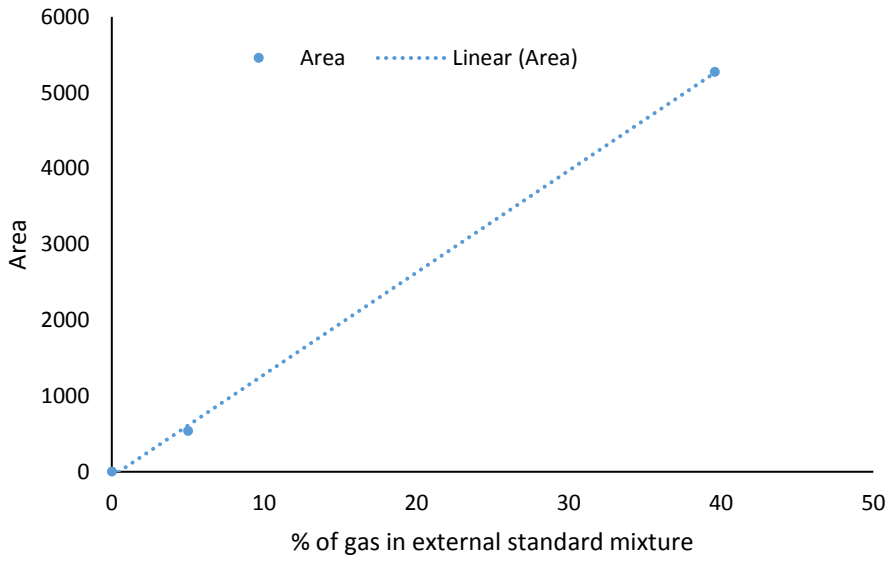

Appendix 1. 8 calibration of ethane, Correlation Coefficient: 1.0000

- ***Ethylene***

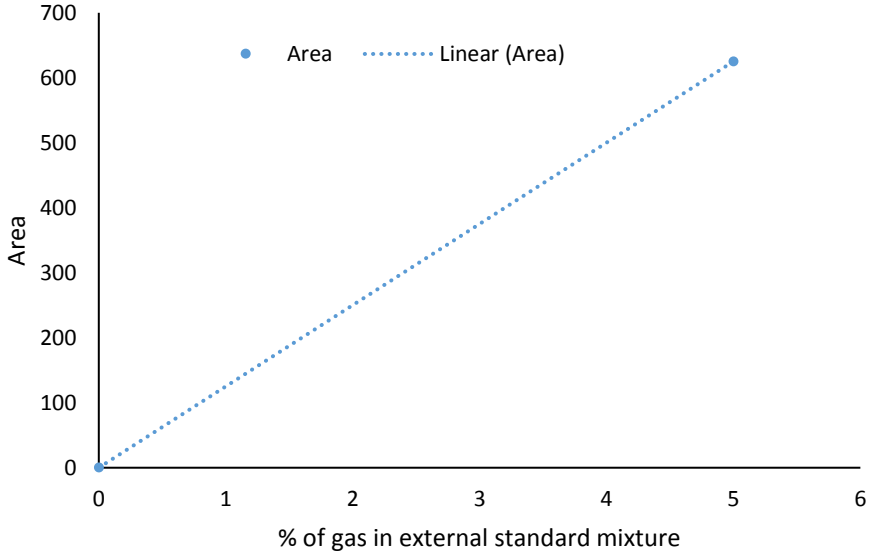

Appendix 1. 9 calibration of ethylene, Correlation Coefficient: 1.0000

- ***Propane***

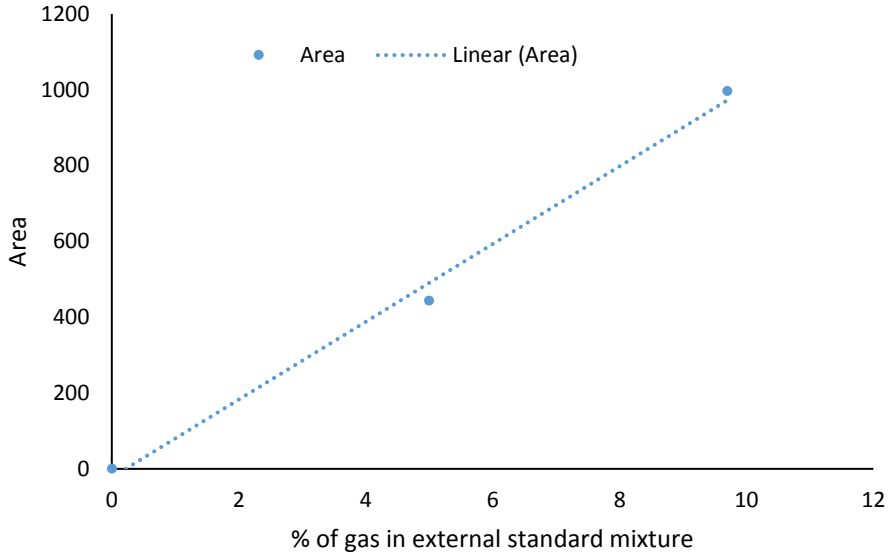

Appendix 1. 10 calibration of propane, Correlation Coefficient: 0.9992

- ***Propylene***

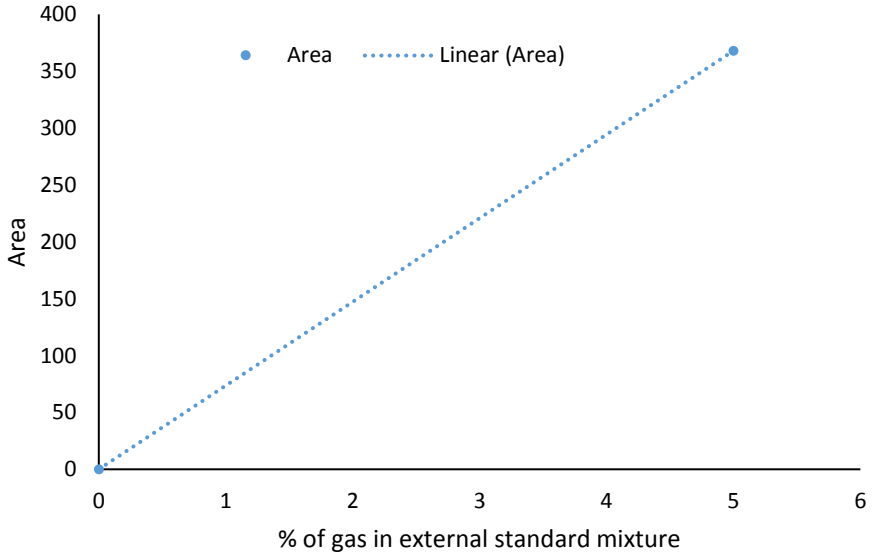

Appendix 1. 11 calibration of propylene, Correlation Coefficient: 1.0000

Micro-GC method -Varian CP-4900

Data Acquisition:	
Channel 1	
Sampling Frequency	100.0 Hz
Run Time	150 s
Channel 2	
Sampling Frequency	100.0 Hz
Run Time	150 s
Injector:	
Channel 1	
Injection Time	30 ms
Injector Temperature Setpoint	50 °C
Channel 2	
Injection Time	30 ms
Injector Temperature Setpoint	50 °C
Column:	
Channel 1	
Column Temperature Setpoint	100 °C
EGC Mode	Static
EGC Initial Pressure	100.0 kPa
Channel 2	
Column Temperature Setpoint	100 °C
EGC Mode	Static
EGC Initial Pressure	100.0 kPa
Detector:	
Channel 1	
Detector State	ON
TCD Temp. Limit Check	ON
Invert Signal	YES
Detector Sensivity	Auto

Channel 2	
Detector State	ON
TCD Temp. Limit Check	ON
Invert Signal	YES
Detector Sensivity	Auto

Miscellaneous:	
Stabilization Time	25 s
Sample Time	21 s
Sample Line Temperature Setpoint	35 °C
Backflush Time Channel 1	13.0 s
Backflush Time Channel 2	0.0 s

Peak table and identified peaks at different retention time

Channel 1- CP-4900 Backflush Column Module, 10m MS5 (TCD)

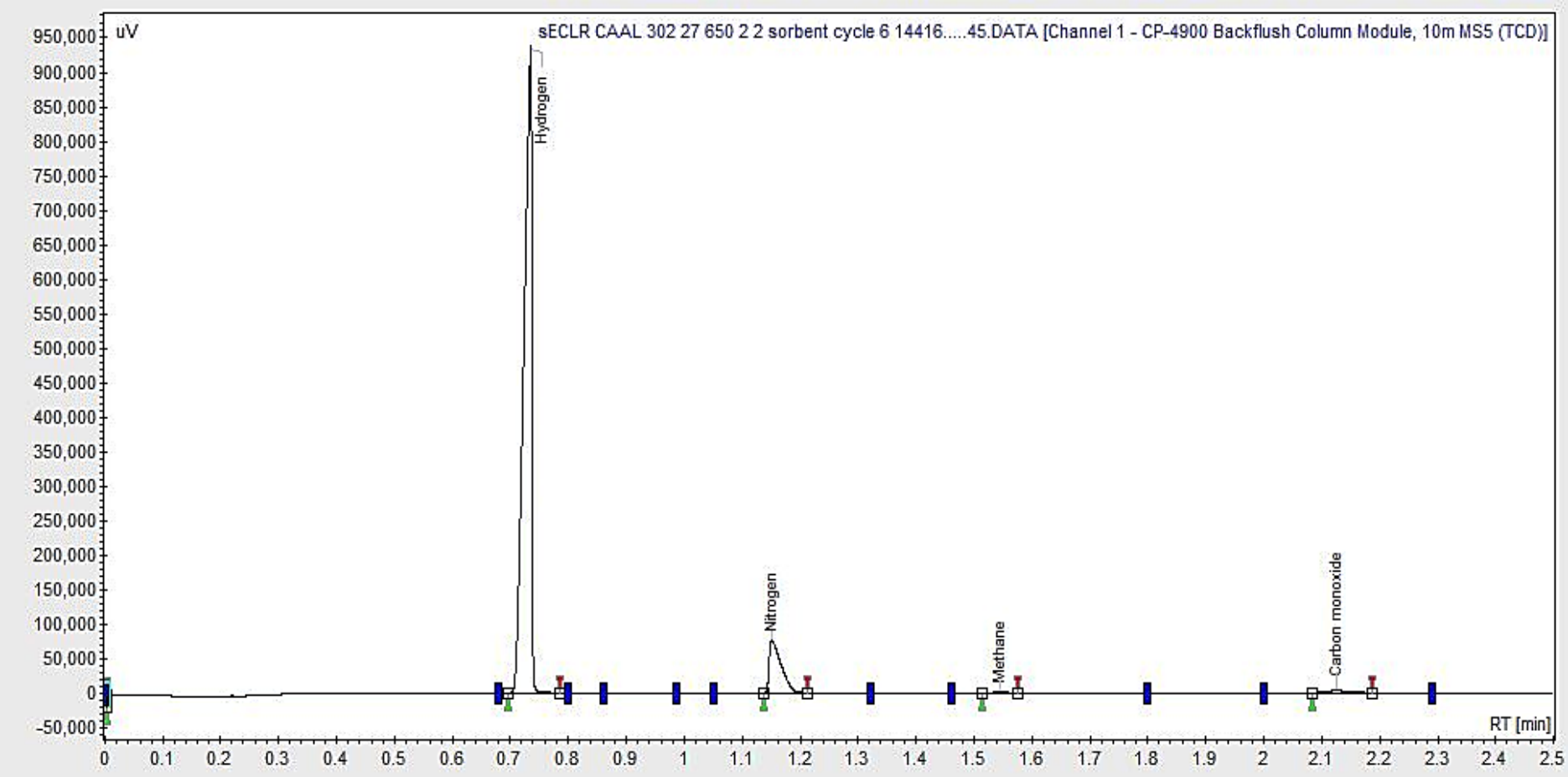

Peak Table

	Name	**Tim (min)**	**Quantity (%)**	**Height(uV)**	**Area (uV.Min)**	**Area % (%)**
1	UNKNOWN*	0.00	0.00	7634.0	6.3	0.038
2	Hydrogen	0.73	33.83	938314.7	14592.7	88.168
3	Nitrogen	1.15	48.08	75637.2	1793.3	10.835
4	Methane	1.54	0.16	483.7	16.3	0.098
5	Carbon monoxide	2.13	3.81	3133.2	142.5	0.0861
5						
Total			85.88	1025202.8	16551.1	100.000

- * Unknown peak detected due to computer noise < 0.05% Area%

Channel 2 - CP-4900 Backflush Column Module, 10m PPQ (TCD)

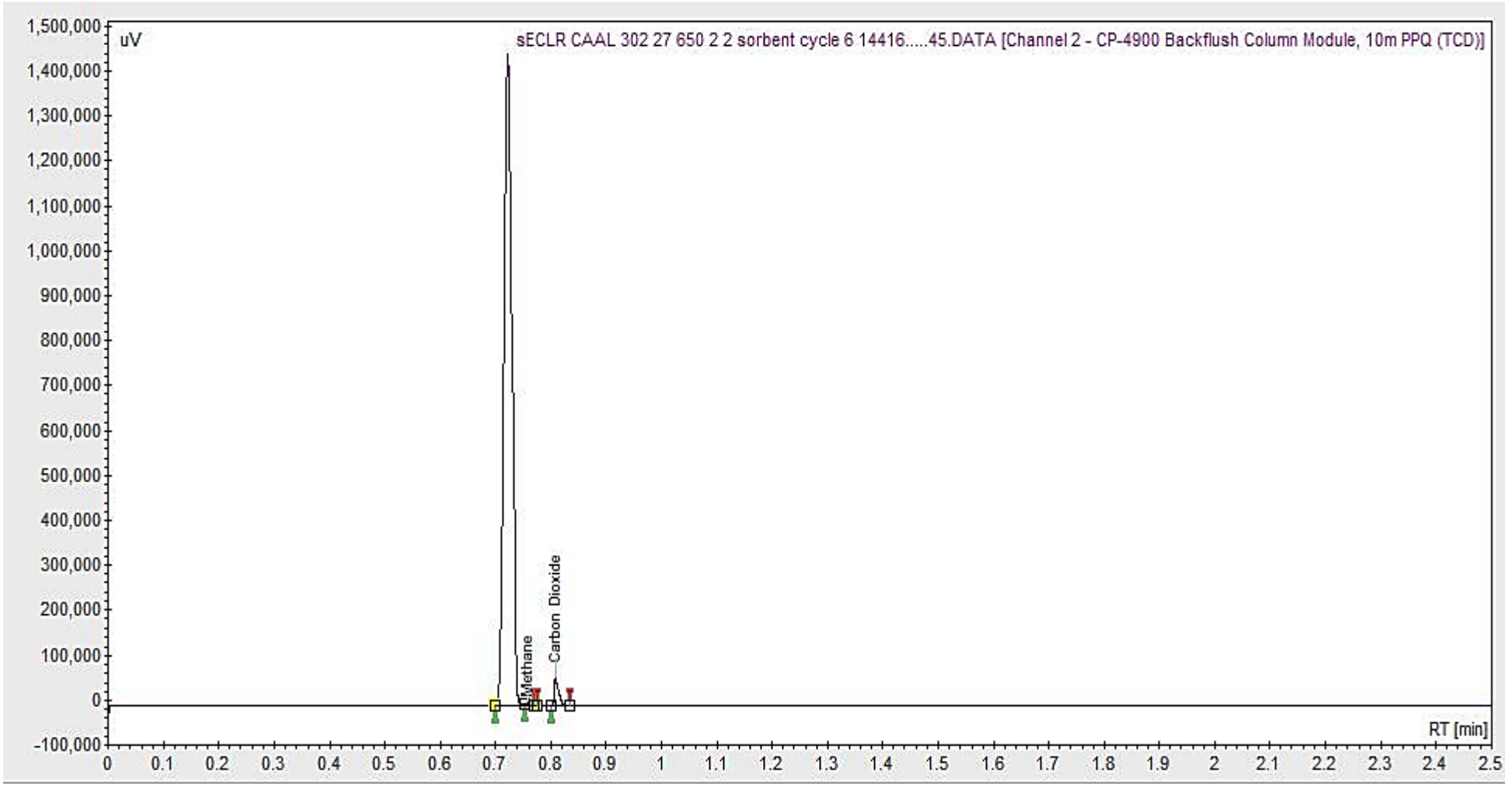

Peak table

	Name	**Tim (min)**	**Quantity (%)**	**Height(uV)**	**Area (uV.Min)**	**Area % (%)**
1	UNKNOWN*	0.72	0.00	1448806.9	24471.3	97.709
2	Methane	0.76	0.22	5152.4	36.0	0.144
3	Carbon dioxide	0.81	16.25	58753.1	537.7	2.147
5						
Total			16.47	1512712.4	25045.1	100.000

- * Unknown peak detected are other gases detected and passed as air in the Pora plot column

Appendix 2 Carbon balance Calculation

- ***CLSR***

The carbon balance for the CLSR process was calculated using the following parameters;

1- Reaction time = 7200 seconds for all cycles
2- Carbon is fully oxidised during each oxidation cycle; *SEM images and EDX* profiling indicates that all filamentous and nearly all carbon formed during the reducing phase is oxidised during the oxidation cycle, this is also evident through CHNS analysis.
3- Carbon in is the same for all reduction cycles as the same volumetric flowrate of 0.978 ml/Hr is utilised for all runs
4- The condensate collected for steam to carbon ration after the reforming cycle was between 3.2 ml and 3.8 ml; hence an average of 3.5 ml was utilised for all samples

The overall carbon balance is calculated as follows;

$$\text{Overall carbon balance} = \text{Total C in} - \text{total C out}$$

The total carbon into the system is calculated as

$$\text{Total C in (mol)} = (\dot{n}_{\text{total flow in}} \times y_{\text{C in feed}}) \times \text{time}$$

$$= \left(\frac{\textbf{Volumetric flowrate of acetic acid} \times \textbf{density of acetic acid}}{\textbf{molar mass of acetic acid}} \times \mathbf{y_{C\ in\ feed}}\right) \times \textbf{time}$$

This is calculated as 6.82E-02 mol for all CLSR runs

The total carbon out is also calculated as follows;

$$Total\ C\ out\ (mol) = \mathbf{C_{condensate}} + \mathbf{C_{oxidation\ or\ catalyst}} + \mathbf{C_{out\ Process}}$$

Where the carbon in the condensate is calculated from the mass concentration of Carbon derived from TOC analysis;

$$\mathbf{C_{condensate}}\ (mol) = \frac{mass\ concentration\ of\ condensate \times volume\ of\ condensate\ collected}{molar\ mass}$$

The carbon released from the oxidation run is calculated through the integration of the molar flowrate of all carbon products formed over time;

$$\mathbf{C_{oxidation}}\ (\boldsymbol{mol}) = \dot{n}_{Carbon\ oxidised} \times time$$

The carbon formed in the catalyst utilised for the last cycle which is not oxidised is calculated from the carbon weight (%) derived through CHN analysis;

$$\mathbf{C_{catalyst}}\ (\boldsymbol{mol}) = \left(\frac{Carbon\ weight\ Fraction \times mass\ of\ catalyst}{catalyst\ weight\ Fraction}\right) \Big/ molar\ mass\ of\ carbon$$

Finally, carbon from the process gas is calculated similarly to that of $\mathrm{C_{oxidation}}$ with the difference that the carbon utilised is that produced in the reducing phase;

$$\mathbf{C_{process}}\ (\boldsymbol{mol}) = \dot{n}_{Carbon\ produced} \times time$$

The carbon unaccounted for is calculated also;

$$\mathbf{C_{unaccounted\ for}}\ (\%) = \frac{Overall\ balance}{Total\ C\ in} \times 100$$

The results for the 5 CLSR cycles at reforming temperature set as 650 °C and oxidation temperature set as 800 °C at steam to carbon ratio 3 with 2 g of catalyst and 2 g of sand is given in the following table;

	C in (feed) (mol)	Fuel Conversion (%)	C-out Process (mol)	C oxidised (mol)	C condensate	Total carbon out	Overall Balance	Carbon Unaccounted for
1	6.82E-02	93.06	6.35E-02	5.04E-03	1.99E-05	6.86E-02	-3.30E-04	-4.83E-01
2	6.82E-02	85.92	5.86E-02	6.19E-03	4.48E-05	6.49E-02	3.38E-03	4.95E+00
3	6.82E-02	85.86	5.86E-02	9.64E-03	3.39E-05	6.83E-02	-2.96E-05	-4.34E-02
4	6.82E-02	91.76	6.26E-02	7.19E-03	1.39E-05	6.98E-02	-1.58E-03	-2.31E+00
5	6.82E-02	84.45	5.76E-02	7.91E-03	9.96E-06	6.55E-02	2.69E-03	3.94E+00

- ***SE-CLSR***

Carbon in =.

$$Carbon\ from\ feedstock\ +\ carbon\ from\ CaCO3\ present\ in\ Calcined\ sorbent$$

Parameter estimations

1- Reaction time = 7200 seconds for all cycles

2- Carbon is fully oxidised during each oxidation cycle; *SEM images and EDX profiling indicates that all filamentous carbon formed during the reducing phase is oxidised during the oxidation cycle, this is also evident through CHNS results which shows a great similarity in carbon present in oxidised Cat + sorbent and Fresh catalyst and sorbent.*

3- *Carbon in is the same for all reduction cycles as the same flowrate is 0.978 ml/Hr is utilised for all runs*

4- *Carbon from $CaCO_3$ from calcined sorbent remains relatively the same across the cycles (4.5% as detected from XRD analysis)*

5- *The carbon on catalyst surface realised after CHNS analysis after 20 cycles can be deduced by subtracting total carbon found from CHNS of the used Cat/sorbent mixture and the CHNS of the Blank (Fresh Cat/Sorbent).*

A- Mole flow rate of C in acetic acid= 9.47667E-06 Mol/S

No of moles in 7200 seconds= 0.06823199 mol

B- - Mass of sorbent= 2 g

% of $CaCO_3$ from XRD analysis = 4.5%

Mass of $CaCO_3$= 0.09 g

Mole weight $CaCO_3$= 100.0869 g/mol

Mol of $CaCO_3$= 0.000899219 mol

Overall Carbon In = 0.06823199 + 0.000899219

= 0.069131209 mol

Carbon OUT

Carbon Out = $Carbon\ from\ Condensate\ +\ Carbon\ Oxidised\ +\ Carbon\ from\ Process\ output$

(For cycle 1-19)

$$Carbon\ from\ Condensate\ +\ Carbon\ from\ used\ catalyst\ +\ Carbon\ from\ Process\ output$$

(For cycle 20)

Carbon from Condensate (after TOC Run) = $\frac{\boldsymbol{Conc\ of\ TO\ Carbon\ \left(\frac{g}{L}\right) * Vol\ of\ collected\ condensate\ (L)}}{\boldsymbol{molar\ mass\ of\ C\ \left(\frac{g}{mol}\right)}}$

Carbon from Process Output and oxidised= $nOut * (\ Molar\ fraction\ of\ CO\ +\ Molar\ fraction\ of\ CO_2\ +\ \ Molar\ fraction\ of\ CH_4)$

Carbon from oxidation run= $nOut * (\ Molar\ fraction\ of\ CO\ +\ Molar\ fraction\ of\ CO_2)$

Carbon from Used Catalyst from cycle 20 (after CHNS) = $Carbon\ from\ Catalyst\ Surface\ +\ Carbon\ from\ Calcination\ of\ Sorbent$

Carbon Unaccounted for = $(Cin - Cout)/Cin\ * 100$

The full carbon balance calculated from 20 cycles of SE-CLSR is given in the following table;

	C (feed) (Mol) $x10^2$	Fuel Conversion (%)	Carbonation time (s)	De-Carbonation time (oxidation Run)	C- out Process (mol) $x10^2$	C –oxidation run (mol) $x10^2$	C- condensate (mol) $x10^5$	Total carbon out (mol) $x10^2$	Balance $x10^3$	Carbon Unaccounted for
1	6.91	91.76	3150.00	1800	3.91	3.09	5.13	7.00	-0.883	-1.28
2	6.91	80.90	2700.00	1500	3.13	3.51	2.00	6.65	2.66	3.85
3	6.91	81.10	2850.00	1500	3.15	3.56	8.49	6.71	2.01	2.91
4	6.91	83.91	2700.00	1350	3.74	2.87	1.86	6.61	3.05E	4.41
5	6.91	82.89	2550.00	1200	3.84	4.31	1.94	8.15	-12.4E	-17.9
6	6.91	87.35	2550.00	1050	3.26	3.54	1.87	6.80	1.13	1.63
7	6.91	91.81	2700.00	1050	4.20	2.71	1.98	6.92	-0.0217	-0.0313
8	6.91	89.56	2700.00	1050	3.58	3.15	1.42	6.73	1.80	2.61
9	6.91	86.72	2250.00	900	3.24	2.93	2.29	6.17	7.44	1.08
10	6.91	85.77	2400.00	900	4.11	2.81	1.90	6.92	-0.0835	-1.21
11	6.91	84.62	1800.00	1050	3.56	2.98	1.54	6.54	3.71	5.37
12	6.91	86.01	1950.00	1050	3.87	3.24	2.75	7.12	-2.04	-2.95
13	6.91	88.44	1350.00	750	3.61	2.82	1.69	6.44	4.78	6.91
14	6.91	87.58	1500.00	750	3.82	2.64	1.95	6.46	4.51	6.53
15	6.91	91.24	1500.00	750	3.91	2.17	1.98	6.08	8.37	12.1
16	6.91	90.45	1650.00	750	4.71	1.67	3.81	6.38	5.28	7.64
17	6.91	86.84	1650.00	900	4.77	1.94	3.66	6.71	1.98	2.87

	C- (feed) (Mol) $x10^2$	Fuel Conversion (%)	Carbonation time (s)	De-Carbonation time (oxidation Run)	C- out Process (mol) $x10^2$	C –oxidation run (mol) $x10^2$	C- condensate (mol) $x10^5$	Total carbon out (mol) $x10^2$	Balance $x10^3$	Carbon Unaccounted for
18	6.91	92.06	1800.00	900	3.57	2.43	2.61	6.00	9.10	13.2
19	6.91	90.68	1950.00		4.43	1.81	3.06	6.25	6.64	9.61
20	6.91	93.69	1800.00		5.60	8.77	2.90	6.48	4.35	6.29

Appendix 3: Ni content in condensate

The Nickel content in the condensate collected for CLSR and SECLSR runs was calculated from the mass concentration of Ni detected from the condensate derived from ICP-MS;

$$Ni_{weight\ in\ condensate} = \ mass\ concentration_{Ni} \times Volume_{condensate\ coleected}$$

Its efficiency is calculated as;

$$Efficiency\ (\%) = \frac{Ni_{weight\ in\ condensate}}{Ni_{weight\ in\ catalyst}} \times 100$$

Appendix 4: SEM-EDX images

EDX for CLSR used catalyst after 10 cycles:

Reforming temperature = 650 °C	Oxidation temperature = 800 °C
Steam to carbon ratio = 3	Catalyst B
WHSV = 2.5 hr $^{-1}$	10 cycles of reforming

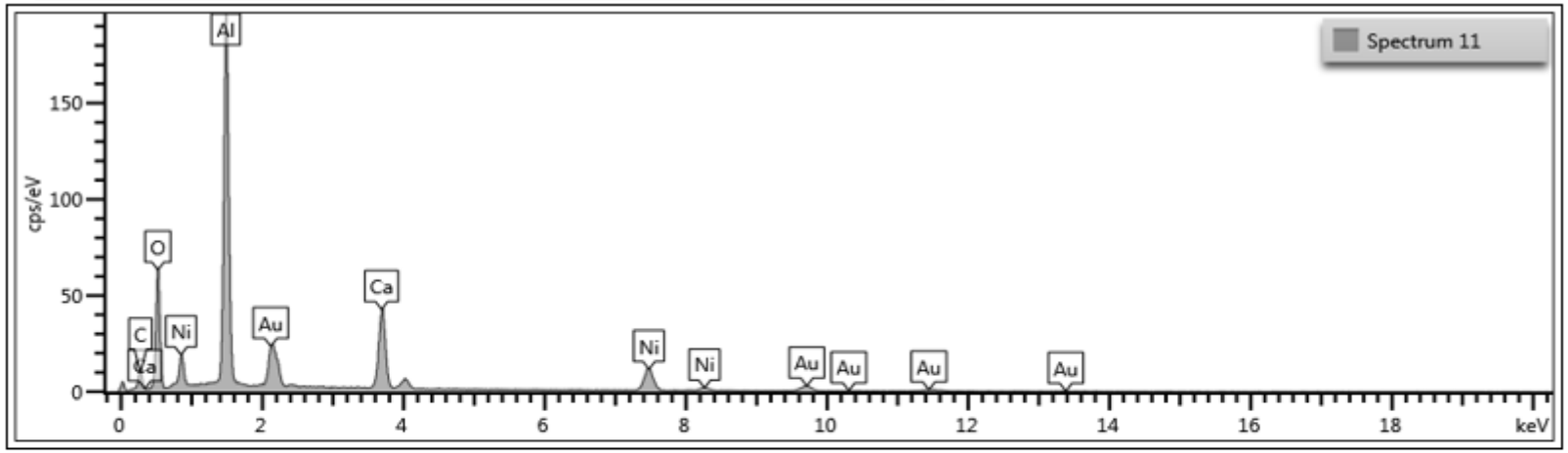

Spectrum 11

Element	Wt%	Wt% Sigma
C	11.47	0.41
O	30.98	0.30
Al	25.88	0.20
Ca	9.80	0.11
Ni	10.22	0.17
Au	11.65	0.24
Total:	100.00	

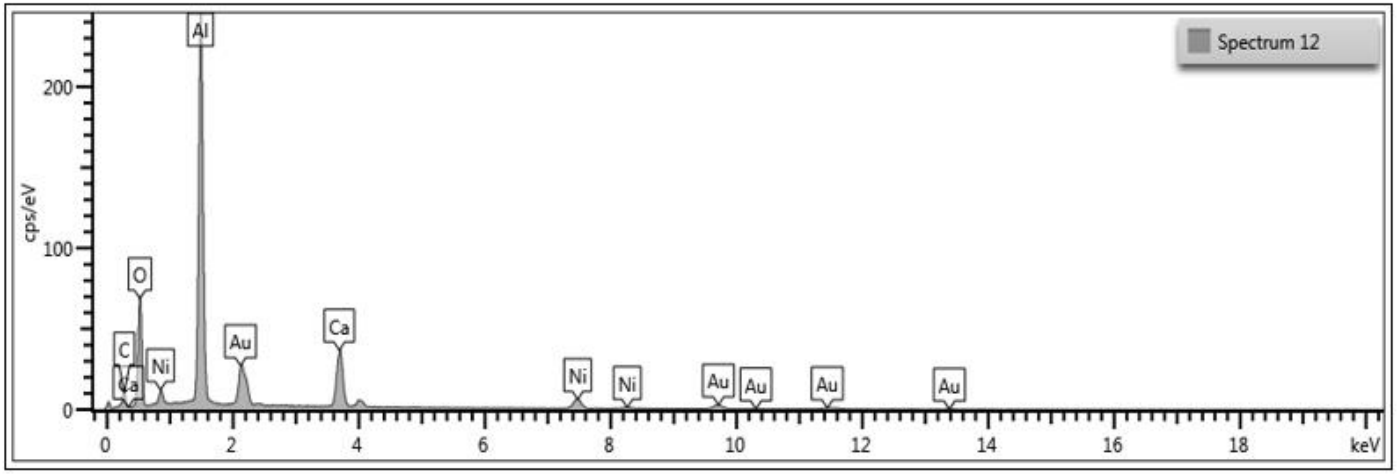

Spectrum 12

Element	Wt%	Wt% Sigma
C	12.02	0.44
O	32.60	0.31
Al	29.27	0.23
Ca	8.26	0.10
Ni	5.13	0.14
Au	12.73	0.25
Total:	100.00	

Electron Image 6

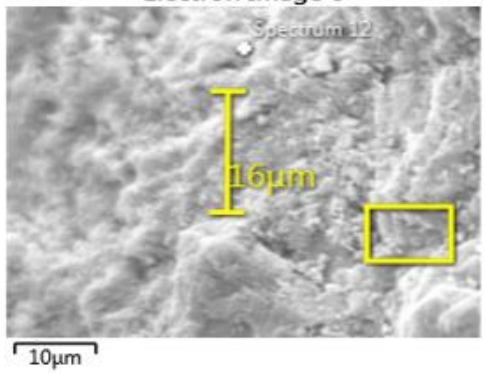

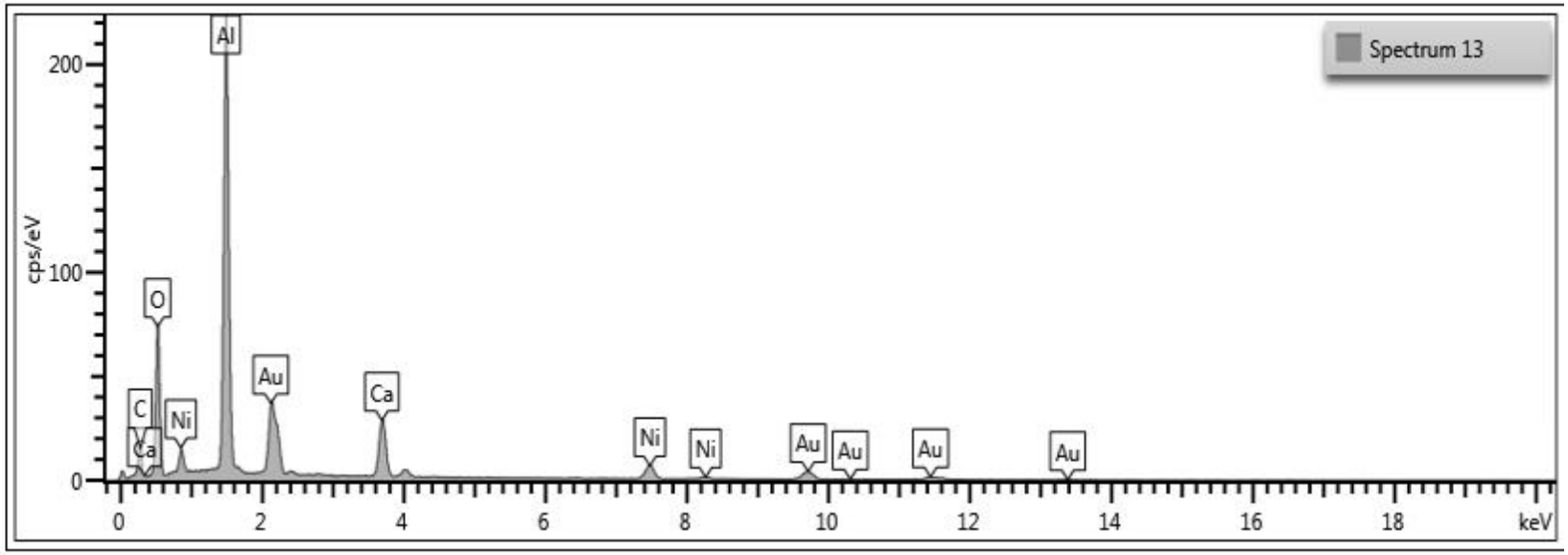

Spectrum 13

Element	Wt%	Wt% Sigma
C	14.16	0.43
O	32.26	0.30
Al	25.16	0.20
Ca	6.30	0.09
Ni	5.45	0.14
Au	16.67	0.26
Total:	100.00	

Electron Image 6

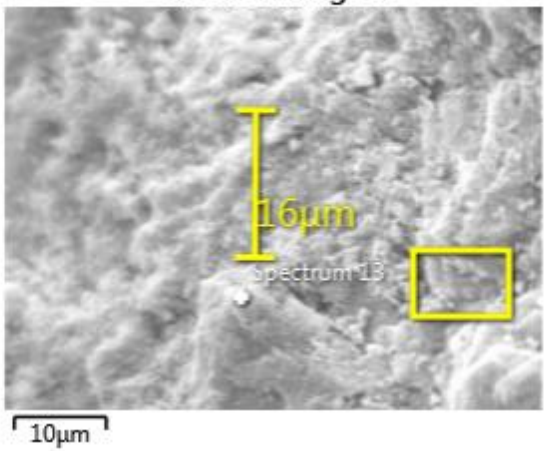

EDX profile oxidized catalyst B;

It is essential to state the amount of carbon estimated could be attributed to the carbon plates utilized, it however shows a similar carbon estimation with fresh catalyst

Reforming temperature = 650 °C	Oxidation temperature = 800 °C
Steam to carbon ratio = 3	Catalyst B
WHSV = 2.5 hr^{-1}	1 cycle of reforming

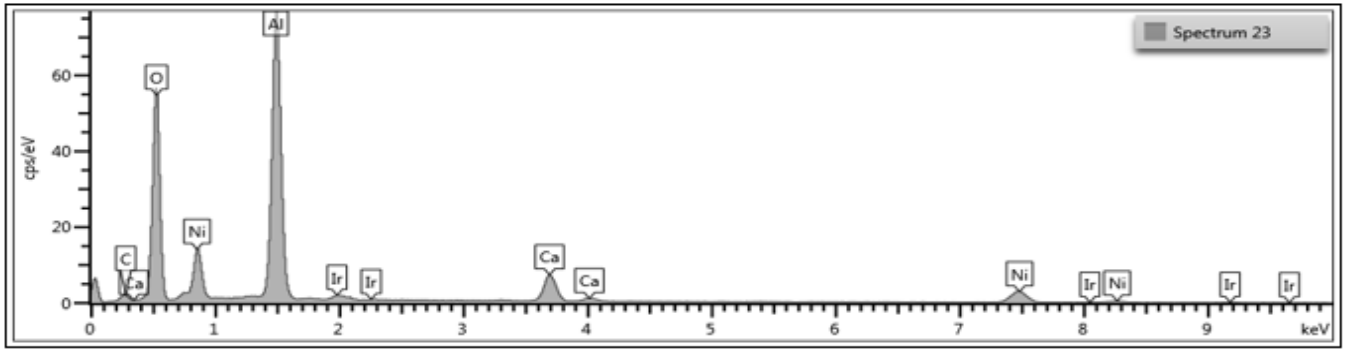

Spectrum 23

Element	Wt%	Wt% Sigma
C	4.14	0.29
O	42.64	0.26
Al	30.03	0.19
Ca	5.92	0.09
Ni	15.27	0.26
Ir	2.00	0.16
Total:	100.00	

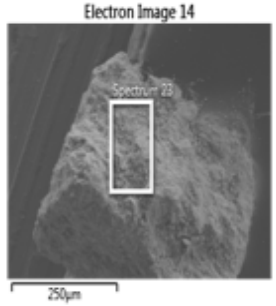

EDX profile Fresh Catalyst B

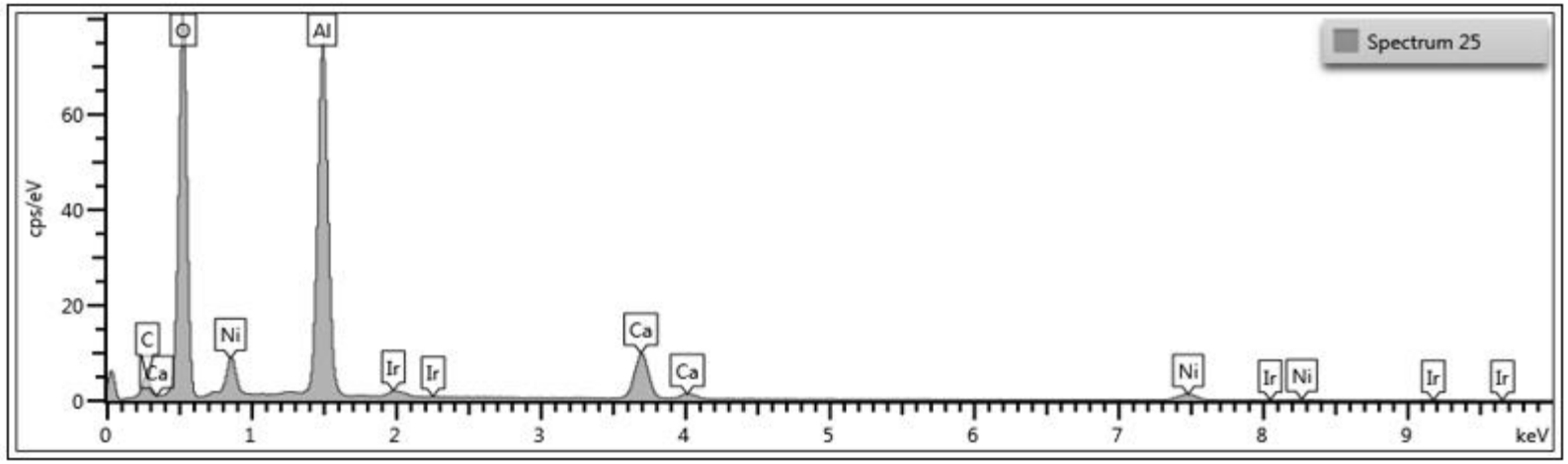

Spectrum 25

Element	Wt%	Wt% Sigma
C	7.88	0.25
O	53.27	0.23
Al	24.21	0.14
Ca	6.99	0.08
Ni	5.96	0.17
Ir	1.70	0.12
Total:	100.00	

Electron Image 16

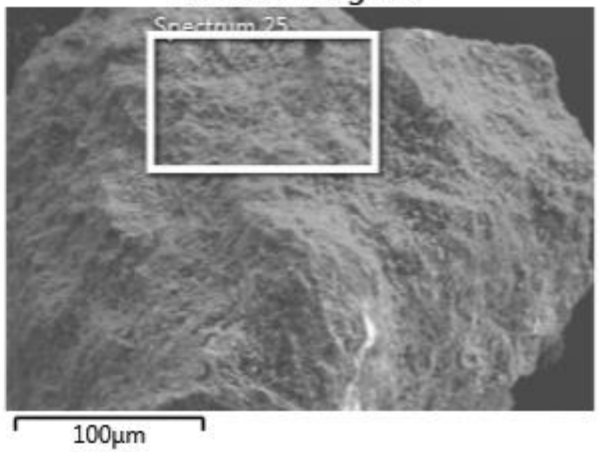

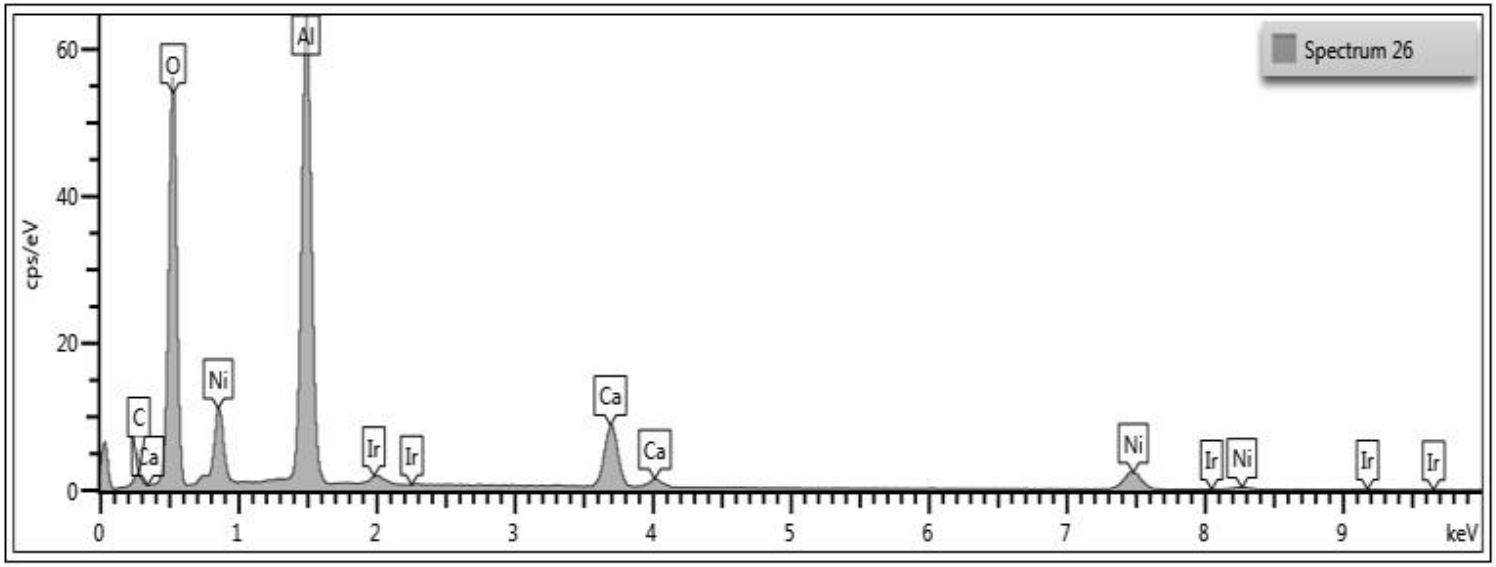

Spectrum 26

Element	Wt%	Wt% Sigma
C	4.32	0.26
O	46.23	0.25
Al	26.67	0.17
Ca	7.76	0.09
Ni	13.05	0.24
Ir	1.96	0.15
Total:	100.00	

Electron Image 17

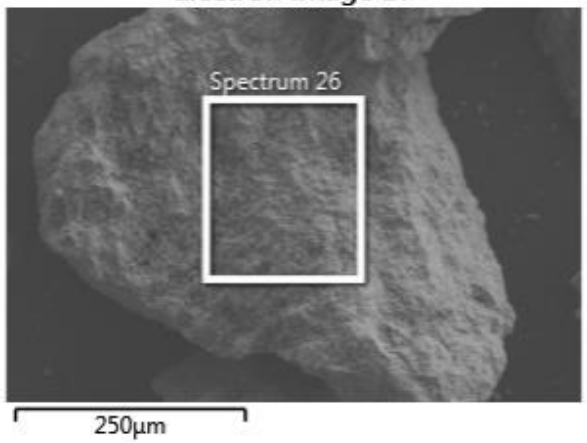

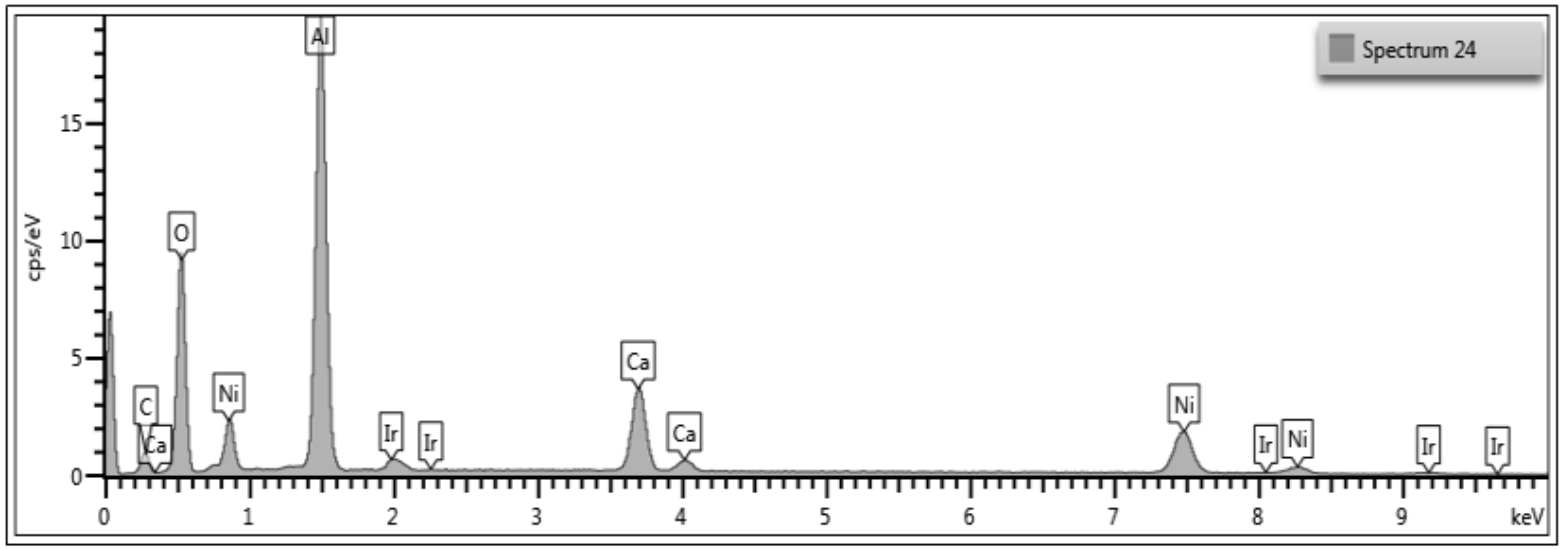

Spectrum 24

Element	Wt%	Wt% Sigma
C	7.55	0.26
O	26.69	0.21
Al	25.73	0.17
Ca	9.31	0.10
Ni	28.08	0.29
Ir	2.66	0.14
Total:	100.00	

Electron Image 15

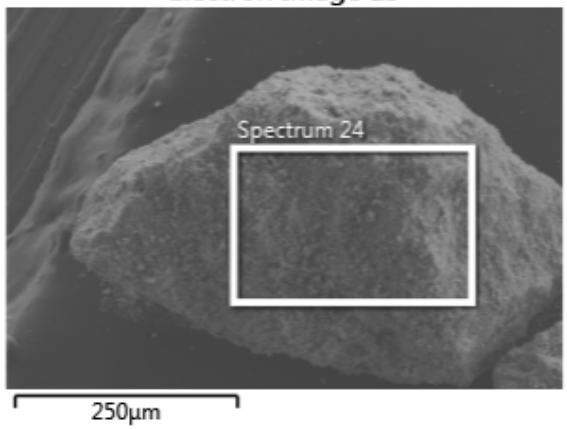

EDX profile oxidized catalyst A coated with gold;

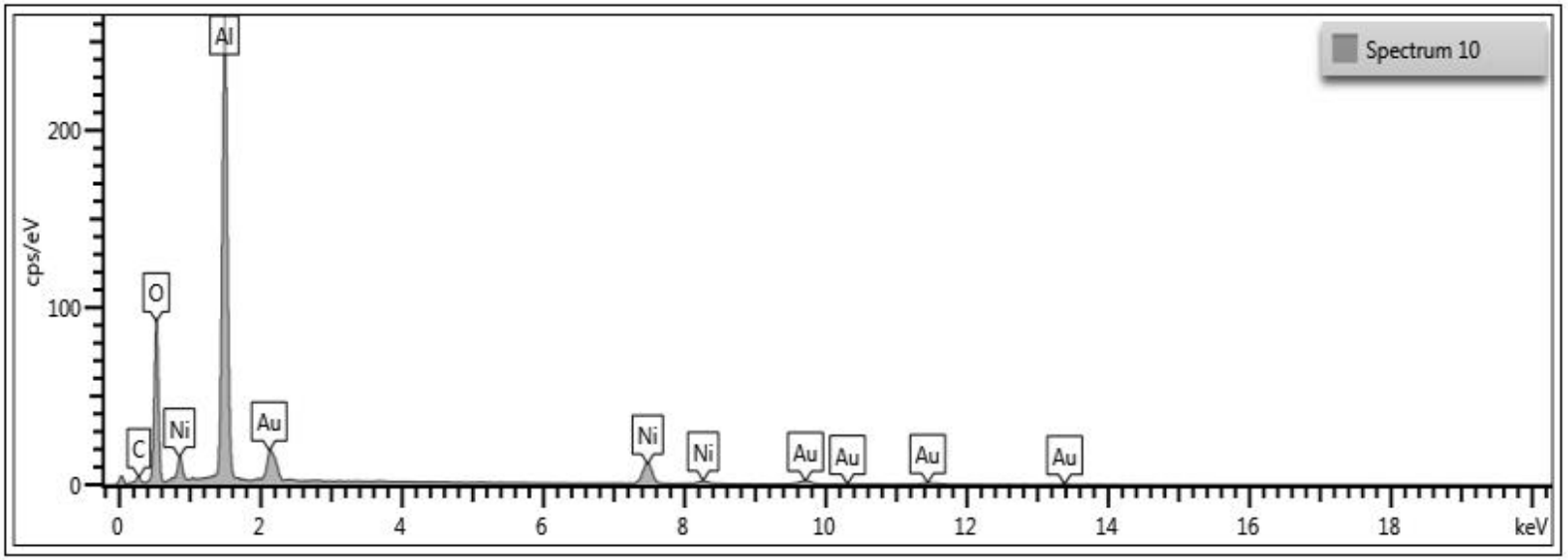

Spectrum 10

Element	Wt%	Wt% Sigma
C	5.66	0.40
O	35.03	0.28
Al	37.43	0.25
Ni	11.29	0.19
Au	10.58	0.25
Total:	100.00	

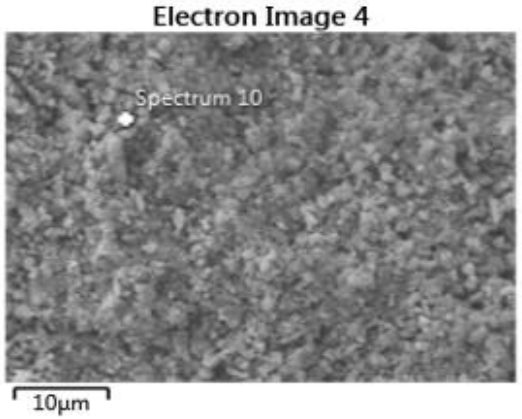

EDX profile Fresh catalyst and sorbent Mix for SE-CLSR

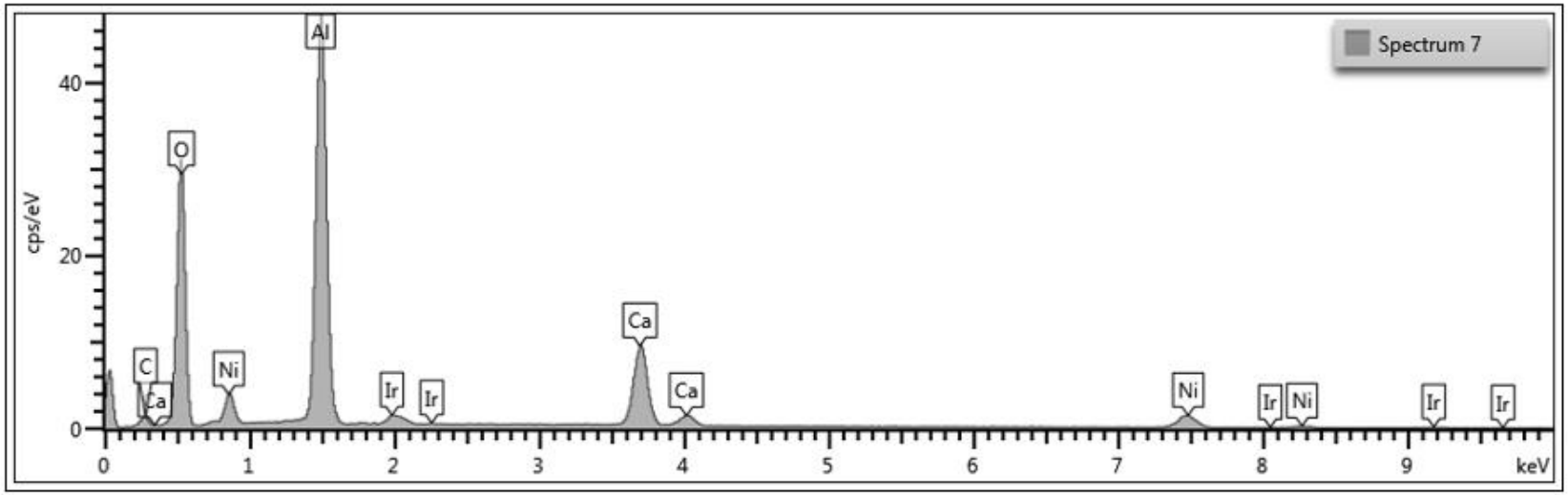

Spectrum 7

Element	Wt%	Wt% Sigma
C	3.98	0.26
O	42.44	0.26
Al	27.89	0.18
Ca	12.05	0.12
Ni	10.96	0.25
Ir	2.69	0.17
Total:	100.00	

Electron Image 4

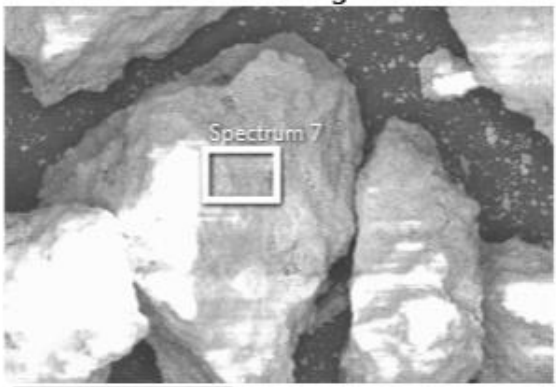

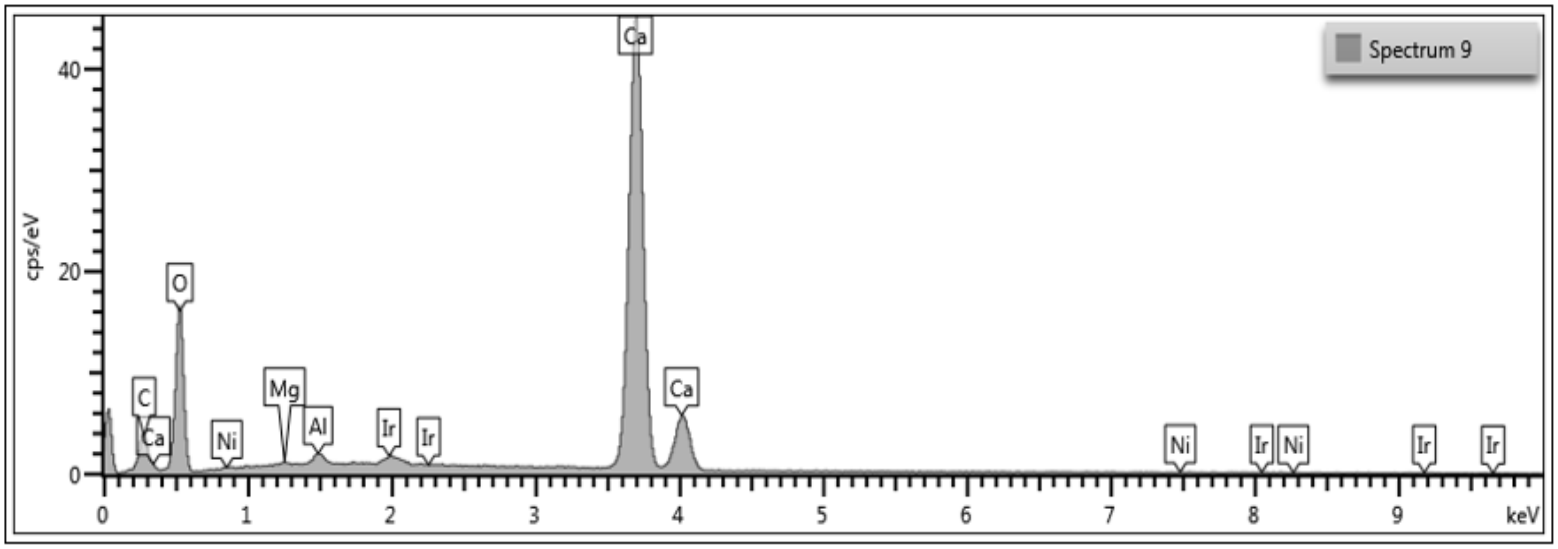

Spectrum 9

Element	Wt%	Wt% Sigma
C	4.78	0.15
O	42.90	0.28
Mg	0.12	0.04
Al	0.54	0.04
Ca	50.01	0.27
Ni	0.22	0.13
Ir	1.43	0.15
Total:	100.00	

Electron Image 6

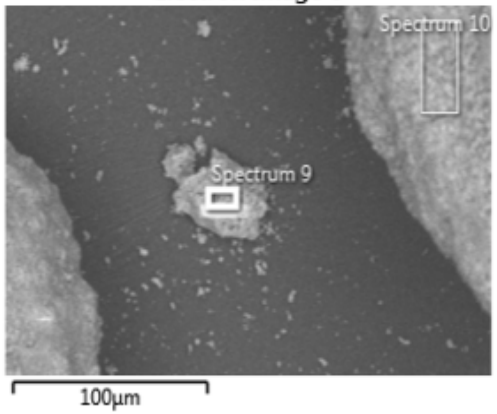

EDX profile Oxidised catalyst and sorbent Mix for SE-CLSR

Reforming temperature = 650 °C	Oxidation temperature = 850 °C
team to carbon ratio = 3	Catalyst B and $CaCO_3$
	8 cycles of reforming

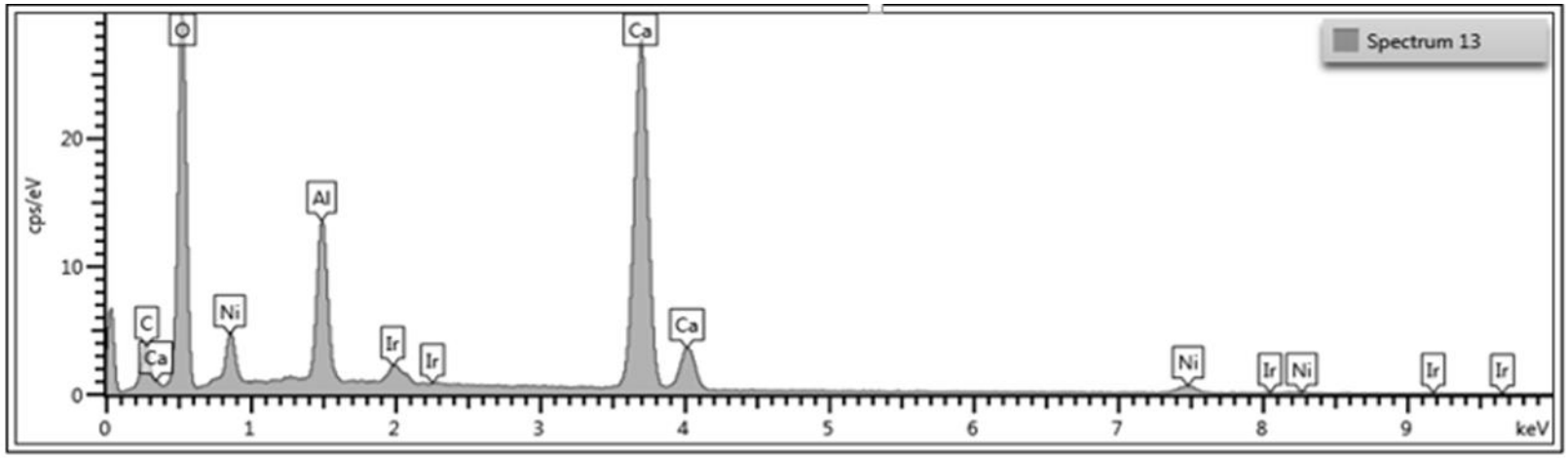

Spectrum 13

Element	Wt%	Wt% Sigma
C	5.61	0.18
O	51.45	0.25
Al	6.63	0.07
Ca	29.95	0.18
Ni	3.87	0.16
Ir	2.49	0.14
Total:	100.00	

Electron Image 8

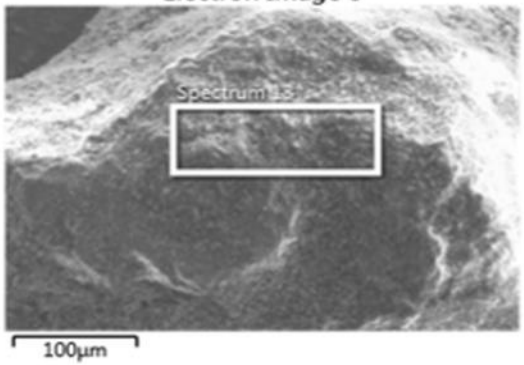

EDX profile used catalyst and sorbent Mix for SE-CLSR after 20 cycles of SE-CLSR

Reforming temperature = 650 °C	Oxidation temperature = 850 °C
Steam to carbon ratio = 3	Catalyst B and $CaCO_3$
	20 cycles of reforming

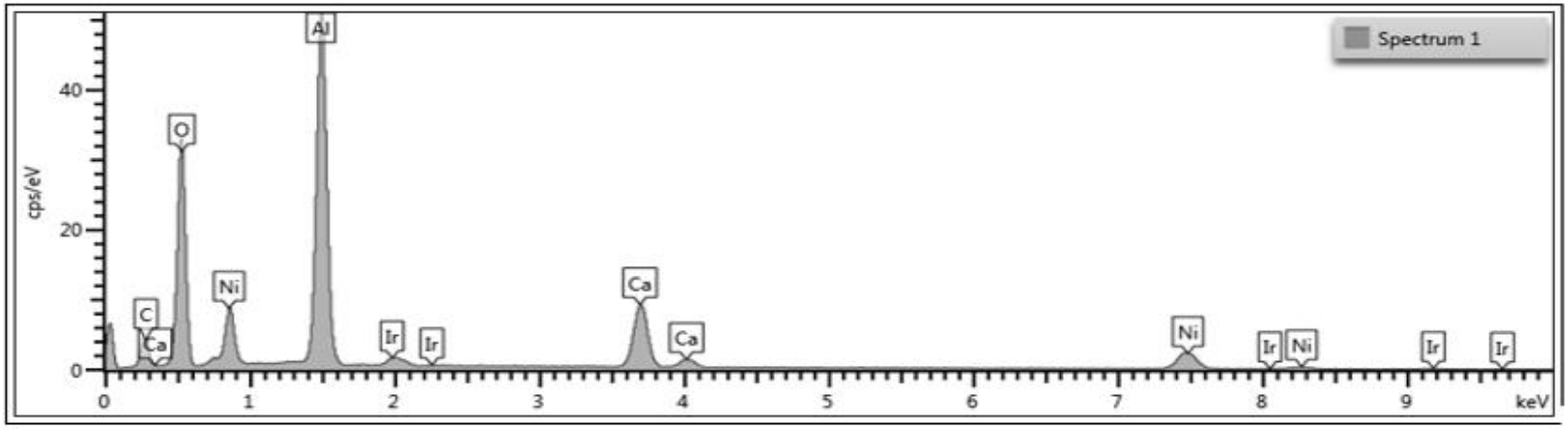

Spectrum 1

Element	Wt%	Wt% Sigma
C	14.38	0.32
O	40.83	0.25
Al	22.37	0.14
Ca	8.68	0.09
Ni	13.75	0.21
Total:	100.00	

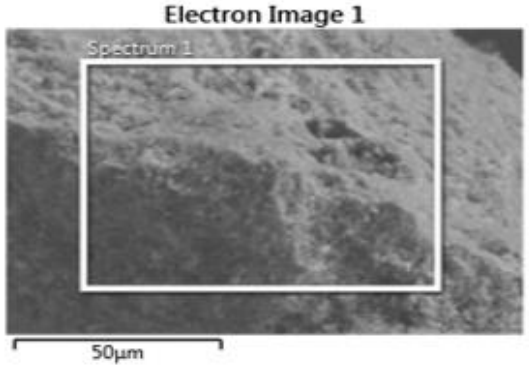

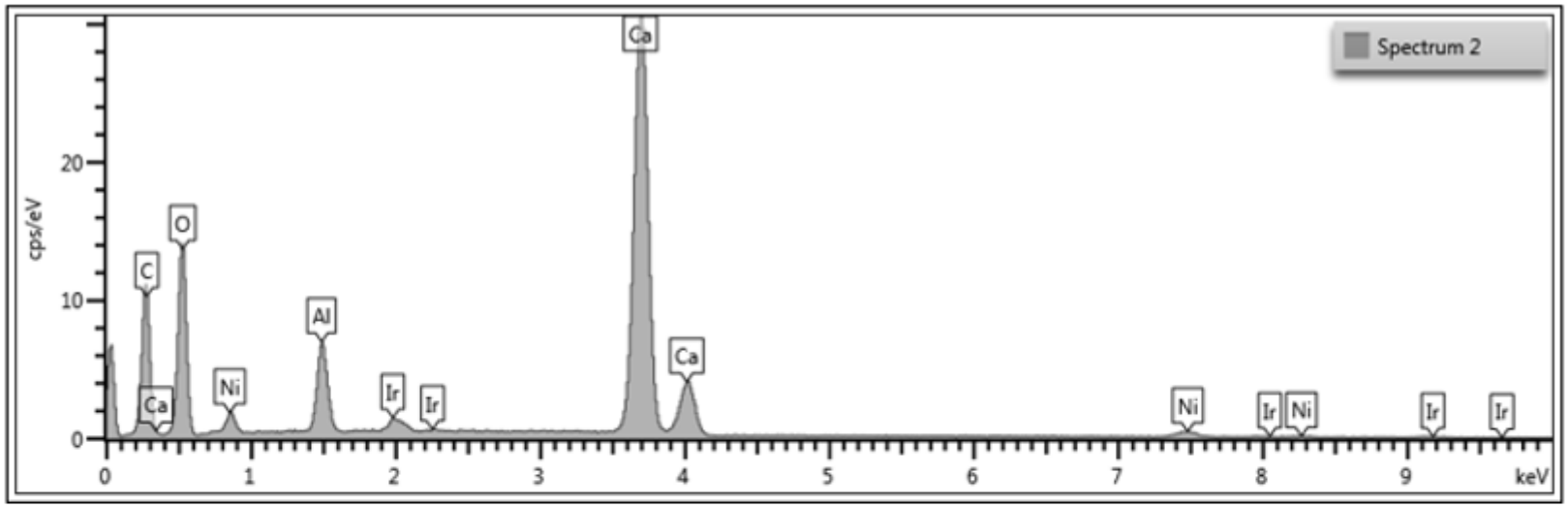

Spectrum 2

Element	Wt%	Wt% Sigma
C	21.47	0.24
O	38.91	0.27
Al	3.29	0.05
Ca	33.64	0.20
Ni	2.69	0.15
Total:	100.00	

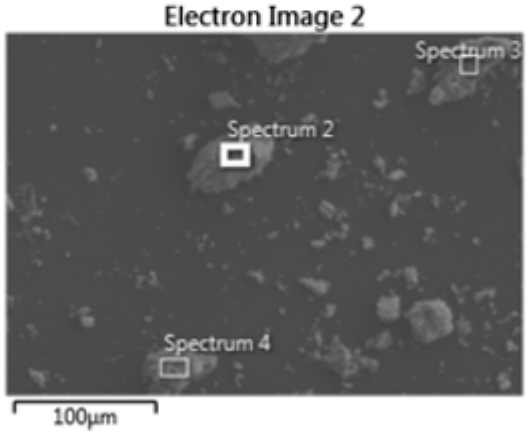

Nomenclature

catalyst A	18 % wt. NiO on α alumina
Catalyst B	15% wt. NiO on Calcium aluminate
sccm	standard cubic centimetre per minute
$\dot{n}_{out,dry}$	total molar flow rate dry basis
$\dot{n}_{c,gas}$	rate of the gasification of carbon
$\dot{n}_{Ni \rightarrow NiO}$	Rate of nickel oxidation
$y_{CO}, y_{CO_2}, y_{O_2}$	Molar fractions of CO, CO2 and O2
$n_{Ni,t}, n_{Ni,i}$	Number of moles of nickel oxidised and number of moles of nickel in catalyst
$\dot{n}_{O_2,in}$	Molar flow rate of oxygen in
Sel_i	Selectivity of individual constituent
CHN	Carbon, hydrogen and nitrogen elemental analysis
ICP-Ms test	Inductively coupled plasma mass spectrometry
TOC	Total organic carbon analysis
SEM-EDX	Scanning Electron Microscope- Energy Dispersive X-ray Analysis
TEM	Transmission Electron Microscope
TGA-FTIR	Thermogravimetric analysis coupled to Fourier transform infrared spectroscopy
TPO	temperature-programmed oxidation
WHSV	Weight hourly space velocity
X_{HAc} and X_{H2O}	Conversion fraction of fuel and water
Equil	equilibrium
Wt.%	Weight percentage
DTG	Derivative Thermogravimetric Analysis
C-in gas, C oxidised, C condensate	Carbon in process gas, carbon in oxidation cycle, carbon in condensate
XRD	X-ray powder diffraction
MBET	Multipoint Brunauer–Emmett–Teller method
Micro-GC	micro gas chromatogram
CEA	Chemical Equilibrium with Applications
BJH	Barrett-Joyner-Halenda method
PEFB	Palm empty fruit bunch
CLSR	Chemical looping reforming

SE-SR, SE-CLSR	Sorption enhanced steam reforming , sorption enhanced CLSR
PB,BT,SS	Pre breakthrough, breakthrough and steady state phase
SR	Steam reforming
HAc	Acetic acid
T_{OX}	Temperature of Oxidation
T_{SR}	Temperature of Steam reforming
$\mathbf{n_{Cgas}}$	Number of moles of carbon gasified in air feed stage
S/C	Steam to carbo ratio
cc/g	cubic centimetre per gram
OC	Oxygen carrier
$\mathbf{X_{Ni\rightarrow NiO}}$, $\mathbf{X_{C-gas}}$	Extent of Nickel and Carbon Oxidation
$\dot{\mathbf{n}}_{\mathbf{i,in}}$ and $\dot{\mathbf{n}}_{\mathbf{i,out}}$	molar flow rate in and out of specie I respectively
n_i	number of moles of specie i
y_i and y_a	molar fraction of specie i and all gases in the outlet gas respectively
W_i	Molar weight of specie i